

One-dimensional approach of transport phenomena of dissolved matter in rivers

A. van Mazijk

De verdediging van het proefschrift en de daarbij behorende stellingen is vastgesteld op dinsdag 17 september 1996 om 13.30 uur in de Senaatszaal van de Aula van de Technische Universiteit Delft, Mekelweg 5 te Delft.

Na de promotie wordt een receptie gehouden in één van de zalen van de Aula.

Stellingen

Stellingen behorende bij het proefschrift van A. van Mazijk, 1996,
One-dimensional approach of transport phenomena of dissolved matter in rivers.

- 1 Hoewel de voortplantingssnelheid van een stofwolk in een rivier het beste wordt beschreven met het zwaartepunt van de wolk in het tijddomein, noodzaakt de praktijk veelal tot het beschouwen van de piekconcentratie.
- 2 Analytische oplossingen van de differentiaalvergelijkingen, die het stoftransport in een rivier met stagnante zones beschrijven, suggeren ten onrechte dat de invloed van deze zones op de stoftransportsnelheid toeneemt met de afstand.
- 3 Het is niet de verblijftijd in de stagnante zones van de met de hoofdstroom uitwisselende stof, die de voortplantingssnelheid van de stofwolk beïnvloedt, maar het volume van deze zones, dat met de hoofdstroom uitwisselt.
- 4 De verdeling van het concentratieverloop in het tijddomein van een zich langs de rivier voortplantende stofwolk is van nature scheef.
- 5 De blijvende scheve verdeling in het tijddomein van het over de dwarsdoorsnede gemiddelde concentratieverloop van een zich langs de rivier voortplantende stofwolk, wordt het beste benaderd door het Chatwin-model met een scheefheidscoëfficiënt gelijk aan de eenheid.
- 6 Het vergroten van de meetnauwkeurigheid van tracermetingen ter bepaling van de coëfficiënt, die de stofuitwisseling tussen het stroomvoerende en het stagnante deel van de dwarsdoorsnede van een rivier beschrijft, heeft weinig zin.
- 7 De verdunningsmethode ter bepaling van de afvoer is niet geschikt voor rivieren met een grote breedte-diepte verhouding (≥ 20), die als scheepvaartweg worden gebruikt.
- 8 Saeijs suggereert ten onrechte, dat Nederland behoort tot de waterarmste landen van de wereld.
(Saeijs, H.L.F., *Levend water en een wereldstad*, Inaugurele rede, Erasmus Universiteit Rotterdam, 1995)

- 9 Door het hoogwater van de Rijn en de Maas in 1995 is de betekenis van het Nederlandse spreekwoord: "Als het kalf verdrongen is, dempt men de put" enigszins afgezwakt.
- 10 Vanwege het belang voor de volksgezondheid van een goede drinkwatervoorziening en afvalwaterbehandeling, zou de Technische Universiteit Delft bij de herinvoering van het 5-jarig curriculum de onderwijsruimte voor de opleiding van de gezondheidstechnicus bij de Faculteit der Civiele Techniek moeten verdubbelen.
- 11 De individualisering van de *lifestyle* in de westerse wereld vormt een milieu-bedreigende ontwikkeling.
(Naar aanleiding van de inaugurele rede van prof. dr. A.C. Kuijsten, Universiteit van Amsterdam, 26 april 1996)
- 12 De jurist Wisse stelt terecht, dat de gelijkheidsdrang in de Europese wetgeving op den duur leidt tot een maatschappij, waarin geen ruimte is voor sociale netwerken, waarbinnen de menselijke persoon zijn eigenheid kan beleven.
(Wisse, G.J.M., *Is een mens niet meer dan een dier dat kan denken?*, Katholiek Nieuwsblad, 29 maart 1996).
- 13 De Bijbel verhaalt de aardse geschiedenis van de mensheid vanuit een hemels perspectief tot circa een eeuw na de geboorte van Christus.
- 14 Iedere wetenschapper behoort ernaar te streven een goede boodschapper te zijn.

*The fear of the Lord is
the beginning of knowledge
(Proverbs 1:7)*

One-dimensional approach of transport phenomena of dissolved matter in rivers



PROEFSCHRIFT

ter verkrijging van de graad van doctor
aan de Technische Universiteit Delft,
op gezag van de Rector Magnificus Prof.ir. K.F. Wakker,
in het openbaar te verdedigen ten overstaan van een commissie,
door het College van Dekanen aangewezen,
op dinsdag 17 september 1996 te 13.30 uur

Albertus VAN MAZIJK
civiel ingenieur
geboren te Utrecht

Dit proefschrift is goedgekeurd door de promotor:
Prof.dr.ir. M. de Vries

Samenstelling promotiecommissie:

Rector Magnificus Prof.dr.ir. M. de Vries	voorzitter em. hgl. Technische Universiteit Delft, promotor
Prof.dr.ir. C. van den Akker	Technische Universiteit Delft
Prof.ir. J.H. Kop	em. hgl. Technische Universiteit Delft
Prof.dr.ir. H.J. de Vriend	Universiteit Twente
Prof.Dr.-Ing. Dr.-Ing.E.h. E.J. Plate	Universität Karlsruhe
Dr.-Ing.E.h. D. Ruchay	Bundesministerium für Umwelt, Naturschutz und Reaktorsicherheit
Dr.ir. C. Kranenburg	Technische Universiteit Delft

Abstract

For the prediction of the transport of a pollution cloud in the River Rhine and its main tributaries the Rhine Alarm-Model has been developed: a one-dimensional transport-model for dissolved matter, based on the analytical solution of the convection-dispersion equation for an instantaneous release after Taylor. In order to reproduce the observed skewness of concentration distributions, the Taylor solution has been adapted by the third Hermite-polynomial after Chatwin.

For the calibration and verification of the model a series of tracer experiments has been carried out from Basel (Switzerland) downstream to the Dutch Rhine-branches. The parameters of the model concern the lag coefficient, representing the difference between the actual transport-velocity and the mean flow-velocity, and the longitudinal dispersion-coefficient. The decay of substances was not taken into account. In case of a completely mixed situation over the river cross-section the lag coefficient is mainly determined by the exchange of mass with the dead zones along the river banks (groyne-fields). For a non-completely mixed situation the transversal velocity-distribution causes differences between the transport velocity and the mean flow-velocity, for instance downstream of a release from a river bank. Moreover, deviations of the actual hydrological conditions from the model schematization are covered by the lag coefficient.

Beside a detailed analysis of the calibrated model-parameters, the relation between the lag coefficient and the ratio of the cross-sectional areas of the dead-zone and the main stream (dead-zone parameter) has been quantified in particular. For that purpose a numerical dead-zone model has been developed. It is shown that the lag coefficient varies with the dead-zone parameter. However, the variation is smoothed by the longitudinal dispersion-coefficient. Therefore, a minimum distance between two successive measuring-stations is needed for a good agreement between the lag coefficient and the mean dead-zone parameter, given by a Péclet number of 10 till 15. This agreement also presumes a completely mixed situation in the dead zones, which depends on the dimensions of the dead zones as well as the flow velocity in the main stream. After the presented conditions the groyne-fields along the Dutch Rhine-branches are completely mixed. However, in case of a suppressed flow the influence of the dead zone becomes negligible. Large dead-zones, like river harbours will only partly exchange with the main stream. A practical upper-limit for the dead-zone parameter seems to be 0.5. The coefficient for the mass transfer between the dead zones and the main stream only influences the shape of the concentration distribution, but not the transport velocity related to the time-centroid of the distribution. It is shown that tracer experiments with degradable substances are unsuitable for the determination of this parameter.

In case of a bank release, the lag coefficient can be estimated by an analytical description of the transversal velocity-distribution. A first verification by the results of two tracer experiments has been carried out.

Samenvatting

Eéndimensionale benadering van transportverschijnselen van opgeloste stoffen in rivieren

Voor de voorspelling van het transport van een verontreinigingsgolf in de Rijn en haar belangrijkste zijrivieren is het Rijnalarmmodel ontwikkeld: een één-dimensionaal transportmodel voor opgeloste stoffen, gebaseerd op de analytische oplossing van de convectie-diffusie vergelijking voor een momentane puntlozing volgens Taylor. Teneinde de veelal waargenomen scheefheid van gemeten concentratie-verdelingen te kunnen reproduceren is deze Taylor-oplossing aangepast volgens Chatwin met de derde Hermiet polynoom.

Voor de ijking en validatie van de modelparameters is een reeks van tracer metingen uitgevoerd van Basel tot in de Nederlandse Rijnakken. De modelparameters zijn de longitudinale dispersiecoëfficiënt en de stoftransportcoëfficiënt. De laatste beschrijft het verschil tussen de actuele transportsnelheid van een verontreinigingsgolf en de gemiddelde stroomsnelheid. De afbraak van de geloosde stof is buiten beschouwing gebleven. In het geval van een volledig gemengde situatie over de dwarsdoorsnede van de rivier wordt de stoftransportcoëfficiënt hoofdzakelijk bepaald door de stofuitwisseling tussen de hoofdstroom en de stagnante zones langs de rivieroever, zoals kribvakken. Bij een onvolledig gemengde situatie is het de snelheidsverdeling over de dwarsdoorsnede van de rivier, die de verschillen tussen de gemiddelde stroomsnelheid en de stoftransportsnelheid veroorzaakt, zoals die bijvoorbeeld zijn waar te nemen benedenstrooms van een oeverlozing. Ook worden afwijkingen van de werkelijk optredende hydrologische omstandigheden als gevolg van de gehanteerde modelschematisatie met de stoftransportcoëfficiënt weergegeven.

Naast een gedetailleerde analyse van de geijkte modelparameters, is met name de relatie tussen de stoftransportcoëfficiënt en de verhouding van de oppervlakten van het stroomvoerend dwarsprofiel en de stagnante zone (= stagnante-zone-coëfficiënt) gekwantificeerd. Voor dat doel is een numeriek stagnante-zone-model ontwikkeld. Het blijkt dat de stoftransportcoëfficiënt varieert met de stagnante-zone-coëfficiënt. Echter, de variatie van de lokale stoftransportcoëfficiënt wordt afgevlakt door de longitudinale dispersiecoëfficiënt. Derhalve is een minimum afstand tussen twee

opeenvolgende meetstations vereist voor een goede overeenstemming tussen de gemeten stoftransportcoëfficiënt en de gemiddelde stagnante-zone-coëfficiënt. De minimum afstand wordt gegeven door een waarde voor het Péclet getal van 10 à 15. Deze overeenkomst tussen beide coëfficiënten veronderstelt overigens een volledig gemengde situatie in de stagnante zones, die bepaald wordt door de afmetingen van de desbetreffende stagnante zones en de stroomsnelheid in de hoofdstroom. Volgens de gepresenteerde voorwaarden in deze, heerst er in de kribvakken langs de Nederlandse Rijntakken volledige menging. In het geval van een gestuwde rivier wordt de invloed van de kribvakken echter verwaarloosbaar klein. Grote stagnante zones zoals havens, zullen maar gedeeltelijk uitwisselen met de hoofdstroom. Een praktische bovengrens van het effectieve deel van deze stagnante zones op het stoftransport blijkt gegeven te kunnen worden door een stagnante-zone-coëfficiënt van 0,5. De parameter, die de stofuitwisselingssnelheid tussen de hoofdstroom en de stagnante zone beschrijft, blijkt alleen het concentratieverloop te beïnvloeden, maar niet het stoftransport, gerelateerd aan het zwaartepunt van de concentratieverdeling in het tijddomein. Aangetoond wordt dat tracerproeven met afbreekbare stoffen ongeschikt zijn voor de bepaling van deze parameter.

In geval van een oeverlozing kan de stoftransportcoëfficiënt met behulp van een analytische beschrijving van het transversale snelheidsprofiel worden benaderd. Een eerste validatie van deze benadering is uitgevoerd op basis van twee tracerproeven.

Table of contents

Abstract	iii
Samenvatting	iv
1 Introduction	1
2 Mathematical description	
2.1 General	3
2.2 Transverse mixing reach	
2.2.1 Release at a river bank	12
2.2.2 River confluence	21
2.3 Longitudinal mixing reach	
2.3.1 General	27
2.3.2 Two-zone approach	32
2.3.3 Temporal-moment approach	45
3. Tracer experiments River Rhine	
3.1 Introduction	53
3.2 Hydraulic basis of the Rhine Alarm-Model	58
3.3 Calibration and verification	
3.3.1 Calibration methods	62
3.3.2 Results	78
3.4 Discussion	
3.4.1 The canalized Rhine between Basel and Kehl-Kronenhof	84
3.4.2 Significance of the lag coefficient between Kehl-Kronenhof and Lobith	86
3.4.3 Comments on the lag coefficient between Kehl-Kronenhof and Lobith	91
3.4.4 Comments on the dispersion coefficient between Kehl-Kronenhof and Lobith	100
3.4.5 The lag coefficient in the Dutch Rhine-branches	107
4 Dead-zone model	
4.1 Introduction	129
4.2 Mass transfer between the main stream and the dead zone	132
4.3 Numerical approach	
4.3.1 Theoretical description	135
4.3.2 Dimensional analysis	142
	vii

4.3.3	Initial behaviour of the transport velocity in a river without dead zones	145
4.3.4	Initial behaviour of the transport velocity in a river with one single dead-zone parameter	155
4.3.5	The transport velocity in a river with a variable dead-zone parameter	180
4.3.6	Conclusions	197
4.4	The Dutch branches of the River Rhine	
4.4.1	General	200
4.4.2	Transport velocity and the dead-zone parameter	206
4.4.3	Mass-transfer coefficient	224
4.4.4	Conclusions	232
5	Transport velocity in case of a release at a river bank	
5.1	Introduction	235
5.2	Comparison of experimental data with computational results	237
5.3	Practical application	246
6.	Conclusions and recommendations	251
	List of symbols	259
	References	265
	Acknowledgements	269
	Curriculum vitae	271
	Appendices	
A	Linear spreading method	275
B	Influence of islands on the lag coefficient	281
C	Determination of the lag coefficient and the longitudinal dispersion- coefficient in the Rhine Alarm-Model	287
D	Derivation of the convolution integral	297
E	Transport velocity related to the peak concentration after the Chatwin-model	307

Chapter 1

INTRODUCTION

In 1986 during a fire at the Sandoz plant in Schweizerhalle (Switzerland), large quantities of chemicals were washed into the River Rhine with the fire extinguishing water. The chemicals caused considerable damage of the ecosystem and led to limitation of the water use by the waterworks. An analysis of this incident proved the inadequacy of the means which were at that time available for predicting the transport of a pollution cloud in the River Rhine. Consequently the ministers of the Rhine riparian states concerned took the decision in 1988 to charge the International Rhine Commission (IRC) and the international Commission for the Hydrology of the Rhine basin (CHR) with the assignment to develop among others a model, which would enable reliable forecasting of the travel time and concentration distribution of contaminants in the River Rhine.

This 'Rhine Alarm-Model' had to fulfil the following prerequisites:

- The model should be ready to be used operationally in cases of accidental spills, i.e. the results must be available promptly.
- The model must be based on input data that can be provided real-time. These data are information concerning the accident and the water-level data, which can be obtained from the measuring stations by telemetering transmission.
- The model design should be as simple as possible and it should be suitable to be implemented on PC's, so that it can be used without difficulty.

On the basis of these prerequisites and because it was realized that in case of an accident the quantitative information on the spill is very uncertain, a one-dimensional transport model was developed, based on the advection-diffusion-equation. The assumptions in such models are

- only longitudinal dispersion occurs;
- directly after the spill and downstream of transversal inflow the contaminant is completely mixed over the cross-sectional area of the river;
- the flow conditions are steady;
- the decomposition of the pollutant, if occurring at all, only takes place linearly.

The travel times in the model are based on the mean flow-velocity, which is a function of the water level or river discharge. By introducing a *lag coefficient* into the model representing the difference between the one-dimensional mean flow-velocity and the actual transport velocity of a pollutant, the travel times could be adapted by calibration of this lag coefficient.

As a matter of fact by applying this coefficient two-dimensional transport phenomena can be incorporated into the one-dimensional transport model:

- * the influence of the flow-velocity profile over the river cross-section in case of an incompletely mixed situation of the pollutant over the cross section;
- * the influence of dead zones along the bottom and sides of the river, where the flow is nearly stagnant: due to a temporary entrapment of portions of the pollutant in these dead zones the transport velocity of a pollution cloud is reduced.

However, the results of a calibration of the lag coefficient do not show the influence of these two-dimensional aspects on the one-dimensional approach of the transport of contaminants only, but will also give insight into what extent the mean flow-velocity along the river has been modelled correctly.

This study presents an analysis of the lag coefficient in the one-dimensional Rhine Alarm-Model. Based on this analysis proposals are made for improvements of the Rhine Alarm-Model concerning the forecasting of the travel time of a spill. These improvements will also focus on the general implementation of the set-up of the model for other rivers with comparable bathymetry.

The results of the calibration of the longitudinal dispersion-coefficient have not been examined explicitly. The decomposition of the pollutant does not belong to the scope of the study.

Chapter 2

MATHEMATICAL DESCRIPTION

2.1 GENERAL

Transport of dissolved matter in open channels is determined by the flow pattern of the channel. This transport can be described by two simultaneous transport phenomena:

- the substance is transported by the flow velocity: *convective transport* and
- the substance is spread over the depth and the width (cross-sectional area) of the river and in the longitudinal direction, caused by turbulence and the non-uniformity of the flow-velocity profile over the cross-sectional area: *dispersive transport*.

For description of the transport of soluble conservative substances in rivers in terms of concentrations (φ) as a function of time (t) and place (x, y) the balance of mass for a column of water with a depth a and horizontal dimensions dx and dy is considered (Fig. 2.1.1). It holds that the change of the concentration per unit of time is in balance with the gradients in transport (flux) in the x - and y -directions.

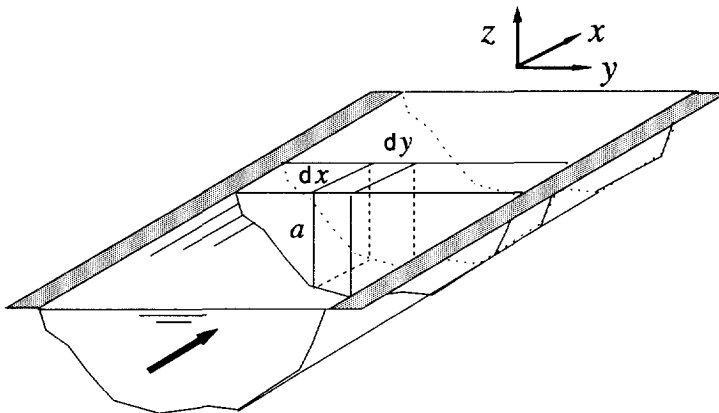


Fig. 2.1.1

Definition sketch

Expressing the transport (flux) in a convective and a dispersive part, while the dispersive transport is approached by the gradient-type (according to Taylor, 1953, 1954) and the convective transport in the transversal direction is neglected, the following convection-dispersion equation is found

$$\frac{\partial \varphi}{\partial t} + u_s \frac{\partial \varphi}{\partial x} - K_x \frac{\partial^2 \varphi}{\partial x^2} - K_y \frac{\partial^2 \varphi}{\partial y^2} = 0 \quad (2.1.1)$$

if the dispersion coefficients K_x and K_y are independent of x and y respectively, while u_s is the mean flow-velocity. In a similar way the one-dimensional description can be derived

$$\frac{\partial \bar{\varphi}}{\partial t} + u_s \frac{\partial \bar{\varphi}}{\partial x} - K \frac{\partial^2 \bar{\varphi}}{\partial x^2} = 0 \quad (2.1.2)$$

Herein stands K for the one-dimensional longitudinal dispersion-coefficient. The over-bar means averaging over the cross-sectional area of the river.

In rivers the release of a substance mostly takes place at the river bank. In these cases there are three mixing phases to be distinguished (Fig. 2.1.2):

- a first phase in which vertical mixing is predominant: the *vertical mixing reach*;
- the second phase in which transversal mixing over the cross-sectional area of the river is predominant: the *transverse mixing reach* and
- the third phase in which longitudinal mixing is predominant for the distribution of the concentration of a released substance: the *longitudinal mixing reach*.

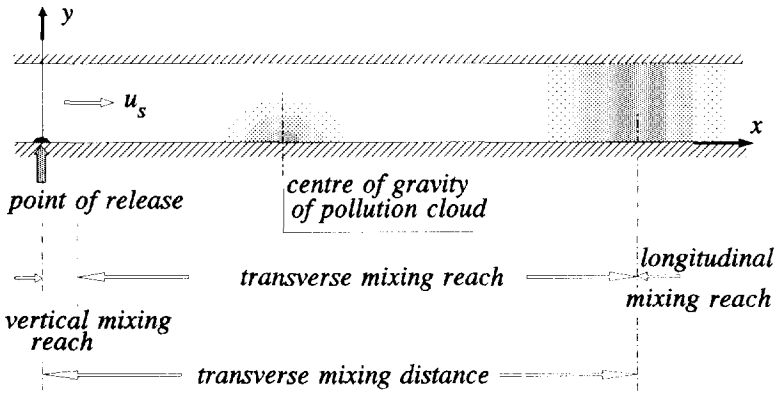


Fig. 2.1.2 Schematic presentation of the phases in the mixing phenomena in a river in case of an instantaneous release

In small and fast streaming brooks vertical and transversal mixing take place so quickly, that it is acceptable to assume a completely mixed situation from the point of release and the one-dimensional model (Eq. 2.1.2) is applicable.

In rivers with a large width/depth ratio (more than 20, as it is in the River Rhine) the distance over which the vertical mixing has become complete, is still relatively short (about 60 till 100 times the average water-depth). In such situations Eq. (2.1.1) gives a reasonable description of the transport phenomena.

For the determination of the distance over which complete mixing takes place, a constant release of a conservative substance (W) from a river bank is considered. By neglecting the longitudinal dispersive transport compared to the transversal one, the following dimensionless solution of Eq.(2.1.1) is found (van Mazijk, 1984)

$$\frac{\varphi(x',y')}{\varphi_0} = \frac{1}{\sqrt{\pi \cdot x'}} \cdot \sum_{n=-\infty}^{n=\infty} \left(\exp \left[- \frac{(y' - 2n)^2}{4 \cdot x'} \right] \right) \quad (2.1.3)$$

wherein

x'	=	$x \cdot K_y / u_s \cdot B^2$
y'	=	y/B
φ_0	=	W/Q
Q	=	river discharge
B	=	river width

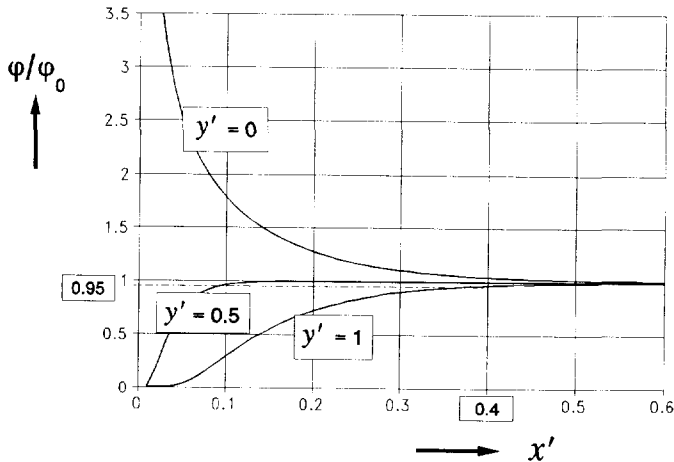


Fig. 2.1.3 Distribution of φ/φ_0 as a function of x' and y' (constant release of a conservative substance at $y' = 0$)

If the released substance is degradable and the decomposition process is linear with a decay coefficient k , Eq.(2.1.3) has to be multiplied with

$$\exp \left(-k \cdot \frac{x}{u_s} \right)$$

In Fig. 2.1.3 the dimensionless concentration $\varphi(x',y')/\varphi_0$ is presented as a function of the dimensionless distance x' for some dimensionless positions in the cross section (y').

If the completely mixed situation is defined by $\varphi/\varphi_0 \geq 0.95$ for $y' = 1$, then the 'transverse mixing distance' $x = L_m$ can be derived from Fig. 2.1.3, being the distance over which the released substance is completely mixed over the cross section. Because the corresponding dimensionless $x' = 0.4$, the transverse mixing distance is

$$L_m \approx 0.4 \cdot \frac{u_s \cdot B^2}{K_y} \quad (2.1.4)$$

This holds also for degradable substances. However in case of a large decay coefficient (k) the concentrations can become so small within the transverse mixing distance, that the variations over the cross section cannot be measured. Even complete disappearance of the substance is possible, which could suggest a smaller transverse mixing distance than the theoretical one ($x' = 0.4$).

Because an instantaneous release of soluble substances shows the same phases in the dispersion phenomena, the transverse mixing distance suits also for these types of releases. It has to be applied for the centre of gravity of the 'cloud'. When after the 'transverse mixing distance'-theory the completely mixed situation is attained, this holds for the whole 'cloud'.

For the transversal dispersion-coefficient K_y , Fischer et al (1979) give the semi-empirical expression

$$K_y = \alpha_y \cdot a \cdot u_* \quad \text{with} \quad \alpha_y = 0.15 \quad (2.1.5)$$

with

a	=	water depth
u_*	=	shear velocity $u_* = \sqrt{(g a i_b)} = u_s \sqrt{(g)/C}$
i_b	=	mean slope of bottom
g	=	acceleration due to gravity
C	=	Chézy-coefficient

As a consequence of the transversal flow caused by variations of the bottom profile and the helicoidal flow in bends and because of additional turbulence caused by

irregularities of the river banks a larger number has to be used for the factor α_y in Eq.(2.1.5). For natural streams Fischer et al (1979) suggest $\alpha_y = 0.3$ to 0.9 with a mean value of 0.6 .

For a reliable estimate of the transverse mixing distance of a certain river the α_y -factor (Eq.2.1.5) should be determined by a tracer experiment. In Table 2.1.1 some data are presented for the branches of the River Rhine.

Table 2.1.1 α_y -factor for the River Rhine

RIVER	α_y -factor	bends	groynes	REFERENCE
Waal (Rhine branch)	0.3 to 0.55	no	yes	Holley (1971,1973)
IJssel (Rhine branch)	0.35 to 0.65	yes	partly	Holley (1971, 1973)
Rhine between Ruhrort and the German-Dutch border	0.54 to 0.81	yes	yes	van Mazijk (1987)

For the one-dimensional longitudinal dispersion-coefficient K Fischer et al (1979) give the following semi-empirical expression

$$K = 0.011 \frac{u_s^2 \cdot B^2}{a \cdot u_*} \quad (2.1.6)$$

Based on measurements in natural streams Fischer et al (1979) conclude that the actual dispersion-coefficient can be 4 times larger or smaller than the one calculated by Eq.(2.1.6). Therefore when Eq.(2.1.6) is used in transport models, the factor 0.011 in Eq.(2.1.6) is replaced by a coefficient α_x , which has to be calibrated by tracer experiments

$$K = \alpha_x \frac{u_s^2 \cdot B^2}{a \cdot u_*} \quad (2.1.7)$$

For the River Rhine transverse mixing distances between 50 and 100 km are found by Eq.(2.1.4), considering the following averaged values:

$$\begin{aligned} a &= 5 \text{ m} \\ u_* &= 1 \text{ m/s} \\ B &= 150 \text{ to } 200 \text{ m} \\ C &= 50 \text{ m}^{1/2}/\text{s} \\ \alpha_y &= 0.6 \end{aligned}$$

This means that for a good description of the transport phenomena in this river a two-dimensional description is necessary.

However, in case an instantaneous spill of a pollutant takes place by accident, detailed information about the duration and magnitude of the spill and the hydrological conditions in the river itself are mostly not available, the one-dimensional description after Eq.(2.1.2) is used for the prediction of the arrival time and the maximum concentration along the river. This means that a completely mixed situation over the cross-sectional area of the river at the point of release is assumed c.q. the transverse mixing distance is not taken into account.

For a river with a constant discharge Q with a more or less constant cross-sectional area A , the solution of Eq.(2.1.2) for an instantaneous spill M of a conservative substance is given by

$$\bar{\varphi}(x,t) = \frac{M/A}{\sqrt{4 \cdot \pi \cdot K \cdot t}} \exp \left[- \frac{(x - u_s \cdot t)^2}{4 \cdot K \cdot t} \right] \quad (2.1.8)$$

In Fig. 2.1.4 a presentation of the concentration distribution after Eq.(2.1.8) is given for three moments. The location of the peak concentration is determined by the time t and the mean flow velocity u_s . The dispersion coefficient and the time determine the spreading of the substance in the longitudinal direction and hence the arrival time of the front of the pollutant.

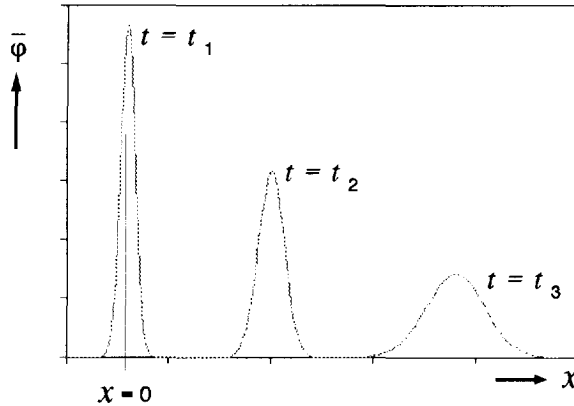


Fig. 2.1.4 Concentration distributions after the *Taylor-model*

The mixing processes in rivers by application of this one-dimensional *Taylor-model* are supposed to be represented by the longitudinal dispersion-coefficient K .

Applying the Taylor-model for the prediction of the arrival time of a pollutant, it has to be realised that within the transverse mixing distance the pollutant is partly spread over the cross-sectional area of the river and the transport velocity c of the pollutant is related to the flow velocity over this part of the cross section. Hence the transport velocity differs from the mean flow-velocity u_s , which is used by the one-dimensional description. In case of a release at the river bank the transport velocity c will be smaller than the mean flow-velocity u_s as long as the substance is spread over half the width of the river (Fig. 2.1.5). The same effects occur downstream of tributaries (Fig. 2.1.6).

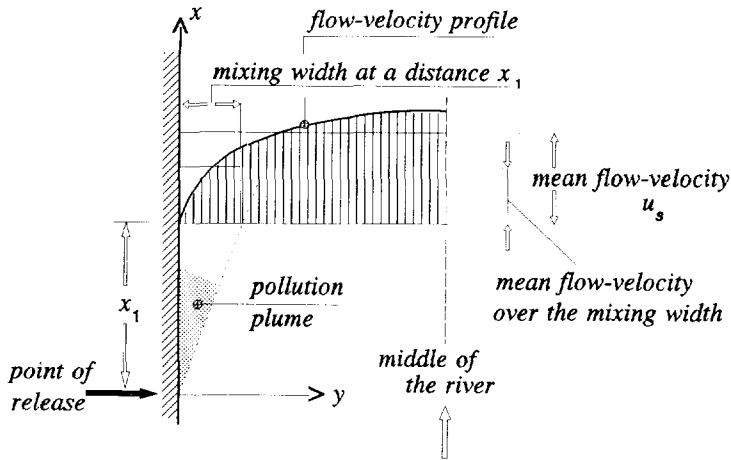


Fig. 2.1.5 Schematic presentation of the difference between the transport velocity and the mean flow-velocity in case of a continuous release at a river bank

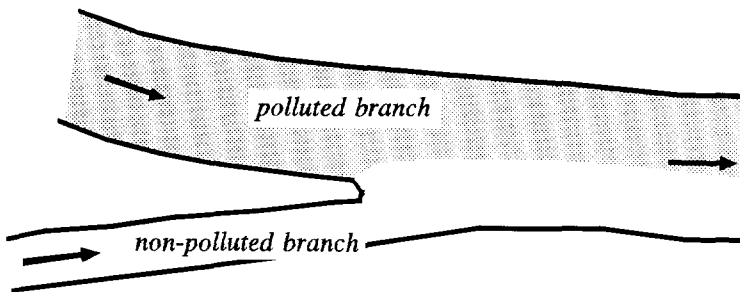


Fig. 2.1.6 Confluence of a polluted main-stream and a non-polluted tributary

The difference between the transport velocity (c) and the mean flow-velocity (u_s) can be taken into account by introducing into the one-dimensional description the *lag coefficient* β after Eq.(2.1.9)

$$c = \frac{u_s}{1 + \beta} \quad (2.1.9)$$

Thus in Eq.(2.1.8) the flow velocity u_s is replaced by the transport velocity c after

$$\bar{\varphi}(x,t) = \frac{M/A}{\sqrt{4 \cdot \pi \cdot K \cdot t}} \exp \left[- \frac{(x - c \cdot t)^2}{4 \cdot K \cdot t} \right] \quad (2.1.10)$$

Starting from the point of a completely mixed situation (longitudinal mixing reach) the one-dimensional description should be correct. However, the prediction of the concentration distribution in the time domain by the Taylor-model can still deviate from observed distributions (Fig. 2.1.7):

- the distribution is skew;
- the arrival time of the pollutant at a certain distance $x = L$ from the point of release, related to the centroid of the concentration distribution in the time domain is not equal to the travel time based on the mean flow-velocity, e.g. equal to L/u_s .

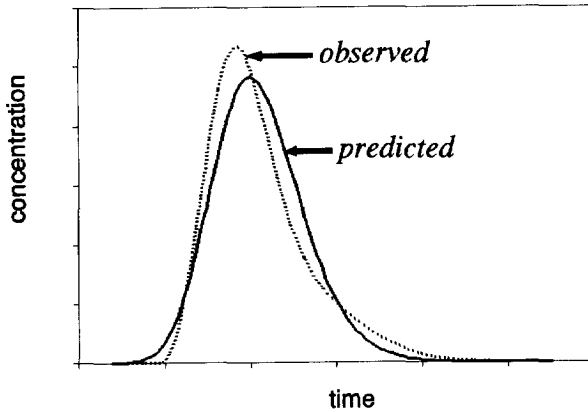


Fig. 2.1.7 Characteristic difference between observed and predicted distributions (Thackston and Schnelle, 1970)

These differences are mainly caused by the exchange of the pollutant between the main stream and the dead zones of the river, being parts of the cross section

without a net flow, like zones between groynes (Hays et al., 1966) or small regions along the bottom and sides of the river due to irregularities, where the flow is nearly stagnant (Fig. 2.1.8).

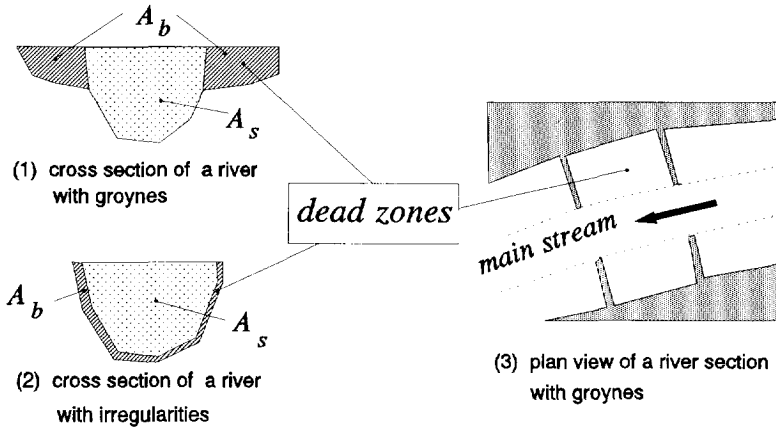


Fig. 2.1.8 Natural and artificial dead-zones in rivers

In the one-dimensional approach the flow-velocity distribution in a river with dead zones can be schematized by a slow-moving zone with a net flow equal to zero and a fast-moving zone, representing the main stream (Reichert and Wanner, 1991). The difference between the transport velocity of a pollutant in the main stream (c) and the mean flow-velocity in the main stream (u_s) is again given by Eq.(2.1.9). In this case the lag coefficient is called the 'dead-zone' parameter and defined by

$$\beta = \frac{A_b}{A_s} \quad (2.1.11)$$

with A_s = cross-sectional area of the main stream
 A_b = cross-sectional area of the dead zone

This means that the two-dimensional aspects of the transport velocity, concerning

- the incomplete spreading of a pollutant over the river cross-section in relation to the cross-sectional flow-velocity profile, and
- the exchange of pollutant between the main stream and the dead zones of a river

can be represented in the one-dimensional Taylor-model by a lag coefficient β .

For a good reconstruction of the skewness of the concentration distribution the Edgeworth series can be applied (Chatwin 1980). Considering only the first term of the series, in Sub-section 2.2.2 it will be shown that Eq.(2.1.8) transforms for a

fixed point $x = L$ into

$$\bar{\varphi}(L, t) = \frac{M/A}{\sqrt{4 \cdot \pi \cdot K \cdot t}} \cdot \exp \left[- \frac{(L - c \cdot t)^2}{4 \cdot K \cdot t} \right] * \left[1 - \frac{G_t}{6} \cdot H_3 \left(\frac{L - c \cdot t}{\sqrt{2 \cdot K \cdot t}} \right) \right] \quad (2.1.12)$$

in which $A = A_s + A_b$.

The skewness of the concentration distribution is represented by the Hermite polynomial $H_3[z] = z^3 - 3z$ with the skewness coefficient G_t . For a good reconstruction of the concentration distribution G_t should not be much more than unity.

Because Eq.(2.1.12) is based on the application of the Edgeworth series by Chatwin (1980), this model will be denoted further on as the *Chatwin-model*.

2.2 TRANSVERSE MIXING REACH

2.2.1 Release at a river bank

For the application of the one-dimensional Taylor-model after Eq.(2.1.10) or the one-dimensional Chatwin-model over the transverse mixing distance after Eq. (2.1.12) the lag coefficient has to be determined.

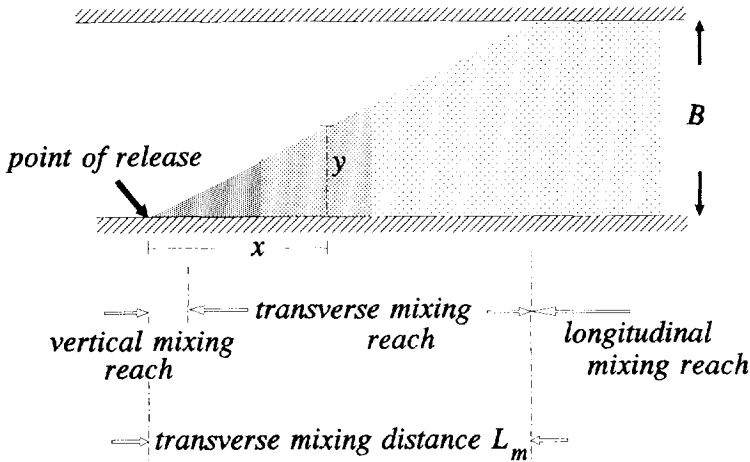


Fig. 2.2.1 The three mixing phases for a continuous release at a river bank

Two different analytical methods are considered:

- The first is called the '*linear-spreading method*'. This method assumes a linear increase of the 'spreading width' of the pollutant with the distance from the point of release (Fig. 2.2.1). The distance of the completely mixed situation over the whole cross-sectional area of the river is given by Eq. (2.1.4). Over the 'spreading width' a completely mixed situation is assumed (Fig. 2.2.3).
- The second one is called the '*flux method*'. This method assumes a specific concentration profile over the width depending of the distance from the point of release after Eq.(2.1.3).

For the determination of the lag coefficient in both cases the same exponential velocity-profile is used, with a variable n after Eq.(2.2.1).

It yields for $y \leq 0.5 B$

$$u(y) = \frac{n+1}{n} \cdot \left(\frac{y}{0.5B} \right)^{\frac{1}{n}} \cdot u_s \quad (2.2.1)$$

and for $0.5 B < y < B$

$$u(y) = \frac{n+1}{n} \cdot \left(\frac{B-y}{0.5B} \right)^{\frac{1}{n}} \cdot u_s \quad (2.2.2)$$

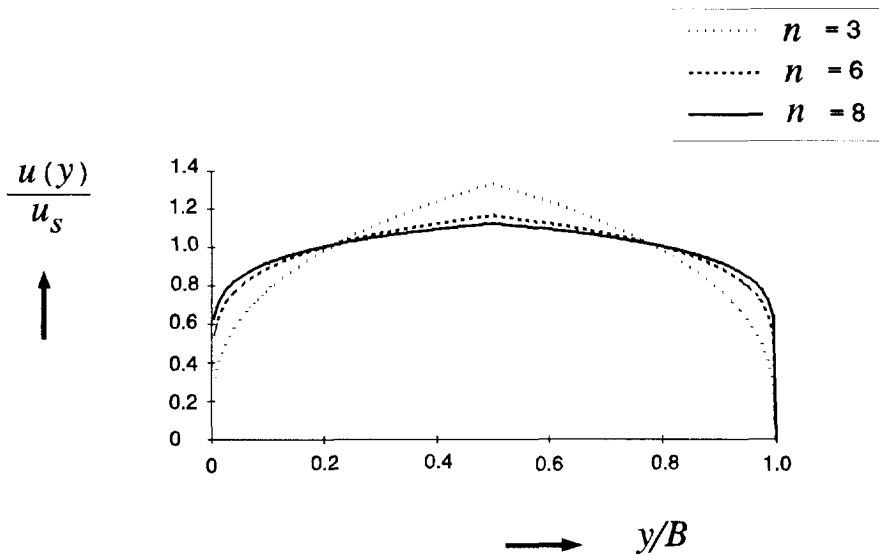


Fig. 2.2.2 Exponential velocity-profile

linear-spreading method

flux method

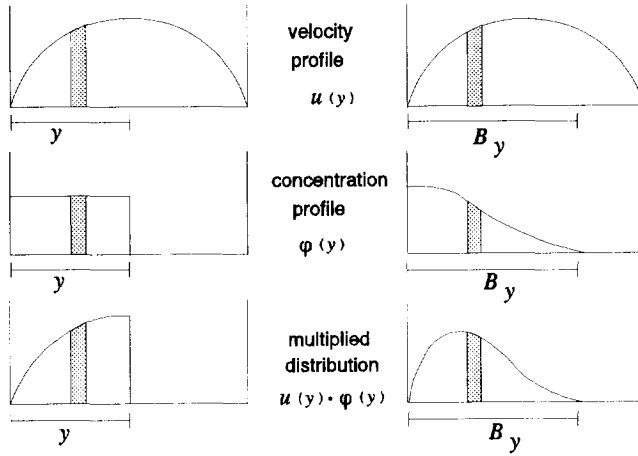


Fig. 2.2.3 The two different analytical methods

In practice the transport velocity c is determined by measuring the travel time T of the pollution over a certain distance x_0

$$c = \frac{x_0}{T} \quad (2.2.3)$$

This means that the local travel-time T_c per unit of distance is given by ($x_0 \Rightarrow 1$)

$$T_c = \frac{1}{c} \quad (2.2.4)$$

in which T_c is the travel time in seconds per meter, if the dimension of the transport velocity c is given in m/s.

Linear-spreading method

In case of the linear increase of the 'spreading width' with the distance (see Fig. 2.2.1) the travel time T_c at a certain distance x is assumed to be equal to the mean travel time over the spreading width y defined by (see also Appendix A)

$$T_c(x) = \frac{1}{c(x)} = \overline{\left(\frac{1}{u(y)} \right)} = \frac{1}{y} \int_0^y \frac{1}{u(\psi)} d\psi \quad (2.2.5)$$

with

$$y = \frac{x}{L_m} \cdot B \quad (2.2.6)$$

Substitution of Eqs (2.2.1) and (2.2.6) into Eq.(2.2.5) the integration of Eq. (2.2.5), applying the dimensionless distance $X = x/L_m$ gives for $X \leq 0.5$

$$T_c(X) = \frac{1}{c(X)} = \frac{n^2}{n^2 - 1} \cdot (2 \cdot X)^{-\frac{1}{n}} \cdot \frac{1}{u_s} \quad (2.2.7)$$

In a similar way the travel time for values of $X > 0.5$ can be derived (Appendix A)

$$T_c(X) = \frac{1}{c(X)} = \frac{n^2}{n^2 - 1} \cdot \frac{1}{2X} \cdot \left[2 - (2 - 2 \cdot X)^{\frac{n-1}{n}} \right] \cdot \frac{1}{u_s} \quad (2.2.8)$$

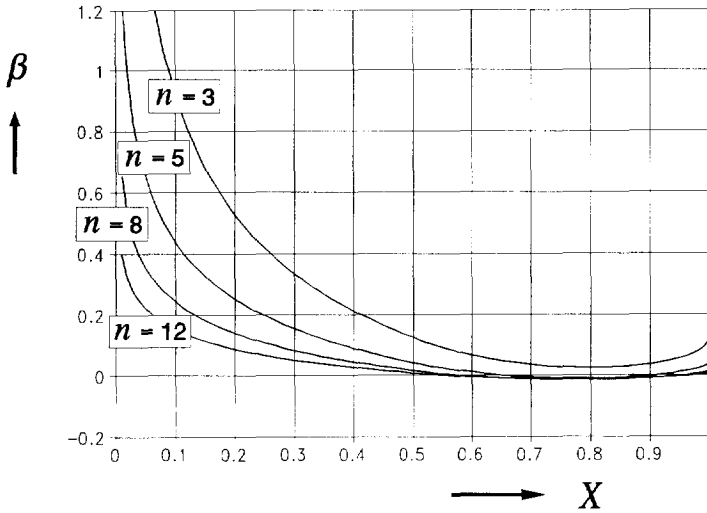


Fig. 2.2.4 Effect of the flow-velocity profile on the transport velocity for a number of n -values after Eqs (2.2.1) and (2.2.2)

The lag coefficient β as a function of the dimensionless distance X over the transverse mixing distance L_m can now be given by substitution of the Eqs (2.2.7)

and (2.2.8) into Eq.(2.1.9)

for $y \leq 0.5 B$

$$\beta(X) = \frac{u_s}{c(X)} - 1 = \frac{n^2}{n^2 - 1} \cdot (2 \cdot X)^{-\frac{1}{n}} - 1 \quad (2.2.9)$$

and for $0.5 B < y < B$

$$\beta(X) = \frac{n^2}{n^2 - 1} \cdot \frac{1}{2X} \cdot \left[2 - (2 - 2 \cdot X)^{\frac{n-1}{n}} \right] - 1 \quad (2.2.10)$$

In Fig. 2.2.4 the relations after Eqs (2.2.9) and (2.2.10) are presented graphically. It is shown that after the linear-spreading method the lag coefficient is positive up to half the transverse mixing distance. For distances larger than half the transverse mixing distance the lag coefficient becomes negative with a minimum value of -0.015 for $n = 8$. In rivers the n -value is about 8 to 12, so that the negative lag-coefficient can be neglected, since for practical applications lag coefficients smaller than 0.05 lie within the accuracy of measured transport-velocities.

In the Taylor-model as well as in the Chatwin-model the flow-velocity is assumed to be constant over the river reach concerned. Therefore an overall value of the lag coefficient over this reach has to be determined. The overall value over the distance X from the point of release is found by averaging the 'local' value given by Eqs (2.2.9) and (2.2.10) over this distance (see also Appendix A).

It yields for $X \leq 0.5$

$$\overline{\beta(X)} = \frac{1}{X} \int_0^X \left[\frac{n^2}{n^2 - 1} \cdot (2 \cdot \xi)^{-\frac{1}{n}} - 1 \right] d\xi \quad (2.2.11)$$

and for $0.5 < X < 1$

$$\overline{\beta(X)} = \frac{1}{X} \int_0^X \left[\frac{n^2}{n^2 - 1} \cdot \frac{1}{2\xi} \cdot \left(2 - (2 - 2 \cdot \xi)^{\frac{n-1}{n}} \right) - 1 \right] d\xi \quad (2.2.12)$$

Figure 2.2.5 shows the graphical presentation of the numerical evaluation of these equations for $n = 10$. The overall lag-coefficient is about 0.06 over the transverse

mixing distance L_m . For distances $X < 0.2$ the overall value is more than 0.20. In the River Rhine with L_m -values of more than 50 km the influence of the non-uniformity of the velocity profile over the river cross-section is significant for the transport velocity of a pollutant, released at the river bank.

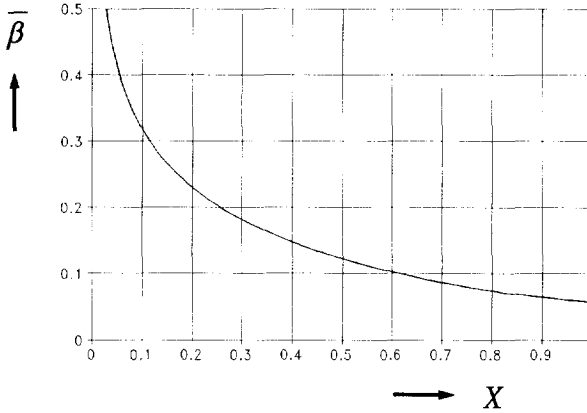


Fig. 2.2.5 Distribution of the overall value of the lag coefficient with the distance from the point of release for $n = 10$

Flux method

In the flux method the average travel-time of a pollution is related to the mass transport (flux)

$$F(x,y) = u(y) \cdot \varphi(x,y) \quad (2.2.13)$$

Thus the definition of the average travel-time becomes

$$T_c(x) = \frac{\int T_c(x,y) \cdot F(x,y) \, dy}{\int F(x,y) \, dy} \quad (2.2.14)$$

Substitution of Eqs (2.2.5) and (2.2.13) into Eq.(2.2.14) gives

$$T_c(x) = \frac{1}{c(x)} = \frac{\int \varphi(x,y) \, dy}{\int u(y) \cdot \varphi(x,y) \, dy} \quad (2.2.15)$$

Applying the dimensionless expression for the concentration contribution after Eq.(2.1.3) the inverse mean-value of the transport velocity of the pollution cloud

becomes

$$\frac{1}{c(x')} = \frac{\int_0^{B_{y'}} \frac{\varphi(x', y')}{\varphi_0} dy'}{\int_0^{B_{y'}} u(y') \cdot \frac{\varphi(x', y')}{\varphi_0} dy'} \quad (2.2.16)$$

wherein $B_{y'}$ is the dimensionless width over which the pollutant has been spread ($= B_y / B$), defined by $\varphi(x, y) / \varphi_0 \geq 0.01$ (see Fig. 2.2.3).

Therefore the distribution of the lag coefficient β after Eq.(2.1.9) as a function of the dimensionless distance x' can be described by, using the exponential velocity distribution after Eqs (2.2.1) and (2.2.2)

for $0 < y' \leq 0.5$

$$\beta(x') = \frac{\int_0^{B_{y'}} \frac{\varphi(x', y')}{\varphi_0} dy'}{\int_0^{B_{y'}} \frac{n+1}{n} \cdot (2 \cdot y')^{\frac{1}{n}} \cdot \frac{\varphi(x', y')}{\varphi_0} dy'} - 1 \quad (2.2.17)$$

for $0.5 < y' \leq 1$

$$\beta(x') = \frac{\int_0^{B_{y'}} \frac{\varphi(x', y')}{\varphi_0} dy'}{\int_0^{B_{y'}} \frac{n+1}{n} \cdot (2 - 2 \cdot y')^{\frac{1}{n}} \cdot \frac{\varphi(x', y')}{\varphi_0} dy'} - 1 \quad (2.2.18)$$

The relation between the dimensionless distances x' and X is given by

$$x' = 0.4 \cdot X \quad (2.2.19)$$

The determination of the lag coefficient after Eqs (2.2.17) and (2.2.18) is executed numerically, because no analytical solution as for the *linear-spreading method* can be derived.

For some n -values of the exponential velocity-distribution the results are presented in Fig. 2.2.6.

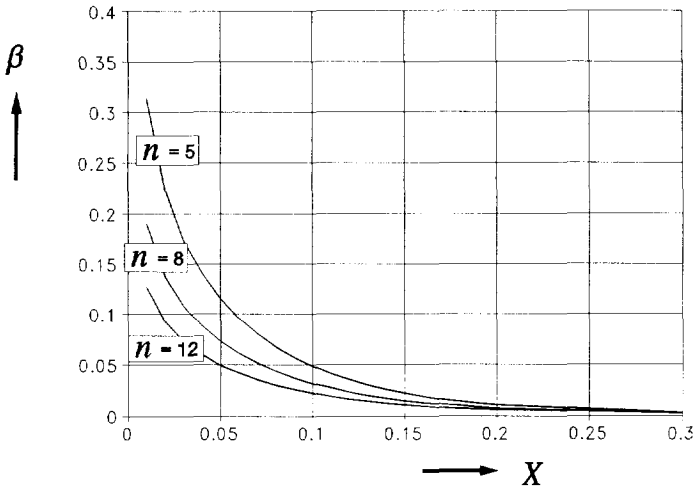


Fig. 2.2.6 Effect of the flow-velocity profile on the transport velocity for a number of n -values after Eqs (2.2.1) and (2.2.2), applying the *flux method*

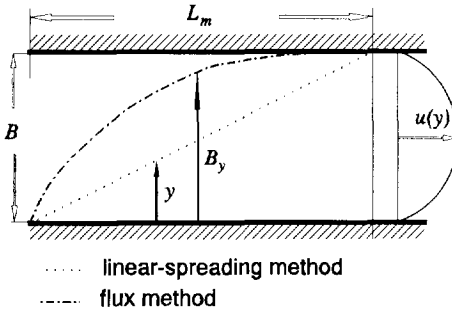


Fig. 2.2.7 Difference of the pollutant width along the river for the *linear-spreading method* and the *flux method*

The influence of the velocity distribution on the transport velocity is significant up to a distance of 0.2 of the transverse mixing distance. At this distance the value of the lag coefficient is about 0.02. The *linear-spreading method* at this distance gives higher values (see Fig. 2.2.4). The reason for these differences between the two methods is the difference in spreading of the pollutant over the width of the river. Near the point of release the pollutant is spread actually over a larger part of the river width than assumed by the *linear-spreading method* (Fig. 2.2.7),

whereas the *flux method* describes the spreading correctly. This means that at a certain location the mean flow-velocity over the spreading width (i.e. the transport

velocity of the pollutant) is smaller in case of the *linear-spreading method* than in case of the *flux method*, using the same n -value. In other words to get the same lag coefficients for both methods the n -value has to be chosen larger in case of the *linear-spreading method* than in case of the *flux method*. In Fig. 2.2.8 the distribution of the overall value of the lag coefficient after the flux method for $n = 10$ is compared with the linear-spreading method for some n -values. In order to get a certain agreement the n -values have to become much more larger than the usual values for rivers. Thus it is the extremely large n -value of 36 in case of the *linear-spreading method*, which gives a good agreement of the distribution of the lag coefficient with the distribution found by the *flux method*.

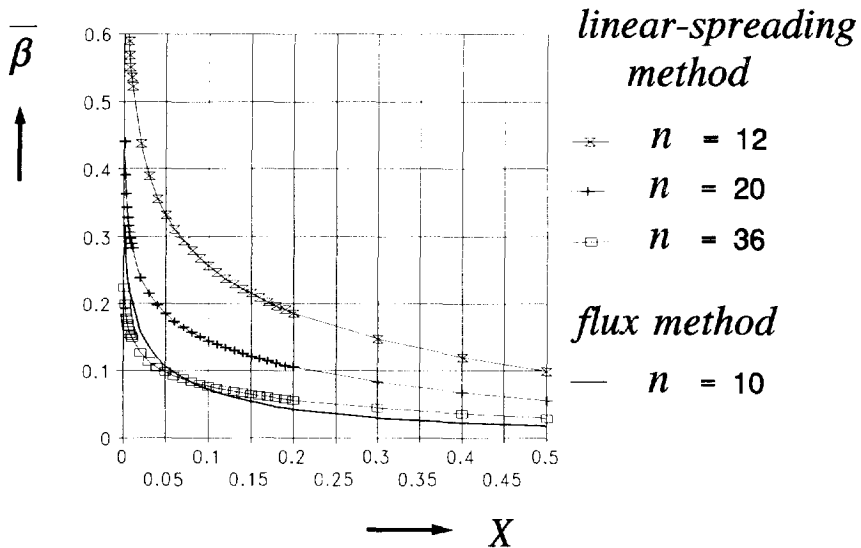


Fig. 2.2.8 Overall β -value for several n -values in case of the *linear-spreading method* in comparison with the *flux method* with $n = 10$

This means that actually the influence of the velocity profile on the transport velocity is not as much as it was found by the *linear-spreading method*. For instance in case of the *flux method* the overall value is about 0.04 at a distance of $X = 0.2$ instead of 0.20 in case of the *linear-spreading method*. However, for the River Rhine with transverse mixing distances of more than 50 km, the influence of the non-uniformity of the velocity profile over the river cross-section is still significant for the transport velocity of a pollutant, released at the river bank.

2.2.2 River confluence

In case of a river confluence also the mixing zone over the width (second phase) is important (see Fig. 2.2.9).

When upstream the concentration in the polluted river has reached an equilibrium (Noppenny, 1988) the conditions at the begin of the confluence are defined by

$$\begin{aligned} \varphi(0,y) &= 0 & \text{if } y/B > B_1/B \\ \varphi(0,y) &= (B/B_1) * W/Q & \text{if } y/B < B_1/B \end{aligned} \quad (2.2.20)$$

The final solution of the concentration distribution downstream of the river confluence is given by

$$\frac{\varphi(x',y')}{\varphi_0} = \frac{B}{2B_1} \left[\sum_{n=-\infty}^{n=\infty} \operatorname{erf} \left(\frac{y' - 2n + \frac{B_1}{B}}{2\sqrt{x'}} \right) - \sum_{n=-\infty}^{n=\infty} \operatorname{erf} \left(\frac{y' - 2n - \frac{B_1}{B}}{2\sqrt{x'}} \right) \right] \quad (2.2.21)$$

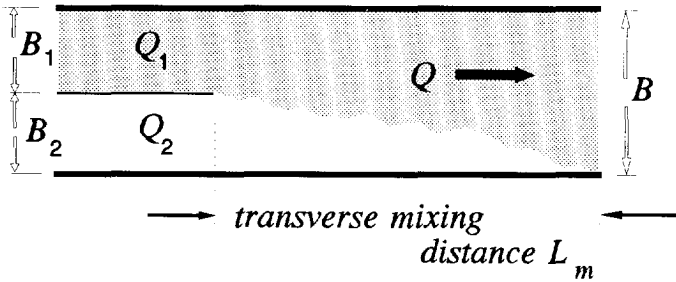


Fig. 2.2.9 Mixing at a confluence starting with a width ratio B_1/B in case of a constant release

For the determination of the distribution of the lag coefficient as a function of the distance from the point of confluence the flux method is applied. For practical use the error-function has been approached with the function (Abramowitz, 1965)

$$\operatorname{erf}(x) = 1 - \frac{1}{(1 + c_1x + c_2x^2 + c_3x^3 + c_4x^4)^4} \quad (2.2.22)$$

with

$$\begin{aligned} c_1 &\approx 0.278393 & c_3 &\approx 0.000972 \\ c_2 &\approx 0.230389 & c_4 &\approx 0.078108 \end{aligned}$$

and

$$\operatorname{erf}(-x) = -\operatorname{erf}(x)$$

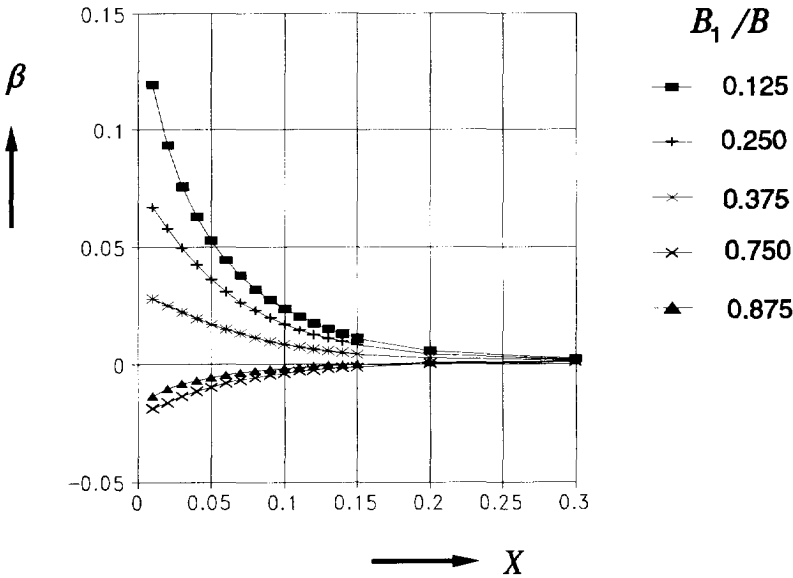


Fig. 2.2.10 The lag coefficient β downstream of a confluence for several width-ratios B_1/B after Fig. 2.2.9 with $n = 10$ in the exponential velocity-profile

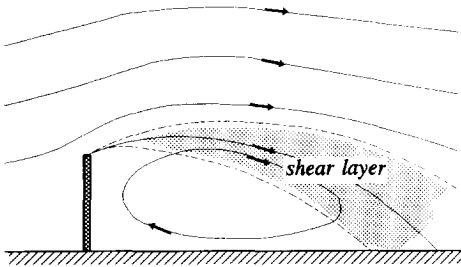


Fig. 2.2.11 Flow pattern near a groyne after Lean and Weare (1979)

In Fig. 2.2.10 the distribution of the lag coefficient is presented for several values of the width ratio B_1/B . Immediately downstream of the confluence an exponential velocity-profile after the Eqs (2.2.1) and (2.2.2) over the *total* width B is assumed.

This assumption is justified by the fact that the adaptation of the flow velocity of the tributary to the flow velocity in the main stream takes place over a relative-

ly short distance (Noppene, 1988). Noppene (1988) made this conclusion by referring to Lean and Weare (1979), who examined the turbulence generated by a shear layer due to a breakwater (Fig. 2.2.11). They stated that the shear layer mixing will dominate over that due to the bed-generated turbulence for a distance of up to 100 till 150 times the depth. This means for the River Rhine that the adaptation length will be of the order of 0.5 km.

TABLE 2.2.1 Main tributaries of the River Rhine

Tributary	Width			polluted branch		Angle of intersection
	River Rhine upstream	tributary	River Rhine downstream	River Rhine	tributary	
	(m)	(m)	(m)	B_1/B after Fig. 2.2.9		
AARE	200	150	200	1	0.75	40°
NECKAR	225	75	275	0.82	0.27	22°
MAIN	325	75	400	0.81	0.19	45°
MOSEL	250	100	300	0.83	0.33	30°

The angle of intersection of the main tributaries of the River Rhine is mostly less than 45° (see Table 2.2.1). This means that the flow patterns downstream of the confluences along the River Rhine will probably not show a separation zone after Best (1987) (Fig. 2.2.12). The inflow of the tributary will more or less stick to the

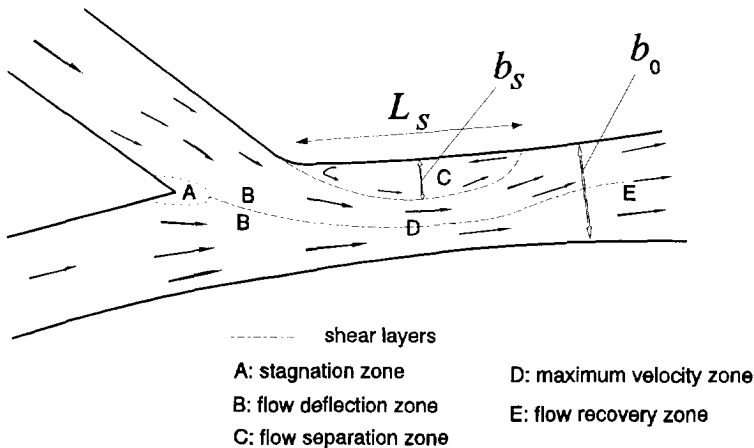


Fig. 2.2.12 A flow dynamics model for a river confluence after Best (1987)

the river bank concerned (Fig 2.2.13). Moreover, the discharge ratio of the main tributaries of the River Rhine ($Q_{tributary}/Q_{Rhine}$) is smaller than 0.25, except for the River Aare (Table 2.2.2). In those situations the main stream will push the outflow of the tributary to the river bank and suppress the growth of a separation zone. In case of the River Aare two parallel river-branches with comparable discharges are coming together (Fig. 2.2.14).

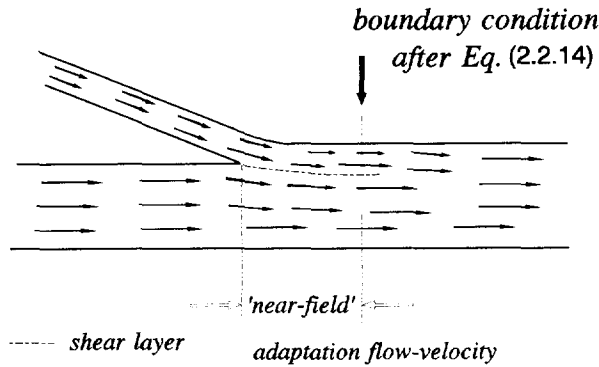


Fig. 2.2.13 Flow pattern downstream of confluences along the River Rhine

TABLE 2.2.2 Long-term mean flow of the River Rhine and its main tributaries (Buck et al., 1993)

Tributary	Tributary		River Rhine		Discharge ratio $Q_{tributary}/Q_{Rhine}$
	measuring station	Discharge (m ³ /s)	measuring station	Discharge (m ³ /s)	
AARE	Stilli	560	Basel	1100	~ 0.5
NECKAR	Rockenau	132	Worms	1400	~ 0.1
MAIN	Frankfurt	188	Mainz	1600	~ 0.1
MOSEL	Cochem	288	Andernach	2000	~ 0.15

These conclusions can also be drawn from investigations on the dimensions of the separation zone in a flume (Best and Reid, 1984). They found for discharge ratios of about 0.1 length- and width-ratios for the separation zone (L_s/b_0 and b_s/b_0 , see Fig. 2.2.12) of less than 0.05.

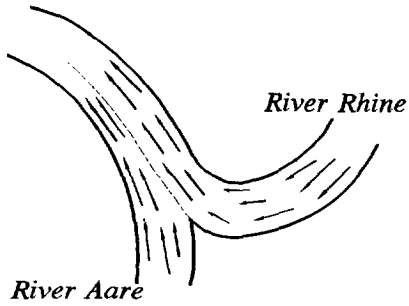


Fig. 2.2.14 Confluence of the River Aare and the River Rhine

Aerial pictures of the confluences of the River Aare and the River Mosel confirm this supposition (Fig. 2.2.15 and 2.2.16). Moreover the boundary condition after Eq.(2.2.20) appears at a short distance ('near-field') downstream of the confluence (Fig. 2.2.17) and the description of the concentration after Eq.(2.2.21), which yields for the 'far-field', is correct.

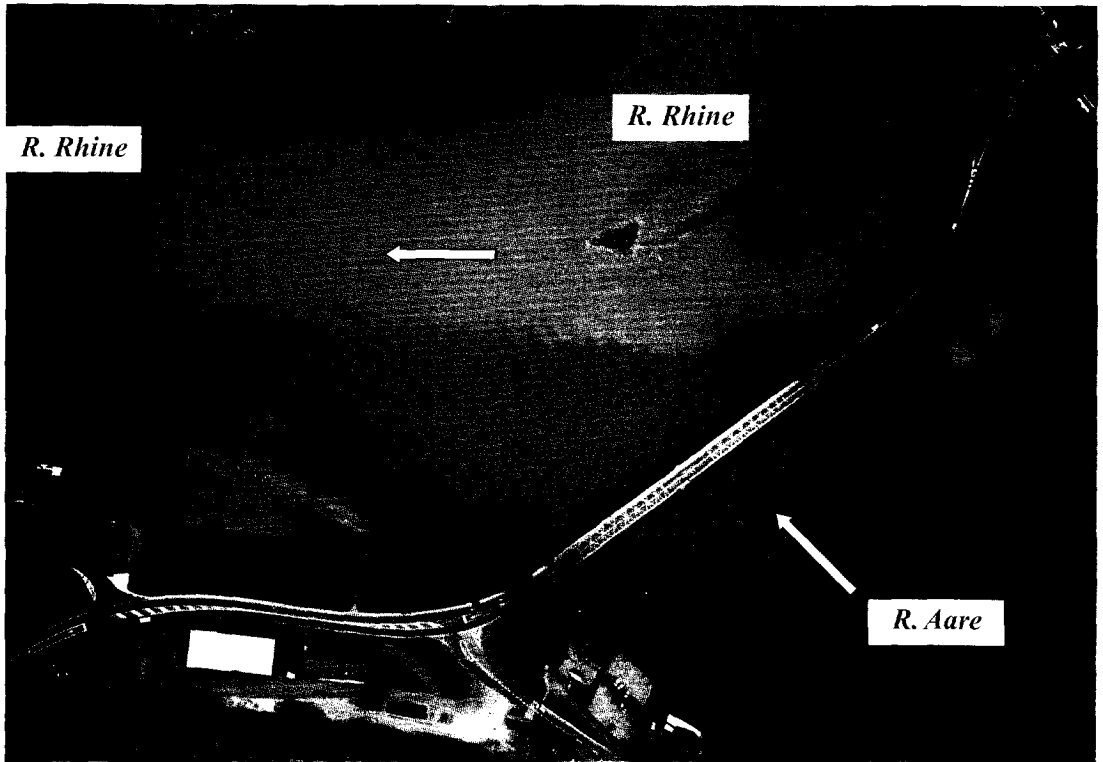


Fig. 2.2.15 Aerial view of the Rhine-Aare confluence during the tracer experiment July 1989
(photo H. Aschwanden, Landeshydrologie und -geologie, Bern, Switzerland)

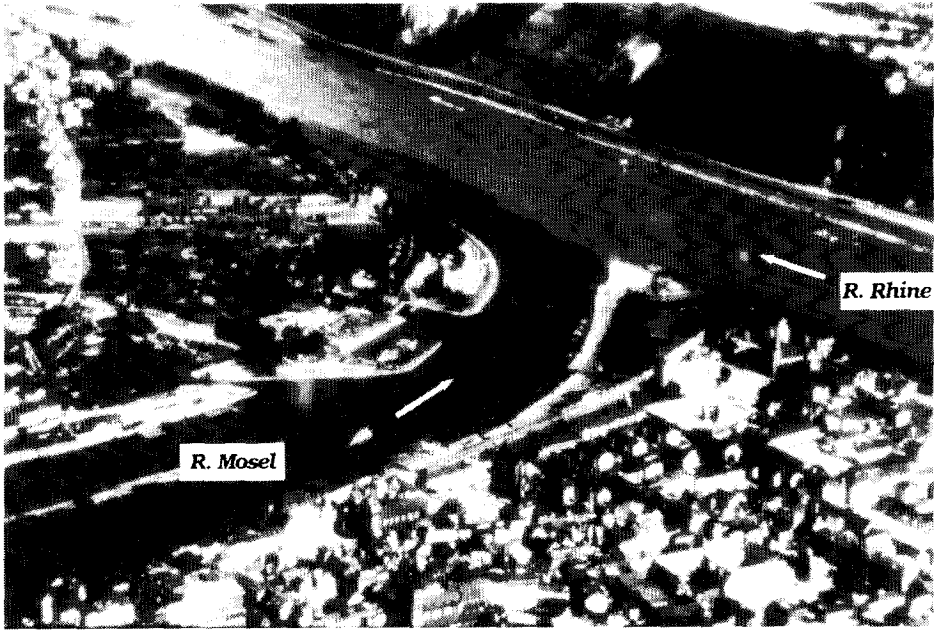


Fig. 2.2.16 Aerial view of the Rhine-Mosel confluence

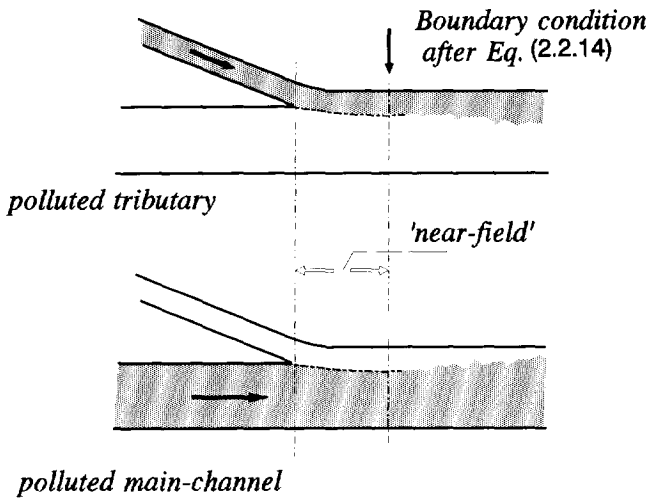


Fig. 2.2.17 Schematic presentation of the mixing at the confluences of the River Rhine

If the River Rhine is polluted, the width ratio B_1/B at the confluences of the main tributaries of the River Rhine is more than 0.8, thus the lag coefficient β after Fig. 2.2.10 will be negligibly small (less than 2%). If one of the main tributaries is polluted the width ratio is 0.20 to 0.30, except for the River Aare. In these cases the lag coefficient is about 5% or less at a dimensionless distance $X = 0.05$, which corresponds with a distance of 5 km in case of a transverse mixing distance of 100 km. Concerning the transport of a pollution cloud over long distances (more than 100 km) this might be negligible.

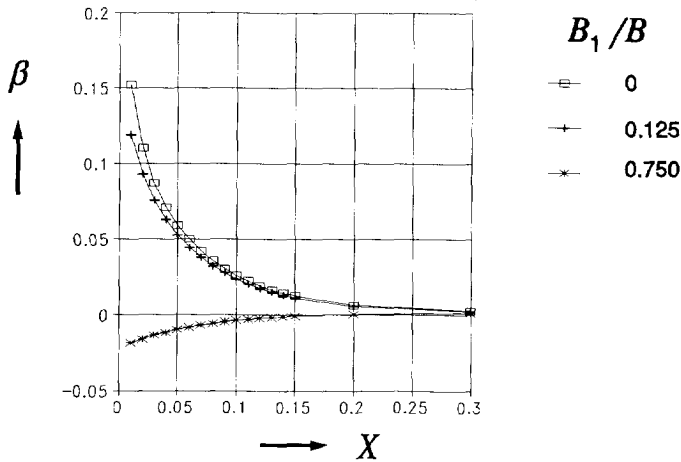


Fig. 2.2.18 Lag coefficient β for a bank release ($B_1/B = 0$) in comparison with two width ratios ($n = 10$)

In case of small tributaries with a width ratio $B_1/B < 0.05$ and a discharge ratio < 0.05 the release of a pollution by this tributary can be considered as a point release at the river bank, i.e. $B_1/B \rightarrow 0$ (Fig. 2.2.18).

2.3 LONGITUDINAL MIXING REACH

2.3.1 General

In case of a completely mixed situation over the cross-sectional area of a river the transport of a pollution cloud is influenced by the exchange of pollutant between the main stream and the 'dead zones' of the river. These dead zones are parts of the cross section without a net flow, like zones between groynes or small regions along the bottom and sides of the river due to irregularities, where the flow is nearly stagnant (see Section 2.1, Fig. 2.1.8). The exchange of the pollutant causes

a temporary entrapment of portions of the pollutant in the dead zones. Due to the delayed release of these entrapped portions, the tail of the concentration distribution is growing. This implies two effects on the concentration-time distribution:

- * the persistence of skewness of the distribution;
- * the deceleration of the transport velocity of the pollutant with respect to the time-centroid of the distribution.

As already mentioned in Section 2.1 (Eq. 2.1.9) the relationship between the transport velocity c of the time-centroid of the distribution and the mean flow-velocity u_s can be given by the *lag coefficient* β , which in this case will be called the *dead-zone parameter*

$$\beta = \frac{u_s}{c} - 1 \quad (2.3.1)$$

wherein β is defined by the ratio of the cross-sectional area of the dead zone A_b and the cross-sectional area of the main stream A_s (Thackston and Schnelle, 1970; Valentine and Wood, 1977)

$$\beta = \frac{A_b}{A_s} \quad (2.3.2)$$

In case of irregularities Thackston and Schnelle (1970) suggest an experimental relation between the dead-zone parameter β and the wall roughness f

$$\frac{\beta}{\beta + 1} = 0.0152 + 0.89 \cdot f^{2.22} \quad (2.3.3)$$

with

$$f = \frac{8 \cdot g \cdot i_b \cdot a}{u_s^2} \quad (2.3.4)$$

wherein

- g = acceleration of gravity
- i_b = slope of the energy gradient, which is equal to the bottom slope in case of uniform flow-conditions and used as a first approximation
- a = average depth

The maximum value of β , measured by Thackston and Schnelle (1970) is 0.06, which corresponds with a wall roughness f equal to 0.26.

In case of the River Rhine with $i_b = 10^{-4}$, $u_s = 1$ m/s, $a = 5$ m, a β -value of 0.016 is found, which means that after Eq.(2.3.3) the influence of the wall roughness can be neglected.

This can also be proved by determination of the influence of the flow-velocity profile on the average transport-velocity c . For the flow-velocity profile over the width of the river the exponential distribution after Eqs (2.2.1) and (2.2.2) is considered. Because of the symmetrical approximation of the velocity distribution only half the width is concerned. Therefore the β -value can be determined after Eq.(2.2.9) by

$$\beta(X) = \frac{n^2}{n^2 - 1} \cdot (2 \cdot X)^{-\frac{1}{n}} - 1 \quad (2.3.5)$$

with $X = 0.5$.

Thus the dead-zone parameter becomes

$$\beta = \frac{n^2}{n^2 - 1} - 1 \quad (2.3.6)$$

Because in rivers the value of the parameter n is approximately 10, the β -value is about 0.01, which is comparable with the result after the experimental relation of Thackston and Schnelle (1970), given by Eq.(2.3.3).

This means that in the River Rhine mainly the artificial dead-zones, made by groynes, have to be taken into account. The definition of the dead-zone parameter β after Eq.(2.3.2) assumed a completely mixed dead-zone, and in succession a transport velocity c , being the average flow-velocity over the main stream and the dead zone

$$c = \frac{u_s \cdot A_s + u_b \cdot A_b}{A_s + A_b} \quad (2.3.7)$$

Because the net flow in the dead zone u_b is equal to zero, Eq.(2.3.7) becomes

$$c = \frac{u_s \cdot A_s}{A_s + A_b} \quad (2.3.8)$$

which can be rewritten into Eq.(2.3.1) or Eq.(2.1.9).

$$c = \frac{u_s}{1 + \beta} \quad (2.3.9)$$

In case of islands in the river, two river branches can be distinguished with different lengths and mean flow-velocities without exchange of the pollutant (Fig. 2.3.1). When the concentration distribution over the cross section at the upstream

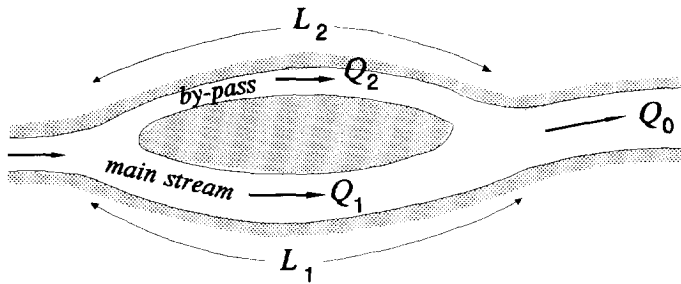


Fig. 2.3.1 Schematization of an island in a river

end of the island is assumed to be homogeneous, the mass will distribute over the branches in the same ratio as the discharges. Applying the *flux method* the average travel-time of the pollutant T_c from the upstream end of the island to the downstream end can be given by (see also Eq. 2.2.14)

$$T_c = \frac{Q_1 \cdot \frac{L_1}{u_1} + Q_2 \cdot \frac{L_2}{u_2}}{Q_1 + Q_2} \quad (2.3.10)$$

wherein

- Q = discharge of the branch
- L = length of the branch
- u = mean flow-velocity in the branch
- subscript 1: main-stream branch
- subscript 2: by-pass branch

The 'time of arrival' of the water is determined by the mean flow-velocity over the total area of the two branches (*flow time*) with a correction to counteract for the difference in length

$$T_u = \frac{L_1}{\left(\frac{u_1 \cdot A_1 + u_2 \cdot A_2 \cdot \frac{L_1}{L_2}}{A_1 + A_2} \right)} = \frac{L_1}{\left(\frac{Q_1 + Q_2 \cdot \frac{L_1}{L_2}}{\frac{Q_1}{u_1} + \frac{Q_2}{u_2}} \right)} \quad (2.3.11)$$

The lag coefficient β can be found by

$$\beta = \frac{T_c}{T_u} - 1 \quad (2.3.12)$$

Substitution of Eqs (2.3.10) and (2.3.11) into Eq.(2.3.12) yields

$$\beta = \frac{\left(1 + \frac{A_2 \cdot L_2}{A_1 \cdot L_1}\right)}{1 + \frac{Q_2}{Q_1}} \cdot \frac{\left(1 + \frac{Q_2 \cdot L_1}{Q_1 \cdot L_2}\right)}{1 + \frac{A_2}{A_1}} - 1 \quad (2.3.13)$$

Setting as a first approximation $\frac{A_2}{A_1} \approx \frac{Q_2}{Q_1} \cdot \left(\frac{L_2}{L_1}\right)^{1/2}$ Eq.(2.3.13) becomes (see also Appendix B)

$$\beta = \frac{\left(1 + \frac{Q_2}{Q_1} \cdot \left[\frac{L_2}{L_1}\right]^{1.5}\right) \cdot \left(1 + \frac{Q_2 \cdot L_1}{Q_1 \cdot L_2}\right)}{\left(1 + \frac{Q_2}{Q_1}\right) \cdot \left(1 + \frac{Q_2}{Q_1} \cdot \left[\frac{L_2}{L_1}\right]^{0.5}\right)} - 1 \quad (2.3.14)$$

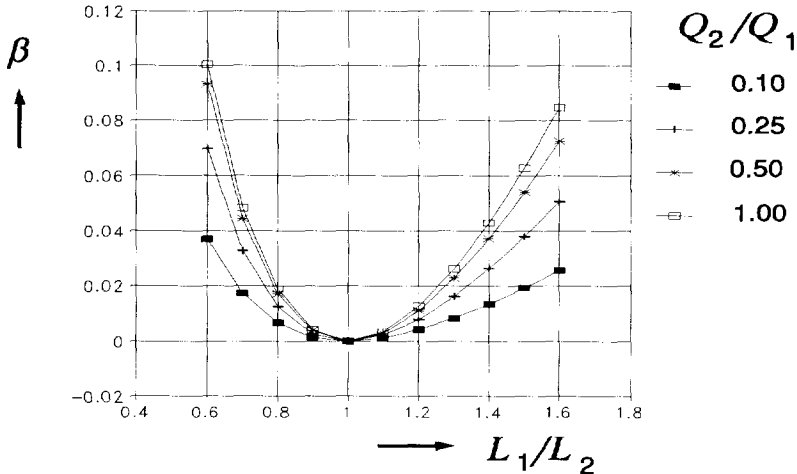


Fig. 2.3.2 Influence of the length ratio of the river branches surrounding an island on the lag coefficient β for some discharge ratios

Equation (2.3.14) is presented graphically in Fig. 2.3.2. In case the branches have the same length the travel time of the flow T_u is the same as the travel time of the pollutant T_c . Thus the lag coefficient β will only give values differing from zero when branches of different length are concerned. However, the lengths of the branches surrounded islands in the River Rhine do not show significant differences (Fig. 2.3.3) and their influences on the transport velocity will be negligible.

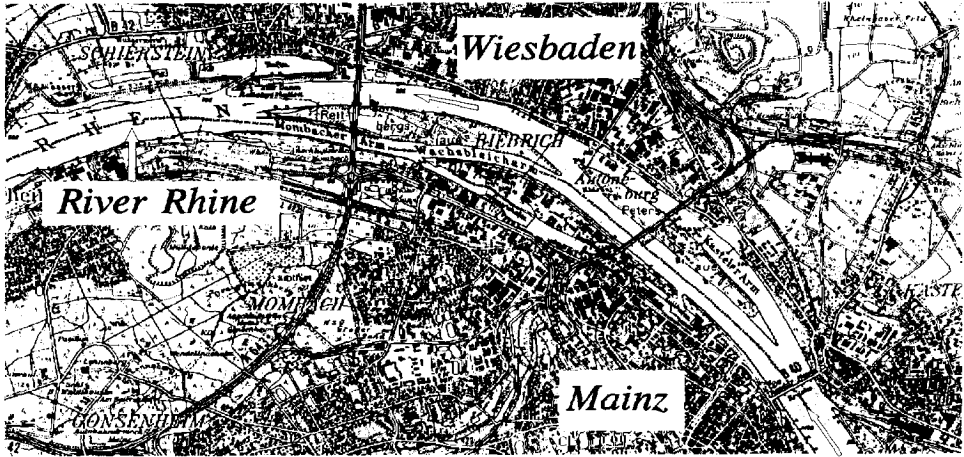


Fig. 2.3.3 The islands in the River Rhine downstream of the tributary Main

In case the travel time of the flow T_u should only be based on the mean flow-velocity in the main stream, Eq.(2.3.14) becomes (Appendix B)

$$\beta = \frac{1 + \frac{Q_2}{Q_1} \cdot \left(\frac{L_2}{L_1}\right)^{1.5}}{1 + \frac{Q_2}{Q_1}} - 1 \quad (2.3.15)$$

Again the lag coefficient will only differ from zero, if the lengths of the branches are significantly different.

2.3.2 Two-zone approach

The description of the concentration distribution in case of *dead zones* made by groynes, will be approached by a two-zone model: a *fast-moving zone*, representing the main stream and a *slow-moving zone* representing regions along the bottom and

sides of the river due to irregularities or groynes, where the flow is nearly stagnant: the *dead zones*.

Concerning this two-zone model Eq.(2.1.2) is valid for each zone, extended with a term representing the exchange between the two zones (for convenience the overbars have been dropped)

$$\frac{\partial \varphi_s}{\partial t} + u_s \frac{\partial \varphi_s}{\partial x} - K_s \frac{\partial^2 \varphi_s}{\partial x^2} = -D_s(\varphi_s - \varphi_b) \quad (2.3.16)$$

$$\frac{\partial \varphi_b}{\partial t} + u_b \frac{\partial \varphi_b}{\partial x} - K_b \frac{\partial^2 \varphi_b}{\partial x^2} = D_b(\varphi_s - \varphi_b) \quad (2.3.17)$$

wherein the subscript *s* indicates the parameters in the fast-moving zone and the subscript *b* the parameters in the slow-moving zone. The coefficients D_s and D_b concern the mass transfer between the two zones. In case of dead zones the flow velocity in the slow-moving zone u_b becomes zero. Assuming a well-mixed situation in the dead zone, there is no dispersive transport in this zone, so Eq.(2.3.17) becomes

$$\frac{\partial \varphi_b}{\partial t} = D_b(\varphi_s - \varphi_b) \quad (2.3.18)$$

Neglecting the dispersive transport in the main stream as well Eq.(2.3.16) becomes

$$\frac{\partial \varphi_s}{\partial t} + u_s \frac{\partial \varphi_s}{\partial x} = -D_s(\varphi_s - \varphi_b) \quad (2.3.19)$$

Considering this degenerated pair of coupled Eqs (2.3.19) and (2.3.18), the concentration in the dead zone φ_b can be eliminated by differentiation of Eq.(2.3.19) after the time *t*

$$\frac{\partial^2 \varphi_s}{\partial t^2} + u_s \frac{\partial^2 \varphi_s}{\partial x \partial t} = -D_s \left(\frac{\partial \varphi_s}{\partial t} - \frac{\partial \varphi_b}{\partial t} \right) \quad (2.3.20)$$

which gives with Eq.(2.3.18)

$$\frac{\partial^2 \varphi_s}{\partial t^2} + u_s \frac{\partial^2 \varphi_s}{\partial x \partial t} = -D_s \frac{\partial \varphi_s}{\partial t} + D_s \cdot D_b \cdot (\varphi_s - \varphi_b) \quad (2.3.21)$$

Substitution of Eq.(2.3.19) into Eq.(2.3.21) yields

$$\frac{\partial^2 \varphi_s}{\partial t^2} + u_s \frac{\partial^2 \varphi_s}{\partial x \partial t} + (D_s + D_b) \frac{\partial \varphi_s}{\partial t} + u_s \cdot D_b \cdot \frac{\partial \varphi_s}{\partial x} = 0 \quad (2.3.22)$$

Concerning an instantaneous spill the concentration distribution in the time as well as in the space domain will change slowly at large distances from the point of release. So in this case the second derivatives can be neglected in relation to the first derivatives and Eq.(2.3.22) becomes

$$\frac{\partial \varphi_s}{\partial t} + \left(\frac{u_s \cdot D_b}{D_s + D_b} \right) \cdot \frac{\partial \varphi_s}{\partial x} = 0 \quad (2.3.23)$$

From Eq.(2.3.23) it is clear that for large distances the transport velocity c of a substance becomes

$$c = \frac{u_s \cdot D_b}{D_s + D_b} = \frac{u_s}{1 + D_s/D_b} \quad (2.3.24)$$

Considering the definition for the mass-transfer coefficients D_s and D_b respectively in case of dead zones

$$D_s = \frac{P}{A_s} \cdot E \quad D_b = \frac{P}{A_b} \cdot E \quad (2.3.25)$$

with

$$P = \alpha_s \cdot P_s \quad (2.3.26)$$

wherein

A_s	=	cross-sectional area of the main stream
A_b	=	cross-sectional area of the dead zone
α_s	=	constant of proportionality in relation to the contact area between main stream and dead zone ($0 < \alpha_s < 1$)
P_s	=	wetted perimeter
E	=	transfer velocity of the pollutant

Equation (2.3.24) becomes

$$c = \frac{u_s}{1 + \beta} \quad (2.3.27)$$

with the dead-zone parameter (see also Fig. 2.1.8)

$$\beta = \frac{A_b}{A_s} \quad (2.3.28)$$

In case of the two-zone model Chikwendu and Ojiakor (1985) solved the pair of coupled Eqs (2.3.16) and (2.3.17), using Fourier transforms. However, the Fourier-inversion integrals could not be solved in a general way. In case of equal dispersion-coefficients in both zones ($= K$) an exact solution was found for large distances from the point of release

$$\frac{\varphi(x,t)}{\varphi_0} = \frac{a}{\sqrt{4\pi Kt}} \cdot \exp \left(- \frac{\left[x - \left(\frac{a_1}{a} \cdot u_1 + \frac{a_2}{a} \cdot u_2 \right) \cdot t \right]^2}{4Kt} \right) \quad (2.3.29)$$

with

- φ_0 = the concentration at the point of release in both zones, after the initial condition $\varphi(x,0) = \varphi_0 \cdot \delta(x)$ with $\delta(x)$, being the Diracdelta-function
- a = the total water depth
- a_1 = the depth of the fast zone (flow velocity u_1)
- a_2 = the depth of the slow zone (flow velocity u_2)

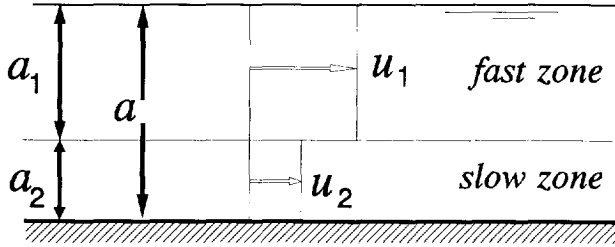


Fig. 2.3.4 Channel, showing slow zone and fast zone

According to Eq.(2.1.8) the transport velocity c is

$$c = \frac{a_1}{a} \cdot u_1 + \frac{a_2}{a} \cdot u_2 \quad (2.3.30)$$

If the slow zone is completely stagnant, so $u_2 = 0$ and $u_1 = u_s$, Eq.(2.3.30) becomes

$$c = \frac{a_1}{a} \cdot u_1 = \frac{u_s}{1 + a_2/a_1} \quad (2.3.31)$$

which is equal to Eq.(2.3.27), if $A_s = a_1 \cdot B$ and $A_b = a_2 \cdot B$ with B is the width of the channel and Eq.(2.3.28) is per meter width of the channel (Fig. 2.3.4).

Further Chikwendu and Ojiakor (1985) present approximations for the concentration distributions in case of small values of the mass-transfer coefficient, which, however, means a reduction of the influence of the slow zone with the distance and consequently the transport velocity c tends to the flow velocity in the fast zone $u_1 = u_s$. This is just in contrast with the conclusion, given by Eq.(2.3.31).

It is also possible to apply the method of the characteristics in solving the Eqs (2.3.18) and (2.3.19). Substitution of Eq.(2.3.18) into Eq.(2.3.19) gives

$$\frac{\partial \varphi_s}{\partial t} + u_s \frac{\partial \varphi_s}{\partial x} + \frac{D_s}{D_b} \cdot \frac{\partial \varphi_b}{\partial t} = 0 \quad (2.3.32)$$

In order to get a second equation with the derivatives of the concentrations in the main flow φ_s and the stagnant zone φ_b Eq.(2.3.18) is differentiated after the time t

$$\frac{\partial^2 \varphi_b}{\partial t^2} = D_b \left(\frac{\partial \varphi_s}{\partial t} - \frac{\partial \varphi_b}{\partial t} \right) \quad (2.3.33)$$

If the second derivative of the concentration in the stagnant zone φ_b after the time t is approximately equal to zero, the second equation will be

$$\frac{\partial \varphi_s}{\partial t} - \frac{\partial \varphi_b}{\partial t} = 0 \quad (2.3.34)$$

The set of equations for the characteristic method becomes

$$\begin{aligned} u_s \frac{\partial \varphi_s}{\partial x} + \frac{\partial \varphi_s}{\partial t} + \frac{D_s}{D_b} \cdot \frac{\partial \varphi_b}{\partial t} &= 0 \\ \frac{\partial \varphi_s}{\partial t} - \frac{\partial \varphi_b}{\partial t} &= 0 \\ \frac{dx}{dt} \frac{\partial \varphi_s}{\partial x} + \frac{\partial \varphi_s}{\partial t} &= \frac{d\varphi_s}{dt} \\ \frac{dx}{dt} \frac{\partial \varphi_b}{\partial x} + \frac{\partial \varphi_b}{\partial t} &= \frac{d\varphi_b}{dt} \end{aligned} \quad (2.3.35)$$

and in matrix notation

$$\begin{vmatrix} u_s & 1 & 0 & D_s/D_b \\ 0 & 1 & 0 & -1 \\ dx/dt & 1 & 0 & 0 \\ 0 & 0 & dx/dt & 1 \end{vmatrix} \cdot \begin{vmatrix} \partial\phi_s/\partial x \\ \partial\phi_s/\partial t \\ \partial\phi_b/\partial x \\ \partial\phi_b/\partial t \end{vmatrix} = \begin{vmatrix} 0 \\ 0 \\ d\phi_s/dt \\ d\phi_b/dt \end{vmatrix} \quad (2.3.36)$$

The characteristic direction in the (x,t) -domain can be derived by setting

$$\begin{vmatrix} u_s & 1 & 0 & D_s/D_b \\ 0 & 1 & 0 & -1 \\ dx/dt & 1 & 0 & 0 \\ 0 & 0 & dx/dt & 1 \end{vmatrix} = 0 \quad (2.3.37)$$

which gives besides the physically irrelevant solution $dx/dt = 0$

$$dx/dt = \frac{u_s}{D_s/D_b + 1} \quad (2.3.38)$$

This result is equal to Eq.(2.3.24). This means that the condition for which Eq.(2.3.34) is valid, also concerns large distances from the point of release. As a matter of fact the change of the concentration in the time domain in the main stream and the stagnant zone are equal (see Eq. 2.3.34).

A combination of Eq.(2.3.19) with Eq.(2.3.18), assuming a constant difference between the concentration in the main stream and in the stagnant zone

$$\frac{1}{D_b} \frac{\partial\phi_b}{\partial t} = \phi_s - \phi_b = W = \text{constant} \quad (2.3.39)$$

gives for dx/dt the value u_s , which will suit quite well for short distances from the point of release, where the concentration in the stagnant zones is still more or less negligible in comparison with the concentration in the main stream.

For the dead-zone model with the pair of coupled Eqs (2.3.16) and (2.3.18) Hays et al. (1966) tried to get a solution by Laplace transforms. The solution of the Laplace transform for the main stream is

$$\varphi(L,s) = \frac{M}{A_s} \frac{\exp \left(\left\{ u_s - \sqrt{u_s^2 + 4 \cdot K_s \cdot \left(1 + \frac{A_b}{A_s} \cdot \Gamma \right) \cdot s} \right\} \cdot \left[\frac{L}{2K_s} \right] \right)}{\sqrt{u_s^2 + 4 \cdot K_s \cdot \left(1 + \frac{A_b}{A_s} \cdot \Gamma \right) \cdot s}} \quad (2.3.40)$$

with

L = distance from the point of release

s = Laplace variable

$$\Gamma = \frac{1}{s/D_b + 1}$$

The complex inversion integral of Eq.(2.3.40) gives the concentration in the time domain. Hayes et al (1966) suggest

$$\varphi(L,t) = \frac{1}{2 \cdot \pi \cdot i} \int_{-i \cdot \infty}^{+i \cdot \infty} \varphi(L,s) \cdot e^{st} ds \quad (2.3.41)$$

so that s only takes imaginary values.

Because Eq.(2.3.41) cannot be solved analytically, only a numerical solution is possible (Thackston and Schnelle, 1970).

For the degenerated pair of coupled Eqs (2.3.19) and (2.3.18) Kranenburg (1988) found for an instantaneous release M for $0 < x < u_s \cdot t$

$$\varphi_s(x,t) = \frac{M}{A_s \cdot u_s} \exp \left[- D_b \cdot t + (D_b - D_s) \frac{x}{u_s} \right] \cdot \left[\delta \left\{ t - \frac{x}{u_s} \right\} + \int_0^{D_s D_b \frac{x}{u_s}} I_0 \left(2 \sqrt{\alpha \left[t - \frac{x}{u_s} \right]} \right) d\alpha \right] \quad (2.3.42)$$

with I_0 being the modified Bessel-function of the 0th order.

Equation (2.3.42) consists of two 'waves':

- (1) the first 'wave' concerns a decreasing δ -function with a propagation velocity u_s

$$\varphi_s(x, t) = \frac{M}{A_s \cdot u_s} \exp \left[- D_b \cdot t + (D_b - D_s) \frac{x}{u_s} \right] \cdot \left[\delta \left\{ t - \frac{x}{u_s} \right\} \right] \quad (2.3.43)$$

which gives for $x = u_s \cdot t$ ($\delta = 1$)

$$\varphi_s(x) = \frac{M}{A_s \cdot u_s} \exp \left[- D_s \frac{x}{u_s} \right] \quad (2.3.44)$$

(2) the second 'wave' propagates more slowly with a velocity c_1

$$\begin{aligned} \varphi_s(x, t) = \frac{M}{A_s \cdot u_s} \exp \left[- D_b \cdot t + (D_b - D_s) \frac{x}{u_s} \right] \cdot \\ \cdot \left[\int_0^{D_s D_b \frac{x}{u_s}} I_0 \left(2 \sqrt{\alpha \left[t - \frac{x}{u_s} \right]} \right) d\alpha \right] \end{aligned} \quad (2.3.45)$$

If α is substituted by

$$\alpha = \frac{z^2}{4 \left(t - \frac{x}{u_s} \right)} \quad (2.3.46)$$

Equation (2.3.45) becomes

$$\begin{aligned} \varphi_s(x, t) = \frac{M}{A_s \cdot u_s} \exp \left[- D_b \cdot t + (D_b - D_s) \frac{x}{u_s} \right] \cdot \\ \cdot \left[\frac{1}{2 \left(t - \frac{x}{u_s} \right)} \cdot \int_0^p z \cdot I_0(z) dz \right] \end{aligned} \quad (2.3.47)$$

with

$$p = 2 \sqrt{D_s D_b \frac{x}{u_s} \cdot \left(t - \frac{x}{u_s} \right)}$$

For large values of p it holds (Abramowitz and Stengun, 1965)

$$\int_0^p z \cdot I_0(z) dz = \sqrt{\frac{p}{2\pi}} \cdot e^p$$

Thus Eq.(2.3.47) reduces to

$$\begin{aligned} \varphi_s(x, t) = & \frac{M}{2\sqrt{\pi} \cdot A_s \cdot u_s} \cdot \frac{[D_s \cdot D_b \cdot (x/u_s) \cdot (t - x/u_s)]^{1/4}}{t - x/u_s} \cdot \\ & \cdot \exp \left[-D_b \cdot t + (D_b - D_s) \cdot (x/u_s) + 2\sqrt{D_b \cdot D_s \cdot (x/u_s) \cdot (t - x/u_s)} \right] \end{aligned} \quad (2.3.48)$$

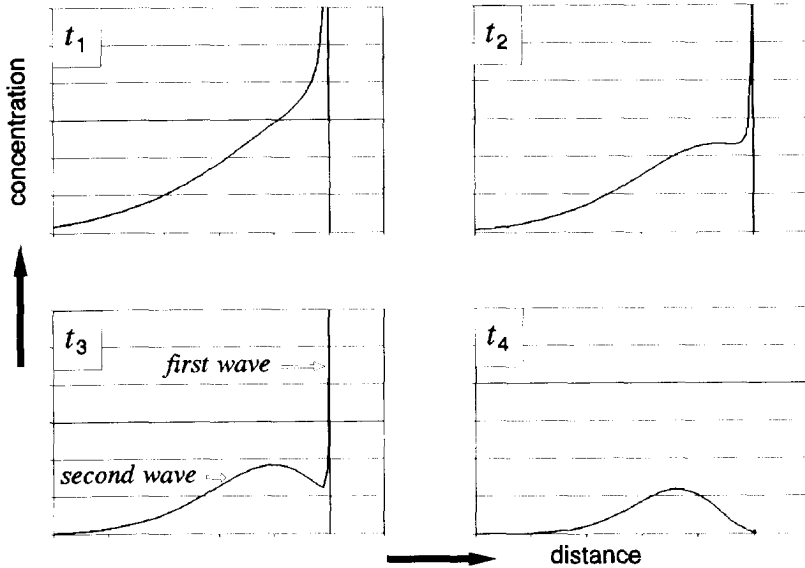


Fig. 2.3.5 Characteristic concentration-distributions after Eq.(2.3.49)

The propagation velocity c_1 of this second 'wave' is found by setting the argument of the exponential function equal to zero

$$c_1 = \frac{x}{t} = \frac{u_s}{1 + D_s/D_b} = c$$

which corresponds with Eq.(2.3.24).

For the determination of c_1 for shorter distances Eq.(2.3.47) has to be solved.

In Fig. 2.3.5 a more qualitative presentation of Eq.(2.3.48) in combination with Eq.(2.3.44) is given for four times $T = t_1, \dots, t_4$

$$\begin{aligned} \frac{\varphi_s(x, T)}{\bar{\varphi}} = \frac{1}{2\sqrt{\pi}} \cdot \frac{[D_s \cdot D_b \cdot (x/u_s) \cdot (T - x/u_s)]^{1/4}}{T - x/u_s} \cdot \\ \cdot \exp \left[-D_b \cdot T + (D_b - D_s) \cdot (x/u_s) + 2\sqrt{D_b \cdot D_s \cdot (x/u_s) \cdot (T - x/u_s)} \right] + \\ + \exp \left[-D_s T \right] \end{aligned} \quad (2.3.49)$$

with

$$\bar{\varphi} = M / (A_s \cdot u_s) ; D_s = \beta \cdot D_b , \text{ and } 0 \leq x / u_s \leq T,$$

with numerical values:

$$t_1 = 200 \text{ s}, t_2 = 300 \text{ s}, t_3 = 400 \text{ s}, t_4 = 800 \text{ s}; \beta = 0.2 \text{ and } D_b = 0.05 \text{ s}^{-1}$$

The first wave vanishes after a certain time, e.g. $T = t_4$

Beer and Young (1983) developed an aggregated dead zone model in order to be able to represent the dispersive transport, as well as the skewness of a concentration distribution. Therefore they interpret Eq.(2.3.18) as representing a mixing tank in which there is an input of solute of concentration φ_s and, under the assumption of complete mixing within the volume, an export of solute of concentration φ_b . The residence time of the fluid in the tank is defined as $1/D_b$. Because models composed of serially connected, completely mixed compartments of the form of Eq.(2.3.18) show also dispersive transport, Beer and Young proposed the same description for rivers in combination with purely convective transport ('plug flow') considering Eq.(2.3.16) without the dispersive transport

$$\frac{d\varphi_s}{dt} = \frac{\partial \varphi_s}{\partial t} + u_s \frac{\partial \varphi_s}{\partial x} = -D_s(\varphi_s - \varphi_b) \quad (2.3.50)$$

in which the two left-hand side terms represent the plug flow and the right-hand side term incorporates the dispersive effects of the aggregated dead zones.

In other words in this model the dead zones are a tool in representing the dispersive transport, so they have not any relation with the stagnant zones along a river and consequently nothing to do with the resulting retardation of the transport of substances in relation to the mean flow-velocity in the main stream of the river.

Reichert and Wanner (1991) developed a model which describes the initial period of the transport of a released substance more correctly. Considering the cross-sectional flow-velocity profile in a river, they divided the cross section in two parts: a layer along the river banks, where the flow velocity is very small and a central part. In their approach the layer along the river banks is the stagnant zone with a flow velocity equal to zero (Fig. 2.3.6). The flow velocity u_c in the main stream is defined by

$$u_c = (1 + \beta) \cdot u_s \quad (2.3.51)$$

which means, that the convective transport-velocity of the substance is larger than the mean flow-velocity. This agrees with the initial transport-velocity for a release in the middle of a river.

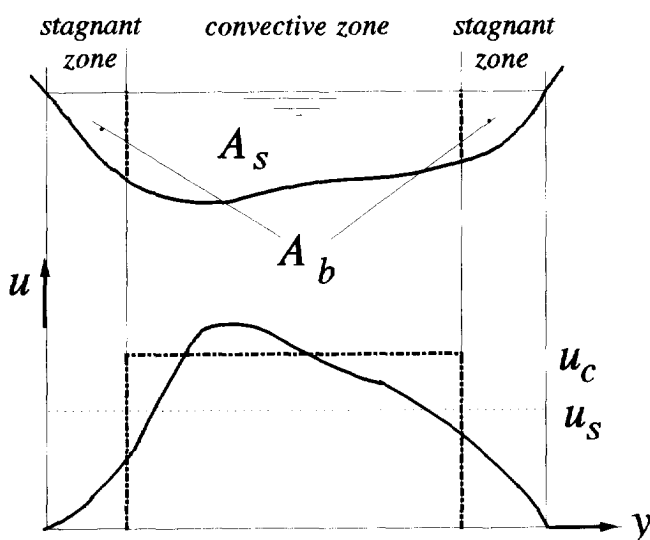


Fig. 2.3.6 River cross-section (above) and transverse profile of vertically averaged flow-velocity

Reichert and Wanner pointed out that, however, their model equations are similar to those, used for the description of dead-zone effects, their equations serve to model the effects of transverse velocity gradients and not those of dead zones.

As a matter of fact their model is a two zone model, like that of Chikwendu and Ojiakor (1985), based on Eqs (2.3.18) and (2.3.19), but without the dispersive transport.

Valentine and Wood (1977) describe tests in a flume with peripheral dead-zones at the bottom (Fig. 2.3.7). The description of the concentration in the main stream is two dimensional in the vertical plane and is of the form of

$$\frac{\partial \varphi_s}{\partial t} + u_s \frac{\partial \varphi_s}{\partial x} - K_{xs} \frac{\partial^2 \varphi_s}{\partial x^2} - K_{zs} \frac{\partial^2 \varphi_s}{\partial z^2} = 0 \quad (2.3.52)$$

with $\varphi_s = \varphi_s(x, z, t)$.

The equation for the concentration in the bottom dead zones is given by

$$\frac{\partial \varphi_b}{\partial t} = D_b \cdot (\varphi_{sz} - \varphi_b) \quad (2.3.53)$$

wherein φ_{sz} is the average concentration in the flow zone just above the boundary and

$$D_b = \frac{E}{d} = \frac{0.02 \cdot u_s}{d} \quad (2.3.54)$$

d = depth of the trapped eddy in the dead zone (Fig. 2.3.7).

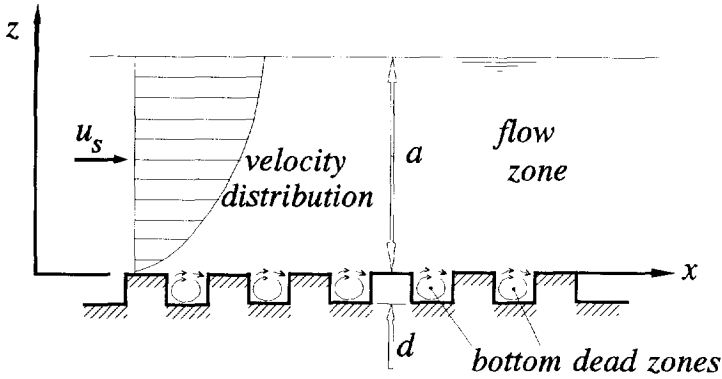


Fig. 2.3.7 Sketch of idealized two-dimensional model

By the Aris (1956) moment-transform method Eqs (2.3.52) and (2.3.53) are rewritten. The transforms are defined by

$$\Phi_{sp} = \int_0^{\infty} \varphi_s \cdot x^p \cdot dx \quad \text{and} \quad \Phi_{bp} = \int_0^{\infty} \varphi_b \cdot x^p \cdot dx$$

The Aris-moment equations were solved numerically.

Valentine and Wood presents 1979 a simplified three-dimensional description of the concentration distribution in a test flume with dead zones along the bottom as well as along the walls (Fig. 2.3.8). Based on the results of their two-dimensional model (Valentine and Wood, 1977) they concluded that the contribution of the longitudinal turbulent diffusion to the variance of a dispersing cloud is negligible. Thus their description of the concentration in the main stream becomes of the form of

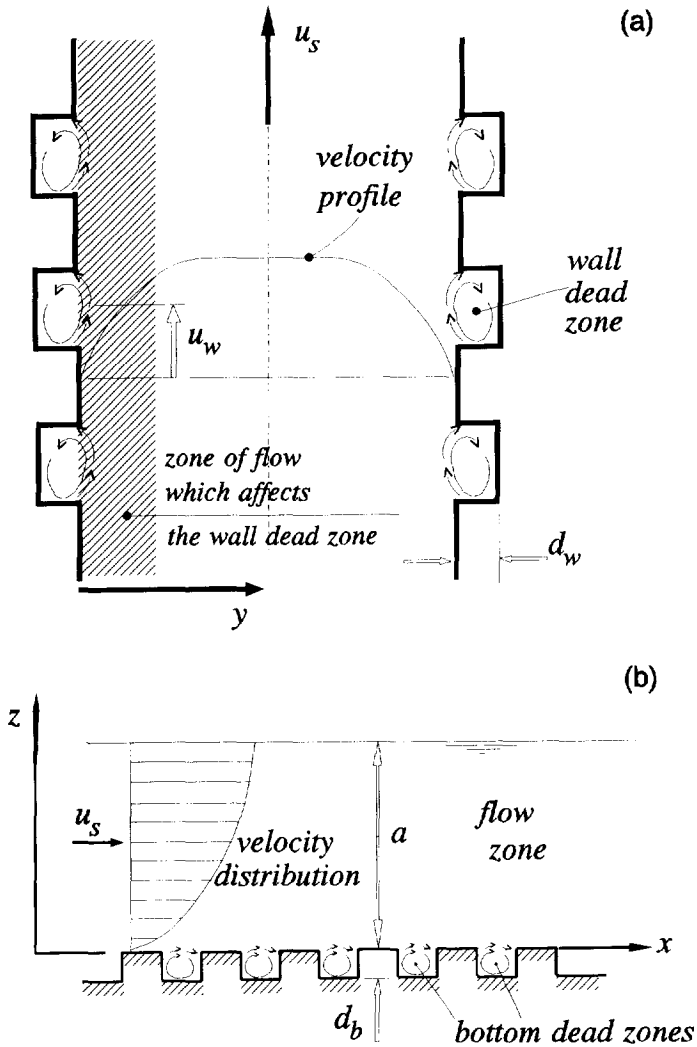


Fig. 2.3.8 Idealized three-dimensional model:
(a) Plan at mid-depth
(b) longitudinal section

$$\frac{\partial \varphi_s}{\partial t} + u_s \frac{\partial \varphi_s}{\partial x} - K_{ys} \frac{\partial^2 \varphi_s}{\partial y^2} - K_{zs} \frac{\partial^2 \varphi_s}{\partial z^2} = 0 \quad (2.3.55)$$

with $\varphi_s = \varphi_s(x, y, z, t)$.

The equations for the concentration in the bottom and wall dead zones, are given by

$$\frac{\partial \varphi_{bb}}{\partial t} = D_{bb} \cdot (\varphi_{sz} - \varphi_{bb}) \quad (2.3.56)$$

and

$$\frac{\partial \varphi_{bw}}{\partial t} = D_{bw} \cdot (\varphi_{sy} - \varphi_{bw}) \quad (2.3.57)$$

wherein

φ_{sz} = average concentration in the flow zone just above the bottom
 φ_{sy} = average concentration in the flow zone just aside of the walls

The coefficients D_{bb} and D_{bw} are defined by

$$D_{bb} = \frac{E}{d_b} = \frac{0.02 \cdot u_s}{d_b} \quad (2.3.58)$$

and

$$D_{bw} = \frac{E_w}{d_w} = \frac{0.02 \cdot u_w}{d_w} \quad (2.3.59)$$

with (see also Fig. 2.3.8)

d_b = depth of the trapped eddy in the bottom dead zone

d_w = depth of the trapped eddy in the wall dead zone

u_w = average velocity in the vicinity of the walls

The same solution method as was used in their two-dimensional model (Valentine and Wood, 1977) was followed, applying the Aris-moment-transform method and solving the resulting equations numerically.

2.3.3 Temporal-moment approach

Because there is no analytical solution for the set of Eqs (2.3.16) and (2.3.17) considering a two-zone model, as well as for the set of Eqs (2.3.16) and (2.3.18) considering the dead-zone model, the moments of the concentration distribution are

considered. For a good reconstruction c.q. approximation of the concentration distribution in the time domain $\varphi_s(L, t) \approx \varphi_E(L, t)$ at a certain measuring point $x = L$, Chatwin (1980) applies the Edgeworth's form of the Gram-Charlier series of Type A (Kendall and Stuart, 1958)

$$\varphi_E(L, t) = \frac{m_0}{\sqrt{2 \cdot \pi \cdot \sigma_t^2}} \cdot \exp \left[-\frac{\tau^2}{2} \right] * \left[1 + \frac{G_t}{6} \cdot H_3(\tau) + \frac{\Gamma_t}{24} \cdot H_4(\tau) + \frac{G_t^2}{72} \cdot H_6(\tau) \right] \quad (2.3.60)$$

with

$$\tau = (t - \mu_t) / (\sigma_t)$$

the Hermite polynomials

$$H_3(\tau) = \tau^3 - 3 \cdot \tau$$

$$H_4(\tau) = \tau^4 - 6 \cdot \tau^2 + 3$$

$$H_6(\tau) = \tau^6 - 15 \cdot \tau^4 + 45 \cdot \tau^2 - 15$$

and	m_0	=	zeroth moment	[kg · m ⁻³ · s]
	μ_t	=	centroid in the time domain	[s]
	σ_t^2	=	variance	[s ²]
	G_t	=	skewness	[-]
	Γ_t	=	kurtosis	[-]

By applying the mathematical description of the moments of a distribution the parameters m_0 , μ_t , and σ_t^2 are defined by

$$m_0 = \int_{-\infty}^{\infty} \varphi_s(L, t) \, dt \quad (2.3.61)$$

$$\mu_t = \frac{1}{m_0} \int_{-\infty}^{\infty} t \cdot \varphi_s(L, t) \, dt \quad (2.3.62)$$

$$\sigma_t^2 = \frac{1}{m_0} \int_{-\infty}^{\infty} (t - \mu_t)^2 \cdot \varphi_s(L, t) \, dt \quad (2.3.63)$$

while the skewness and the kurtosis are defined by

$$G_t = \frac{|g_t|}{|\sigma_t^3|} \quad (2.3.64)$$

$$\Gamma_t = \frac{\gamma_t}{\sigma_t^4} - 3 \quad (2.3.65)$$

with

$$g_t = \frac{1}{m_0} \int_{-\infty}^{\infty} (t - \mu_t)^3 \cdot \varphi_s(L, t) dt \quad (2.3.66)$$

$$\gamma_t = \frac{1}{m_0} \int_{-\infty}^{\infty} (t - \mu_t)^4 \cdot \varphi_s(L, t) dt \quad (2.3.67)$$

For a good reconstruction of the concentration distribution by Eq.(2.3.60), the skewness G_t and the kurtosis Γ_t should not be much more than unity.

The mass M passing at the measuring point can be found by

$$M = m_0 \cdot Q \quad (2.3.68)$$

assuming that the river discharge Q is constant during the passage of the pollutant at $x = L$.

According to the dead-zone model of Nordin and Troutman (1980) the centroid in the time domain μ_t and the variance σ_t^2 of the concentration distribution can be written as functions of x , u_s , K and β

$$\mu_t = \left(\frac{x}{u_s} + \frac{2 \cdot K}{u_s^2} \right) \cdot (1 + \beta) \quad (2.3.69)$$

$$\sigma_t^2 = \left(\frac{x}{u_s} + \frac{4K}{u_s^2} \right) \cdot \frac{2K}{u_s^2} \cdot (1 + \beta)^2 + \left(\frac{x}{u_s} + \frac{2K}{u_s^2} \right) \cdot \frac{2 \cdot \beta}{D_b} \quad (2.3.70)$$

in which D_b is the constant of proportionality for the exchange of pollutant between the main stream and the dead zone (see also Eq. 2.3.17).

For a first approximation of Eqs (2.3.69) and (2.3.70) the order of magnitude of the two terms between the brackets of these equations are now considered. At small distances x from the point of release, this distance is of the order 10^3 m, while the dispersion coefficient K is relatively small and of the order 10^1 m²/s (Fig. 1.10, Spreafico and van Mazijk, 1993, p.98, Fig. 5.4.7). If the mean flow velocity u_s is of the order 10^0 m/s, the first term (x/u_s) is of the order 10^3 and the second term (K/u_s^2) of the order 10^1 . At larger distances, x is of the order 10^4 till 10^5 m and the dispersion coefficient K becomes of the order 10^2 till 10^3 m²/s.

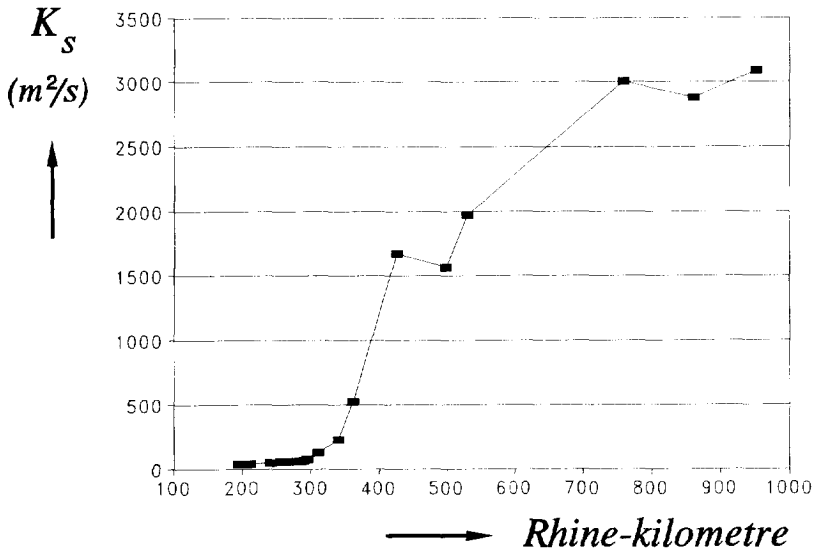


Fig. 2.3.9 Development of the dispersion coefficient K_s along the River Rhine between Basel and the Netherlands, based on the tracer experiment April 1989 (Spreafico and van Mazijk, 1993)

This means, that the order of magnitude of the terms between the brackets becomes

$$O\left(\frac{x/u_s}{K/u_s^2}\right) = O\left(\frac{x \cdot u_s}{K}\right) = O\left(\frac{10^3 \cdot 1}{10}\right) = 10^2$$

and Eqs (2.3.69) and (2.3.70) can be reduced to

$$\mu_t = \left(\frac{x}{u_s}\right) \cdot (1 + \beta) \quad (2.3.71)$$

$$\sigma_t^2 = \left(\frac{2 \cdot x}{u_s^3} \right) \cdot \left[K \cdot (1 + \beta)^2 + \frac{\beta \cdot u_s^2}{D_b} \right] \quad (2.3.72)$$

For a further comparison of the magnitude of the two terms between the square brackets in Eq.(2.3.72), the expression for D_b is considered (see Eqs 2.3.25 and 2.3.26)

$$D_b = \frac{\alpha_s \cdot P_s}{A_b} \cdot E \quad (2.3.73)$$

After Valentine and Wood (1977) the transfer velocity of the pollutant can be given by (Eq. 2.3.54)

$$E \approx 0.02 \cdot u_s \quad (2.3.74)$$

Because the hydraulic radius for rivers with a large width/depth ratio (as the River Rhine) is defined by $R = A_s / P_s \cong a$ (a = water depth), it can be shown, that for $\alpha_s=1$ the second term between the square brackets of Eq.(2.3.72) becomes

$$\frac{\beta \cdot u_s^2}{D_b} \approx 50 \cdot \beta^2 \cdot u_s \cdot a \quad (2.3.75)$$

Considering the following average values, according to the River Rhine

$$\begin{array}{lll} \beta & \approx & 10^{-1} \text{ till } 10^{-2} \\ u_s & \approx & 1 \text{ m/s} \\ a & \approx & 5 \text{ m} \end{array}$$

the value of the expression of Eq.(2.3.75) is less than 2.5 m²/s. Because the longitudinal dispersion-coefficient K is at large distances of the order 10² m²/s or more, Eq.(2.3.72) can be reduced to

$$\sigma_t^2 = \left(\frac{2 \cdot x}{u_s^3} \right) \cdot [K \cdot (1 + \beta)^2] \quad (2.3.76)$$

Substituting $x / u_s = t$ gives

$$\sigma_t^2 = \left(\frac{2 \cdot t}{u_s^2} \right) \cdot [K \cdot (1 + \beta)^2] \quad (2.3.77)$$

Based on these expressions the transport velocity c and the longitudinal dispersion-coefficient for the dead zone model K_s can be derived by (Nordin and Sabol, 1974)

$$c = \left(\frac{d\mu_t}{dx} \right)^{-1} \quad (2.3.78)$$

and

$$K_s = \frac{u_s^2}{2} \cdot \left(\frac{d\sigma_t^2}{dt} \right) \quad (2.3.79)$$

Substitution of Eq.(2.3.71) into Eq.(2.3.78) and Eq.(2.3.76) into Eq.(2.3.79) gives respectively

$$c = \frac{u_s}{1 + \beta} \quad (2.3.80)$$

$$K_s = K \cdot (1 + \beta)^2 \quad (2.3.81)$$

Notice, that Eq.(2.3.80) is equal to the definition of the dead-zone parameter β after Eqs (2.3.27) and (2.3.28).

For $x = L$ Eqs (2.3.71) and (2.3.77) can be rewritten, applying Eqs (2.3.80) and (2.3.81)

$$\mu_t = \left(\frac{L}{c} \right) \quad (2.3.82)$$

$$\sigma_t^2 = \left(\frac{2 \cdot t}{u_s^2} \right) \cdot K_s = \left(\frac{2 \cdot t}{c^2} \right) \cdot K \quad (2.3.83)$$

Substituting Eqs (2.3.68), (2.3.82) and (2.3.83) into Eq.(2.3.60) gives

$$\begin{aligned} \varphi_E(L, t) = & \frac{M/Q}{\sqrt{4 \cdot \pi \cdot K \cdot t/c^2}} \cdot \exp \left[- \frac{(t - L/c)^2}{4 \cdot K \cdot t/c^2} \right] \cdot \\ & * \left[1 + \frac{1}{6} \cdot H_3 \left(\frac{t - L/c}{\sqrt{2 \cdot K \cdot t/c^2}} \right) + \frac{1}{24} \cdot H_4 \left(\frac{t - L/c}{\sqrt{2 \cdot K \cdot t/c^2}} \right) + \frac{1}{72} \cdot H_6 \left(\frac{t - L/c}{\sqrt{2 \cdot K \cdot t/c^2}} \right) \right] \end{aligned} \quad (2.3.84)$$

with G_t and Γ_t equal to unity.

For the development of the accidental spill-model for the River Rhine Eq.(2.3.84) was used, neglecting the Hermite polynomials $H_4(\tau)$ and $H_6(\tau)$ (see also Eq.2.1.12)

$$\varphi_E(L,t) = \frac{M/Q}{\sqrt{4 \cdot \pi \cdot K \cdot t/c^2}} \cdot \exp \left[- \frac{(t - L/c)^2}{4 \cdot K \cdot t/c^2} \right] * \left[1 + \frac{1}{6} \cdot H_3 \left(\frac{t - L/c}{\sqrt{2 \cdot K \cdot t/c^2}} \right) \right] \quad (2.3.85)$$

Applying Eq.(2.3.85) (*Chatwin-model*) for the development of an accidental spill-model the following parameters have to be calibrated:

- * the transport velocity c of a substance, e.g. the dead-zone parameter β after Eq.(2.3.80) and
- * the longitudinal dispersion-coefficient K .

Using the semi-empirical expression for the longitudinal dispersion-coefficient K as derived by Fischer et al. (1979)

$$K = \alpha_x \cdot \frac{u_s^2 \cdot B^2}{a \cdot u_*} \quad (2.3.86)$$

with α_x = coefficient of proportionality
 B = width of the main stream
 a = depth of the main stream
 u_* = shear velocity: $u_* = u_s \cdot \sqrt{(g) / C}$

wherein g = acceleration of gravity
 C = Chézy-coefficient, after Strickler $C = 25 \cdot (a/k_N)^{1/6}$
 k_N = equivalent sand roughness after Nikuradse

the calibration of K means the calibration of the coefficient of proportionality α_x .

In Chapter 3 the calibration and verification of these parameters in the Rhine Alarm-Model are discussed in detail.

Chapter 3

TRACER EXPERIMENTS RIVER RHINE

3.1 INTRODUCTION

The *lag coefficient* as well as the *longitudinal dispersion-coefficient* in the Rhine Alarm-Model were calibrated and verified by means of tracer experiments (Spreafico & van Mazijk, 1993) in Switzerland, France, Germany and the Netherlands (Fig. 3.1.1).

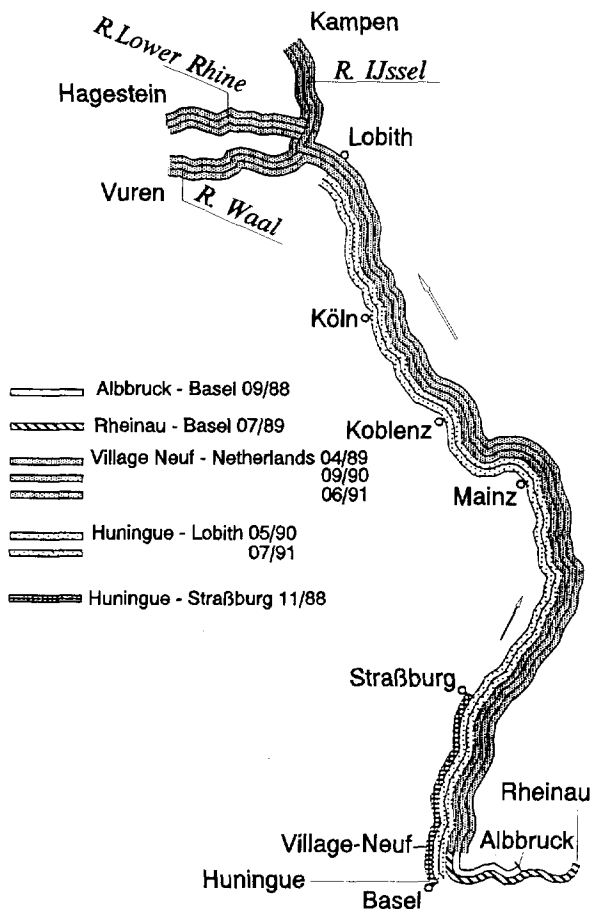


Fig. 3.1.1 Tracer experiments in the River Rhine between Lake of Constance and the Rhine branches in the Netherlands

The three main experiments were carried out from Basel (Village Neuf, Begin of the Rheinseiten Canal, River-kilometre 174.1, Fig. 3.1.2) up to the Rhine branches in the Netherlands: the River Waal (Vuren, River-kilometre 951.8), the River Lower Rhine (Hagestein, River-kilometre 946.5) and the River IJssel (Kampen, River-kilometre 994.5).

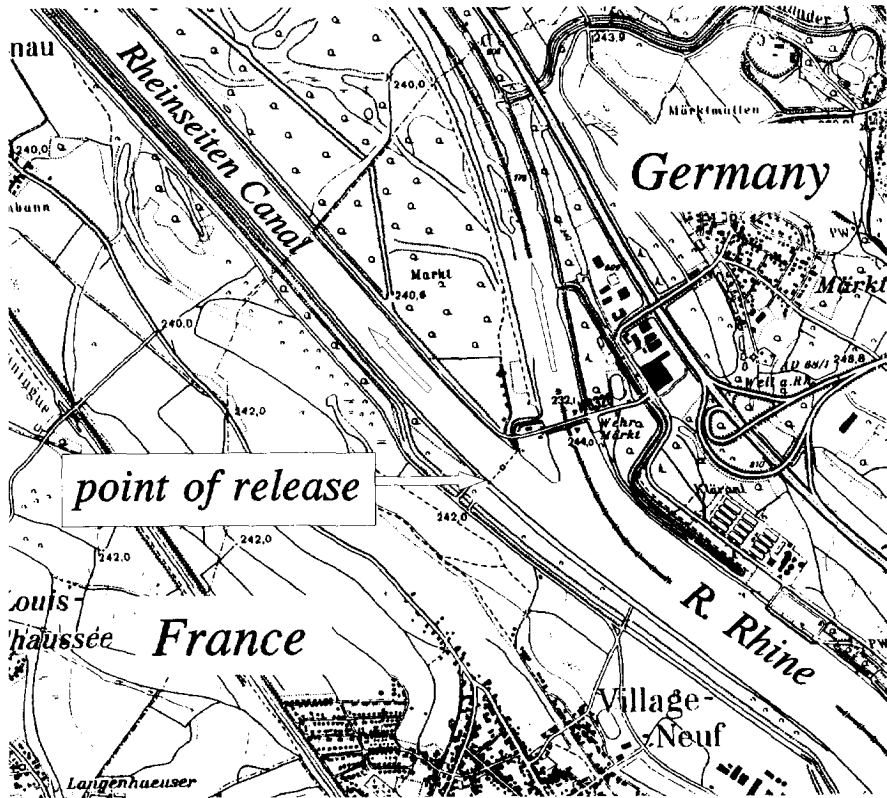


Fig. 3.1.2 Situation of the point of release in Village-Neuf

The experiments are indicated by the month and the year the tracer was released:

- * April 1989 (04/89) with a more or less normal-flow in the River Rhine at the measuring station Rheinfelden ($Q_{\text{Rheinfelden}} = 1170 \text{ m}^3/\text{s}$);
- * September 1990 (09/90) with a mean low-water discharge ($Q_{\text{Rheinfelden}} = 663 \text{ m}^3/\text{s}$) and
- * June 1991 (06/90) with a relatively high-water discharge at Rheinfelden ($Q_{\text{Rheinfelden}} = 1820 \text{ m}^3/\text{s}$)

Figure 3.1.3 shows the discharge distribution along the River Rhine between Rheinfelden and Lobith during the experiments concerned, in comparison with the discharges for mean high-water, normal-flow and mean low-water conditions.

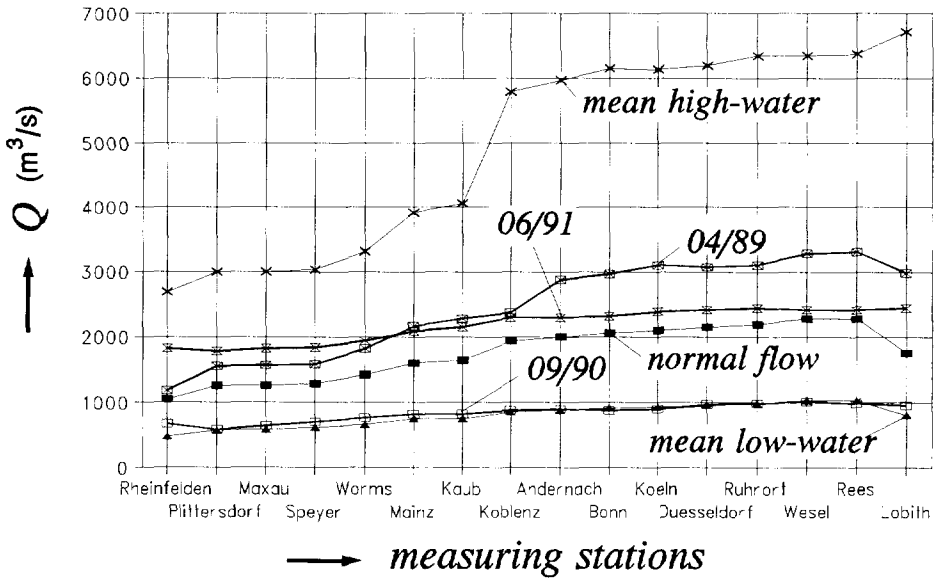


Fig. 3.1.3 Longitudinal distribution of the river discharge Q during the tracer experiments in comparison with the mean low-water, normal flow and mean high-water discharges of the River Rhine

Because the Rhine Alarm-Model is a one-dimensional transport model, assuming a completely mixed situation at the point of release, the tracer was poured into the Rheinseiten Canal in the middle of the canal, just upstream of a power station in order to get very quickly a homogeneous distribution of the tracer over the cross section of the canal.

In case of the experiments between Basel (Huningue) and Lobith the tracer was poured into the river from the left bank: experiments 05/90 and 07/91. The tracer experiment between Basel (Huningue) and Straßburg (11/88) was a first attempt, with unfortunately incomplete results. The river-discharge conditions during the experiment 05/90 lie between those of the experiments 04/89 and 09/90: $Q_{\text{Rheinfelden}} = 1008 \text{ m}^3/\text{s}$ (Fig. 3.1.4). The river-discharge conditions of the experiment 07/91 are comparable with those of the experiment 06/91.

The two experiments in Switzerland were realized in the Upper-Rhine River from Albbruck to Basel (09/88) with $Q_{\text{Rheinfelden}} = 1068 \text{ m}^3/\text{s}$ and from Rheinau to Basel (07/89) with $Q_{\text{Rheinfelden}} = 700 \text{ m}^3/\text{s}$ (Fig. 3.1.1).

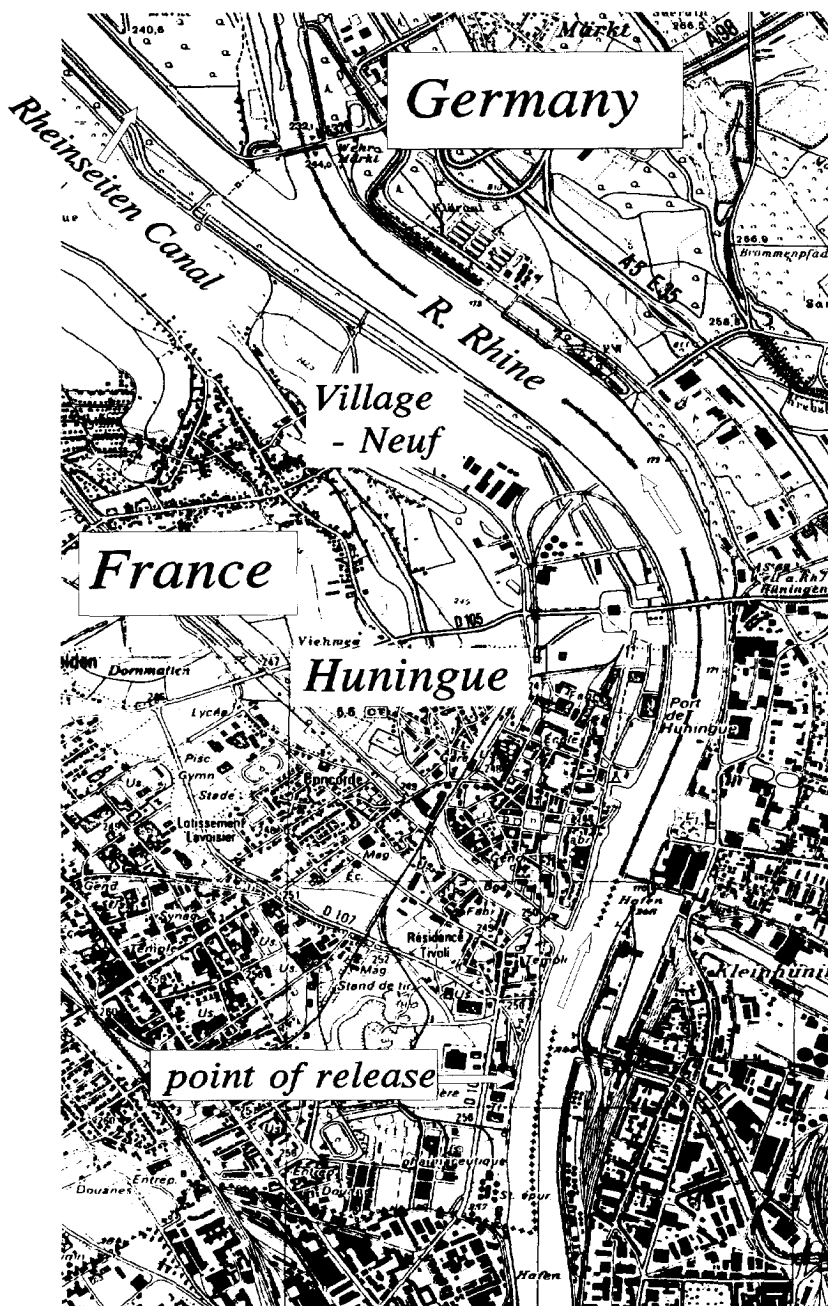


Fig. 3.1.4 Point of release at the left bank of the River Rhine in case of the tracer experiments Huningue - Lobith (05/90 and 07/91)

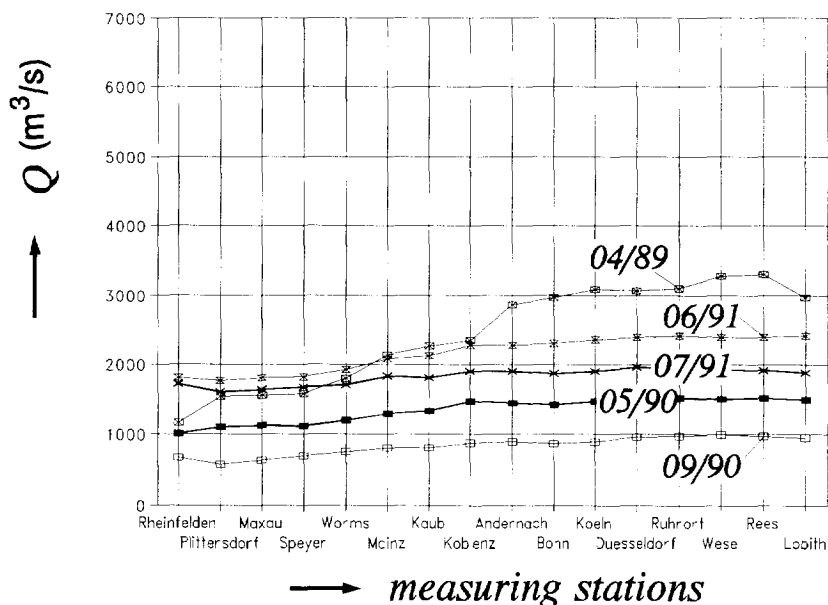


Fig. 3.1.5 Longitudinal distributions of the river discharge Q during the tracer experiments 05/09 and 07/91 in comparison with the discharges during the experiments 04/89, 09/90 and 06/91

For the tracer experiments an artificial tracer was used: the fluorescence tracer Rhodamine or Uranine. Due to the expected travel time of the tracer Rhodamine WT with a half-life period of 1300 hours was chosen in case of the experiments between Basel and the Netherlands. In case of the experiments in the Upper-Rhine River Uranine with a half-life period of 11 hours was used. For the experiments 05/90 and 07/91 with measurements between Basel and Lobith the tracer Rhodamine B with a half-life period of 780 hours was released. All these tracers have a very low detection limit.

The measured fluorescence can be corrected for background values, due to pollutant spills downstream of the point of release of the tracer.

The decomposition of the tracer elements is mainly caused by photosynthesis. This means that the actual value of the half-life period of the tracer depends on the turbidity of the river water and the climatic conditions, during the tracer experiment. For instance a tracer experiment with Uranine in the River Aare executed in 1993, showed a half-life of about 48 hours instead of the 11 hours, based on measurements under laboratory conditions.

For the analysis of the influence of tributaries and dead zones on the transport velocity the tracer experiments 04/89, 09/90 and 06/91 are considered. The results of the experiments 05/90 and 07/91 are used for the examination of the influence of the transversal mixing on the one-dimensional approach of the transport velocity in case of a release at the river bank.

The results of the experiments in the Upper-Rhine River were analyzed in detail by van Kuik and van Mazijk (1994). They studied the influence of tributaries and suppressed flow by weirs on the lag coefficient in general and the influence of the River Aare and the suppressed flow at the vicinity of water-power stations on this coefficient especially.

3.2 HYDRAULIC BASIS OF THE RHINE ALARM-MODEL

In order to represent the morphological variations along the River Rhine in the Rhine Alarm-Model the river was split up in a series of branches, which could subdivided in a series of sub-branches. This schematization of the River Rhine into branches and nodes is based on stationary flow conditions. In each branch the discharge is constant and related to a water-level measuring-station for which 'water-level-discharge' relation exists (Figs 3.2.1 and 3.2.2). At the nodes the

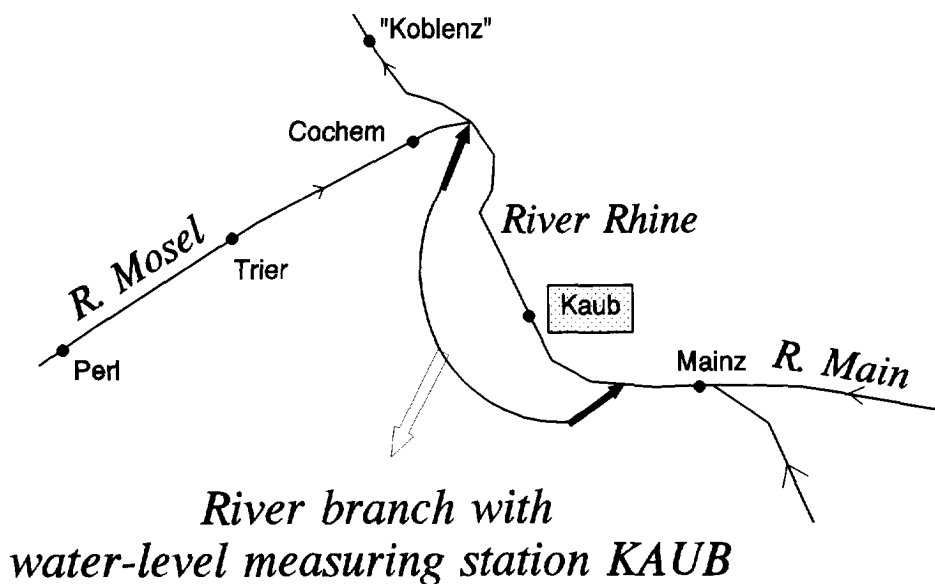
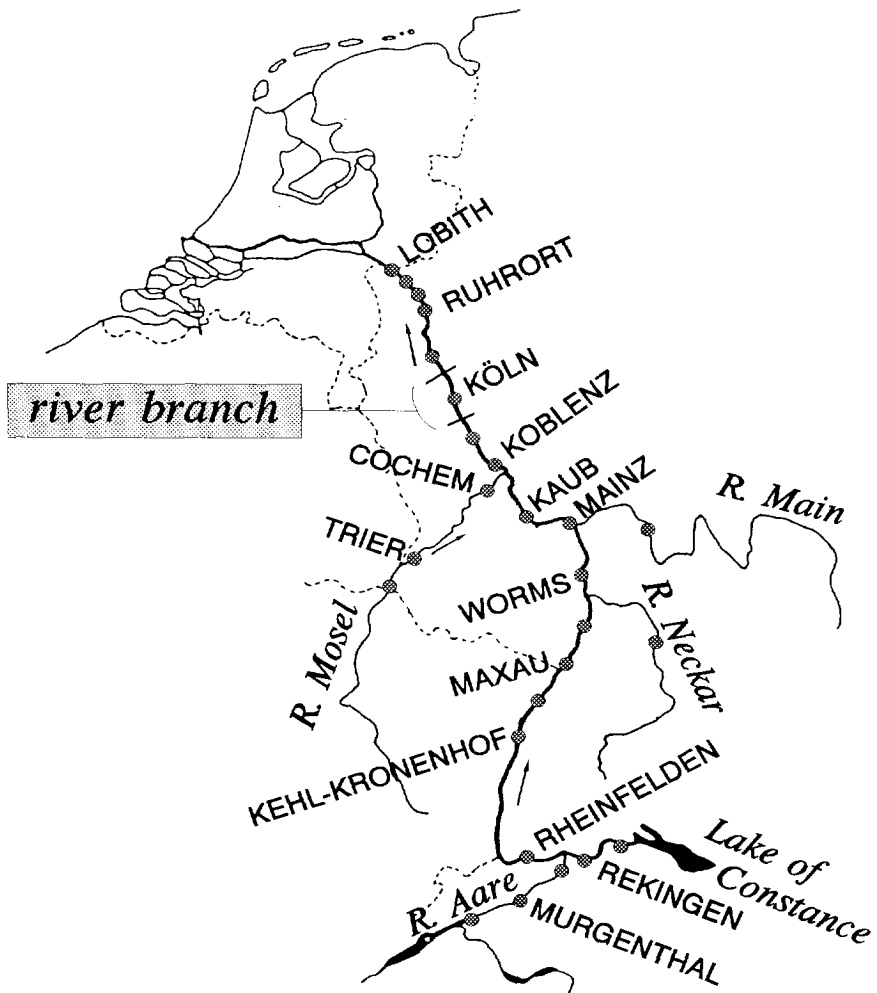


Fig. 3.2.1 Example of a river branch with water-level measuring-station



• *water-level measuring-stations*

Fig. 3.2.2

River Rhine with its main tributaries and the water-level stations (*notice not all stations are named*)

discharge can vary stepwise. In each sub-branch the mean flow-velocity is constant and is determined by the representative discharge and cross-sectional area of the sub-branch concerned.

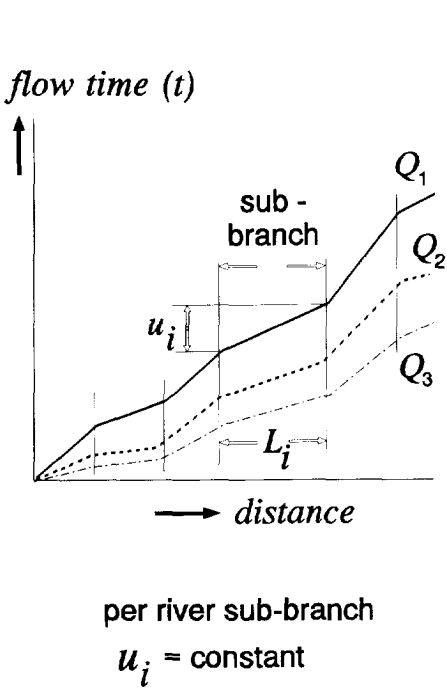


Fig. 3.2.3 Flow time as a function of the distance within a river branch for several river discharges, i.e. water levels

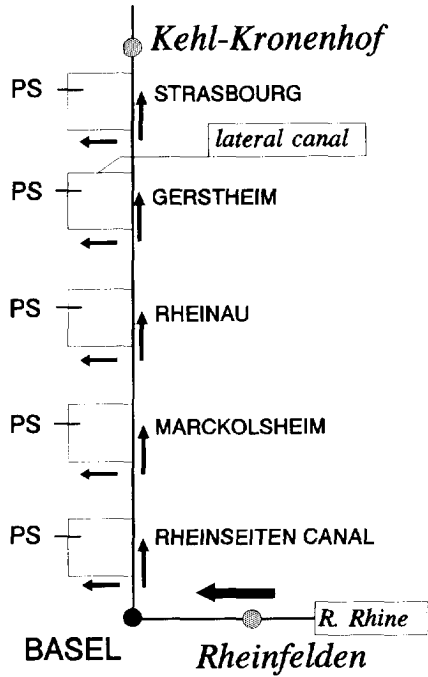


Fig. 3.2.4 The River Rhine between Basel and Kehl-Kronenhof
(PS = power station)

With the sub-branch length L_i and the mean flow-velocity u_i the flow time of the sub-branch per discharge can be determined: $T_i = L_i/u_i$ (Fig. 3.2.3). Because for each branch or sub-branch respectively the discharge is determined by the water-level discharge relation at the measuring stations concerned, the Rhine Alarm-Model uses water-level/flow-time relations for the computation of the travel time of a pollution cloud.

Between Village-Neuf (River-kilometre 173.6) and Kehl-Kronenhof (River-kilometre 292.2) the River Rhine has several lateral branches: canals with power stations (Fig. 3.2.4). These canals are located at the French territory. For the discharge ratio between the canals and the River Rhine, France and Germany made an agreement. This agreement implies a maximum discharge through the canals of

1400 m³/s and a minimum discharge through the River Rhine of 30 m³/s. The discharge ratio is related to the discharge at the water-level station Rheinfelden. The discharge at the water-level station Kehl-Kronenhof is also referred to the measured discharge at Rheinfelden-station.

For the application of the Rhine Alarm-Model it has to be realized that the maximum discharge of 1400 m³/s will be exceeded regularly. Moreover, up till a discharge of 1400 m³/s the discharge control system will be steered by the energy demand of the Electricité de France (EDF): rise-level control. That means that up to a canal discharge of 1200 m³/s the water is stored at night and during periods of high energy demand during the day the stored water is discharged. Therefore the discharge in the canal will be vary more irregularly than in the River Rhine itself. Consequently the flow time of the suppressed-flow river-reach between Basel and Kehl-Kronenhof will not be as constant as it is supposed to be.

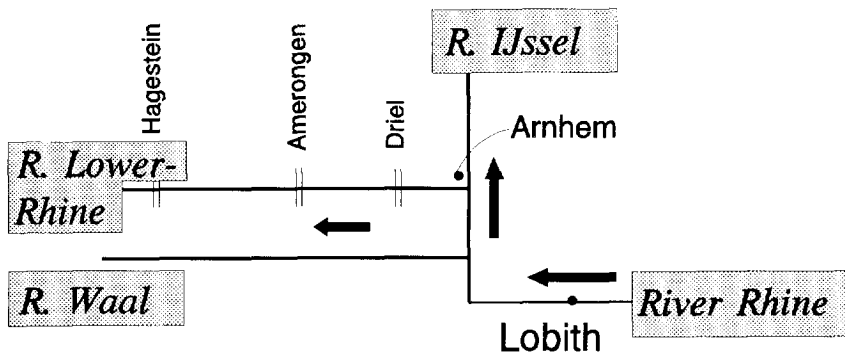


Fig. 3.2.5 The Dutch branches of the River Rhine with the weirs at Driel, Amerongen and Hagestein

The discharge in the Dutch branches of the River Rhine (River Waal, Lower-Rhine River, River IJssel) are related to the water-level station Lobith at the Dutch-German border. The steering of the discharges over these branches is achieved by controlling the weirs at Driel, Amerongen and Hagestein (Fig. 3.2.5). The purpose of the control system is to guarantee a minimum discharge in the River IJssel, whereas the discharge in the Lower-Rhine River stays at 25 m³/s. However, in case of low-water situations these discharge conditions are not always realised, because the control system of the weirs is based on water-level regulation and not on the river discharge.

3.3 CALIBRATION AND VERIFICATION

3.3.1 Calibration methods

In the Rhine Alarm-Model the concentration distribution in the time domain is computed after the Chatwin-model (see Eq. 2.3.85)

$$\varphi_E(L,t) = \frac{M/Q}{\sqrt{4 \cdot \pi \cdot K \cdot t/c^2}} \cdot \exp \left[- \frac{(t - L/c)^2}{4 \cdot K \cdot t/c^2} \right] * \left[1 + \frac{1}{6} \cdot H_3 \left(\frac{t - L/c}{\sqrt{2 \cdot K \cdot t/c^2}} \right) \right] \quad (3.3.1)$$

Now the calibration of the Rhine Alarm-Model concerns two parameters (see also Section 2.3.3):

- the transport velocity c after Eq.(2.3.80)

$$c = \frac{u_s}{1 + \beta} \quad (3.3.2)$$

i.e. *the lag coefficient* β , by which the model flow-time T_u is corrected in order to get a good fit with the measured transport-time T_c of the tracer

$$\beta = \frac{T_c}{T_u} - 1 \quad (3.3.3)$$

- the longitudinal dispersion-coefficient (Eq. 2.3.86) after Fischer et al. (1979)

$$K = \alpha_x \cdot \frac{u_s^2 \cdot B^2}{a \cdot u_*} \quad (3.3.4)$$

i.e. *the coefficient of proportionality* α_x in Eq.(3.3.4).

For the calibration of these parameters the main condition concerned the arrival time of the peak of the concentration distribution of the tracer cloud in the time domain at the distinguished measuring stations. This condition dominates the calibration of the lag coefficient β .

The longitudinal spreading of the tracer cloud with the corresponding concentration distribution is calibrated by fitting the coefficient of proportionality α_x . Because this coefficient directly affects the concentration distribution, it influences indirectly the time of the peak value of the concentration distribution and consequently the calibrated lag-coefficient value. However, initially this influence will be secondary.

The determination of the value of the lag coefficient is based on comparison of the measured concentration distribution with the computed one by the Rhine Alarm-Model. The condition for a good fit of the travel time of the tracer T_c , related to the peak value of the concentration distribution is given by (Fig. 3.3.1)

$$T_d = \frac{(T_c)_{meas.} - (T_c)_{comp.}}{(T_c)_{meas.}} < 0.05 \quad (3.3.5)$$

wherein T_d is the deviation of the measured travel time from the calculated one in terms of percentage (*deviation of travel time*).

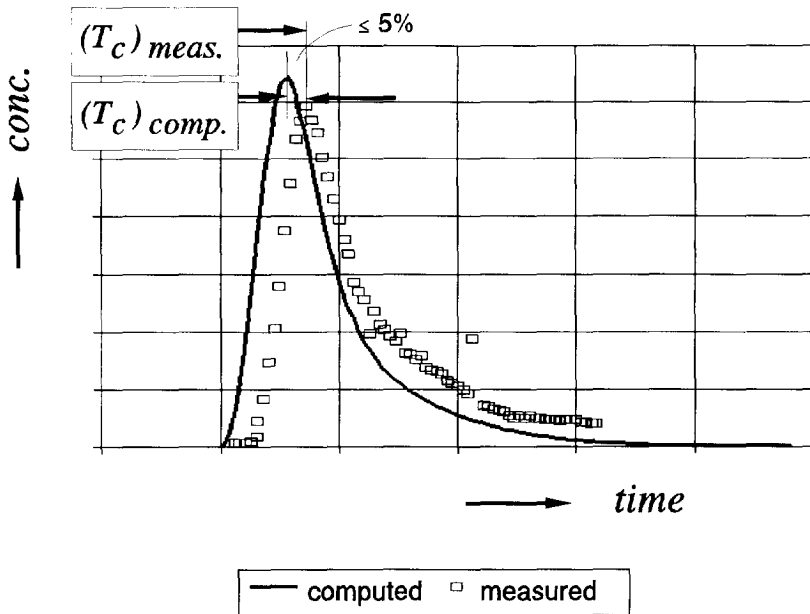


Fig. 3.3.1 Criterion for the comparison of the measured with the calculated transport-time of the tracer

For the fit of the concentration distribution itself, i.e. the spreading of the tracer cloud the deviation between the computed concentrations $(\varphi_{comp.})_i$ and the measured values $(\varphi_{meas.})_i$ is considered

$$\sigma = \left(\frac{\sum_{i=1}^n \left(\frac{(\varphi_{comp.})_i - (\varphi_{meas.})_i}{(\varphi_{comp.})_i} \right)^2}{n} \right)^{1/2} \quad (3.3.6)$$

with σ = the mean deviation
 n = number of considered values

Because in practice the forecasting of the arrival time of the front as well as the peak concentration of a pollution cloud is normative, the determination of the mean deviation σ only considers concentration values $(\varphi_{meas.})_i$ larger than $0.3 \cdot (\varphi_{comp.})_{\max}$, while $(\varphi_{comp.})_{\max}$ is the peak value of the computed concentration distribution. In this way the 'tail' of the concentration distribution is not taken into account.

The best fit of the concentration distribution is found by minimizing the derivatives of σ after α_x and β ($d\sigma/d\alpha_x$ and $d\sigma/d\beta$).

For the calibration of the coefficient of proportionality α_x the computed and measured rate of tracer must be equal at the measuring station concerned. Therefore the input data for the released quantity of tracer in the model M was determined for each measuring station, using the measured concentrations after

$$M = Q \cdot \sum_{i=1}^n (\varphi_{meas.})_i \cdot dt_i \quad (3.3.7)$$

with Q = the mean river-discharge at the river branch concerned
 dt_i = time interval between two concentration measurements

In Eq.(3.3.7) the flux due to the dispersion is neglected, which is acceptable in case of small concentration gradients. At relatively small distances from the point of release this condition is already achieved. Because all tracer experiments were carries out over long distances (more than 10 km) Eq.(3.3.7) will give a good estimation of the flux.

The resulting rates give insight into the degradation of the used tracer. However, for a good determination of these rates the concentration distribution in the time domain has to be complete, which is hardly possible. Besides the detection limit the length of the tail will be mostly too long to be measured completely. Therefore the calculated rate by Eq.(3.3.7) is a first approximation for the calibration. The actual rate has been determined by trial and error during the minimizing-process of the mean deviation between the measured and computed concentration-distribution.

To avoid these iteration processes for the calibration of the lag coefficient β and

the coefficient of proportionality α_x the moments of the measured concentration-distributions are considered (van Mierlo, 1993).

For the calibration of the lag coefficient the travel time of the tracer cloud is related to the time-centroid of the concentration distribution at a measuring station with a distance L from the point of release (see also Eqs (2.3.61) and (2.3.62))

$$\mu_t = \frac{\int_{-\infty}^{+\infty} t \cdot \varphi_{meas.}(L, t) \cdot dt}{\int_{-\infty}^{+\infty} \varphi_{meas.}(L, t) \cdot dt} \quad (3.3.8)$$

The overall lag-coefficient over the distance L is found by

$$\bar{\beta} = \frac{\mu_t}{T_u} - 1 \quad (3.3.9)$$

For the calibration of the coefficient α_x the variance in the time domain is considered

$$\sigma_t^2 = \frac{\int_{-\infty}^{+\infty} (t - \mu_t)^2 \cdot \varphi_{meas.}(L, t) \cdot dt}{\int_{-\infty}^{+\infty} \varphi_{meas.}(L, t) \cdot dt} \quad (3.3.10)$$

After Eq.(2.3.76) it yields

$$K = \frac{1}{(1 + \bar{\beta})^2} \cdot \left(\frac{u_s^3}{2 \cdot L} \right) \cdot \sigma_t^2 \quad (3.3.11)$$

By substituting of Eq.(2.3.86) into Eq.(3.3.11) the relation between the overall value of coefficient of proportionality and the variance becomes

$$\bar{\alpha}_x = \frac{1}{(1 + \bar{\beta})^2} \cdot \frac{a \cdot u_*}{B^2} \cdot \left(\frac{u_s}{2 \cdot L} \right) \cdot \sigma_t^2 \quad (3.3.12)$$

wherein the parameters B , u_s , u_* and a have to be considered as mean values over the distance L .

The significance of the tail of the concentration distribution to the time-centroid

increases with its length. However, a longer tail does not only mean a larger value for time-centroid, but also larger values for the skewness of the concentration distribution. Because there are differences in completeness of the measured concentration-distributions, for instance when the measuring time was too short to get the complete tail of the distribution, it is necessary to use a truncation criterion in order to have comparable results. For the criterion the skewness parameter G_t is used (Eq. 2.3.64)

$$G_t = \frac{|g_t|}{|\sigma_t^3|} \quad (3.3.13)$$

with

$$g_t = \frac{\int_{-\infty}^{+\infty} (t - \mu_t)^3 \cdot \varphi_{meas.}(L, t) \cdot dt}{\int_{-\infty}^{+\infty} \varphi_{meas.}(L, t) \cdot dt} \quad (3.3.14)$$

In the Rhine Alarm-Model G_t is equal to unity in order to get a good reconstruction of the concentration distribution after the Chatwin-model (Eq. 2.3.85). Therefore concentration distribution is truncated for $G_t \approx 1$. Because G_t depends on the value of the time-centroid μ_t which value has to be calculated previously, the determination of the truncation time t_c is an iterative process

$$G_t(t_c) = \frac{\left| \frac{\int_{-\infty}^{t_c} (t - \mu_t(t_c))^3 \cdot \varphi_{meas.}(L, t) \cdot dt}{m_0(t_c)} \right|}{\left(\frac{\int_{-\infty}^{t_c} (t - \mu_t(t_c))^2 \cdot \varphi_{meas.}(L, t) \cdot dt}{m_0(t_c)} \right)^{3/2}} \approx 1 \quad (3.3.15)$$

with

$$m_0(t_c) = \int_{-\infty}^{t_c} \varphi_{meas.}(L, t) \cdot dt \quad (3.3.16)$$

Figure 3.3.2 gives an illustration for the measured concentration-distribution at Rhine-kilometre 362 of the tracer experiment 04/89 (Maximiliansau) and Fig. 3.3.3 presents the corresponding distribution of the skewness for the non-truncated and the truncated situation.

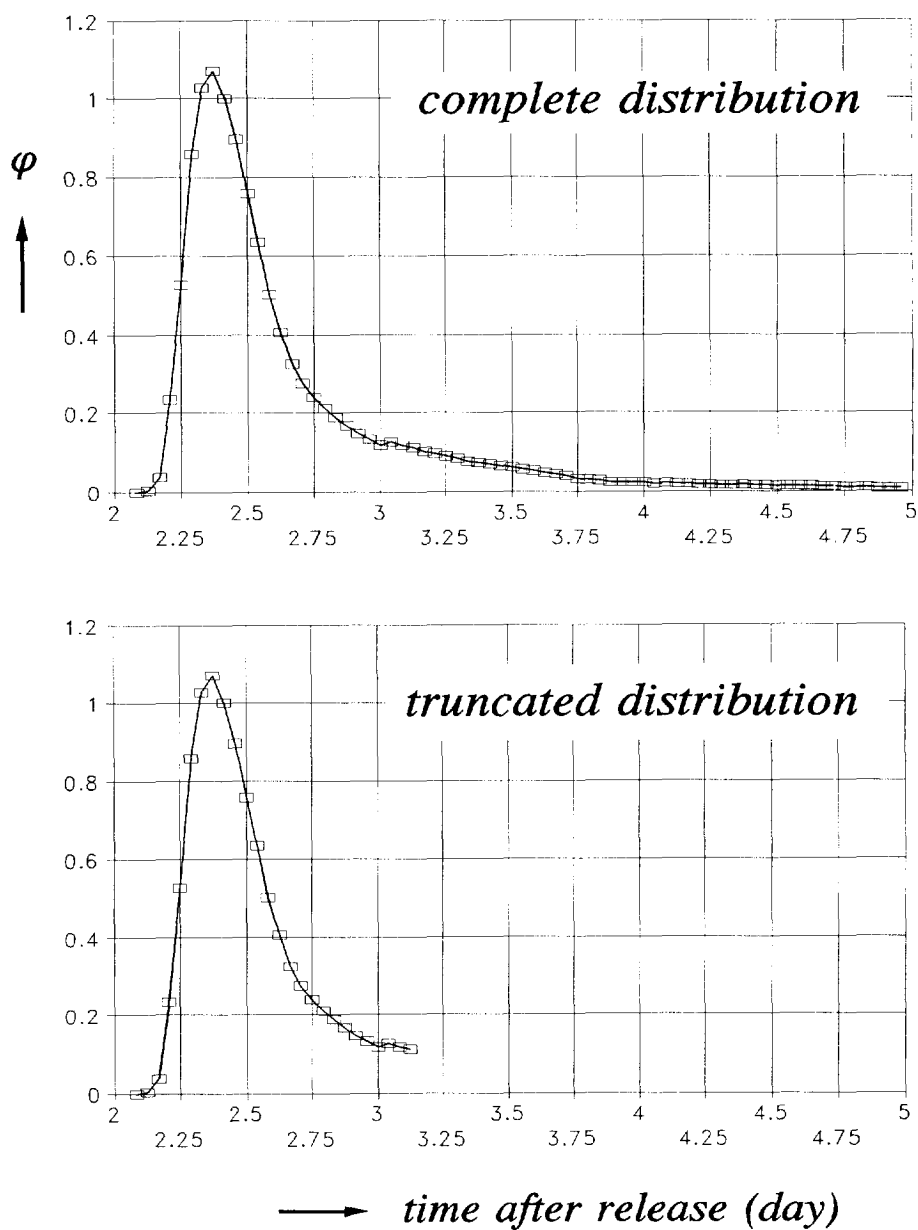


Fig. 3.3.2 Measured concentrations φ at station Maximiliansau (Rhine-kilometre 362), tracer experiment 04/89

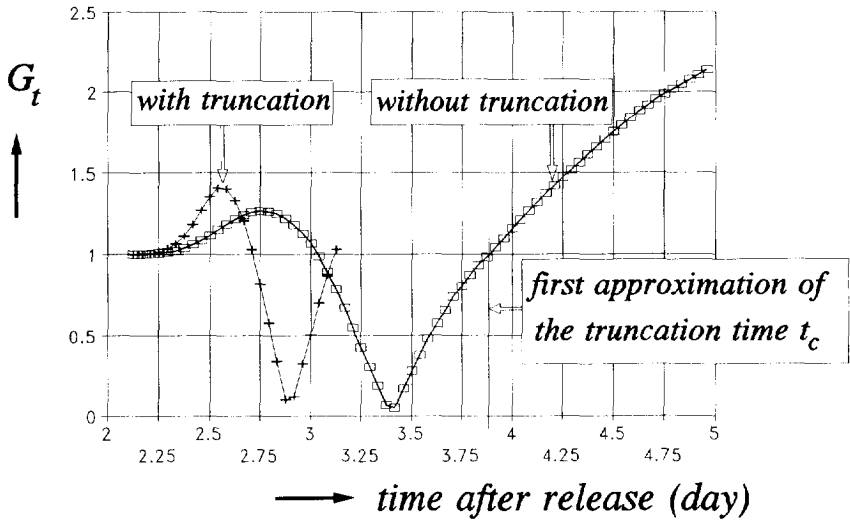


Fig. 3.3.3 Distribution of the skewness G_t , measuring-station Maximiliansau (Rhine-kilometre 362), tracer experiment 04/89

If the measuring time of a concentration distribution is too short to achieve a skewness equal to unity this method does not give reliable values for the time-centroid and variance. However, determination of the time-centroid and the variance as well as the flux by minimizing the difference between the measured distribution and the theoretical approximation after Eq.(2.3.60) is *independent* of the completeness of the measured concentration-distribution. Taking for the skewness G_t and the kurtosis Γ_t the value one and neglecting the fourth ($H_4(\tau)$) and sixth ($H_6(\tau)$) Hermite polynomials, Eq.(2.3.60) becomes

$$\varphi_E(L, t) = \frac{m_0}{\sqrt{2 \cdot \pi \cdot \sigma_t^2}} \cdot \exp \left[-\frac{\tau^2}{2} \right] \cdot \left[1 + \frac{1}{6} \cdot H_3(\tau) \right] \quad (3.3.17)$$

with

$$\tau = (t - \mu_t) / (\sigma_t)$$

and the third Hermite-polynomial

$$H_3(\tau) = \tau^3 - 3 \cdot \tau$$

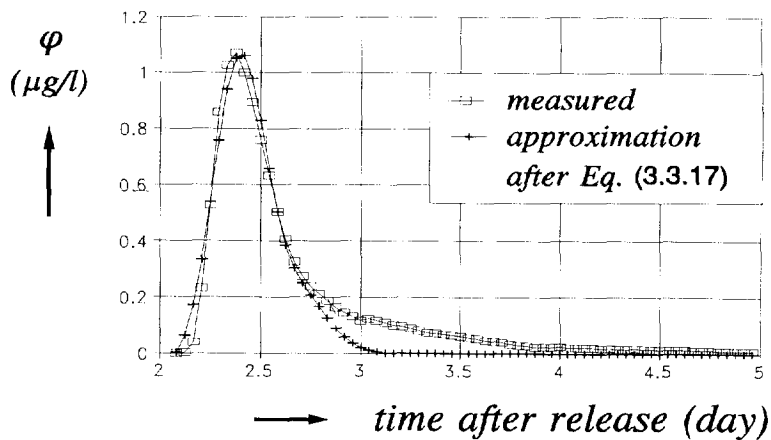


Fig. 3.3.4 Comparison of the measured concentration at Maximiliansau (Rhine-kilometre 362) and the approximation after Eq.(3.3.17), tracer experiment 04/89

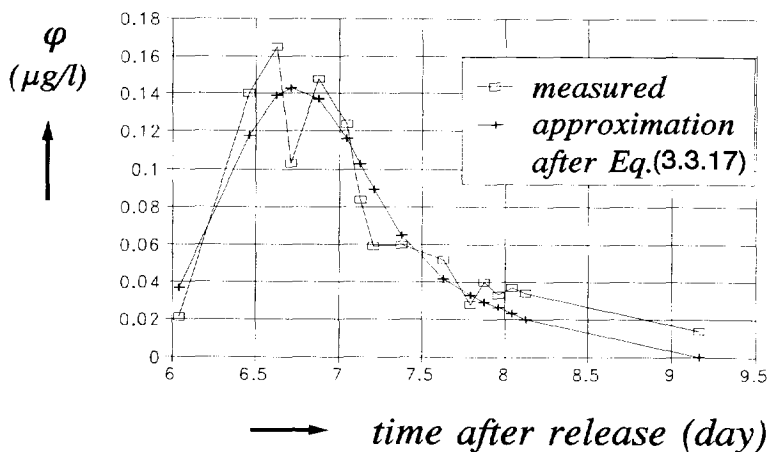


Fig. 3.3.5 Comparison of the measured concentration at Lobith (Rhine-kilometre 862.2) and the approximation after Eq.(3.3.17), tracer experiment 04/89

For the comparison of the measured distribution with the computed distribution after Eq.(3.3.17) a derivative-free Gauss-Newton algorithm, called DUD-method (*Doesn't Use Derivatives*) is applied (Ralston and Jennrich, 1978)¹⁾. In Fig. 3.3.4 and 3.3.5 the measured distributions at stations Maximiliansau (Rhine-kilometre 362) and Lobith (Rhine-kilometre 862.2) are compared with the theoretical approximations after Eq.(3.3.17) with the optimized values of the flux m_0 , the time-centroid μ_t and the variance σ_t for the tracer experiment 04/89.

For the calibration of the Rhine Alarm-Model the lag coefficient β has to be determined per river (sub-)branch i . However, the time-centroid μ_t , based on the moments of the measured concentration-distributions after Eq.(3.3.8) or the DUD-method, gives the overall-value after Eq.(3.3.9). The relation between this overall-value $\bar{\beta} = \beta_j$, considering the travel time over the distance from the point of release to the end of sub-branch j , and the local value β_i per river (sub-)branch can be given by (van Mierlo (1993), see also Appendix C)

$$\beta_j = \frac{\sum_{i=1}^j \left(\frac{\Delta x_i}{u_i} \cdot \beta_i \right)}{\sum_{i=1}^j \frac{\Delta x_i}{u_i}} \quad (3.3.18)$$

wherein Δx_i is the length of sub-branch i .

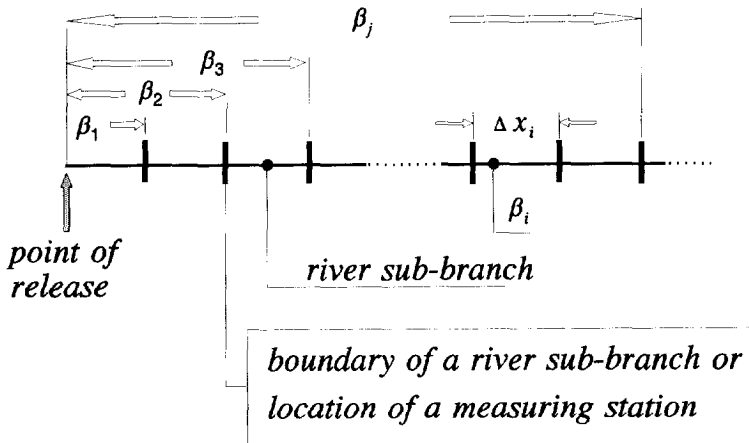


Fig. 3.3.6 Model schematization with sub-branches and the relation between the overall value β_j and the local value β_i per sub-branch

¹⁾ The applied computer-program was developed by Delft Hydraulics.

For practical reasons mostly it is not possible to coincide the measuring stations of a tracer experiment with the boundaries of the (sub-)branches of the model (Fig. 3.3.6). Moreover from a financial point of view it is not possible to carry out concentration measurements at all model-branch boundaries. Therefore the lag coefficients of the (sub-)branches between two successive measuring stations have to be taken equal. If the river reaches between two successive measuring stations are numbered by $1, \dots, m$ and the model (sub-)branches between two successive measuring stations by n_{m-1}, \dots, n_m while n indicates the (sub-)branch concerned, counted from the point of release, Eq.(3.3.18) can be rewritten into

$$\beta_{n_m} = \frac{\beta_1 \sum_{i=1}^{n_1} \frac{\Delta x_i}{u_i} + \beta_2 \sum_{i=n_1+1}^{n_2} \frac{\Delta x_i}{u_i} + \dots + \beta_m \sum_{i=n_{m-1}+1}^{n_m} \frac{\Delta x_i}{u_i}}{\sum_{i=1}^{n_m} \frac{\Delta x_i}{u_i}} \quad (3.3.19)$$

Starting from the point of release the local lag-coefficients per river reach between two successive measuring stations are determined stepwise (see also Fig. 3.3.7)

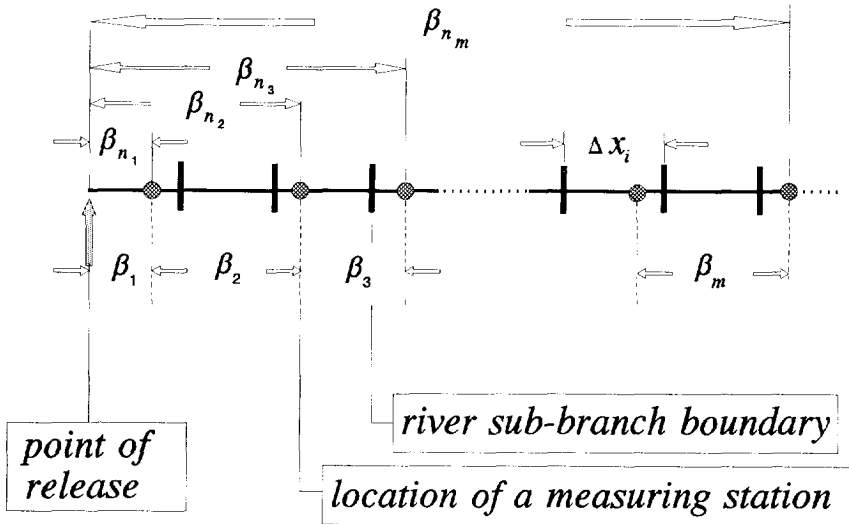


Fig. 3.3.7 Model schematization with sub-branches and the relation between the overall value β_{n_m} and the local value β_m between successive measuring-stations

$$\beta_1 = \frac{\beta_{n_1} \sum_{i=1}^{n_1} \frac{\Delta x_i}{u_i}}{\sum_{i=1}^{n_1} \frac{\Delta x_i}{u_i}} = \beta_{n_1} \quad (3.3.20)$$

$$\beta_2 = \frac{\beta_{n_2} \sum_{i=1}^{n_2} \frac{\Delta x_i}{u_i} - \beta_1 \sum_{i=1}^{n_1} \frac{\Delta x_i}{u_i}}{\sum_{i=n_1+1}^{n_2} \frac{\Delta x_i}{u_i}} \quad (3.3.21)$$

or generally written

$$\beta_m = \frac{\beta_{n_m} \sum_{i=1}^{n_m} \frac{\Delta x_i}{u_i} - \left(\beta_1 \sum_{i=1}^{n_1} \frac{\Delta x_i}{u_i} + \beta_2 \sum_{i=n_1+1}^{n_2} \frac{\Delta x_i}{u_i} + \dots + \beta_{m-1} \sum_{i=n_{m-2}+1}^{n_{m-1}} \frac{\Delta x_i}{u_i} \right)}{\sum_{i=n_{m-1}+1}^{n_m} \frac{\Delta x_i}{u_i}} \quad (3.3.22)$$

From the concentration distributions of two successive measuring-stations the lag coefficient of the river reach m can be found directly after Eq.(3.3.9) by

$$\beta_m = \frac{(\mu_t)_m - (\mu_t)_{m-1}}{(T_u)_m - (T_u)_{m-1}} - 1 \quad (3.3.23)$$

with $(\mu_t)_m$ = time-centroid of the concentration distribution at the upstream boundary of the river reach m
 $(\mu_t)_{m-1}$ = time-centroid of the concentration distribution at the downstream boundary of the river reach m
 $(T_u)_m$ = flow time from the point of release to the upstream boundary of the river reach m
 $(T_u)_{m-1}$ = flow time from the point of release to the downstream boundary of the river reach m

If the location of the measuring station is between the boundaries of a sub-branch the lag coefficient of this branch ($\beta_{composed}$) is the average value of the lag

coefficients of the upstream and downstream river-reach

$$\beta_{composed} \cdot \left(\frac{\Delta x_i}{u_i} + \frac{\Delta x_{i+1}}{u_{i+1}} \right) = \frac{\beta_i \cdot \Delta x_i}{u_i} + \frac{\beta_{i+1} \cdot \Delta x_{i+1}}{u_{i+1}} \quad (3.3.24)$$

wherein β_i = upstream value of the lag coefficient
 β_{i+1} = downstream value of the lag coefficient

Because the flow velocity in a sub-branch is constant $u_i = u_{i+1}$, thus Eq.(3.3.24) can be simplified by

$$\beta_{composed} = \frac{\beta_i \cdot \Delta x_i + \beta_{i+1} \cdot \Delta x_{i+1}}{\Delta x_i + \Delta x_{i+1}} \quad (3.3.25)$$

For the determination of the coefficient of proportionality $(\alpha_x)_i$ per sub-branch the composed longitudinal dispersion-coefficient \overline{K}_s after the Rhine Alarm-Model (van Mazijk et al.(1991), see also Eq. 2.3.85) is considered

$$\overline{K}_s = \frac{K}{c^2} \cdot t \quad (3.3.26)$$

wherein K = longitudinal dispersion-coefficient after Eq.(2.3.86)
 c = transport velocity of the pollutant

The relation between the overall value (subscript $j \rightarrow n_m$) and the local values (subscript i) is given by

$$(\overline{K}_s)_{n_m} = \sum_{i=1}^{n_m} \frac{K_i}{c_i^2} \cdot T_i = \frac{K_{n_m}}{c_{n_m}^2} \cdot T_{n_m} \quad (3.3.27)$$

wherein T is the transport time T_c .

Applying Eq.(2.3.86)

$$K = \alpha_x \cdot \frac{u_s^2 \cdot B^2}{a \cdot u_*} = \alpha_x \cdot \frac{u_s \cdot B^2 \cdot C}{a \sqrt{g}} \quad (3.3.28)$$

and the relation between the variance of the tracer cloud and the dispersion coefficient after Eq.(2.3.83)

$$\sigma_t^2 = \left(\frac{2 \cdot t}{c^2} \right) \cdot K \quad (3.3.29)$$

the overall value of the coefficient of proportionality can be determined, using the second moment of the concentration distributions, by the expression (see van Mierlo, 1993)

$$(\alpha_x)_{n_m} = \frac{(\sigma_t)_{n_m}^2}{2} \cdot \frac{a_{n_m} \cdot \sqrt{g}}{B_{n_m}^2 \cdot C_{n_m} \cdot (1 + \beta_{n_m})^2} \cdot \frac{\sum_{i=1}^{n_m} \Delta x_i}{\left[\sum_{i=1}^{n_m} \frac{\Delta x_i}{u_i} \right]^2} \quad (3.3.30)$$

with

$$a_{n_m} = \frac{\sum_{i=1}^{n_m} a_i \cdot \Delta x_i}{\sum_{i=1}^{n_m} \Delta x_i} \quad B_{n_m} = \frac{\sum_{i=1}^{n_m} B_i \cdot \Delta x_i}{\sum_{i=1}^{n_m} \Delta x_i} \quad C_{n_m} = \frac{\sum_{i=1}^{n_m} C_i \cdot \Delta x_i}{\sum_{i=1}^{n_m} \Delta x_i}$$

and

$$\beta_{n_m} = \frac{(\mu_t)_{n_m}}{\sum_{i=1}^{n_m} \frac{\Delta x_i}{u_i}} - 1$$

Based on Eq.(3.3.27) with Eqs (3.3.2) and (3.3.28) the relation between the overall $[(\alpha_x)_{n_m}]$ and local $[(\alpha_x)_i]$ value of the coefficient of proportionality can be given by (Appendix C)

$$(\alpha_x)_{n_m} = \frac{a_{n_m}}{B_{n_m}^2 \cdot C_{n_m} \cdot (1 + \beta_{n_m})^3} \cdot \frac{\sum_{i=1}^{n_m} \Delta x_i}{\left[\sum_{i=1}^{n_m} \frac{\Delta x_i}{u_i} \right]^2} \cdot \sum_{i=1}^{n_m} \left[\frac{(\alpha_x)_i \cdot B_i^2 \cdot C_i \cdot \Delta x_i}{a_i} \cdot \frac{\Delta x_i}{u_i^2} \cdot (1 + \beta_i)^3 \right] \quad (3.3.31)$$

Given the overall values $(\alpha_x)_{n_m}$ after Eq.(3.3.30) van Mierlo (1993) derived the following relation for the local value of the coefficient per river reach m (see also Appendix C)

$$(\alpha_x)_m = \frac{(\alpha_x)_{n_m} \cdot H_{n_m} \cdot \left[\sum_{i=1}^{n_m} \frac{\Delta x_i}{u_i} \right]^2 \cdot (1 + \beta_{n_m})^3}{P_{n_m} \cdot \sum_{i=1}^{n_m} \Delta x_i} + \quad (3.3.32)$$

$$- \left[(\alpha_x)_1 \cdot \frac{P_{n_1}}{P_{n_m}} + (\alpha_x)_2 \cdot \frac{P_{n_2}}{P_{n_m}} + \dots + (\alpha_x)_{m-1} \cdot \frac{P_{n_{m-1}}}{P_{n_m}} \right]$$

with

$$P_{n_m} = \sum_{i=n_{m-1}+1}^{n_m} H_i \cdot \frac{\Delta x_i}{u_i^2} \cdot (1 + \beta_i)^3$$

and

$$H_q = \frac{B_q^2 \cdot C_q}{a_q}$$

wherein q stands for the subscript concerned.

For the direct determination of the longitudinal dispersion-coefficient and in succession the coefficient of proportionality $(\alpha_x)_m$ per river reach, the measured concentration-distributions at two successive stations have to be used. In this case the analytical solution of the one-dimensional convection-dispersion equation (Eq. 2.1.2) for a given concentration distribution $\varphi_0(x_{m-1}, t)$ at the upstream boundary has to be applied (Appendix D)

$$\varphi(x_m, t) = \Theta \cdot \int_0^t \varphi(x_{m-1}, t - \tau) \cdot \frac{\Delta x_m}{\sqrt{4 \cdot \pi \cdot (K_s)_m \cdot \tau^3}} \cdot \exp \left[- \frac{(\Delta x_m - c_m \cdot \tau)^2}{4 \cdot (K_s)_m \cdot \tau} \right] \cdot d\tau \quad (3.3.33)$$

wherein (see also Fig. 3.3.8)

- Δx_m = $x_m - x_{m-1}$
- x_m = x -coordinate of the downstream boundary of the river reach m
- x_{m-1} = x -coordinate of the upstream boundary of the river reach m
- Θ = rate of loss of matter over the distance Δx_m
- c_m = mean transport-velocity of the pollutant over the river reach m
- $(K_s)_m$ = longitudinal dispersion-coefficient over the river reach m , related to the transport velocity c_m

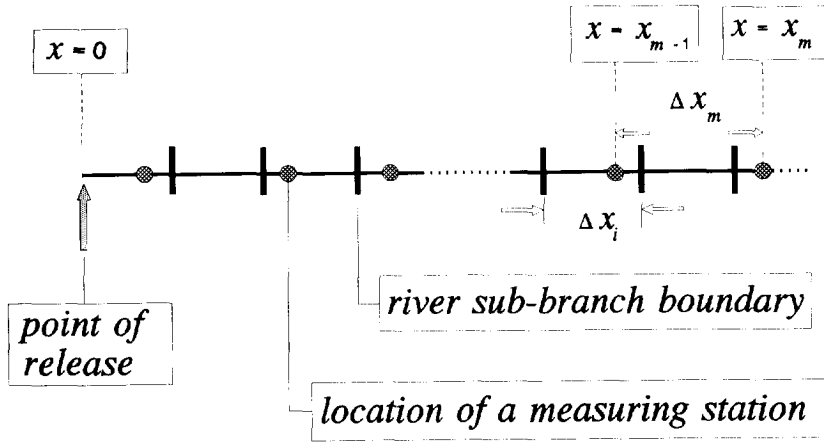


Fig. 3.3.8 Definition of x -coordinate and distances concerning the sub-branches and river reaches between successive measuring stations

The parameters Θ , c_m and $(K_s)_m$ are determined by comparing the computed concentration-distribution $\varphi(x_m, t)$ after Eq.(3.3.33) with the measured distribution, using the measured concentration-distribution $\varphi(x_{m-1}, t)$ as the upstream boundary condition. In the framework of the evaluation of the tracer experiments in the River Rhine, Bremicker (1989) optimized the parameters by the Gauss-Newton iteration algorithm (Hartley, 1961 and Jennrich & Sampson, 1968) after the nonlinear-least-squares method.

With the optimized value of the longitudinal dispersion-coefficient $(K_s)_m$ the coefficient of proportionality can be found from the Eqs 2.3.80, 2.3.81 and 2.3.86

$$(K_s)_m = K_m \cdot (1 + \beta_m)^2 = (\alpha_x)_m \cdot \frac{(u_s)_m \cdot B_m^2 \cdot C_m}{a_m \cdot \sqrt{g}} \cdot (1 + \beta_m)^2 \quad (3.3.34)$$

$$(\alpha_x)_m = (K_s)_m \cdot \frac{a_m \cdot \sqrt{g}}{c_m \cdot B_m^2 \cdot C_m} \cdot \frac{1}{(1 + \beta_m)^3} \quad (3.3.35)$$

in which the subscript m indicates the mean value of the concerned parameter over the distance Δx_m .

In case the location of a measuring station lies between the boundaries of a sub-branch the composed value of α_x can be found by analogy with Eq.(3.3.24) after

$$(\alpha_x)_{composed} = \frac{(\alpha_x)_i \cdot \Delta x_i + (\alpha_x)_{i+1} \cdot \Delta x_{i+1}}{\Delta x_i + \Delta x_{i+1}} \quad (3.3.36)$$

In the Sub-section 3.3.2 the results of the calibration of the parameters β and α_x in the Rhine Alarm-Model, based on the tracer experiments 04/89 and 06/91 are summarized. For the calibration the tracer experiment 06/91 was only partly considered for several reasons (van Mazijk and van Mierlo 1992). The hydrological conditions during the tracer experiment 06/91 downstream of Koblenz are more or less equal to normal conditions, while the conditions during the tracer experiment 04/89 are normal upstream of Koblenz (Fig. 3.1.3). Moreover, the tracer experiment 04/89 includes only one station (Düsseldorf, Rhine-kilometre 759.6) between Koblenz (River-kilometre 592) and Lobith (River-kilometre 862.2) the measured concentration-distribution could be used for the calibration by the optimization-method after Eqs (3.3.5) and (3.3.6). In case of the tracer experiment 06/91 there have been four measuring-stations between Koblenz and Lobith (Table 3.3.1).

TABLE 3.3.1 Measuring stations between Koblenz and Lobith (tracer experiment 06/91)

Measuring station	Rhine-kilometre
Koblenz	590.35
Bad Honnef	640.0
Köln	689.5
Düsseldorf	759.6
Wesel	814.0
Lobith	862.2

The applied calibration-method in Sub-section 3.3.2 concerns the optimization-method, in which the transport velocity of the tracer cloud is related to the peak value of the measured concentration-distributions (Eqs (3.3.5) and (3.3.6)). The methods wherein the time-centroid of the concentration distribution is considered, are used for the evaluation of the results in Section 3.4.

3.3.2 Results

Figure 3.3.9 presents the comparison of the measured and the calculated concentration-distributions after the calibration of the parameters β and α_x for a few measuring stations of the tracer experiment 04/89.

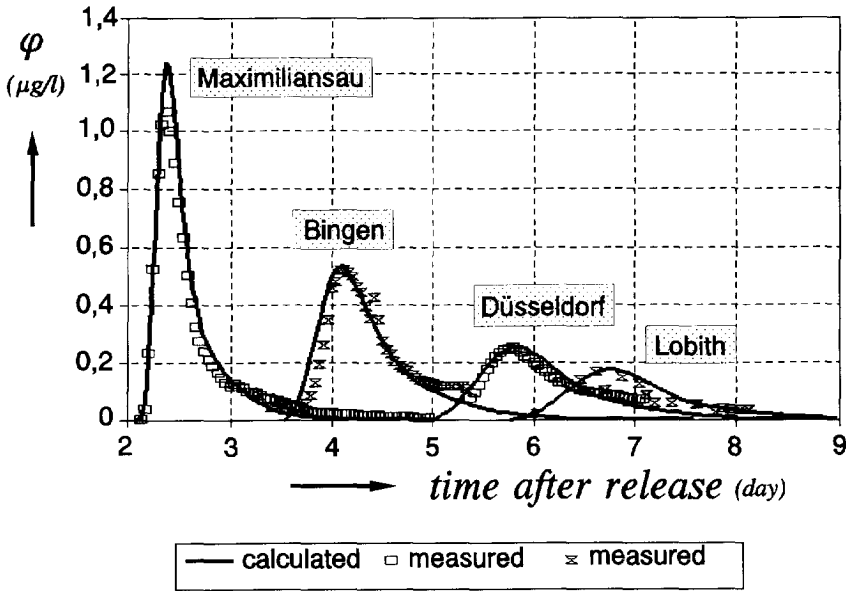


Fig. 3.3.9 Comparison of calculated and measured concentration-distribution, tracer experiment 04/89

In Fig. 3.3.10 the travel time T_u of the water particles, based on the water-level/flow-time relations in the Rhine Alarm-Model during the tracer experiment, is compared with the travel time T_c of the measured peak-concentration of the tracer. The difference between these two travel-times results into the values of the lag coefficient β after Eq.(3.3.3).

The distribution of the lag coefficient β in the Rhine Alarm-Model is presented in Fig. 3.3.11. In this figure the position of the main tributaries are marked, as well as the end of the lateral branches between Basel and Kehl-Kronenhof (see also Fig. 3.2.4). The German-Dutch border is marked by the water-level station Lobith.

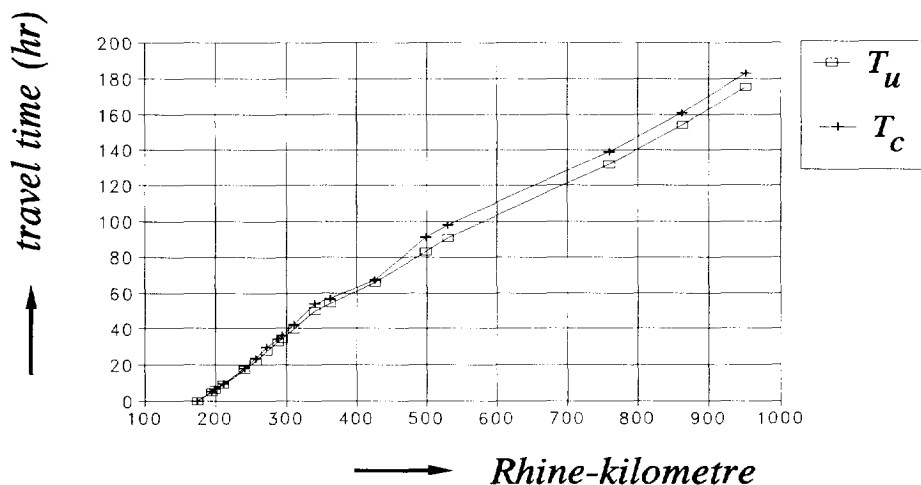


Fig. 3.3.10 Travel time of the peak-concentration compared with the mean flow-time, tracer experiment 04/89

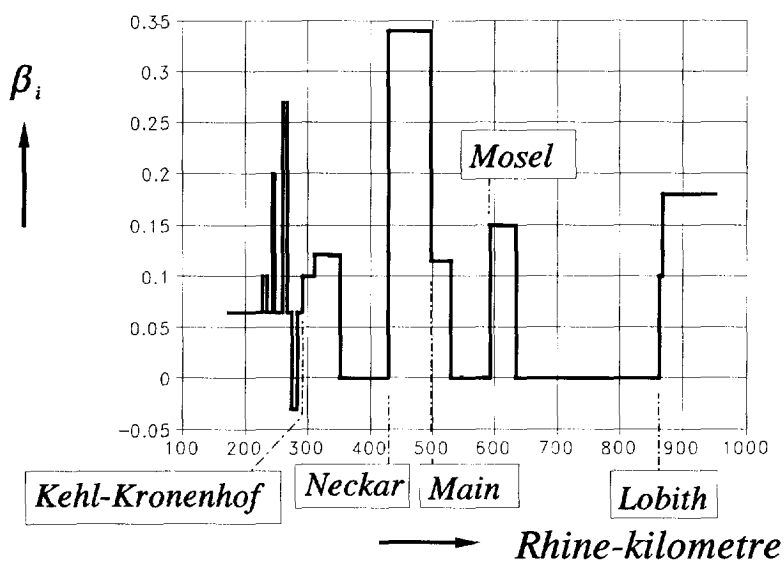


Fig. 3.3.11 Distribution of the lag coefficient β from Basel (Rhine-kilometre 173.6) to Vuren on the R. Waal (Rhine-kilometre 951.8)

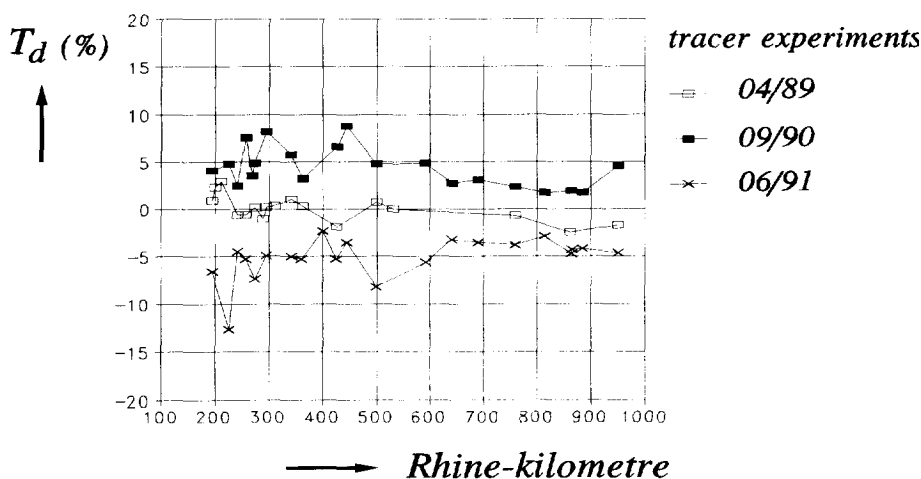


Fig. 3.3.12 Deviation T_d of the measured travel-time from the calculated time after Eq.(3.3.5) for three tracer experiments after calibration by the experiment 04/89

With these values for the β -coefficient the relative difference between the calculated and measured travel-time of the peak concentration of the tracer T_d after Eq.(3.3.5) lies within the 5%-limit (see Fig. 3.3.12). It should be noticed that the resulting β -values are also influence by the optimization of the α_x -parameter as well as the flux M (see also Eq. 3.3.7). Therefore only β -values of 0.05 or more are significant.

Including the additional calibration for the River Rhine reach between Koblenz and Lobith by the tracer experiment 06/91 the 5%-limit for the arrival time of the peak concentrations also holds quite well for the tracer experiments 09/90 and 06/91 (Fig. 3.3.12).

The distribution of the calibrated α_x -value in the Rhine Alarm-Model is presented in Fig. 3.3.13. After Fischer et al. (1979) the semi-empirical value of α_x is 0.011, but can be 4 times smaller and larger. Tracer experiments in the Albert Canal and the Kempen Canals (Belgium) gave values of about ten times smaller, due to the small flow-velocities and therefore relatively uniform flow-velocity profiles over the cross section (Craenenbroeck et al., 1985). Thus it can be concluded that the calibrated values for the canal-reaches between Basel and Kehl-Kronenhof (Rhine-kilometre 292.2) confirm the values of the Belgium canals, while the values for the river-reaches correspond with those, found by Fischer et al. (1979).

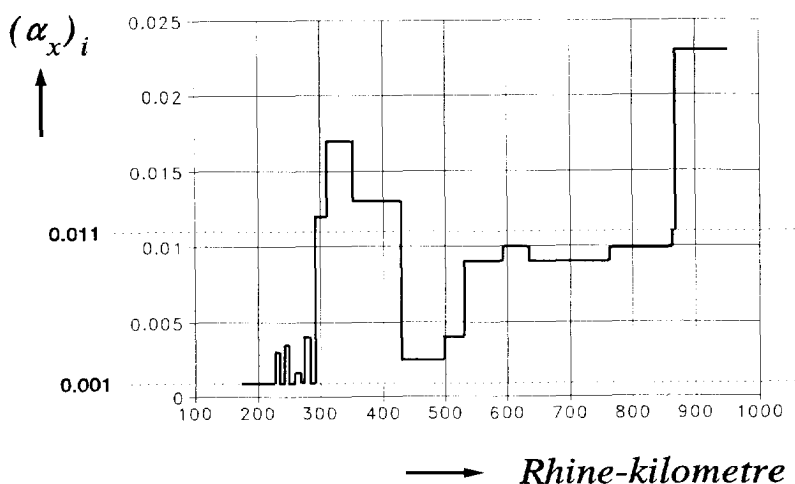


Fig. 3.3.13 Distribution of the coefficient of proportionality α_x from Basel (Rhine-kilometre 173.6) to Vuren on the R. Waal (Rhine-kilometre 951.8)

As already indicated in section 3.2 the three branches of the River Rhine in the Netherlands are represented explicitly in the Rhine Alarm-Model: the River Waal from the bifurcation at Pannerden (Rhine-kilometre 867.2) till Vuren (Rhine-

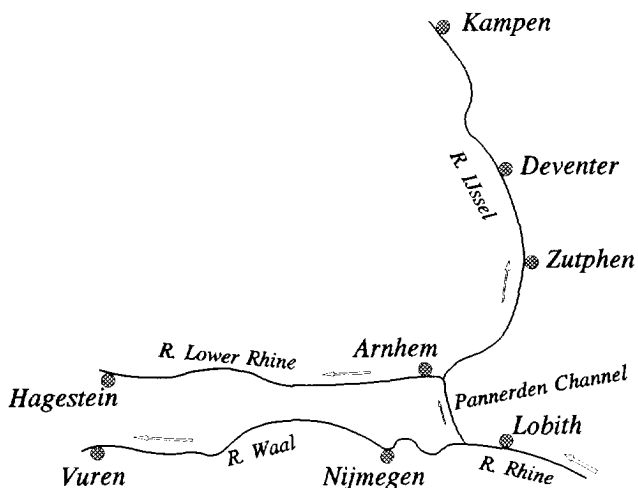


Fig. 3.3.14 Overview of the Rhine branches in the Netherlands downstream of Lobith

kilometre 951.8), the Pannerden Channel from the bifurcation at Pannerden till the bifurcation near Arnhem (Rhine-kilometre 878.5) and from this bifurcation the River Lower Rhine till Hagestein (Rhine-kilometre 946.5) and the River IJssel till Kampen (Rhine-kilometre 994.5). An overview of the Rhine branches is given in Fig. 3.3.14.

In Fig. 3.3.15 the calibrated lag-coefficients β_i for the River-Rhine branches in the Netherlands are presented explicitly.

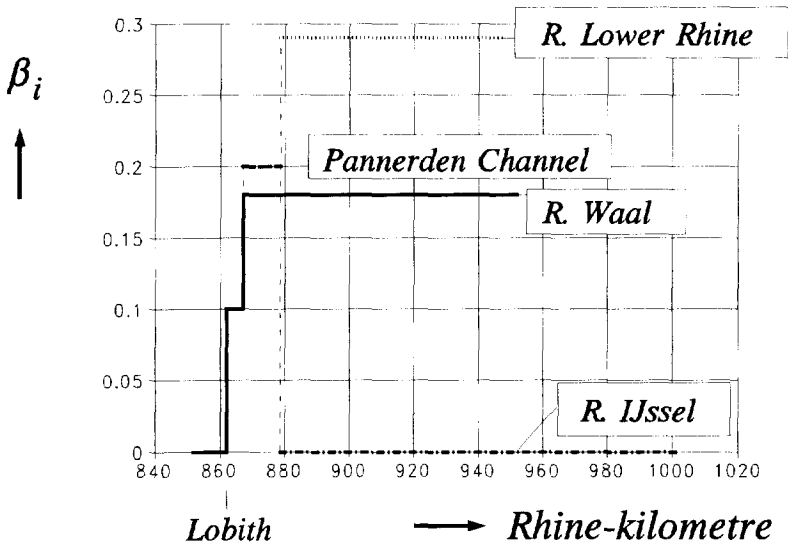


Fig. 3.3.15 Distribution of the lag coefficient β along the Rhine branches in the Netherlands

TABLE 3.3.2 Deviation of the travel time T_d after Eq.(3.3.5) along the Dutch branches of the River Rhine

measuring station	tracer experiment		
	04/89	09/90	06/91
Arnhem (Rhine-km 876.9)	-	5 %	-
Nijmegen (Rhine-km 884.73)	-	3 %	- 3.6 %
Vuren (Rhine-km 951.8)	- 1.75 %	5 %	- 4.0 %
Hagestein (Rhine-km 946.5)	- 1.7 %	-	- 2.8 %
Kampen (Rhine-km 994.5)	- 2.3 %	4 %	-

For the calibration only concentration measurements at Lobith, Vuren, Hagestein and Kampen were available (tracer experiment 04/89). During the tracer experiments 09/90 and 06/91 also concentration distributions at Arnhem and Nijmegen were carried out. The results of these additional measuring-stations were indirectly taken into account for the determination of the parameters by the optimization-method after Eqs (3.3.5) and (3.3.6) related to the peak value of the concentration distribution (van Mazijk and van Mierlo, 1992). The deviation of the travel time T_d after Eq.(3.3.5) for the tracer experiments is presented in Table 3.3.2.

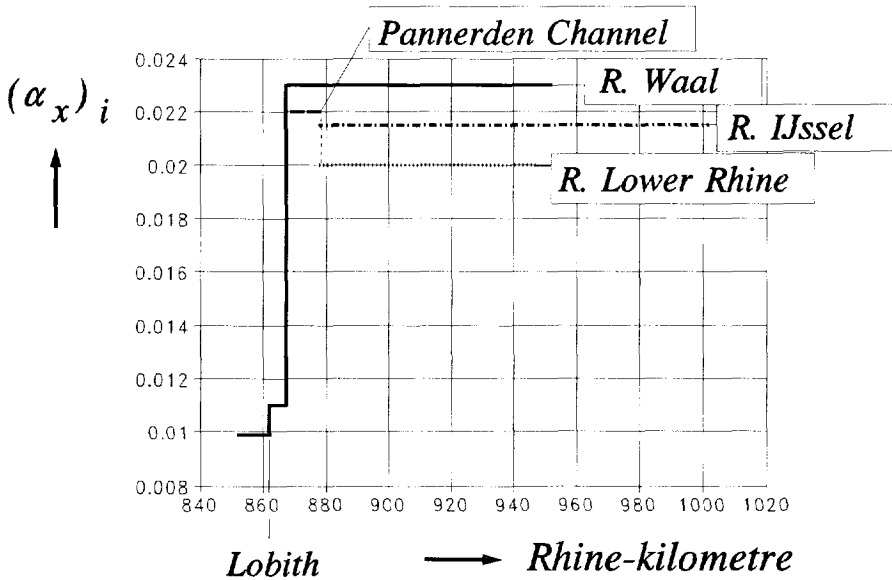


Fig. 3.3.16 Distribution of the coefficient of proportionality α_x along the Rhine branches in the Netherlands

In Fig. 3.3.15 the calibrated α_x -values for the Dutch branches of the River Rhine are presented. The α_x -values are twice the semi-empirical value of 0.011 (Fischer et al., 1979), which is within the margin of the factor four, Fischer et al. (1979) found for natural streams. The reason for these relatively large values could be the presence of the groyne-fields along the Rhine branches in the Netherlands. The additional turbulence, they excite as well as their influence on the cross-sectional velocity-profile, can increase the longitudinal dispersion.

3.4

DISCUSSION

3.4.1 The canalized Rhine between Basel and Kehl-Kronenhof

The calibrated values of the lag coefficient β between Basel and the water-level measuring-station Kehl-Kronenhof will represent the difference between the flow velocity based on the German-French agreement concerning the discharge ratio between the canals and the River Rhine, and the actual flow-velocity. However, this difference depends on the rise-level control by the power stations. Because for small river-discharges the storage period of water will be longer than during larger river-discharges, the difference between the mean flow-velocity after the German-French agreement and the actual velocity will be *larger* in case of *small* river-discharges and *smaller* in case of *larger* discharges. Consequently the deviation T_d will be positive in case of the tracer experiment 09/90 with a smaller discharge than during the experiment 04/89, and negative in the case of the experiment 06/91 with a larger discharge (Fig. 3.3.12).

For verification of this statement the β -values of the canal and river branches in the Rhine Alarm-Model between Basel and Kehl-Kronenhof are calibrated additionally by the experiments 09/90 and 06/91 (van Mazijk and van Mierlo, 1992). The results of this calibration are summarized in Table 3.4.1.

TABLE 3.4.1 Mean values of the lag coefficient β between Basel and Kehl-Kronenhof

	Tracer experiment		
	04/89	09/90	06/91
River discharge at Rheinfelden (m ³ /s)	1170	660	1820
β -value	0.095	0.22	0.023

Using these calibrated values of β for the verification of the Rhine Alarm-Model by the tracer experiments 09/90 and 06/91 the deviation T_d downstream of Kehl-Kronenhof reduces (Fig. 3.4.1). This proves a significant influence of the rise-level control on the transport velocity, which can be hardly taken into account in the Rhine Alarm-Model. On one hand it is difficult to get on-line information about the rise-level control-system and on the other hand the level-discharge manipulations at the power stations result into a variation of the flow-velocity over a relatively short time-interval, which cannot be represented by the Rhine Alarm-Model. Moreover the calibrated lag-coefficient β between Basel and Kehl-Kronenhof represents an artificial manipulation and does not give information about natural transport phenomena.

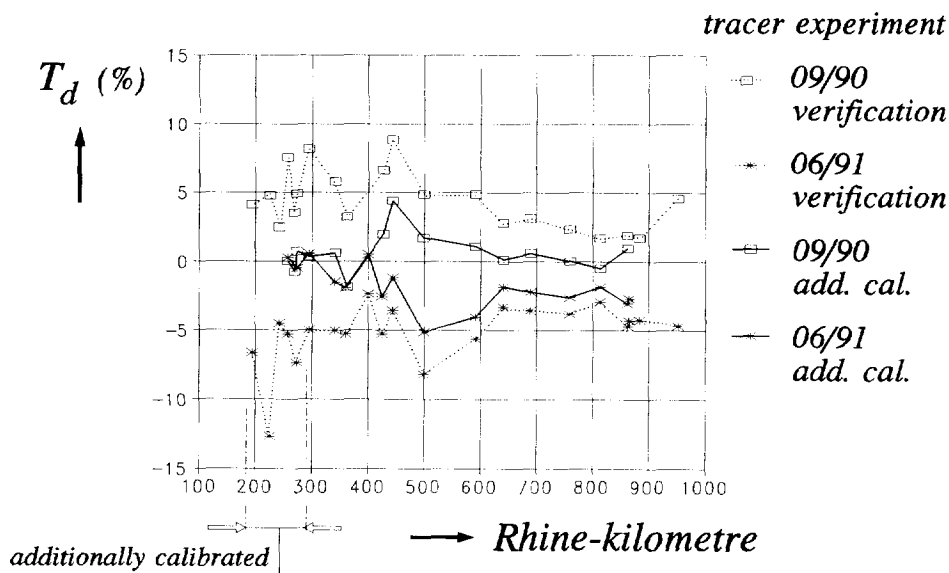


Fig. 3.4.1 Influence of the rise-level control between Basel and Kehl-Kronenhof on the travel time of the tracer

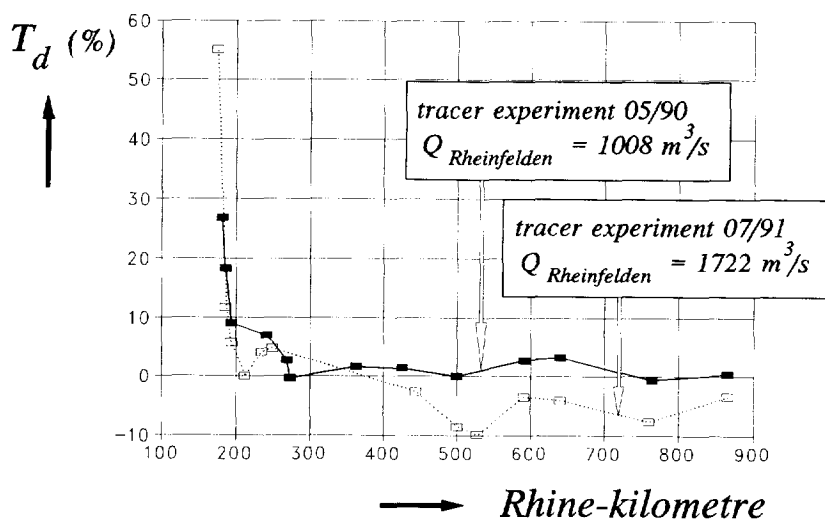


Fig. 3.4.2 Deviation of travel time T_d in case of a release at the bank of the river (tracer experiments 05/90 and 07/91)

Therefore further analysis of the calibrated β -values of the River Rhine between Basel and Kehl-Kronenhof will not be executed, except in relation to the results of the verification by the tracer experiments 05/90 and 07/91, carried out between Huningue and Lobith (Fig. 3.1.1). In case of these experiments the tracer was released at the left bank of the river, about 5 km upstream of the bifurcation of the River Rhine and the Rheinseiten Canal (Fig. 3.1.4).

Especially just downstream of the point of release, where the tracer is not completely mixed over the cross section of the river or canal, the deviation T_d of the travel time is more than 10% (Fig. 3.4.2). This deviation can be explained by the incomplete cross-sectional mixing of the tracer and the flow-velocity profile over the cross-sectional area of the river or canal.

3.4.2 Significance of the lag coefficient between Kehl-Kronenhof and Lobith

Comparison of the 'measured' time-centroid after Eq.(3.3.8) with the truncation condition after Eq.(3.3.15) with the optimized time-centroid after the DUD-method (Ralston and Jennrich, 1978) with Eq.(3.3.17) shows a good agreement (Fig. 3.4.3). Although the concentration distribution of the last measuring-station Lobith is missing a part of the tail (Fig. 3.3.5), this does not disturb this agreement.

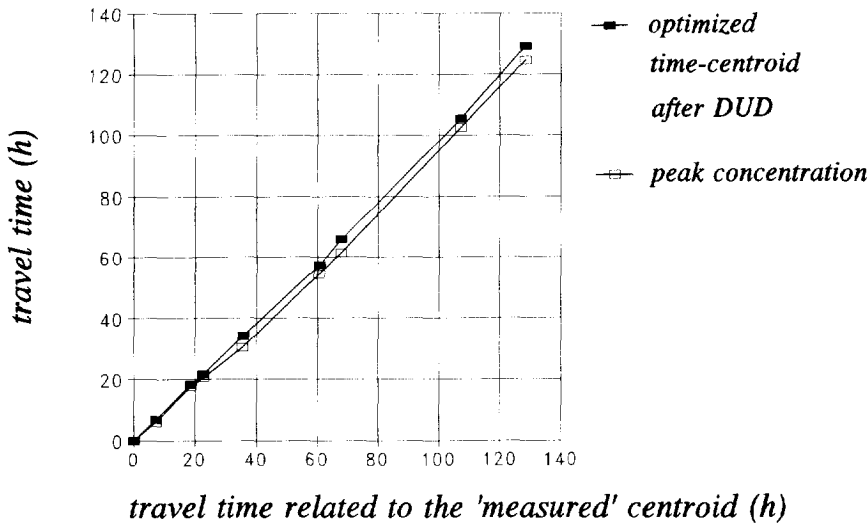


Fig. 3.4.3 Relation between the travel time, based on the 'measured' time-centroid after Eq.(3.3.8) and the travel times, based on the peak-concentration and the optimized time-centroid, applying Eq.(3.3.17)

Apparently the incompleteness of the tail of distribution has no significant effect on the *overall* travel-time of the tracer cloud, related to the time-centroid.

The travel time based on the peak concentration is smaller than the travel time based on the time-centroid. This means that the lag coefficient β , based on the peak concentration (Rhine Alarm-Model) should be smaller than the β -value derived from the 'measured' time-centroid after Eq.(3.3.8). Figure 3.4.4 confirms this more or less up till Rhine-kilometre 500.

Downstream of Rhine-kilometre 500 the tracer-experiment 04/89 only includes three measuring stations: Bingen (Rhine-kilometre 530.15), Düsseldorf (Rhine-kilometre 759.6) and Lobith (Rhine-kilometre 862.2). This means that the positive value of the lag coefficient downstream of the River Mosel, found by the additional calibration of the river reach Koblenz-Lobith by the experiment 06/91, has to be excluded for the comparison with the results, based on the 'measured' time-centroid (Fig. 3.4.4). The negative β -values between Rhine-kilometre 500 and 750 are within the range of non-significance (smaller than 5%). The negative β -value of about 6% downstream of the Rhine-kilometre 750 shows that the incompleteness of the tail of the 'measured' concentration-distribution at Lobith (Fig. 3.3.5) might have an significant effect on the *local* travel-time between two successive measuring-stations (see also Fig. 3.4.5).

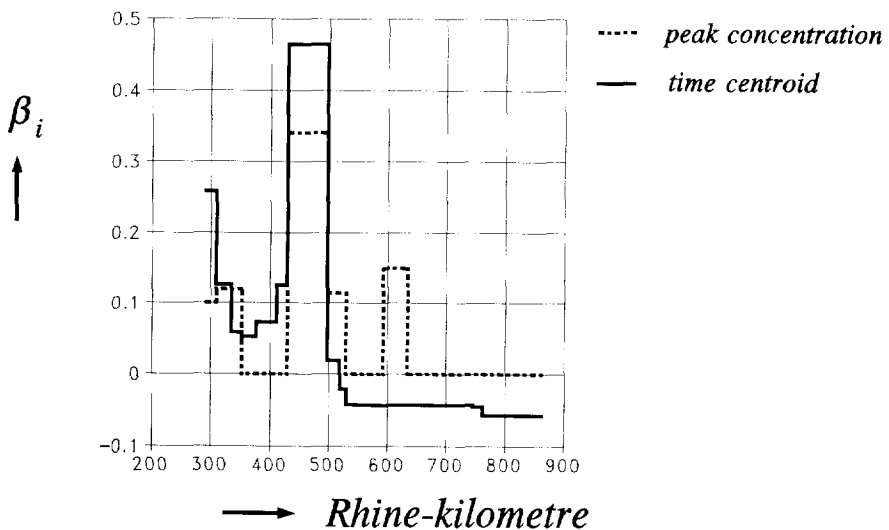


Fig. 3.4.4 Comparison of the distributions of the local lag-coefficient, based on the peak-concentration (Rhine Alarm-Model) and after Eq.(3.3.22), based on the 'measured' time-centroid (Eqs 3.3.8 and 3.3.9)

In Fig. 3.4.5 the local lag-coefficient β is presented per river reach between two successive measuring-stations of the tracer-experiment 04/89 downstream of Kehl-Kronenhof up to Lobith. The β -values are determined after Eq.(3.3.23), using the 'measured' time-centroid after Eq.(3.3.8) with the truncation condition after Eq.(3.3.15) (van Mierlo, 1993) and the optimized value for the time-centroid after the DUD-method. The two methods give comparable distributions with the exception of the last river reach, where the incompleteness of the measured concentration-distribution at Lobith might have caused the negative value instead of the positive one in case of the DUD-method.

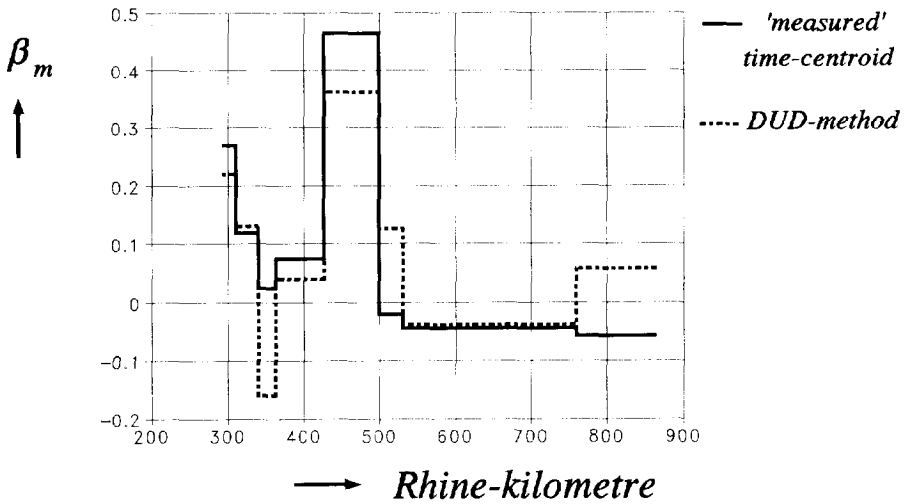


Fig. 3.4.5 Lag coefficient β_m per river reach between two successive measuring-stations from Kehl-Kronenhof downstream to Lobith, tracer experiment 04/89

Although the overall travel-times, based on the 'measured' time-centroid after Eq.(3.3.8) and based on the optimized value after the DUD-method are more or less the same (Fig. 3.4.3), the calculated *local* lag-coefficients β_m after Eq.(3.3.23) can differ significantly (Fig. 3.4.5).

Considering Eq.(3.3.23)

$$\beta_m = \frac{(\mu_t)_m - (\mu_t)_{m-1}}{(T_u)_m - (T_u)_{m-1}} - 1 \quad (3.4.1)$$

with $(\mu_t)_m$ = time-centroid of the concentration distribution at the upstream boundary of the river reach m

- $(\mu_t)_{m-1}$ = time-centroid of the concentration distribution at the downstream boundary of the river reach m
 $(T_u)_m$ = flow time from the point of release to the upstream boundary of the river reach m
 $(T_u)_{m-1}$ = flow time from the point of release to the downstream boundary of the river reach m

it will be clear that small deviations in the time-centroid μ_t or the flow time T_u can give large deviations in the lag coefficient β_m . After the square propagation-law of errors the variance of the lag coefficient β_m can be approximated by

$$\sigma_{\beta_m}^2 = 2 \cdot \sigma_{\mu_t}^2 \cdot \left(\frac{1}{(T_u)_m - (T_u)_{m-1}} \right)^2 + 2 \cdot \sigma_{T_u}^2 \cdot \frac{[(\mu_t)_m - (\mu_t)_{m-1}]^2}{[(T_u)_m - (T_u)_{m-1}]^4}$$

or

$$\sigma_{\beta_m}^2 = 2 \cdot \sigma_{\mu_t}^2 \cdot \frac{1}{(\Delta T_u)_m^2} + 2 \cdot \sigma_{T_u}^2 \cdot \frac{(\Delta \mu_t)_m^2}{(\Delta T_u)_m^4} \quad (3.4.2)$$

- with σ_{μ_t} = standard deviation of the time-centroid
 σ_{T_u} = standard deviation of the flow time

In Table 3.4.2 the data of $(\Delta T_u)_m$ after the Rhine Alarm-Model and $(\Delta \mu_t)_m$ after the DUD-method are presented for the tracer experiment 04/89. The variance of the time-centroid can be estimated at 20 minutes and the variance of the flow-time will be up to 10 till 20 minutes, in accordance with an error in the water-level measurement of about 0.10 m or 5% in the discharge due to inaccuracies in the applied relation between the water level and the river discharge.

TABLE 3.4.2 Data of time-centroid (DUD-method), flow time (Rhine Alarm-Model) and variance of the lag coefficient (tracer experiment 04/89)

river reach between two successive measuring-stations (Rhine-kilometre)	$(\Delta T_u)_m$ (h)	$(\Delta \mu_t)_m$ (h)	β_m	$ \sigma_{\beta_m} $
294.15 - 310.5	5.66	6.9048	0.22	0.11
310.5 - 340.3	10.14	11.4696	0.13	0.06
340.3 - 362	4.07	3.4152	-0.16	0.14
362 - 426.2	11.93	12.4080	0.04	0.05
426.2 - 498.5	17.08	23.2752	0.36	0.04
498.5 - 530.15	7.53	8.4168	0.13	0.08
530.15 - 759.6	41.16	39.5760	-0.04	0.01
759.6 - 862.2	22.49	23.7504	0.06	0.02

In Fig. 3.4.6 the distribution of lag coefficient in accordance to the variance after Table 3.4.2 is presented in comparison with the distribution of the 'measured' time-centroid after Eq.(3.3.8), including the truncation after Eq.(3.3.15).

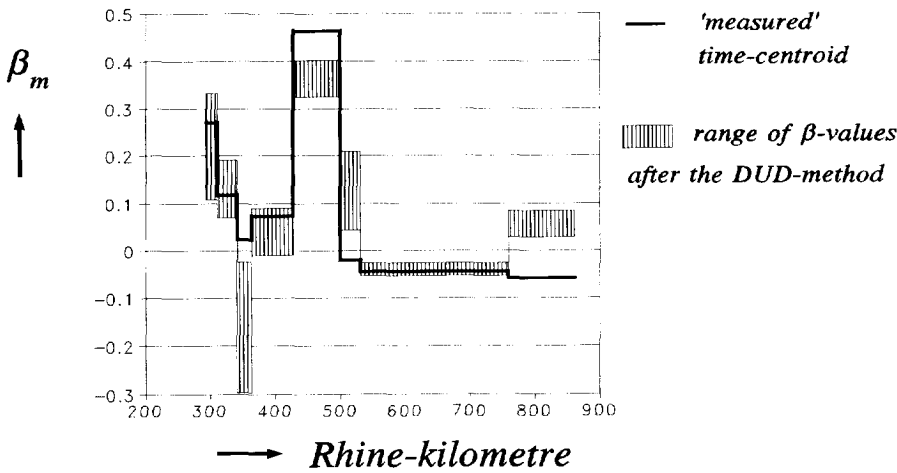


Fig. 3.4.6 Distribution of lag-coefficient

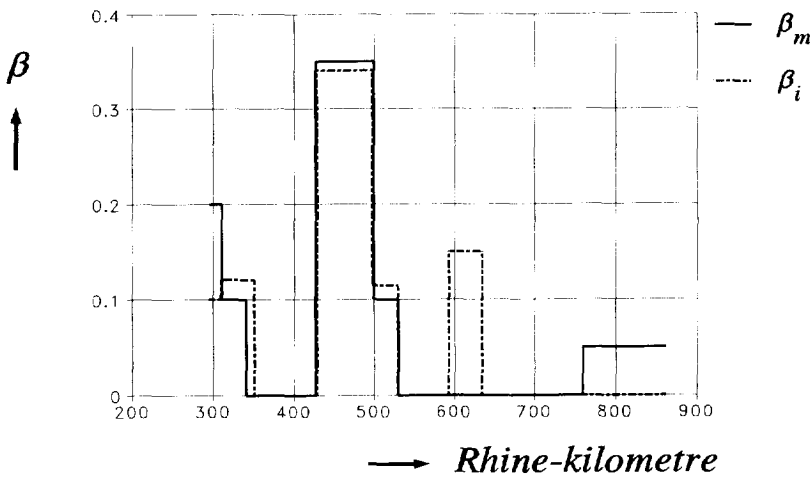


Fig. 3.4.7 Significant values of the lag coefficient. Comparison of the results of the time-centroid (β_m) with the peak-concentration after the Rhine Alarm-Model (β_i)

Figure 3.4.6 shows that the variance of the lag coefficient depends on the distance between two successive tracer measuring-stations: the smaller the distance the larger the error of the lag coefficient becomes. Considering the variance and assuming β_m -values up to 0.05 as non-significant, it can be stated that between the measuring-stations Kehl (Rhine-kilometre 294.15) and Plittersdorf (Rhine-kilometre 340.3) the β_m -value is significantly positive (0.10 till 0.20). Between Plittersdorf and Mannheim (Rhine-kilometre 426.2) the derived β_m -values can be considered as non-significant, which agrees with β_r -values, based on the transport velocity of the peak concentration (Fig. 3.4.4). From Rhine-kilometre 426.2 to 498.5 (Mainz) the value of the lag coefficient is about 0.35 and between Mainz and Bingen (Rhine-kilometre) about 0.10, while over the river reach from Bingen to Düsseldorf (Rhine-kilometre 759.6) the lag coefficient is negligible. Downstream of Düsseldorf the value of β_m tends to a significant value. In Fig. 3.4.7 these conclusions are summarized and compared with the results based on the peak concentration.

3.4.3 Comments on the lag coefficient between Kehl-Kronenhof and Lobith

Figure 3.4.8 presents the schematized River Rhine after the Rhine Alarm-Model between Kehl-Kronenhof and Lobith, including the water-level measuring-stations and the tracer measuring-stations of the experiment 04/89, as well as the additional stations Koblenz (Rhine-kilometre 590.35) and Bad Honnef (Rhine-kilometre 640) of the experiment 06/91.

Mostly a positive β -value indicates stagnant zones with which the tracer exchanges. An examination of the River Rhine between Kehl-Kronenhof and Lobith shows only artificial stagnant zones (groyne-fields) between Rhine-kilometre 290 and 380 and downstream of Rhine-kilometre 650 (Table 3.4.3). Comparing this information with the distribution of the lag coefficient after Fig. 3.4.7, it can be concluded, that the lag coefficient of 0.1 till 0.2 between Rhine-kilometre 294.15 and 340.3, as well as the slight increment of the lag coefficient downstream of Rhine-kilometre 759.6 are caused by groyne-fields. Between Rhine-kilometre 290 and 350 the groyne-fields partly occupy half of the river width (Fig. 3.4.9).

To which extent the rise-level control at the power stations upstream of Rhine-kilometre 290 and the control of the power-stations Gambsheim (Rhine-kilometre 309) and Iffezheim (Rhine-kilometre 334) have influenced the resulting lag-coefficients between Rhine-kilometre 290 and 340, has not been examined.

Apparently the groyne-fields between Rhine-kilometre 350 and 376 as well as between 650 and 760 do not have a significant influence on the local β -value.

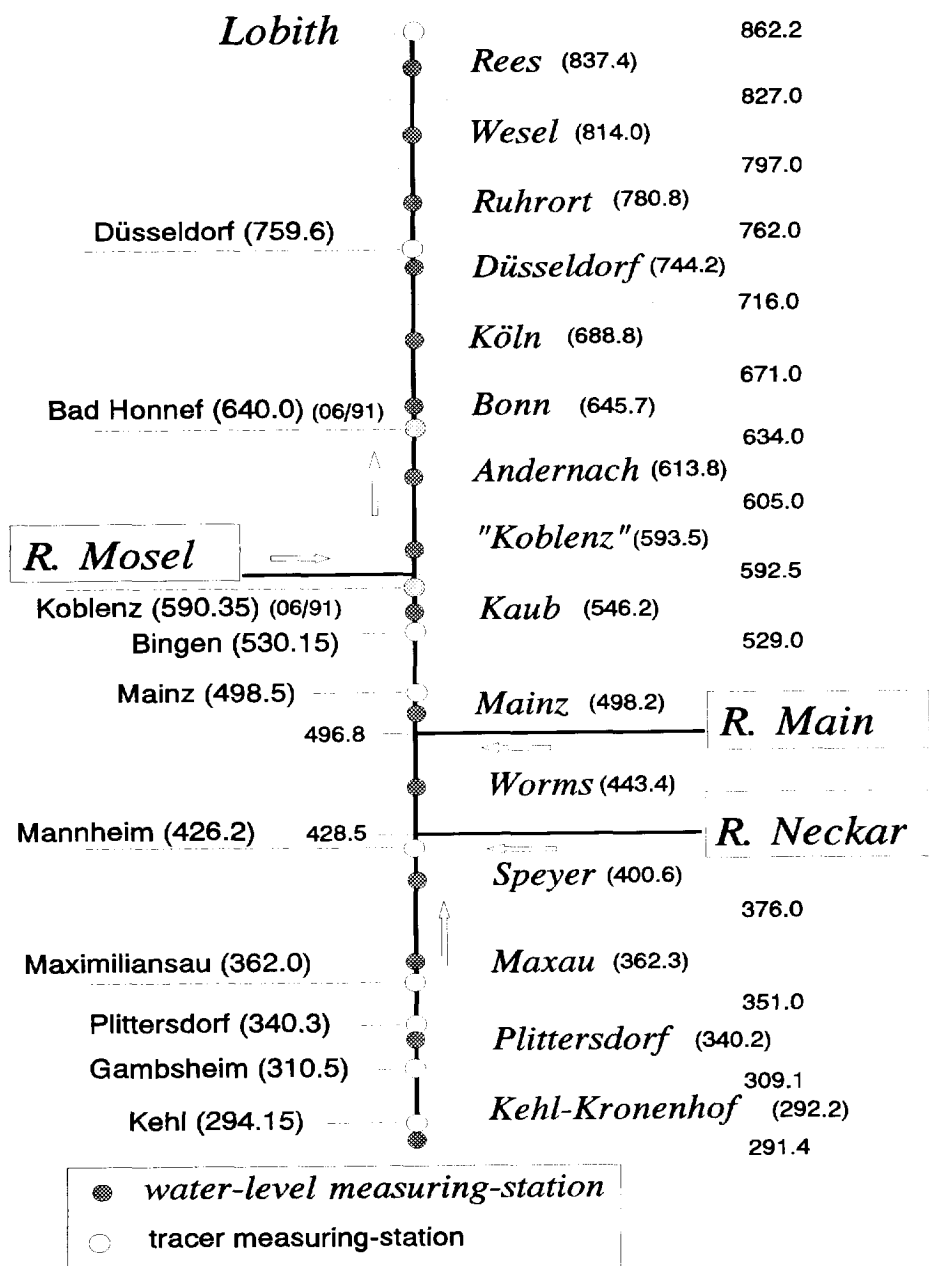


Fig. 3.4.8 Schematic presentation of the River Rhine between Kehl-Kronenhof and Lobith with the tracer measuring-stations, experiment 04/89 and partly 06/91

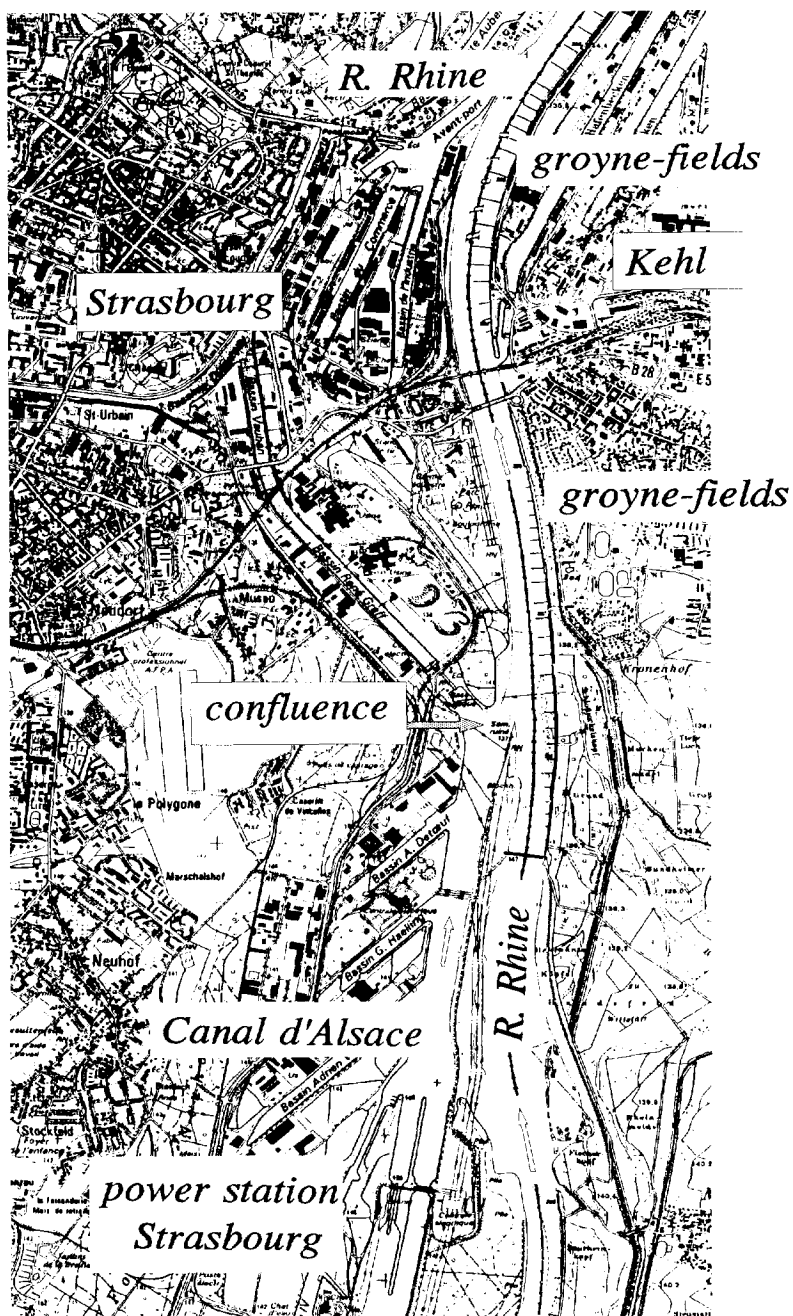


Fig. 3.4.9 Confluence of the River Rhine and the lateral canal (Canal d'Alsace) near the tracer measuring-station Kehl (Rhine-kilometre 294.15)

TABLE 3.4.3 Groyne-fields along the River Rhine between Kehl-Kronenhof and Lobith

Rhine-kilometre	groyne-fields
291 - 299	continuously at the right river-bank
310 - 320	continuously at the right river-bank
320 - 345	fairly continuously at both river-sides
345 - 376	continuously at both river-sides
650 - 740	incidentally at both river-sides
740 - 760	continuously at the left river-bank
760 - 800	incidentally at both river-sides
800 - 846	continuously at the right river-bank
846 - 862	continuously at both river-sides

The large value of the lag coefficient between Rhine-kilometre 426.2 (Mannheim) and Rhine-kilometre 530.15 (Bingen) (see also Fig. 3.4.8) concerns river reaches downstream of the two main tributaries of the River Rhine: the River Neckar at Rhine-kilometre 428.5 and the River Main at Rhine-kilometre 496.8. After the width-ratios of the tributaries and the main river as well as the angle of intersection (see Table 2.2.1) a lag coefficient of 10 till 35% as a result of the cross-sectional flow-velocity profile and an incompletely mixed situation, caused by the inflow of the tributaries cannot be expected in advance (see Section 2.2.2).

TABLE 3.4.4 Lag coefficient β_m for the river reach Mannheim (Rhine-kilometre 426.2) - Mainz (Rhine-kilometre 498.5) in relation to the river discharges

tracer-experiment	River discharges					β_m
	River Rhine water-level measuring-stations			tributaries		
	Speyer	Worms	Mainz	R. Neckar	R. Main	
04/89	1581	1808	2150	227 (14%)	342 (19%)	0.30
09/90	689	748	813	59 (8%)	65 (7%)	0.20
06/91	1827	1929	2084	102 (5%)	155 (8%)	0.02

However, an analysis of the transport of the tracer-cloud between Mannheim and Mainz, based on the time-centroid after the DUD-method for the three tracer-experiments 04/89, 09/90 and 06/91, shows a significant influence of the discharges of the tributaries on the lag coefficient (Table 3.4.4). The discharges of the River Rhine at the water-level measuring-station Worms are during the tracer experiments 04/89 and 06/91 of the same order of magnitude. The discharges of the tributaries are quite different: about 5% of the discharge of the River Rhine in case of the experiment 06/91 and about 15% in case of the experiment 04/89. Consequently high discharges of the tributaries in terms of percentage mean large values of the lag coefficient β_m . Considering the tracer experiments 09/90 and 06/91 the discharges of the tributaries in terms of percentages are more or less the same, while the discharge of the River Rhine differs a factor 2.6 and the lag coefficient a factor 10. Thus for low-water situations the tributaries have relatively more influence on the transport velocity of the tracer cloud than for high-water situations.

The influence of the River Neckar on the transport of the tracer cloud in case of the experiment 04/89 was examined in detail by additionally measured concentration-distributions at Ludwigshafen (Rhine-kilometre 431.0 at the left bank of the river) and Worms (Rhine-kilometre 443.4 in the middle of the river). The results are presented in Table 3.4.5. At the river reach Mannheim-Ludwigshafen the influence of the River Neckar on the tracer transport concerns a river distance of 2.5 km, while at the river reach Worms-Mainz the River Main already influences the transport over a distance of 1.7 km. The influence of the tributaries is evident.

TABLE 3.4.5 Lag coefficient β_m for the river reach Mannheim (Rhine-kilometre 426.2) - Mainz (Rhine-kilometre 498.5), tracer experiment 04/89

river reach		β_m	$ \sigma_{\beta_m} $
Mannheim (km 426.2)	- Ludwigshafen (km 431.0)	1.56	0.77
Ludwigshafen (km 431.0)	- Worms (km 443.4)	0.30	0.20
Worms (km 443.4)	- Mainz (km 498.5)	0.29	0.04

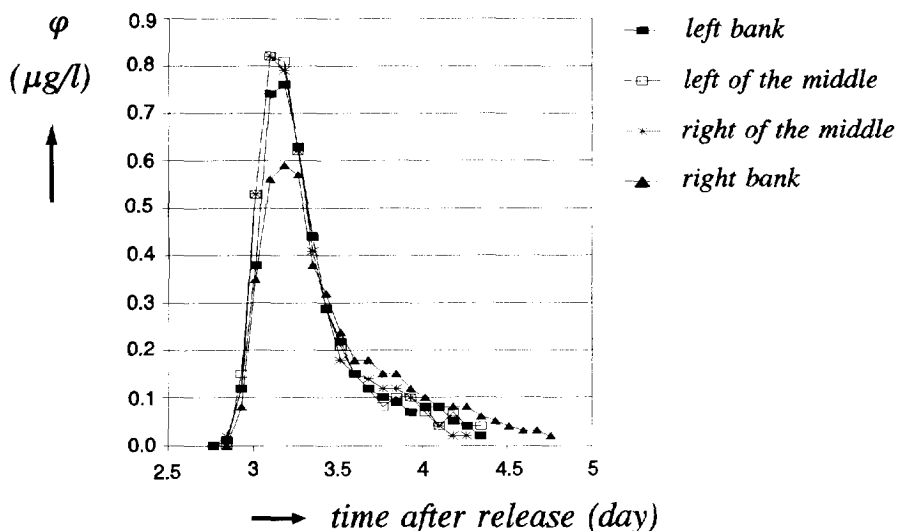


Fig. 3.4.10 Concentration distributions at four positions in the cross section at Mainz, Rhine-kilometre 498.5 (tracer experiment 06/91)

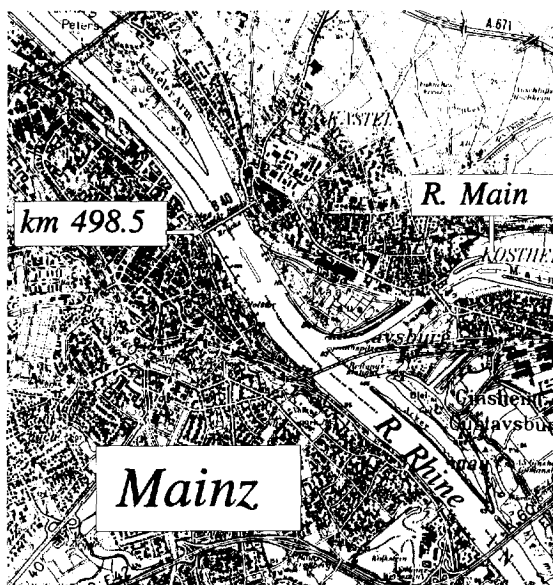


Fig. 3.4.11 Location of the tracer measuring-station Mainz (Rhine-km 498.5)

At short distances downstream of a tributary an inhomogeneous concentration-distribution over the river cross-section will occur. At the river bank the inflow is situated the concentrations will be smaller than in the middle of the stream. Measurements in the cross section at 1.7 km downstream of the inflow of the River Main at the right border of the River Rhine show these differences in Fig. 3.4.10. Figure 3.4.11 shows the location of these measurements.

Considering the time-centroid of the different concentration-distributions, the travel time of the distributions at the river banks are larger (Table 3.4.6).

TABLE 3.4.6 Time-centroid at the measuring-station Mainz (tracer experiment 06/91)

position in the river cross-section	time-centroid (h)
left bank	78
left of the middle of the river	77.5
right of the middle of the river	77.5
right bank	79.5

The time-centroid at the left bank is half an hour later than in the middle of the river and at the left bank about 2 hours. If the difference of 2 hours should be representative for the influence of the tributaries in case of the tracer experiment 06/91, the lag coefficient β_m for the river reach Mannheim - Mainz should become more than 0.10 instead of 0.02.

Referring to the considerations made above it can be concluded that in case of low-water the tributaries Neckar and Main influence the transport of substances significantly ($\beta_m \sim 0.20$). In case of high-water situations there will be also a significant influence, if the discharge of a tributary constitutes a significant part of the total discharge of the River Rhine (more than 10%).

Apparently the retardation of the transport is caused by the exchange of substances between the main stream and the inflow of the tributary with different mean flow-velocities, comparable with the two-zone model after Chikwendu and Ojiakor (1985). For a more detailed quantification of the lag coefficient in relation to the river discharges, flow-patterns downstream of the tributaries have to be measured.

As a matter of fact, the approximation of the two-dimensional transport-phenomena downstream of a tributary by schematizing the polluted river-branch as a number of point releases over a certain width of the river after Eq.(2.2.21) is a simplification, which does not hold quite well (see also Fig. 2.2.10, $B_1/B \sim 0.875$).

The positive lag-coefficient (β_l) downstream of the tributary Mosel (see Fig. 3.3.11) is based on the tracer experiment 06/91: the measured concentration-distributions at Koblenz (Rhine-kilometre 590.35) and Bad Honnef (Rhine-kilometre 640.0) (see also Fig. 3.4.8). Analysis of the transport-time between those two stations after the DUD-method, showed that the calibrated value of 0.15 is not significant (see Table 3.4.7). For comparison also the β_m -value is determined by

TABLE 3.4.7 The lag coefficient downstream of the tributary Mosel (Koblenz) in case of the tracer experiment 06/91

river reach (Rhine-km)	Rhine Alarm- Model β_i	DUD-method β_m		$ \sigma_{\beta_m} $
		peak conc.	time- centroid	
592.5 - 634.0	0.15	-	-	-
590.35 - 640.0	-	0.06	0.02	0.06
426.2 - 498.5 (see Table 3.4.4)	-	-	0.02	0.03

considering the peak value of the optimized concentration-distribution after Eq.(3.3.17) (DUD-method). The results are similar to those found for the river reach Mannheim - Mainz (Table 3.4.4). Likewise the discharges of the tributary and the main river are similar: the discharge of the River Mosel is about 7% of the discharge of the River Rhine upstream of the inflow of the tributary.

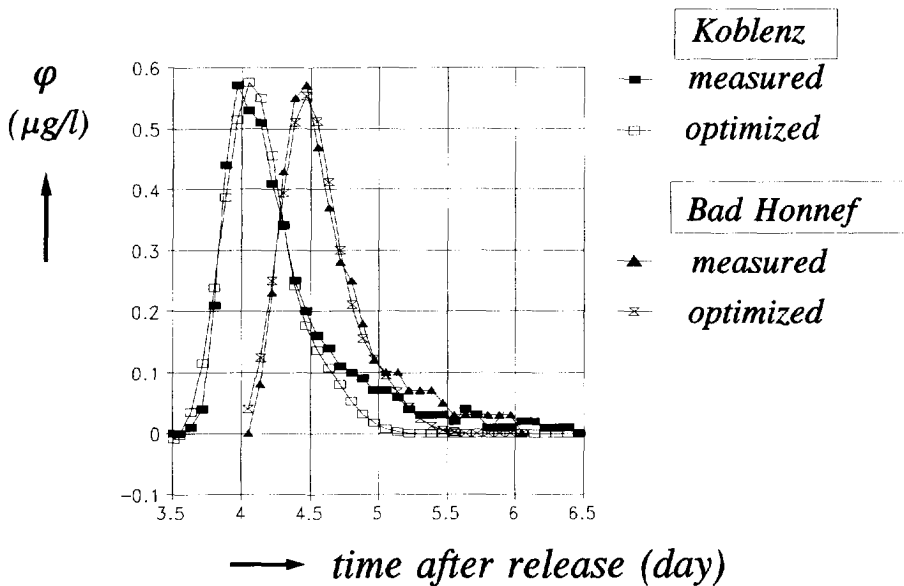


Fig. 3.4.12 Concentration distributions at Koblenz (Rhine-kilometre 590.35) and Bad Honnef (Rhine-kilometre 640), tracer experiment 06/91

The positive value, found after the optimization-method, related to the peak concentration in the Rhine Alarm-Model, might be caused by the deformation of the concentration-distribution between Koblenz and Bad-Honnef, due to the islands in the river bed. In Fig. 3.4.12 the measured concentration-distributions are compared with the optimized distribution after Eq.(3.3.17) (DUD-method). The main deformation concerns the reduction of the length of the tail of the distributions and consequently a reduction of the optimized variance of the distribution. The distributions also show that the distance between the stations Koblenz and Bad Honnef in relation to the travel-time and the variance of the measured concentrations is relatively small. This might have lead to inaccuracies in the determination of the lag coefficient after the applied optimization-method and therefore a relatively unreliable value of the lag coefficient.

Referring to the analysis of the travel-time between Mannheim and Mainz for low-water situations the lag coefficient between Koblenz and Bad Honnef must have a significant value. Analysis of the concentration distributions at Koblenz and Bad Honnef at low-water conditions (tracer-experiment 09/90) after the DUD-method confirm this expectation $\beta_m > 0.05$ (Table 3.4.8)

TABLE 3.4.8 The lag coefficient between Koblenz (Rhine-kilometre 590.35) and Bad Honnef (Rhine-kilometre 640)

tracer-experiment	river discharge		β_m	$ \sigma_{\beta_m} $
	River Rhine (upstream of R.Mosel)	River Mosel		
06/91	2150	140 (7%)	0.02	0.06
07/91	1700	120 (7%)	0.03	0.05
09/90	800	80 (10%)	0.08	0.04
04/89	2350	500 (20%)	0.03	0.06

The measured concentration-distributions at Koblenz and Bad Honnef, during the tracer experiment 04/89 were incomplete and showed measurement errors, which made these measurements inapplicable for the optimization-method, related to the peak concentration. However, by using the DUD-method and adapting the distributions to the most plausible ones by the following corrections (see Fig. 3.4.13):

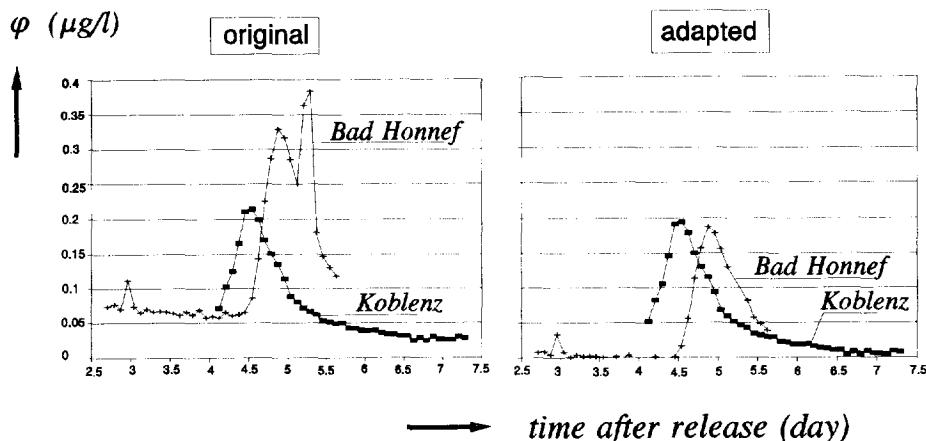


Fig. 3.4.13 Adaptation of the measured concentration-distributions at Koblenz (Rhine-kilometre 590.35) and Bad Honnef (Rhine-kilometre 640), tracer experiment 04/89

- correcting the measured concentrations by an estimated background-concentration;
- dividing the measured concentrations at Bad Honnef by a factor 1.42, according to a revised value of the used reference-substance, which at a later stage was applied for a number of measured distributions of the tracer experiment 04/89 and
- neglecting the second peak-values of the distribution at Bad Honnef, an analysis of the travel time has become possible. The results are presented in Table 3.4.8.

Considering the discharges of the River Rhine and the River Mosel, it can be concluded that in contrast with the inflows of the tributaries Neckar and Main, the inflow of the River Mosel effects the transport of the tracer only in case of low-water conditions.

3.4.4 Comments on the dispersion coefficient between Kehl-Kronenhof and Lobith

After Nordin and Troutman (1980) the variance of the concentration distribution in the time domain increases linear with the distance to the point of release (see also Eq. 2.3.70). In Fig. 3.4.14 this relation is presented for the tracer experiment

04/89, considering the 'measured' variance after Eq.(3.3.10) with the truncation of the tail of the concentration-distribution after Eq.(3.3.15) and the DUD-method, applying Eq.(3.3.17). The 'measured' variances, applying Eq.(3.3.10) on the measured distributions is systematically larger than those determined by minimizing the difference between the measured distribution and the approximation by Eq.(3.3.17) after the DUD-method. However, generally both plots show an increment of the variance with the distance.

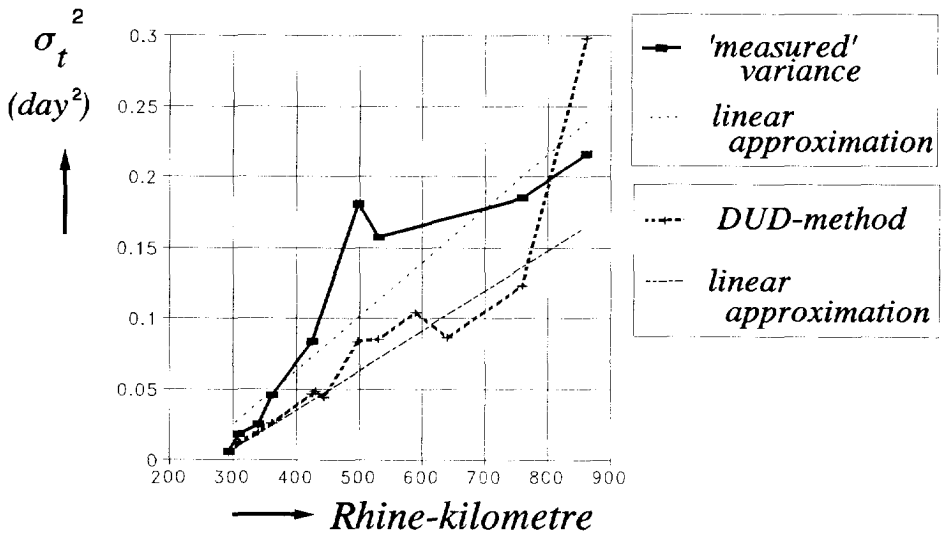


Fig. 3.4.14 Plot of the variance σ_t^2 as a function of the distance, tracer experiment 04/89

The truncation of the tail influences the value of the variance directly. The more the tail is truncated the smaller the variance becomes. As a matter of fact the value of the variance is significantly influenced by the truncation condition and the reliability and the completeness of the measured concentration-distribution. This makes the determination of the coefficient of proportionality α_x , based on the moments of the measured concentration-distributions less objective than the DUD-method, by which the measured concentration-distribution is compared with the approximation after Eq.(3.3.17). This conclusion is in contrast with the determination of the time-centroid, which is restrictedly influenced by the truncation condition (see also Fig. 3.4.3). Due to the mentioned influence of the truncation condition on the determination of the time-variance, the results of this method are not used for further analysis.

In Fig. 3.4.14 the distribution of the time-variance after the DUD-method has two spots, where the variance is decreasing: between Ludwigshafen (Rhine-km 431.0)

and Worms (Rhine-km 443.4) and between Koblenz (Rhine-km 590.35) and Bad Honnef (Rhine-km 640.0). These stations are situated in the vicinity of the main tributaries Neckar and Mosel. To what extent downstream of tributaries the flow patterns for instance can reduce the variance in the time-domain has not been examined. On the other hand these stations were not taken into account for the calibration of the Rhine Alarm-Model, because the measured distributions were not applicable for the used optimization-method, related to the peak concentrations (see also Fig. 3.4.13). Therefore these stations are left aside for the analysis of the coefficient of proportionality α_x .

The extremely large value of the time-variance at Lobith (Rhine-km 862.2) is probably caused by the peculiar distribution of the measured concentration (see Fig. 3.3.5). After the plot of Fig. 3.4.14 a more realistic value could be 0.17 day².

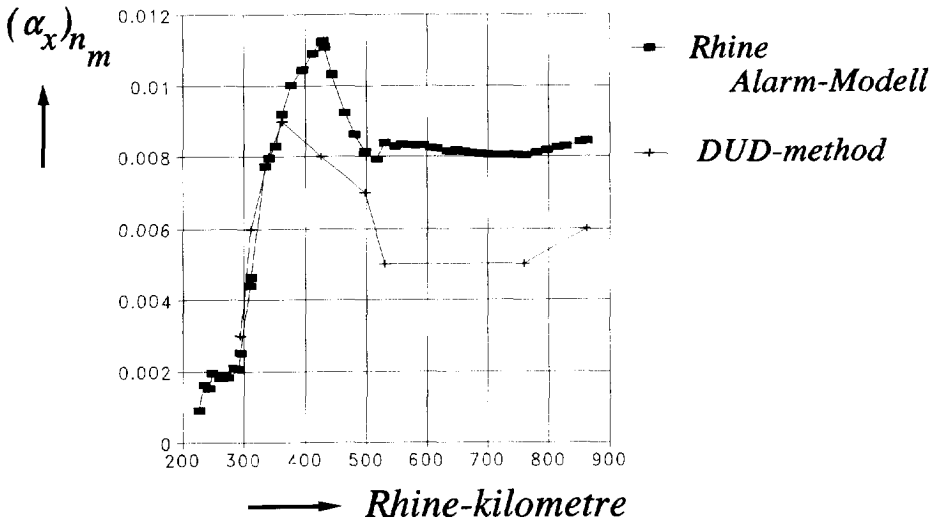


Fig. 3.4.15 Overall value of the proportionality coefficient α_x for the experiment 04/89, based on the Rhine Alarm-Model values after Eq.(3.3.31) and the variance after the DUD-method with Eq.(3.3.30)

In Fig. 3.4.15. the distribution of the overall value of the coefficient of proportionality α_x is presented concerning to the calibrated values $(\alpha_x)_i$ of the Rhine Alarm-Model after Eq.(3.3.31) and the time-variance after Eq.(3.3.30). Both distributions show a decrease of the coefficient between the measuring stations Mannheim (Rhine-km 426.2) and Bingen (Rhine-km 530.15), the river reach where the two main tributaries Neckar and Main flow into the River Rhine. Apparently these tributaries not only cause a significant retardation of the transport velocity (Section 3.4.3), but also influence the concentration distribution in such a way, that

the variance decreases locally. In accordance to this reduction the local values of the proportionality coefficient will be very small over this river reach (Fig. 3.4.16).

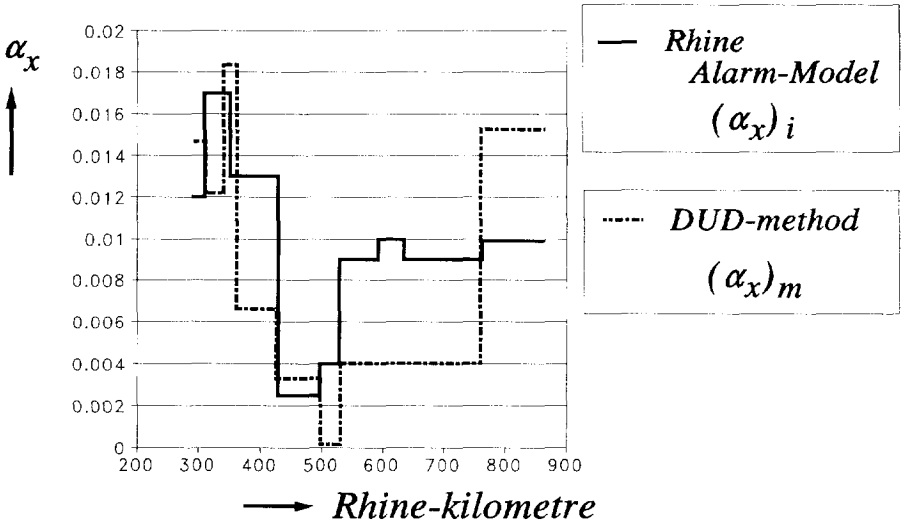


Fig. 3.4.16 Comparison of the distributions of the local value of the coefficient of proportionality α_x after the Rhine Alarm-Model and based on the time-variance after the DUD-method

Downstream of Rhine-kilometre 362 (Maximiliansau) the α_x -coefficient after the Rhine Alarm-Model is systematically larger than the coefficient, based on the time-variance after the DUD-method. A reason for this difference is the applied optimization-method. In case of the calibration of the Rhine Alarm-Model after Eq.(3.3.6), the tail of the concentration distribution is taken into account, while the optimization after the DUD-method considers the peak values as more important than the tail values (see Fig. 3.4.17 and 3.4.18).

In case of the measuring-station Düsseldorf (Fig. 3.4.18) the measured concentration-distribution as well as the optimized distribution after the DUD-method concern a distribution, which is corrected by a background concentration. For the optimization in the Rhine Alarm-Model the non-corrected concentration-distribution was used (Fig. 3.4.19).

The comparisons of the optimized concentration-distributions in Figs 3.4.17 and 18 show that the DUD-method sometimes can give a smaller value, but considering the relative importance of the tail, this method will mostly give the best approximation. Due to the large variation of the α_x -coefficient with a factor 4, as

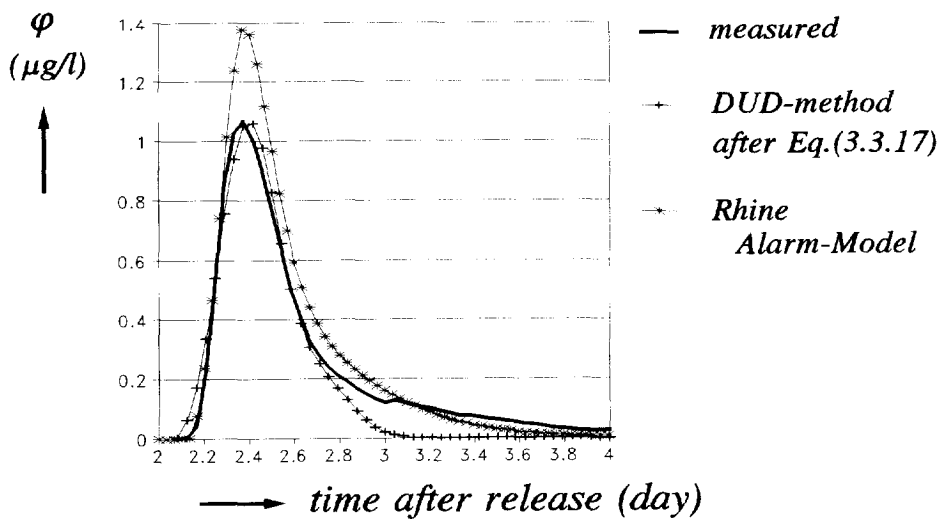


Fig. 3.4.17 Comparison of the measured concentration-distribution at Maximiliansau (Rhine-km 362) with the approximations after the optimization-methods

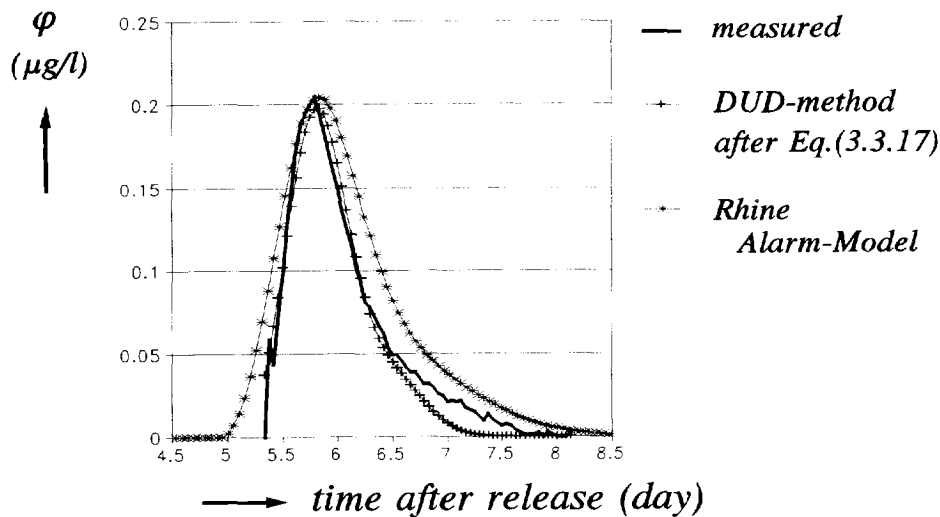


Fig. 3.4.18 Comparison of the measured concentration-distribution at Düsseldorf (Rhine-km 759.6) with the approximations after the optimization-methods with background-concentration correction

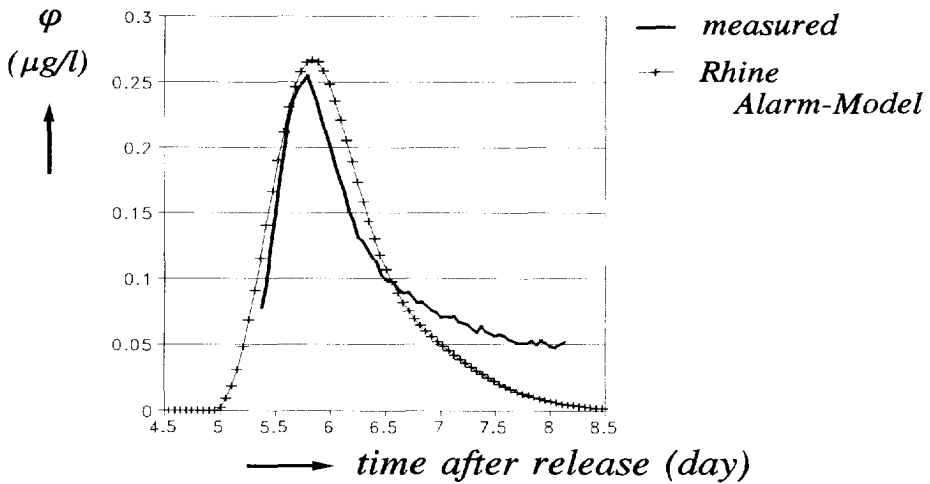


Fig. 3.4.19 Comparison of the measured concentration-distribution at Düsseldorf (Rhine-km 759.6) with the approximations after the optimization-method in the Rhine Alarm-Model without background-concentration correction

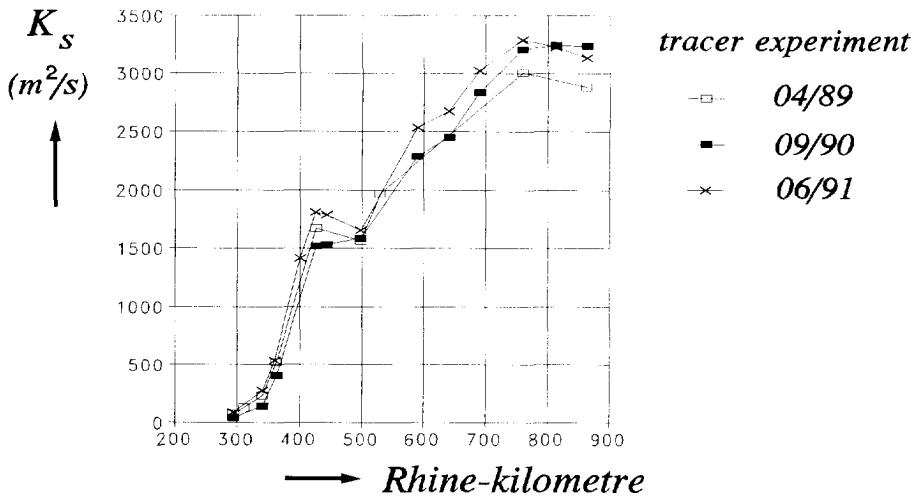


Fig. 3.4.20 Mean longitudinal dispersion-coefficient K_s after Eq.(2.3.81) from the point of release (Rhine-km 174.1) downstream to the measuring station concerned for three tracer experiments (Spreafico & van Mazijk, 1993)

Fischer et al. (1979) suggest, a detailed analysis of the accuracy of this coefficient has not been carried out (see also Table 3.4.9). Referring to the α_x -values found for the River Rhine between Kehl-Kronenhof and Lobith, based on the tracer experiment 04/89, an overall value of 0.007 for this river reach would be an acceptable estimation. This means that the average longitudinal dispersion-coefficient will become about 2500 m²/s (Table 3.4.9). In Fig. 3.4.20 the longitudinal dispersion-coefficient after the Rhine Alarm-Model for the tracer experiments 04/89, 09/90 and 06/91 is presented.

TABLE 3.4.9 The coefficient of proportionality α_x , based on experimental measurements of longitudinal dispersion in open channels, comparison of data after Fischer et al. (1979) and the River Rhine between Kehl-Kronenhof and Lobith

Channel	depth (m)	width (m)	mean flow- velocity (m/s)	shear velocity (m/s)	dispersion coefficient (m ² /s)	proportionality coeff. α_x
Chicago Ship Channel	8.07	48.8	0.27	0.0191	3.0	0.003
Trapeziodal laboratory channel with roughened sides	0.035	0.40	0.25	0.0202	0.123	0.009
	0.047	0.43	0.45	0.0359	0.253	0.011
	0.035	0.40	0.45	0.0351	0.415	0.016
	0.035	0.34	0.44	0.0348	0.250	0.014
	0.021	0.33	0.45	0.0328	0.400	0.012
	0.021	0.19	0.46	0.0388	0.220	0.023
Missouri River	2.70	200	1.55	0.074	1500	0.003
Copper Creek, Virginia (below gage)	0.49	16	0.27	0.080	20	0.042
	0.85	18	0.60	0.100	21	0.015
	0.49	16	0.26	0.080	9.5	0.022
Clinch River, Tennessee	0.85	47	0.32	0.067	14	0.004
	2.10	60	0.94	0.104	54	0.004
	2.10	53	0.83	0.107	47	0.005
Copper Creek, Virginia (above gage)	0.40	19	0.16	0.116	9.9	0.050
Powell River, Tennessee	0.85	34	0.15	0.055	9.5	0.017
Cinch River, Virginia	0.58	36	0.21	0.049	8.1	0.004
Coachella Canal, California	1.56	24	0.71	0.043	9.6	0.002
River Rhine between Kehl-Kronenhof and Lobith	5.7	335	1.30	0.094	~ 2500	0.007

3.4.5 The lag coefficient in the Dutch Rhine-branches

The discharges in the Dutch Rhine-branches (Fig. 3.4.21) are related to the water-level station Lobith (see also Section 3.2). Because the travel times from Lobith to the measuring stations Vuren (R. Waal), Hagestein (R. Lower-Rhine) and Kampen (R. IJssel) are one day or more, depending on the discharge at Lobith, stationary flow conditions are necessary for a correct determination of the lag coefficient, using the flow times of the Rhine Alarm-Model (Table 3.4.10).

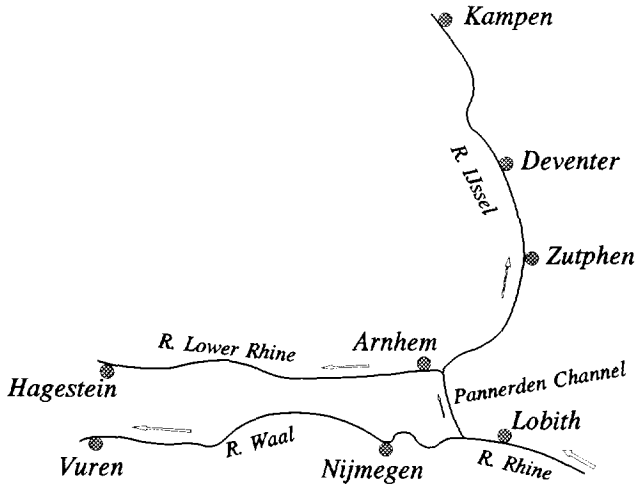


Fig. 3.4.21 Overview of the Rhine branches in the Netherlands downstream of Lobith

TABLE 3.4.10 Flow times during the tracer experiments after the Rhine Alarm-Model (Version 2.1)

tracer experiment	river discharge at Lobith (m ³ /s)	flow times (day)		
		Lobith-Vuren	Lobith-Hagestein	Lobith-Kampen
04/89	2979	0.8867	0.9786	1.6762
09/90	954	1.2125	17.9396	2.7572
06/91	2383	0.9473	1.0549	1.8579

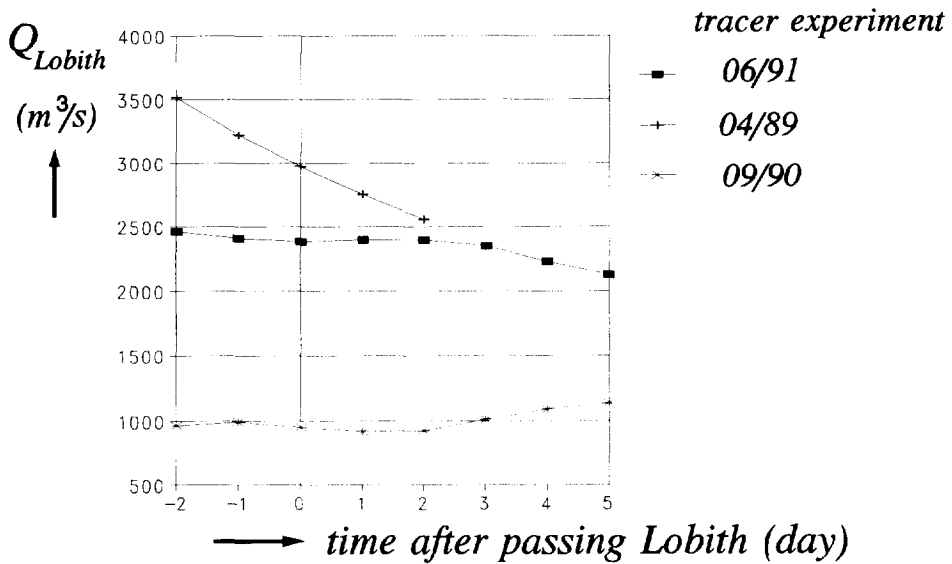


Fig. 3.4.22 Discharge at the water-level station Lobith during the period the tracer is passing

Considering the discharges at Lobith for the tracer experiments 04/89, 09/90 and 06/91 during the period the tracer cloud passes Lobith, it can be concluded that this holds for the tracer experiments 09/90 and 06/91 (Fig. 3.4.22). Because the flow times during the tracer experiment 04/89 are smaller than one day, except for the river reach Lobith - Kampen, the situation during this tracer experiment can also be considered as stationary. However, for the river reach Lobith - Kampen the discharge during the day, the tracer cloud passes the station Lobith, as well as the discharge during the following day have to be considered. In case of the tracer experiment 09/90 the flow time Lobith - Hagestein is more than two weeks, thus the stationary situation had to last this long period, which did not occur. After five days the river discharge at Lobith increases up to values of more than 1300 m^3/s . Therefore special attention will be paid on the results of this river reach below (see also Section 3.2).

In Table 3.4.11 the measuring stations for which the time-centroid could be determined by the DUD-method are presented (van Mazijk, et al., March 1991, June 1991 and December 1992). From these centroids the transport time of the tracer cloud can be determined and compared with the flow time, which gives after Eq.(3.4.1) the lag coefficient per river reach concerned

TABLE 3.4.11 Time-centroid of the measuring stations downstream of Lobith

measuring station	river branch (see also Fig. 3.4.21)	Rhine-kilometre	$(\mu_t)_m$ (day)
tracer experiment 04/89			
Lobith	River Rhine	862.2	6.9383
Vuren	River Waal	951.8	8.0834
Hagestein	River Lower-Rhine	946.5	8.2825
Kampen	River IJssel	994.5	8.7358
tracer experiment 09/90			
Lobith	River Rhine	863.30	11.340
Bimmen	River Rhine	865.02	11.307
Nijmegen	River Waal	884.73	11.691
Vuren	River Waal	951.80	12.749
Arnhem	Pannerden Channel	876.90	11.770
Kampen	River IJssel	994.50	14.046
tracer experiment 06/91			
Lobith	River Rhine	863.30	6.704
Bimmen	River Rhine	865.02	6.532
Nijmegen	River Waal	884.73	6.759
Vuren	River Waal	951.80	7.692
Arnhem	Pannerden Channel	876.90	7.709
Hagestein	River Lower-Rhine	946.50	8.072

$$\beta_m = \frac{(\Delta\mu_t)_m}{(\Delta T_u)_m} - 1 \quad (3.4.3)$$

with $(\Delta\mu_t)_m$ = difference between the time-centroid of two successive measuring-stations (river reach m)
 $(\Delta T_u)_m$ = the flow time between the two successive measuring-stations concerned (river reach m)

Because along the Dutch Rhine-branches groyne-fields are present at both river sides, the difference between the measured transport-velocity and the flow velocity, quantified by this lag coefficient must be caused by these groyne-fields or dead zones. Consequently the determined lag-coefficient β_m is primarily related to the dead-zone parameter β after Eq.(2.1.11)

$$\beta = \frac{A_b}{A_s} \quad (3.4.4)$$

with A_s = cross-sectional area of the main stream
 A_b = cross-sectional area of the dead zone

A comparison of the time-centroids of Lobith and Bimmen (tracer experiments 09/90 and 06/91) shows a difference in such a way that the centroid of the tracer cloud passes Bimmen earlier than Lobith, although Lobith lies upstream of Bimmen. In case of the tracer experiment 09/90 (low river-discharge) the difference is about three quarters of an hour and in case of the experiment 06/91 the difference amounts to 4 hours. A comparison of the measured concentration-distributions shows that the peak values are passing more or less at the same time (Fig. 3.4.23). The differences in concentration values might be caused by the inflow of the tributaries Lippe and Emscher about 50 and 70 km respectively upstream of Lobith at the right bank of the river. The smaller concentration-distribution, measured at the right bank (measuring-station Wesel, Rhine-kilometre 814), just upstream of the River Lippe and 19 km downstream of the River Emscher might confirm this (Fig. 3.4.24).

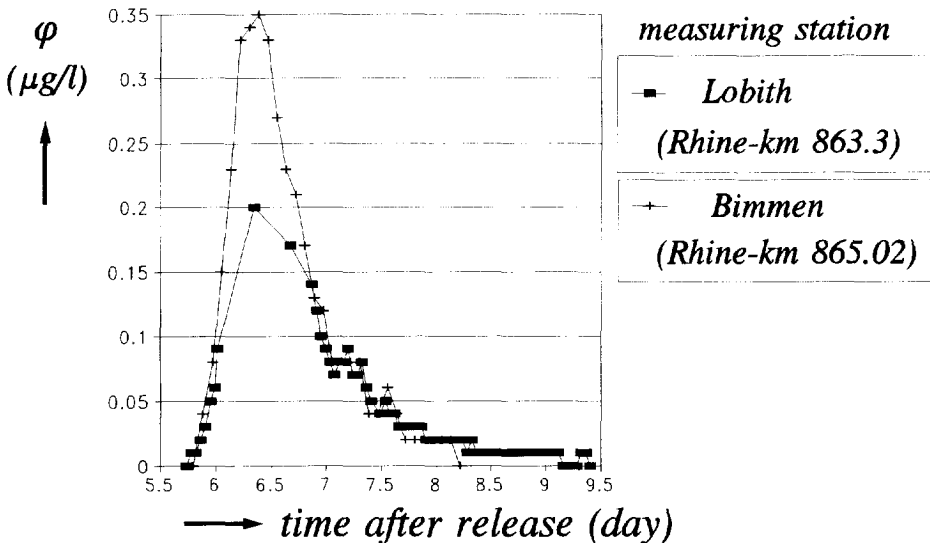


Fig. 3.4.23 Comparison of the measured concentration-distributions at Lobith (right river-bank) and Bimmen (left river-bank), tracer experiment 06/91

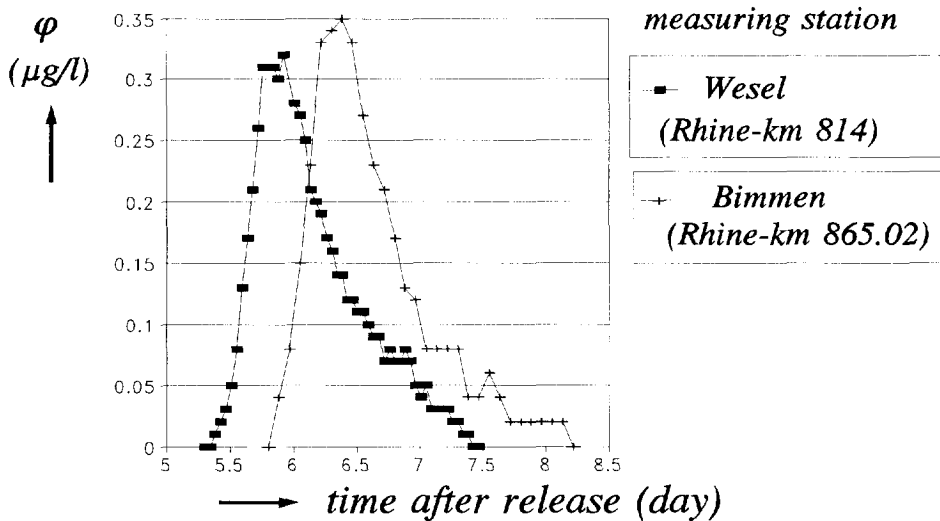


Fig. 3.4.24 Comparison of the measured concentration-distributions at Wesel (right river-bank) and Bimmen (left river-bank), tracer experiment 06/91

In case of the tracer experiment 09/90 the difference between the time-centroids of Lobith and Bimmen are smaller than in case of the experiment 06/91. The reason could be that the used concentration-distribution at Lobith is based on measurements at four spots in the river cross-section and at Bimmen only on measurements at the left bank of the river.

In Table 3.4.12 the time-centroids and the times related to the measured peak-concentrations, are presented. In Table 3.4.13 the derived lag-coefficient for the river reach Lobith/Bimmen - Nijmegen based on these time-centroids as well as on the time of the measured peak-values are collected. The diversification of the determined values of the lag coefficient as well as the magnitude of the variance of this coefficient show that the distance between Lobith/Bimmen and Nijmegen is that short, that inaccuracies will have a very large influence on the results. This can be explicitly shown by comparison of the flow time over the distance Lobith/Bimmen - Nijmegen which is about 0.25 day (Table 3.4.13), and the length of the concentration distribution in the time domain, which amounts a few days (Fig. 3.4.25). This means among others, that a slight deformation of the concentration distribution, caused by a non-homogeneously mixed situation over the cross-sectional area of the river (see also the differences between Lobith and Bimmen in Fig. 3.4.23), can have a large influence on the magnitude of the lag coefficient, which has nothing to do with the actual travel-time of the tracer cloud.

TABLE 3.4.12 Comparison of the time-centroid and the time of the measured peak-value of the concentration distributions at Lobith, Bimmen and Nijmegen

measuring station	Rhine-kilometre	time-centroid $(\mu_t)_m$ (day)	time of peak value $(T_p)_m$ (day)
tracer experiment 09/90			
Lobith	863.30	11.340	10.8292
Bimmen	865.02	11.307	11.0167
Nijmegen	884.73	11.691	11.2458
tracer experiment 06/91			
Lobith	863.30	6.704	6.3438
Bimmen	865.02	6.532	6.3854
Nijmegen	884.73	6.759	6.5938

TABLE 3.4.13 Lag coefficient for the river reach Lobith/Bimmen - Nijmegen

river reach	flow-time (ΔT_u) _m (day)	time-centroid			peak value		
		($\Delta \mu_t$) _m (day)	β_m	$ \sigma_{\beta_m} ^*$	(ΔT_p) _m (day)	β_m	$ \sigma_{\beta_m} ^*$
tracer experiment 09/90							
Lobith-Nijmegen	0.2572	0.351	0.36	0.25	0.4166	0.62	0.26
Bimmen-Nijmegen	0.2336	0.384	0.64	0.29	0.2291	-0.02	0.26
tracer experiment 06/91							
Lobith-Nijmegen	0.2164	0.055	-0.75	0.27	0.2500	0.16	0.29
Bimmen-Nijmegen	0.1994	0.227	0.14	0.32	0.2084	0.05	0.31

*) after Eq.(3.4.2) with $\sigma_{\mu_t} = \sigma_{T_p} = 60$ min. and $\sigma_{\tau_u} = 20$ min.

The higher concentrations measured at Nijmegen on the left bank (Fig. 3.4.25) confirms the difference in concentration values between Lobith (right bank) and Bimmen (left bank) (Fig. 3.4.23). For that reason the lag coefficient of 0.14 based on the time-centroid of the distributions, measured at Bimmen and Nijmegen, might be more true for the river reach Lobith - Nijmegen than the value based on the measurements at Lobith and Nijmegen (Table 3.4.13). In case of the tracer experiment 09/90 the considered concentration-distributions at Lobith as well as at Nijmegen are based on measurements at four spots over the river cross-section.

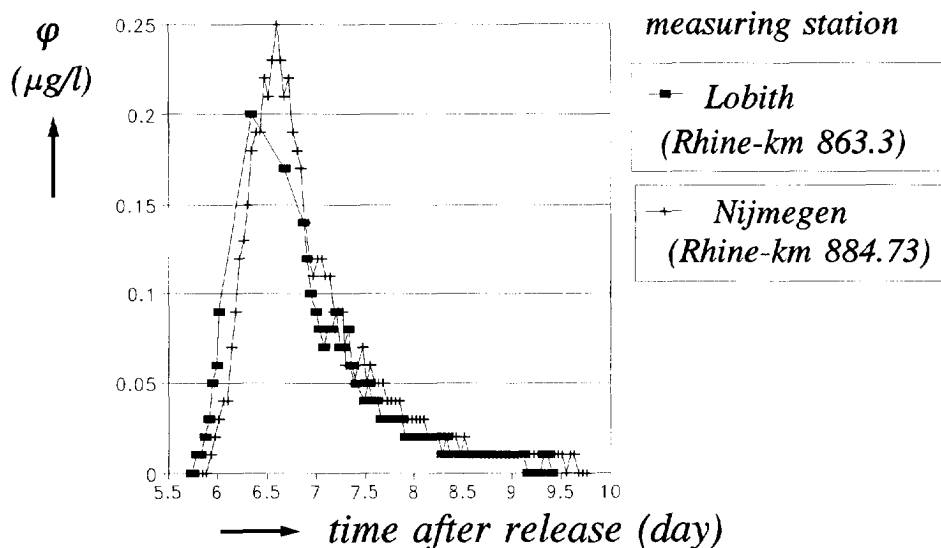


Fig. 3.4.25 Comparison of the measured concentration-distributions at Lobith (right river-bank) and Nijmegen (left river-bank), tracer experiment 06/91

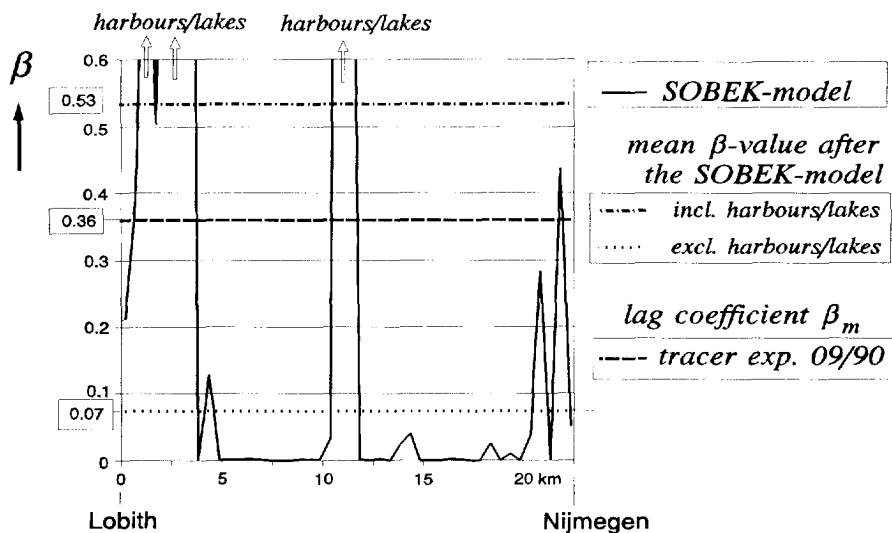


Fig. 3.4.26 Distribution of the dead-zone parameter β along the River Rhine between Lobith (Rhine-km 862.2) and Nijmegen (Rhine-km 884.5) after the SOBEK-model for $Q_{Lobith} = 954 \text{ m}^3/\text{s}$

Therefore the lag coefficient of 0.36 based on the time-centroids of these measured concentration-distributions is more true than the coefficient based on the comparison of the time-centroids of Bimmen and Nijmegen (Table 3.4.13).

In Fig. 3.4.26 this lag coefficient $\beta_m = 0.36$ is compared with the distribution of the dead-zone parameter β ²⁾ along the River Rhine between Lobith and Nijmegen for a river discharge at Lobith of 954 m³/s (tracer experiment 09/90) after the SOBEK-model³⁾. In this situation the mean dead-zone parameter $\beta = 0.07$ if the dead zones, caused by river harbours and lakes with open connections with the River Rhine, are excluded and 0.53 if they are included. Apparently the large value for the lag coefficient ($\beta_m = 0.36$) is the result of the large residence time of the

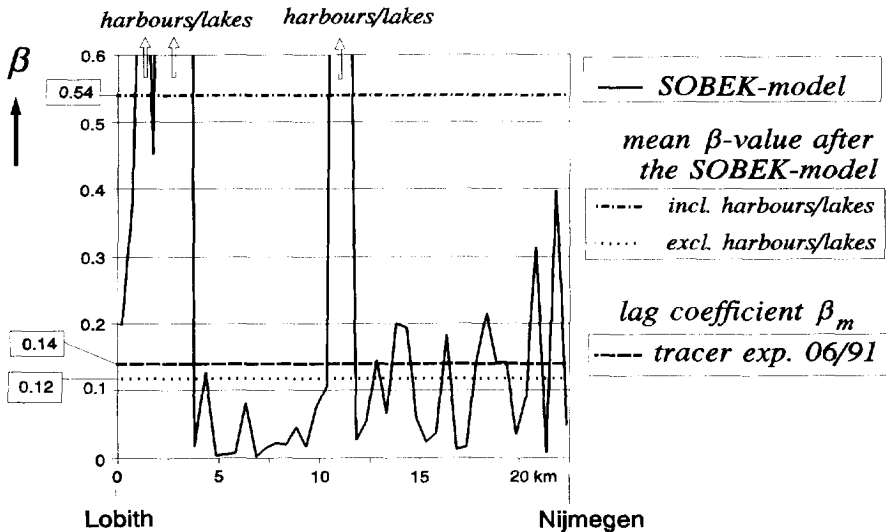


Fig. 3.4.27 Distribution of the dead-zone parameter β along the River Rhine between Lobith (Rhine-km 862.2) and Nijmegen (Rhine-km 884.5) after the SOBEK-model for $Q_{Lobith} = 2383 \text{ m}^3/\text{s}$

²⁾ If the parameter β concerns the ratio of the cross-sectional areas of the stagnant zones and the main stream of a river, the indication of 'dead-zone' parameter will be used; in case the parameter concerns the transport of a pollutant in relation to the flow velocity, the indication of 'lag coefficient' is taken.

³⁾ For hydrodynamic flow and transport calculations the Dutch branches of the River Rhine are schematized in a number of reaches and nodes. The model concerned is SOBEK (Delft Hydraulics & Ministry of Transport, Public Works and Water-management, 1995). By this model the total cross-sectional area as well as the cross-sectional area of the main stream can be calculated every 500 m for a certain river-discharge at Lobith.

tracer cloud as a whole in the river reach concerned (a few days), by which the exchange of tracer with these harbours/lakes can become of a significant influence on the transport velocity. In case of the tracer experiment 06/91 with a river discharge of 2383 m³/s at Lobith the lag coefficient β_m (= 0.14) is comparable with the mean dead-zone parameter β (= 0.12) in case the dead zones, caused by the harbours and lakes are excluded (Fig. 3.4.28).

For the determination of the lag coefficient of the River Waal between Nijmegen (Rhine-kilometre 884.73) and Vuren (Rhine-kilometre 951.8) the tracer experiments 09/90 and 06/91 have to be considered. Table 3.4.14 shows the results.

TABLE 3.4.14 Lag coefficient of the River Waal between Nijmegen and Vuren

tracer experiment	$(\Delta T_u)_m$ (day)	$(\Delta \mu_t)_m$ (day)	β_m	$ \sigma_{\beta_m} ^*)$
09/90	0.9553	1.058	0.11	0.07
06/91	0.7309	0.933	0.28	0.09

*) see Note of Table 3.4.13

In case of the tracer experiment 09/90 the concentration distributions concerned are based on measurements at four spots in the river cross-section at Nijmegen and at two spots in the river cross-section at Vuren. Referring to the non-homogeneously mixed situation at Lobith and Nijmegen (Figs 3.4.23 and 3.4.25) the derived time-centroids for Nijmegen and Vuren are representative for the transport velocity of the tracer cloud. In case of the tracer experiment 06/91 the time-centroid at Nijmegen is based on measurements at the left bank of the river and at Vuren at the right bank. Because effects of non-homogeneously mixed situations reduces with the distance concerned, its influence on the derived lag-coefficient in case of this experiment will be limited. This means that the difference between the

TABLE 3.4.15 Overall lag-coefficient of the River Rhine and the River Waal between Lobith/Bimmen and Vuren

tracer experiment	River discharge at Lobith (m ³ /s)	$(\Delta T_u)_m$ (day)	$(\Delta \mu_t)_m$ (day)	β_m	$ \sigma_{\beta_m} ^*)$
04/89	2979	0.8867	1.1451	0.29	0.07
09/90	954	1.2125	1.4090	0.16	0.05
06/91	2383	0.9303	1.1600	0.25	0.07

*) see Note of Table 3.4.13

measured lag-coefficients of the two tracer experiments in Table 3.4.14 is relevant. Thus the lag coefficient increases with the river discharge. A comparison of the lag coefficient between Lobith and Vuren for the three tracer experiments 04/89, 09/90 and 06/91 confirms this conclusion (Table 3.4.15). Apparently a significant increment of the discharge means an increment of the water-level and consequently an increment of the dead-zone parameter after Eq.(3.4.4).

In Figures 3.4.28 and 3.4.29 the lag coefficients β_m for the River Waal between Nijmegen and Vuren (Table 3.4.14) are compared with the dead-zone parameter β after the SOBEK-model for the two river discharges at Lobith (945 and 2383 m³/s), referring to the tracer experiments 09/90 and 06/91. The observed increment of the dead-zone parameter with the river discharge is confirmed by the SOBEK-model. In contrast to the conclusion made above, that the influence of the stagnant zones, caused by river harbours and lakes is significant for low river-discharges, the comparison of the measured lag-coefficient with the mean values of the dead-zone parameter (incl. and excl. river harbours and lakes) after the SOBEK-model suggests more influence of the river harbours and lakes on the transport velocity of the tracer in case of a larger discharge. However, the overall lag-coefficients β_m for the whole river-reach between Lobith and Vuren for the three tracer experiments 04/89, 09/90 and 06/91 show comparable differences with the mean values

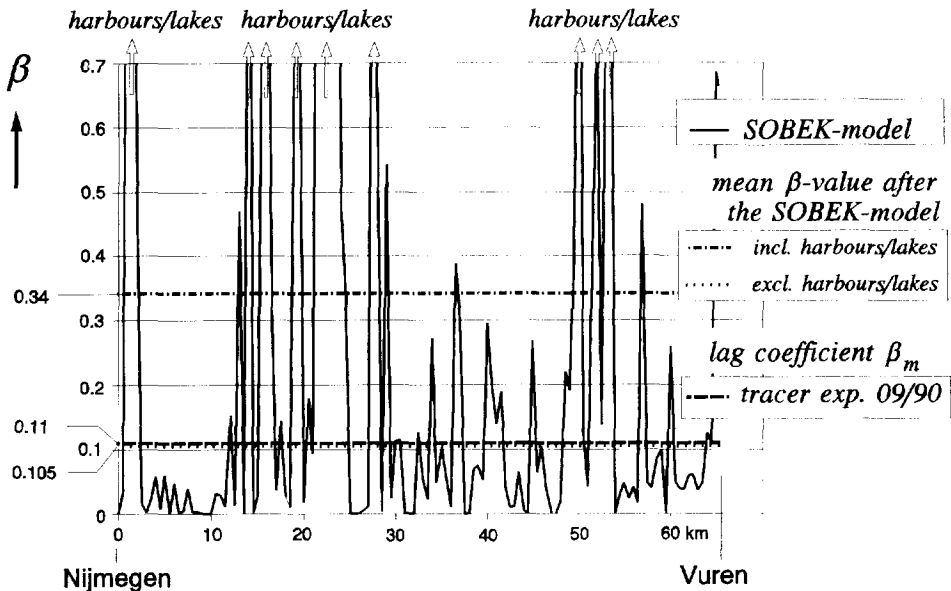


Fig. 3.4.28 Distribution of the dead-zone parameter β along the River Waal between Nijmegen (Rhine-km 884.5) and Vuren (Rhine-km 951.8) after the SOBEK-model for $Q_{Lobith} = 954 \text{ m}^3/\text{s}$

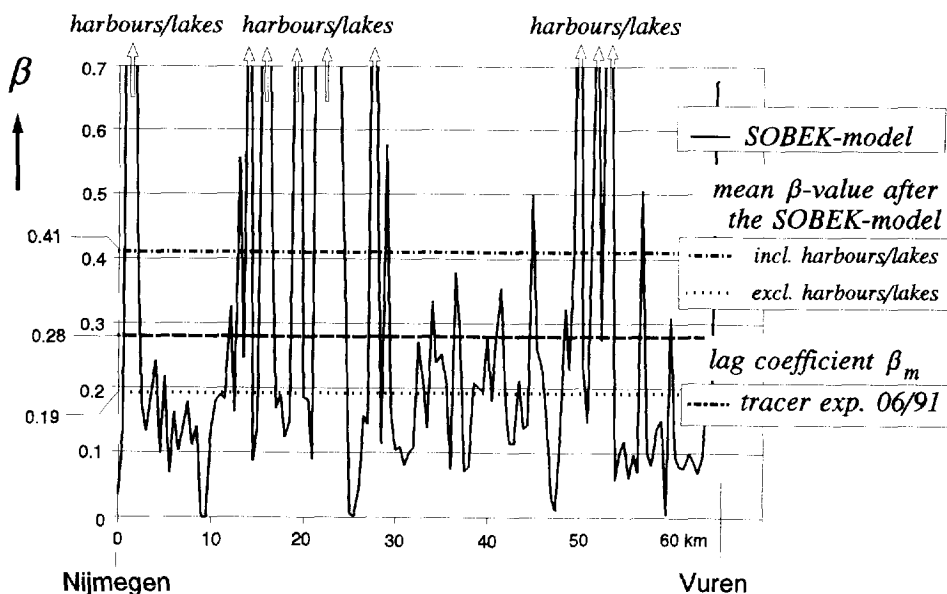


Fig. 3.4.29 Distribution of the dead-zone parameter β along the River Waal between Nijmegen (Rhine-km 884.5) and Vuren (Rhine-km 951.8) after the SOBEK-model for $Q_{Lobith} = 2383 \text{ m}^3/\text{s}$

of the dead-zone parameters after the SOBEK-model (Table 3.4.16). Thus the stagnant zones, caused by the river harbours and lakes have to be taken into account into the dead-zone parameter to a certain degree, depending on the rate of exchange of tracer.

TABLE 3.4.16 Overall lag-coefficient and dead-zone parameter of the River Rhine and the River Waal between Lobith/Bimmen and Vuren

tracer experiment	River discharge at Lobith (m^3/s)	lag coeff. β_m	dead-zone parameter β after SOBEK		lag coefficient after the Rhine Alarm-Model	
			incl. harbours/ lakes	excl. harbours/ lakes	Lobith - Nijmegen	Nijmegen - Vuren
04/89	2979	0.29	0.49	0.22	0.10	0.18
09/90	954	0.16	0.39	0.10		
06/91	2383	0.25	0.44	0.17		

The measurements at Arnhem were executed in the Pannderden Channel (Rhine-kilometre 876.9) just upstream of the bifurcation River Lower-Rhine and River IJssel at Rhine-kilometre 878.5 (Fig. 3.4.21). This station gives the opportunity to determine the lag coefficient of this Channel with a length of 11.3 km, by comparing its measured time-centroid with those of Lobith/Bimmen at about 3.5 km upstream of the bifurcation Waal - Pannderden Channel at Rhine-kilometre 867.2. In Table 3.4.11 the time-centroids based on the measured concentration-distributions after the DUD-method for the tracer experiments 09/90 and 06/91 are presented. In case of the tracer experiment 06/91 the difference between the time-centroids of Lobith/Bimmen and Arnhem is about one day, whereas the flow time

TABLE 3.4.17 Lag coefficient β_m of the Pannderden Channel between Lobith and Arnhem

tracer experiment	$(\Delta T_u)_m$ (day)	$(\Delta \mu_t)_m$ (day)	β_m	$ \sigma_{\beta_m} ^*$
09/90	0.298	0.430	0.44	0.22

*) see Note of Table 3.4.13

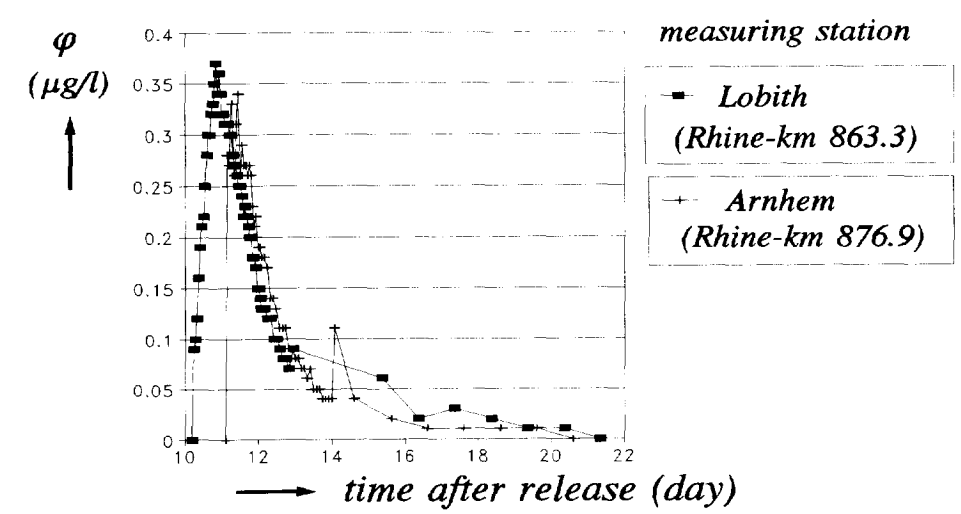


Fig. 3.4.30 Comparison of the measured concentration-distributions at Lobith (cross-sectional mean values) and Arnhem (left river-bank), tracer experiment 09/90

between these stations is about 3 h. Due to this large difference the concentration-measurements at Arnhem of the tracer experiment 06/91 have to be disqualified. In case of the tracer experiment 09/90 the time-centroid at Lobith is based on measurements at four spots in the river cross-section, whereas the time-centroid of Bimmen as well as of Arnhem is based on measurements at the left bank of the river. Referring to the non-homogeneously mixed situation at Lobith/Bimmen only the measurements of Lobith will be taken into account. The results are presented in Table 3.4.17.

Due to the relatively small distance between the measuring stations Lobith and Arnhem (13.6 km) the influence of inaccuracies in the time-centroid is fairly large (50%). Moreover at such small distances the influence of the non-homogeneously mixed situation at Lobith can also disturb the results as well as the fact that the transport time is much smaller than the length of the concentration distributions in the time domain (Fig. 3.4.30). Therefore the derived β_m -value of 0.44 have reduced relevance. On the other hand the relatively large residence-time of the tracer cloud in the river reach Lobith-Arnhem (bifurcation River IJssel) might have caused a more significant influence of the harbours and lakes on the transport of the tracer as it was already observed for the river reach Lobith-Nijmegen. However, in Fig. 3.4.31 the results of the analysis of the dead-zone parameter

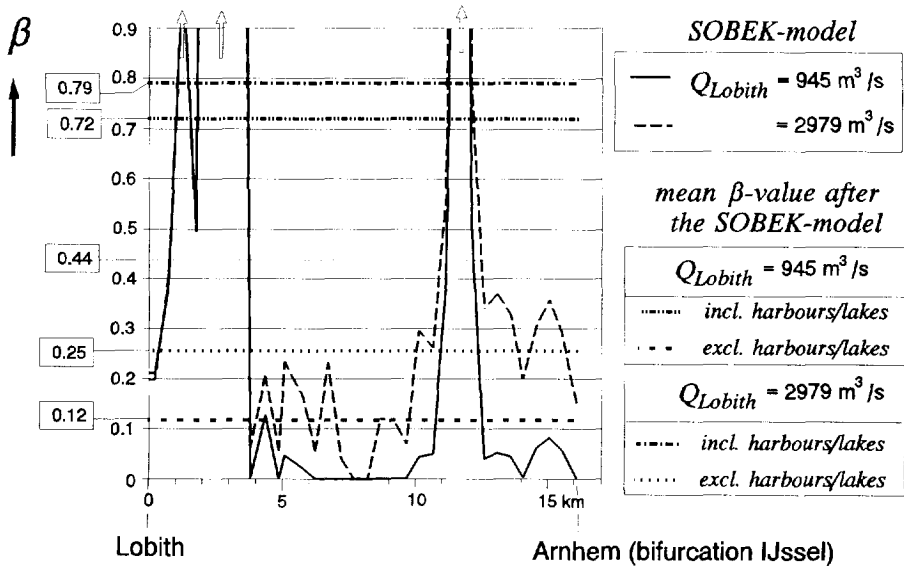


Fig. 3.4.31 Dead-zone parameter along the River Rhine and the Pannerden Channel between Lobith (km 862.2) and Arnhem (bifurcation IJssel, km 878.3) after the SOBEK-model for $Q_{Lobith} = 954$ and $2979 \text{ m}^3/\text{s}$

after the SOBEK-model indicate that a lag coefficient β_m of about 0.20 (including a certain influence of the river harbours and lakes) is more true than the value of 0.44 for the low river-discharge of 954 m³/s at Lobith. After this analysis the dead-zone parameter becomes 0.25 to 0.30 for a river discharge of about 3000 m³/s at Lobith. Moreover, these values after the SOBEK-model agree quite well with the calibrated value of 0.20 for the lag coefficient of the Pannerden Channel in the Rhine Alarm-Model (Table 3.4.18).

TABLE 3.4.18 Overall lag-coefficient and dead-zone parameter for the River Rhine and the Pannerden Channel between Lobith/Bimmen and Arnhem (bifurcation River IJssel)

tracer experiment	River discharge at Lobith (m ³ /s)	lag coeff. β_m	dead-zone parameter β after SOBEK		lag coefficient after the Rhine Alarm-Model	
			incl. harbours/ lakes	excl. harbours/ lakes	Lobith - Pannerden Channel	Pannerden Channel
04/89	2979	-	0.79	0.25	0.10	0.20
09/90	954	0.44	0.72	0.12		

For the River Lower-Rhine the measuring stations Arnhem and Hagestein have to be considered. However, only during the tracer experiment 09/90 the measured concentration-distribution at Arnhem seems to be reliable, whereas the measurement at Hagestein is failing. The reason is that after the Rhine Alarm-Model the tracer should have passed this measuring station about a week later than it actually did (Fig. 3.4.27). As a matter of fact for low-water conditions ($Q_{Lobith} < 1400$ m³/s) the flow times in the Rhine Alarm-Model are based on the weir-regulation-programme S285 of the Dutch Ministry of Transport and Public Works by which the discharges over the Rhine branches are regulated by the weirs in the River Lower-Rhine (see also Section 3.2, Fig. 3.2.5). This programme implies that for low-water conditions the discharge in the River Lower-Rhine is kept constant at 25 m³/s in order to guarantee a minimum discharge of 285 m³/s in the River IJssel. However, an analysis of the flow and transport times between Lobith and Hagestein based on measured time-series of chloride concentrations at Lobith and Hagestein demonstrates that in case of low-water situations the discharge in the River Lower-Rhine can vary substantially (between 0 and 100 m³/s). The main reason is the fact that the steering of the weirs primarily is based on water-level control. Consequently the transport time between Lobith and Hagestein can deviate a week or more from the times after the Rhine Alarm-Model (van Mazijk et al., 1992; van Mazijk, 1993; van Mazijk and Wuijts, 1995).

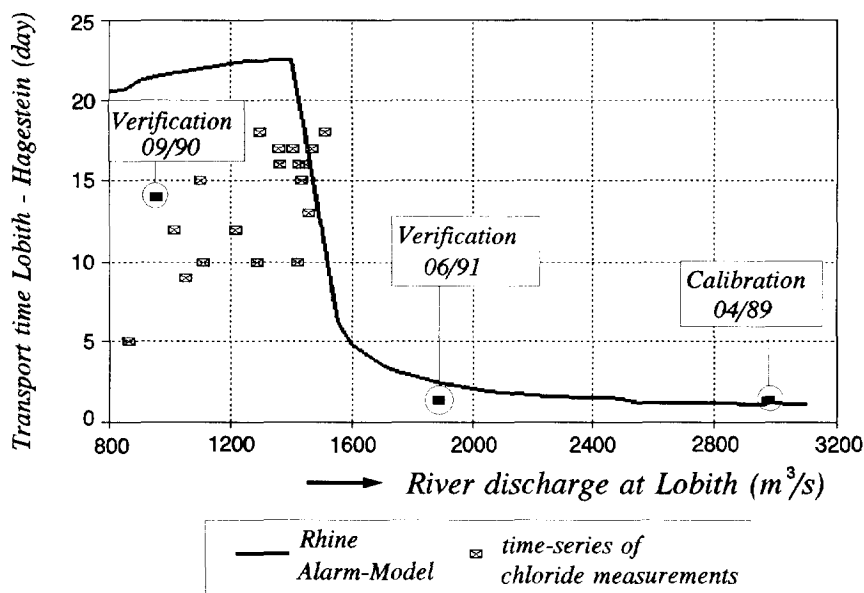


Fig. 3.4.32 Transport time between Lobith and Hagestein in relation to the river discharge at Lobith. Comparison of the Rhine Alarm-Model with the tracer experiments and the time-series of chloride measurements (van Mazijk and Wuijts, 1995)

In case of the tracer experiment 09/90 with a river discharge at Lobith of $954 \text{ m}^3/\text{s}$ at the day the tracer cloud starts passing this station, the related flow time till Hagestein is more than 17 days (Table 3.4.10). However, after eight days the discharge at Lobith has increased up to over $1300 \text{ m}^3/\text{s}$ (see also Fig. 3.4.22), which also can cause a smaller flow time downstream of Arnhem and consequently an earlier arrival of the tracer cloud at Hagestein.

To what extent the actual control-system on the River Lower-Rhine has also influenced the actual discharge in the Panterden Channel and consequently the derived lag-coefficient of 0.44 for this Channel (Table 3.4.17) has not been examined.

Thus, in order to get an indication of the lag coefficient for the River Lower-Rhine the measured concentration-distributions at Lobith/Bimmen and Hagestein during the tracer experiments 04/89 and 06/91 have to be considered. In Table 3.4.19 the results, based on the time-centroids of the distributions concerned after the DUD-method are collected. In case of the tracer experiment 06/91 the mean value of the time-centroids of Lobith and Bimmen are used.

TABLE 3.4.19 Lag coefficient between Lobith/Bimmen and Hagestein

tracer experiment	River discharge at Lobith (m ³ /s)	$(\Delta T_u)_m$ (day)	$(\Delta \mu_t)_m$ (day)	β_m	$ \sigma_{\beta_m} (*)$
04/89	2979	0.9786	1.3442	0.37	0.07
06/91	2383	1.0464	1.4540	0.39	0.06

*) see Note of Table 3.4.13

A comparison of the resulting lag-coefficients (0.37 and 0.39) with the dead-zone parameter after the SOBEK-model, averaged over the river reach Lobith - Hagestein, suggests a relatively large influence of the river harbours and lakes on the transport time of the tracer: the difference between the lag coefficient β_m and the dead-zone parameter β after the SOBEK-model, neglecting the harbours and lakes is about 0.10 (see Table 3.4.20). Considering the lengths of the river reaches Lobith-Pannerden Channel (5.1 km), Pannerden Channel (11 km) and the River Lower-Rhine until Hagestein (66 km) the measured lag-coefficients of 0.39 and 0.37 as well as the dead-zone parameters after SOBEK are representative for the River Lower-Rhine. According to the variance of the derived lag-coefficient, it can be finally concluded that the lag coefficient of the River Lower-Rhine is about 0.30 till 0.35, which agrees quite well with the calibrated lag-coefficient in the Rhine Alarm-Model.

TABLE 3.4.20 Overall lag-coefficient and dead-zone parameter for the River-Rhine reach between Lobith/Bimmen and Hagestein

tracer experiment	River discharge at Lobith (m ³ /s)	lag coeff. β_m	dead-zone parameter β after SOBEK		lag coefficient after the Rhine Alarm-Model		
			incl. harbours/ lakes	excl. harbours/ lakes	(1) *)	(2)	(3)
04/89	2979	0.37	0.97	0.26	0.10	0.20	0.29
06/91	2383	0.39	0.95	0.23			

*) river reaches

- | | | | |
|-----|----------------------------|----------------------------|---------|
| (1) | Lobith - Pannerden Channel | (length of the river reach | 5.1 km) |
| (2) | Pannerden Channel | („ | 11 km) |
| (3) | River Lower-Rhine | („ | 66 km) |

For the River IJssel the measuring stations Arnhem (Pannerden Channel) and Kampen have to be considered. Only during the tracer experiment 09/90 from both

stations concentration-distributions are available. In Table 3.4.21 the results are presented. For comparison of the results of tracer experiments 09/90 with those of the experiment 04/89 the lag coefficient has also be derived for the river reach Lobith - Kampen. It has to be noticed that the flow time between Lobith and Kampen in case of the tracer experiment 09/90 is less than three days (Table 3.4.10), whereas from the time, the tracer passes the measuring-station Lobith, the following three days the discharge at this station is more or less stationary (Fig. 3.4.22). This means that the results cannot be disturbed by discharge variations, so in this way the results should be reliable.

TABLE 3.4.21 Overall lag-coefficient between Lobith/Bimmen and Kampen

tracer experiment	discharge at Lobith (m ³ /s)	River reach	$(\Delta T_u)_m$ (day)	$(\Delta \mu_t)_m$ (day)	β_m	$ \sigma_{\beta_m} ^*$
04/89	2979	Lobith-Kampen	1.6762	1.7975	0.07	0.04
09/90	954	Arnhem-Kampen	2.4592	2.2760	-0.07	0.03
		Lobith-Kampen	2.7572	2.7060	-0.02	0.02

*) see Note of Table 3.4.13

However, a comparison of the derived lag-coefficients β_m for the river reach Lobith - Kampen (Table 3.4.21) with the dead-zone parameter β after the SOBEK-model shows remarkable deviations (Table 3.4.22). Based on the dead-zone parameter the expected values of the lag coefficients for the river reach concerned should be at least in the range of 0.10 till 0.25 instead of the range of 0 till 0.10. Analysis of the measured concentration-distributions at Kampen demonstrates that the approximation of the measured concentration-distribution by the Chatwin-model (Eq. 3.3.17) after the DUD-method does not reproduce the tail of the distribution quite

TABLE 3.4.22 Overall lag-coefficient and dead-zone parameter for the River-Rhine reach between Lobith and Kampen

tracer experiment	River discharge at Lobith (m ³ /s)	lag coeff. β_m	dead-zone parameter β after SOBEK	
			incl. harbours/ lakes	excl. harbours/ lakes
04/89	2979	0.07	0.80	0.20
09/90	954	-0.02	0.84	0.09

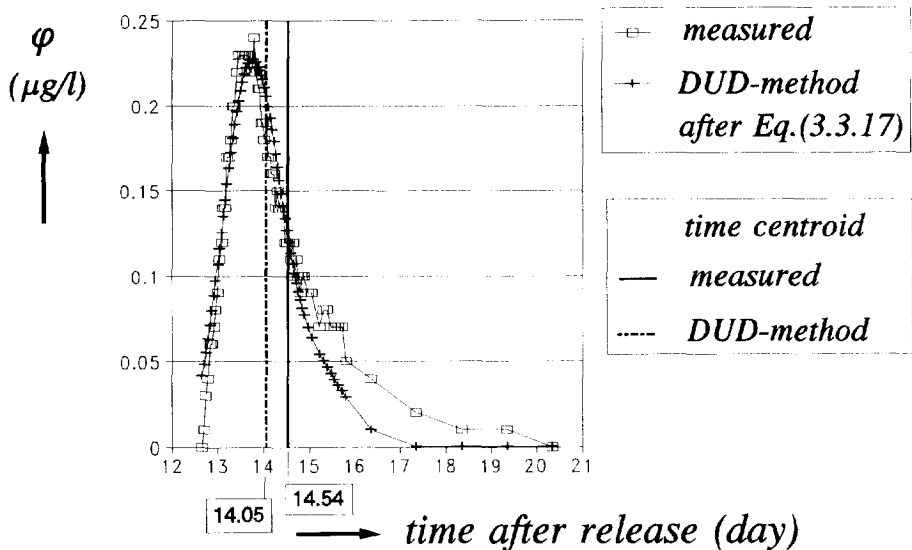


Fig. 3.4.33 Comparison of the measured concentration-distribution with the approximation after the DUD-method and the time-centroids concerned (tracer experiment 09/90, measuring-station Kampen)

well (Fig. 3.4.33). Therefore the resulting time-centroid after the DUD-method is too small. In case of the tracer experiment 09/90 the tail of the concentration distribution is measured completely. Thus the time-centroid based on these measurements after Eqs (2.3.61) and (2.3.62) is correct. In case of the tracer experiment 04/89 the tail of the concentration distribution is not measured completely (Fig. 3.4.34). For a good approximation of the time-centroid the distribution is extrapolated. The lag coefficients for the river reach Lobith - Kampen, based on the improved values of the time-centroid of the measuring-station Kampen, are shown in Table 3.4.23.

TABLE 3.4.23 Overall lag-coefficient between Lobith and Kampen

tracer experiment	discharge at Lobith (m ³ /s)	$(\Delta T_u)_m$ (day)	$(\Delta \mu_t)_m$ (day)	β_m
04/89	2979	1.6762	2.16	0.29
09/90	954	2.7572	3.20	0.16

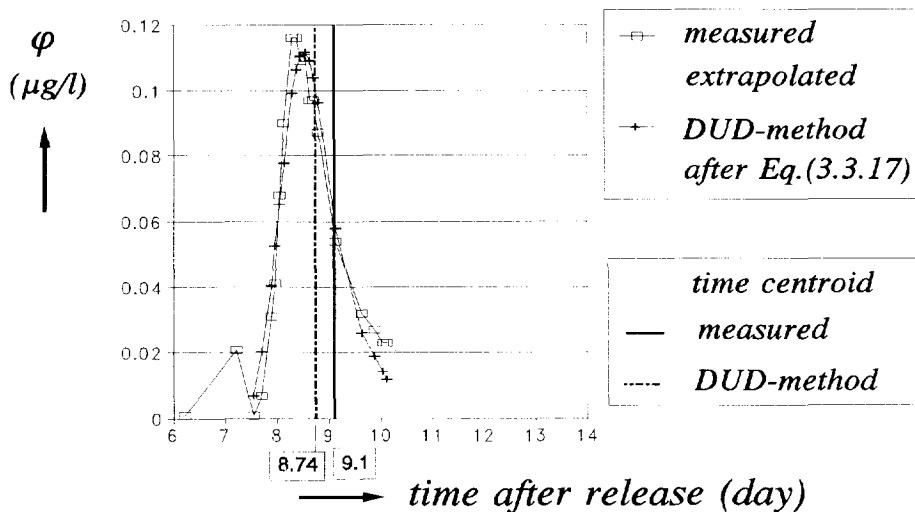


Fig. 3.4.34 Comparison of the measured concentration-distribution with the approximation after the DUD-method and the time-centroids concerned (tracer experiment 04/89, measuring-station Kampen)

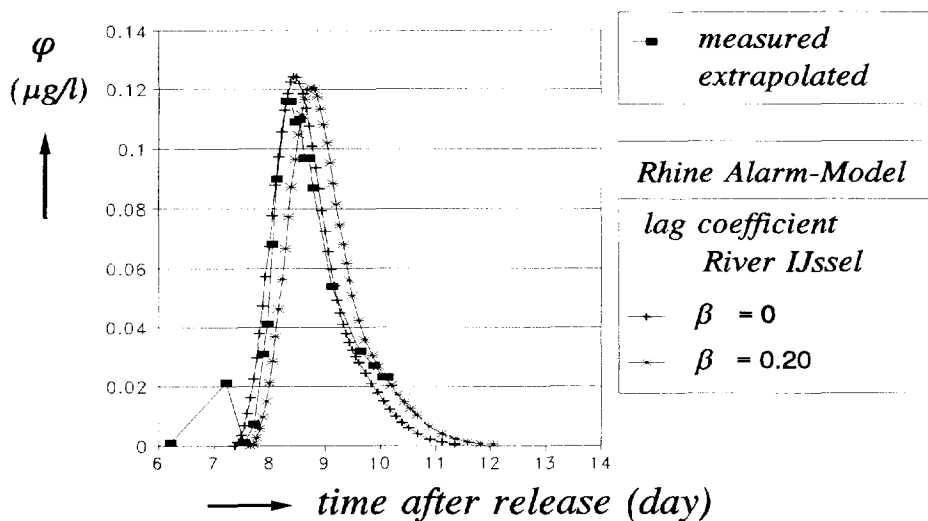


Fig. 3.4.35 Comparison of the measured concentration-distribution at Kampen (tracer experiment 04/89) with the calibrated distribution after the Rhine Alarm-Model for two values of the lag coefficient for the River IJssel

These values of the lag coefficients are in the same proportion to the dead-zone parameters after the SOBEK-model as found for the other Dutch branches of the River Rhine. However, the calibrated value of the lag coefficient in the Rhine Alarm-Model (based on the experiment 04/89) amounts zero. This can be explained by the calibration method. In this method primarily the peak concentration is fitted and in the second place the concentration distribution for which only concentration-values larger than 30% of the peak value (Sub-section 3.3.1) are concerned. The latter criterion means that the tail becomes less important. Moreover, the Rhine Alarm-Model applies the Chatwin-model after Eq.(3.3.17) with a skewness $G_t = 1$, which means that the calibration will have results, which are comparable with those after the DUD-method. Thus it is not always possible to reproduce with the Chatwin-model the steep front of a measured concentration-distribution as well as the complete tail. In Fig. 3.4.35 the measured concentration-distribution at Kampen (tracer experiment 04/89) is compared with the distributions after the Rhine Alarm-Model for two β -values for the River IJssel: $\beta = 0$ (calibration) and $\beta = 0.20$. It illustrates the restrictions of the applicability of the Chatwin-model for the reproduction of the dead-zone parameter β by the lag coefficient β_m .

TABLE 3.4.24 Lag coefficients β_m and dead-zone parameters β in the Dutch branches of the River Rhine ($Q_{Lobith} = 2000$ to $3000 \text{ m}^3/\text{s}$)

river reach	dead-zone parameter SOBEK-model (excl. harbours/lakes)	lag coefficient	
		DUD-method after Eq.(3.3.17)	Rhine Alarm- Model
River Rhine (Lobith-bifurcation Pannerden/Nijmegen)	0.12	0.14	0.10
River Waal (bifurcation Pannerden /Nijmegen-Vuren)	0.20	0.27	0.18
Pannerden Channel	0.25	no reliable measurement	0.20
River Lower-Rhine (bifurcation R. IJssel - Hagestein)	0.25	0.38	0.29
River IJssel (bifurcation R. IJssel - Kampen)	0.15	0.07 (~ 0.25) *)	0

*) based on the time-centroid, determined from the measured concentration-distribution itself by Eqs (2.3.16) and (2.3.62)

In Table 3.4.24 an overview of the significant values of the lag coefficient β_m , determined by the DUD-method after Eq.(3.3.17) as well as by the calibration of the Rhine Alarm-Model, and the dead-zone parameters β after the SOBEK-model is given for normal-flow conditions (river discharges of 2000 to 3000 m³/s at Lobith).

In Chapter 4 the influence of artificial dead-zones (groyne-fields) on the lag coefficient will be examined in detail by a numerical model. The purpose of this examination is to determine the relationships between the dead-zone parameter, based on measured cross-sectional areas of a river and the resulting lag-coefficient. With these relationships it might be possible to feed the values of lag coefficients β into alarm models in advance.

Chapter 4

DEAD-ZONE MODEL

4.1 INTRODUCTION

The transport velocity c of a pollutant in case of dead zones made by groyne-fields is defined by Eq.(2.3.9)

$$c = \frac{u_s}{1 + \beta} \quad (4.1.1)$$

wherein u_s is the flow velocity in the main stream, while the dead-zone parameter β ⁴⁾ is defined by

$$\beta = \frac{A_b}{A_s} \quad (4.1.2)$$

with A_s as the cross-sectional area of the main stream and A_b as the total cross-sectional area of the dead zone (see Fig. 2.1.8, Section 2.1).

However, the transport velocity c , defined by Eqs (4.1.1) and (4.1.2) will be achieved at large distances from the point of release (see Sub-section 2.3.2). This means that in between the effectiveness of the dead-zone influence on the transport velocity c of the resulting concentration-distribution is smaller than based on the value of β defined by Eq.(4.1.2). In this case it is preferred to use the actual dead-zone parameter, i.e. the actual lag-coefficient $\beta_{act.}$ defined by

$$\beta_{act.} = \kappa \cdot \frac{A_b}{A_s} \quad (4.1.3)$$

with κ as the ratio of actuality, representing the actual effect of the stagnant zones on the transport velocity.

After the degenerated pair of coupled Eqs (2.3.19) and (2.3.18) there are two waves to be distinguished at short distances of the point of release (Eq. 2.3.42).

⁴⁾ if the parameter β concerns the ratio of the cross-sectional areas of the stagnant zones and the main stream of a river, the indication of 'dead-zone' parameter will be used; in case the parameter concerns the transport of a pollutant in relation to the flow velocity, the indication of 'lag coefficient' will be taken.

The first wave propagates with the flow velocity u_1 , while the second wave propagates more slowly. Near the point of release the peak concentration is dominated by the first wave. Thus the distribution of the κ -value with the distance from the point of release depends on the definition of the transport velocity. Mostly for the determination of the transport velocity the time-centroid of the concentration distribution is considered. On the other hand the last part of the tail of measured concentration-distributions usually fails. In those cases the peak concentration is often used for the determination of the transport velocity. Therefore the analysis of the distribution of the κ -value in Section 4.3 will concern both definitions.

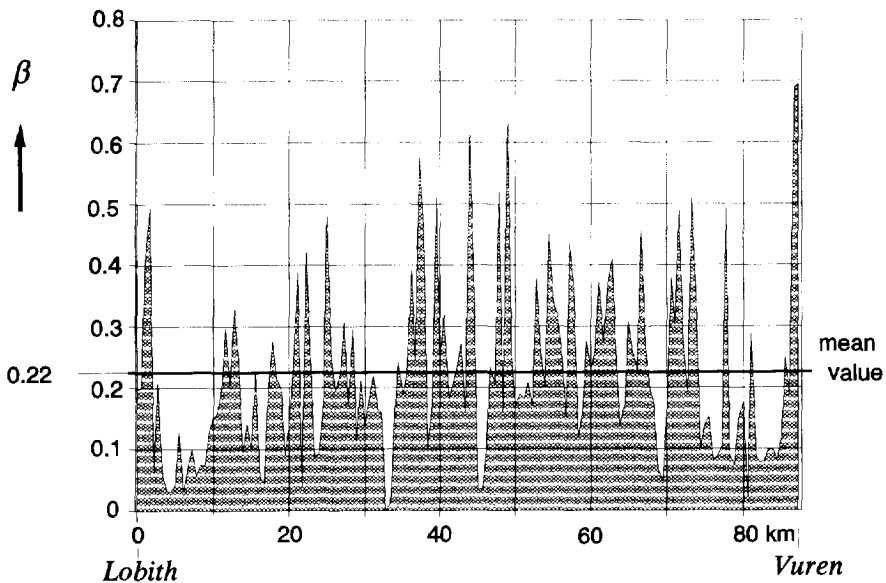


Fig. 4.1.1 Distribution of the dead-zone parameter β after the SOBEK-model along the River Rhine between Lobith and Vuren for $Q_{Lobith} = 3000 \text{ m}^3/\text{s}$, neglecting harbours, lakes etc.

Further it has to be realized that the cross-sectional area of the dead zones along a river branch is not constant. In Fig. 4.1.1 the distribution of the dead-zone parameter after Eq.(4.1.2) is presented for the River Rhine between Lobith (Rhine-km 862.2) at the German-Dutch border and Vuren on the River Waal (Rhine-km 951.8) for the situation during the tracer experiment of April 1989 with a river discharge at the measuring-station Lobith of $2979 \text{ m}^3/\text{s}$ (van Mazijk et al, March 1991). For the determination of the β -values the SOBEK-schematization (Delft Hydraulics & Ministry of Transport, Public Works and Watermanagement, 1995)

of this branch of the River Rhine has been used. By this model the total cross-sectional area as well as the cross-sectional area of the main stream can be determined every 500 m for a certain river-discharge at Lobith. In the presented distribution of the dead-zone parameter (Fig. 4.1.1), stagnant zones caused by river harbours, lakes etc. with an open connection with the river, are left out of consideration. That means that β -values larger than 0.8 are not taken into account. The mean value of 0.22 is the arithmetical average.

Taking the length of the river-reach per calculated β -value into account, a relation between the value of the dead-zone parameter β and the part of the branch of the River Rhine between Lobith and Vuren with values equal to or less than the considered one, can be determined (see Fig. 4.1.2). Thus the β -value is equal to or less than 0.21 over a distance of 50% of the river branch between Lobith and Vuren. This value is in accordance with the arithmetical average for which β -values larger than 0.8 were left out of consideration (Fig. 4.1.1).

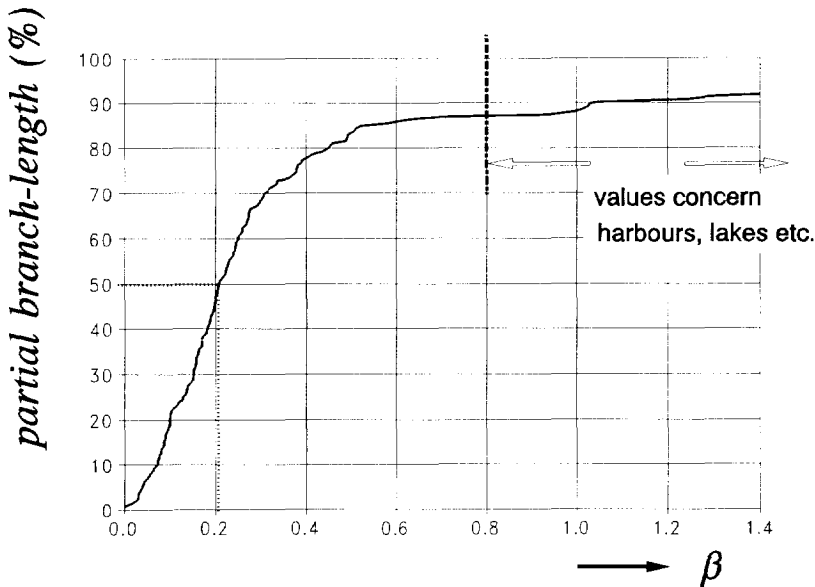


Fig. 4.1.2 Partial branch-length with β -values equal to or less than the considered one for the River Rhine between Lobith and Hagestein

Referring to the fact that at large distances the transport velocity c can be given by Eqs (4.1.1) and (4.1.2), the question is which value the actual lag-coefficient becomes if the dead-zone parameter varies along the river reach concerned. This means that in Section 4.3 not only the influence of the dead zones on the transport velocity of a pollution cloud near the point of release will be examined, but also

the relation between the average dead-zone parameter for a certain river reach and the resulting lag-coefficient. Moreover the distribution of the dead-zone parameter as presented in Fig. 4.1.2 might influence the actual lag-coefficient too.

At last it has to be pointed out that in the dead-zone model after Eqs (4.1.1) and (4.1.2) a completely mixed situation is assumed over the cross-sectional area of the main stream as well as over the cross-sectional area of the dead zones. In Section 4.2 the conditions for this assumption are discussed.

4.2 MASS TRANSFER BETWEEN THE MAIN STREAM AND THE DEAD ZONE

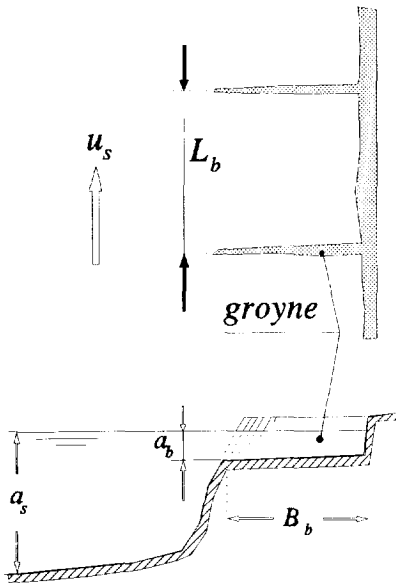


Fig. 4.2.1 Definition sketch of a dead-zone field

Consider a river reach with dead zones, caused by groynes (Fig. 4.2.1). For the description of the exchange of a pollutant between the main stream and the dead zone the longitudinal distance L_b is important. A critical value is the distance for which the velocity head Δh_1 is equal to the loss of energy head Δh_2 over the distance L_b . This distance can be given by applying Chézy's formula for uniform flow conditions (Fig. 4.2.2) (Jansen et al, 1979)

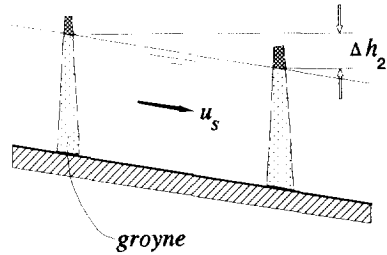


Fig. 4.2.2 Energy loss

$$\Delta h_2 = L_b \cdot \frac{u_s^2}{C^2 \cdot a_s} = \Delta h_1 = \frac{(c_1 \cdot u_s)^2}{2 \cdot g} \quad (4.2.1)$$

or

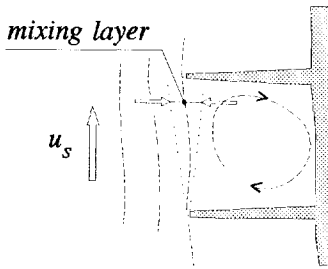
$$L_b = c_1^2 \cdot \frac{C^2 \cdot a_s}{2 \cdot g} \approx c_1^2 \cdot 125 \cdot a_s \quad (4.2.2)$$

with values of about $50 \text{ m}^{1/2}/\text{s}$ for the Chézy-coefficient C .

Because the position of the stagnation point at the downstream groyne lies more or less in the middle of the mixing layer (Fig. 4.2.3), the value of c_1 will be about 0.5 till 0.7, thus

$$L_b \approx 30 \cdot a_s \quad (4.2.3)$$

If $\Delta h_2 \leq \Delta h_1$ an eddy between the groynes can exist (Fig. 4.2.3). After Eqs (4.2.1) and (4.2.2) this condition means



$$L_b \leq 30 \cdot a_s \quad (4.2.4)$$

Now a completely mixed situation can be expected, if the passage-duration of a pollutant at the entrance of the considered groyne-field is larger than the time needed for one turn around of the eddy.

Fig. 4.2.3 Mixing layer downstream of a groyne

Applying the relation given by Booij (1986) between the mean velocity in the main stream u_s and the average velocity in the eddy u_n

$$u_n \approx 0.25 \cdot u_s \quad (4.2.5)$$

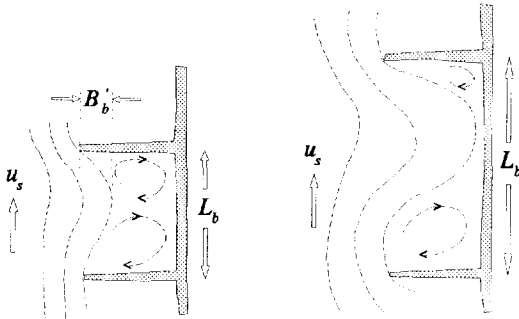


Fig. 4.2.4 Penetration of the dead zone by the main stream

the travel time of one turn around can be estimated. For an eddy with a radius of 50m, - is equal to half of the critical length L_b for a water depth of 3.5m -, and a flow velocity in the main stream of about 1 m/s, this time is about 300 s.

Because the passage-duration mostly will be of the order of hours till days, the assumption of a completely mixed situation in the dead zone will be correct.

In case of

$$L_b > 30 \cdot a_s \quad (4.2.6)$$

the main flow will penetrate into the dead zone and causes smaller eddies, in which a completely mixed situation can be assumed, based on the considerations made above (Fig. 4.2.4). The penetration depth B_b' increases with the length L_b . This means that on one hand the influence of the dead zone is reducing by the decrement of the cross-sectional area of the dead zone, and on the other hand the cross-sectional area of the main flow is increasing, which in succession reduces the mean flow velocity u_s .

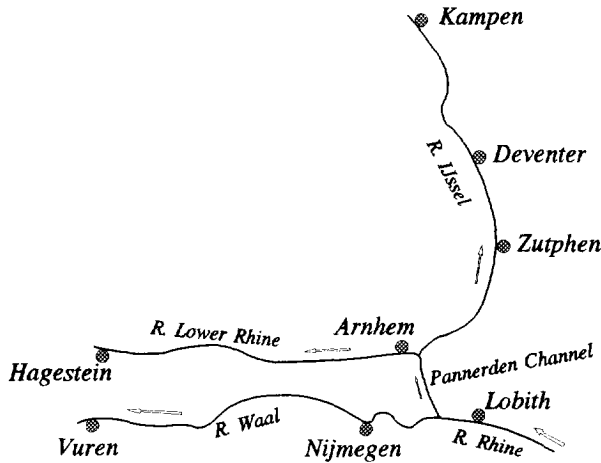


Fig. 4.2.5 Overview of the Rhine branches in the Netherlands downstream of Lobith

Along the branches of the River Rhine in the Netherlands the distance L_b varies from 50 till 135 m. Between Lobith at the German-Dutch border and the water-level gauge station Vuren at the River Waal (Fig. 4.2.5) the distance L_b varies between 75 and 135 m with an average value of 100 m. In the Pannerden Channel and the River Lower Rhine between Arnhem and the water-level gauge station Hagestein distances between 50 and 75 m are found with a predominant value of about 50 m. In the River IJssel branch the distances lie between 25 and 50 m.

The ratio L_b/B_b is always larger than unity and varies between 2 and 4. This means e.g. that for the River IJssel with small values of L_b , the width B_b is about 10 m, so the groyne-fields along the River IJssel are relatively small in relation to the average width of 80 m of the main stream.

Because for average discharge conditions the water depth in the main stream of the Rhine branches varies between 3.5 and 5 m, after Eq.(4.2.3) the length L_b lies

between 100 and 150 m. This means that after Eq.(4.2.4) mostly an eddy between the groynes can exist. Thus it can be concluded that the conditions for a completely mixed situation in the dead zones i.e. the groyne-fields along the Rhine branches in the Netherlands are present.

In case of low-water discharge the weirs in the River Lower Rhine downstream of Arnhem are lowered, so that the water level becomes more or less horizontal and consequently L_b very large. In this case the existence of an eddy is not possible. Due to the very low flow-velocity under these circumstances (0.05 till 0.2 m/s) the mass exchange between the main stream and the dead zones will be limited. Only diffusion and small vortices at the transition between the main stream and the dead zone (groyne-field) are the driving forces. Therefore a completely mixed dead zone can hardly be expected in this case.

As a matter of fact a completely mixed situation in the dead zone does not mean that the concentration in the dead zone (φ_b) is equal to the concentration in the main stream (φ_s). This depends on the transfer velocity E in Eq.(2.3.25), which should be proportional to the flow velocity in the main stream u_s (Valentine and Wood, 1977). The influence of the transfer velocity E on the relation between the dead-zone parameter and the lag coefficient will also be considered in Section 4.3.

4.3 NUMERICAL APPROACH

4.3.1 Theoretical description

In order to examine the relationships between the dead-zone parameter after Eqs (4.1.1) and (4.1.2) and the actual lag-coefficient, the differential equations (2.3.16) and (2.3.18), describing the dead zone model, have to be solved

$$\frac{\partial \varphi_s}{\partial t} + u_s \frac{\partial \varphi_s}{\partial x} - K_s \frac{\partial^2 \varphi_s}{\partial x^2} = -D_s(\varphi_s - \varphi_b) \quad (4.3.1)$$

$$\frac{\partial \varphi_b}{\partial t} = D_b(\varphi_s - \varphi_b) \quad (4.3.2)$$

For a numerical solution of these equations the explicit scheme 'Forward Time, Central Space differences' is used, thus Eqs (4.3.1) and (4.3.2) can be rewritten into difference equations

$$\begin{aligned} \frac{(\varphi_s)_j^{i+1} - (\varphi_s)_j^i}{\Delta t} + u_s \frac{(\varphi_s)_{j+1}^i - (\varphi_s)_{j-1}^i}{2 \cdot \Delta x} - K_s \frac{(\varphi_s)_{j+1}^i - 2 \cdot (\varphi_s)_j^i + (\varphi_s)_{j-1}^i}{\Delta x^2} + \\ + D_s \cdot (\varphi_s)_j^{i+1} - D_s \cdot (\varphi_b)_j^{i+1} = 0 \end{aligned} \quad (4.3.3)$$

$$\frac{(\varphi_b)_j^{i+1} - (\varphi_b)_j^i}{\Delta t} + D_b \cdot (\varphi_b)_j^{i+1} - D_b \cdot (\varphi_s)_j^{i+1} = 0 \quad (4.3.4)$$

To avoid restrictions for the time step Δt in relation to the value of the mass transfer coefficient D_b the last two terms in Eqs (4.3.3) and (4.3.4) are treated implicitly (Wang, 1989). The whole scheme remains effectively explicit.

To solve the concentrations $(\varphi_s)_j^{i+1}$ and $(\varphi_b)_j^{i+1}$ explicitly from Eqs (4.3.3) and (4.3.4), they are rewritten as

$$\begin{aligned} & \{1 + D_s \cdot \Delta t\} \cdot (\varphi_s)_j^{i+1} - \{D_s \cdot \Delta t\} \cdot (\varphi_b)_j^{i+1} = \\ & = (\varphi_s)_j^i - u_s \frac{(\varphi_s)_{j+1}^i - (\varphi_s)_{j-1}^i}{2 \cdot \Delta x} \cdot \Delta t + K_s \frac{(\varphi_s)_{j+1}^i - 2 \cdot (\varphi_s)_j^i + (\varphi_s)_{j-1}^i}{\Delta x^2} \cdot \Delta t \end{aligned} \quad (4.3.5)$$

$$- \{D_b \cdot \Delta t\} \cdot (\varphi_s)_j^{i+1} + \{1 + D_b \cdot \Delta t\} \cdot (\varphi_b)_j^{i+1} = (\varphi_b)_j^i \quad (4.3.6)$$

or in matrix notation

$$\begin{aligned} & \begin{vmatrix} 1 + D_s \cdot \Delta t & -D_s \cdot \Delta t \\ -D_b \cdot \Delta t & 1 + D_b \cdot \Delta t \end{vmatrix} \cdot \begin{vmatrix} (\varphi_s)_j^{i+1} \\ (\varphi_b)_j^{i+1} \end{vmatrix} = \\ & = \begin{vmatrix} (\varphi_s)_j^i - u_s \cdot \frac{(\varphi_s)_{j+1}^i - (\varphi_s)_{j-1}^i}{2 \Delta x} \Delta t + K_s \frac{(\varphi_s)_{j+1}^i - 2(\varphi_s)_j^i + (\varphi_s)_{j-1}^i}{\Delta x^2} \Delta t \\ (\varphi_b)_j^i \end{vmatrix} \end{aligned} \quad (4.3.7)$$

In order to eliminate the concentration in the dead zone in Eq.(4.3.5) the concentration $(\varphi_b)_j^{i+1}$ in Eq.(4.3.6) is written explicitly

$$(\varphi_b)_j^{i+1} = \left(\frac{D_b \cdot \Delta t}{1 + D_b \cdot \Delta t} \right) \cdot (\varphi_s)_j^{i+1} + \left(\frac{1}{1 + D_b \cdot \Delta t} \right) \cdot (\varphi_b)_j^i \quad (4.3.8)$$

Substitution of Eq (4.3.8) into Eq.(4.3.5) gives

$$\begin{aligned}
 \{1 + D_s \cdot \Delta t\} \cdot (\varphi_s)_j^{i+1} - \frac{D_s \cdot D_b \cdot (\Delta t)^2}{1 + D_b \cdot \Delta t} \cdot (\varphi_s)_j^{i+1} - \frac{D_s \cdot \Delta t}{1 + D_b \cdot \Delta t} \cdot (\varphi_b)_j^i = \\
 = (\varphi_s)_j^i - u_s \frac{(\varphi_s)_{j+1}^i - (\varphi_s)_{j-1}^i}{2 \cdot \Delta x} \cdot \Delta t + K_s \frac{(\varphi_s)_{j+1}^i - 2 \cdot (\varphi_s)_j^i + (\varphi_s)_{j-1}^i}{\Delta x^2} \cdot \Delta t
 \end{aligned}
 \tag{4.3.9}$$

or

$$\begin{aligned}
 \left[\frac{1 + D_s \cdot \Delta t + D_b \cdot \Delta t}{1 + D_b \cdot \Delta t} \right] \cdot (\varphi_s)_j^{i+1} = \frac{D_s \cdot \Delta t}{1 + D_b \cdot \Delta t} \cdot (\varphi_b)_j^i + \\
 + (\varphi_s)_j^i - u_s \frac{(\varphi_s)_{j+1}^i - (\varphi_s)_{j-1}^i}{2 \cdot \Delta x} \cdot \Delta t + K_s \frac{(\varphi_s)_{j+1}^i - 2 \cdot (\varphi_s)_j^i + (\varphi_s)_{j-1}^i}{\Delta x^2} \cdot \Delta t
 \end{aligned}
 \tag{4.3.10}$$

Applying the substitution

$$\Lambda = 1 + (D_s + D_b) \cdot \Delta t \tag{4.3.11}$$

or by using the dead zone parameter $\beta = D_s/D_b = A_b/A_s$ after Eqs (2.3.25) and (2.3.28) or (4.1.2)

$$\Lambda = 1 + D_b \cdot (1 + \beta) \cdot \Delta t \tag{4.3.12}$$

Eq.(4.3.10) becomes

$$\begin{aligned}
 (\varphi_s)_j^{i+1} = \frac{\beta \cdot D_b \cdot \Delta t}{\Lambda} \cdot (\varphi_b)_j^i + \\
 + \left(\frac{1 + D_b \cdot \Delta t}{\Lambda} \right) \cdot \left[(\varphi_s)_j^i - u_s \frac{(\varphi_s)_{j+1}^i - (\varphi_s)_{j-1}^i}{2 \cdot \Delta x} \cdot \Delta t \right] + \\
 + \left(\frac{1 + D_b \cdot \Delta t}{\Lambda} \right) \cdot \left[K_s \frac{(\varphi_s)_{j+1}^i - 2 \cdot (\varphi_s)_j^i + (\varphi_s)_{j-1}^i}{\Delta x^2} \cdot \Delta t \right]
 \end{aligned}
 \tag{4.3.13}$$

The concentration in the dead zone will be found in succession by substituting Eq.(4.3.13) into Eq.(4.3.6)

$$\begin{aligned}
 (\varphi_b)_j^{i+1} = & \left[\frac{\beta \cdot (D_b \cdot \Delta t)^2}{\Lambda \cdot (1 + D_b \cdot \Delta t)} + \frac{1}{1 + D_b \cdot \Delta t} \right] \cdot (\varphi_b)_j^i + \\
 & + \left(\frac{D_b \cdot \Delta t}{\Lambda} \right) \cdot \left[(\varphi_s)_j^i - u_s \frac{(\varphi_s)_{j+1}^i - (\varphi_s)_{j-1}^i}{2 \cdot \Delta x} \cdot \Delta t \right] + \\
 & + \left(\frac{D_b \cdot \Delta t}{\Lambda} \right) \cdot \left[K_s \frac{(\varphi_s)_{j+1}^i - 2 \cdot (\varphi_s)_j^i + (\varphi_s)_{j-1}^i}{\Delta x^2} \cdot \Delta t \right]
 \end{aligned}
 \tag{4.3.14}$$

For $\beta = 0$ the concentration in the main stream after Eq.(4.3.13) is independent of the concentration in the dead zone and becomes equal to Eq.(4.3.3) without the two last terms, representing the influence of the dead zone.

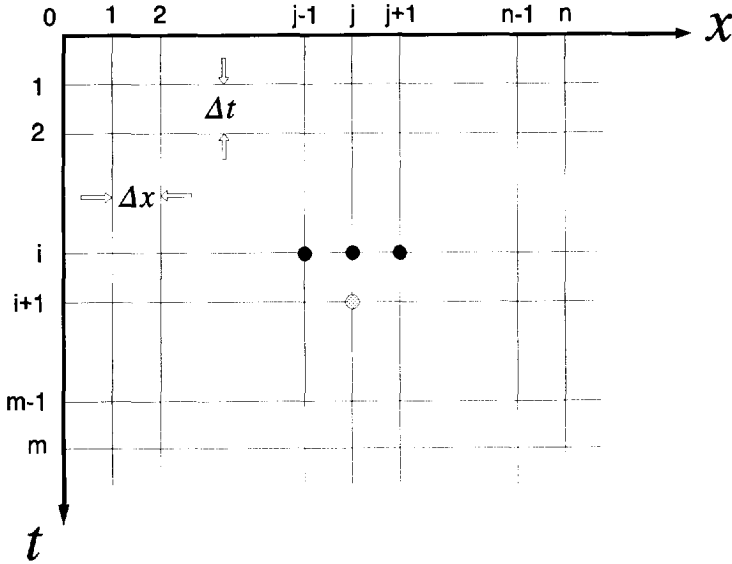


Fig. 4.3.1 Differences scheme for the calculation of the concentrations in the main stream

Because for $t = i \cdot \Delta t$ the concentrations for every value of x are known, the concentrations for $t = (i+1) \cdot \Delta t$ can be determined by Eqs (4.3.13) and (4.3.14) explicitly (Fig. 4.3.1).

The *initial* conditions are

$$\begin{array}{lll} \text{for } t = 0 & \text{and } x > 0 & \varphi_s = 0 \\ & \text{and } x \geq 0 & \varphi_b = 0 \end{array}$$

The last condition means that the concentration $\varphi_b = (\varphi_b)_j^{i=0} = 0$.

The *boundary* condition is given by

$$x = 0 \quad \text{and} \quad t \geq 0 \quad \varphi_s = f(t)$$

As a start for $i = 0$ and 1 ($j = 0$) the concentration is taken constant (see also Fig. 4.3.2)

$$(\varphi_s)_{j=0}^i = \varphi_0 \quad (4.3.15)$$

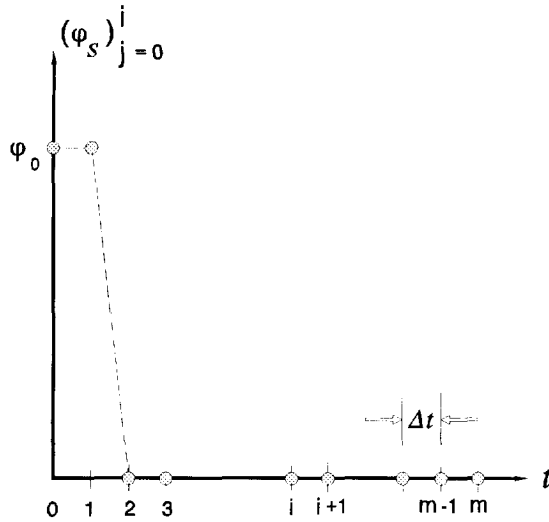


Fig. 4.3.2 Initial concentration-distribution in the main stream; approximation of an instantaneous release

Applying the downstream boundary-condition

$$\frac{\partial^2 \varphi_s}{\partial x^2} = 0$$

the concentrations at this boundary ($j = n$) are found by the following set of equations in according to Eqs (4.3.3) and (4.3.4)

$$\frac{(\varphi_s)_n^{i+1} - (\varphi_s)_n^i}{\Delta t} + u_s \frac{(\varphi_s)_n^i - (\varphi_s)_{n-1}^i}{\Delta x} + D_s \cdot (\varphi_s)_n^{i+1} - D_s \cdot (\varphi_b)_n^{i+1} = 0 \quad (4.3.16)$$

and

$$\frac{(\varphi_b)_n^{i+1} - (\varphi_b)_n^i}{\Delta t} + D_b \cdot (\varphi_b)_n^{i+1} - D_b \cdot (\varphi_s)_n^{i+1} = 0 \quad (4.3.17)$$

This means that for the downstream boundary the Eqs (4.3.13) and (4.3.14) become

$$\begin{aligned} (\varphi_s)_n^{i+1} &= \frac{\beta \cdot D_b \cdot \Delta t}{\Lambda} \cdot (\varphi_b)_n^i + \\ &+ \left(\frac{1 + D_b \cdot \Delta t}{\Lambda} \right) \cdot \left[(\varphi_s)_n^i - u_s \frac{(\varphi_s)_n^i - (\varphi_s)_{n-1}^i}{\Delta x} \cdot \Delta t \right] \end{aligned} \quad (4.3.18)$$

$$\begin{aligned} (\varphi_b)_n^{i+1} &= \left[\frac{\beta \cdot (D_b \cdot \Delta t)^2}{\Lambda \cdot (1 + D_b \cdot \Delta t)} + \frac{1}{1 + D_b \cdot \Delta t} \right] \cdot (\varphi_b)_n^i + \\ &+ \left(\frac{D_b \cdot \Delta t}{\Lambda} \right) \cdot \left[(\varphi_s)_n^i - u_s \frac{(\varphi_s)_n^i - (\varphi_s)_{n-1}^i}{\Delta x} \cdot \Delta t \right] \end{aligned} \quad (4.3.19)$$

Concerning the stability of the calculations in case of $\beta = 0$, the values of the time (Δt) and space steps (Δx) are limited. The conditions for the stability are in succession (Vreugdenhil, 1989)

$$\Delta t < \frac{2 \cdot K_s}{u_s^2} \quad (4.3.20)$$

and

$$\Delta t \leq \frac{\Delta x^2}{2 \cdot K_s} \quad (4.3.21)$$

However, the conditions for the values of Δt and Δx are not only determined by Eqs (4.3.20) and (4.3.21), but also by the distance over which the value of β varies.

In Eqs (4.3.13) and (4.3.14) as well as in Eqs (4.3.18) and (4.3.19) the coefficients D_s and D_b are supposed to be constant, as well as the longitudinal dispersion-coefficient K_s and the mean flow-velocity u_s . However, the dead zone parameter β ($= D_s/D_b = A_b/A_s$) varies along the river (see Section 4.1), as well as the coefficient D_b , according to the variance of the dead zone cross-sectional area A_b (Eq. 2.3.25). Therefore Eqs (4.3.13) and (4.3.14) should be rewritten

$$\begin{aligned}
 (\varphi_s)_j^{i+1} = & \frac{\beta_j \cdot (D_b)_j \cdot \Delta t}{\Lambda_j} \cdot (\varphi_b)_j^i + \\
 & + \left(\frac{1 + (D_b)_j \cdot \Delta t}{\Lambda_j} \right) \cdot \left[(\varphi_s)_j^i - u_s \frac{(\varphi_s)_{j+1}^i - (\varphi_s)_{j-1}^i}{2 \cdot \Delta x} \cdot \Delta t \right] + \\
 & + \left(\frac{1 + (D_b)_j \cdot \Delta t}{\Lambda_j} \right) \cdot \left[K_s \frac{(\varphi_s)_{j+1}^i - 2 \cdot (\varphi_s)_j^i + (\varphi_s)_{j-1}^i}{\Delta x^2} \cdot \Delta t \right]
 \end{aligned}
 \tag{4.3.22}$$

and

$$\begin{aligned}
 (\varphi_b)_j^{i+1} = & \left[\frac{\beta_j \cdot [(D_b)_j \cdot \Delta t]^2}{\Lambda_j \cdot [1 + (D_b)_j \cdot \Delta t]} + \frac{1}{1 + (D_b)_j \cdot \Delta t} \right] \cdot (\varphi_b)_j^i + \\
 & + \left(\frac{(D_b)_j \cdot \Delta t}{\Lambda_j} \right) \cdot \left[(\varphi_s)_j^i - u_s \frac{(\varphi_s)_{j+1}^i - (\varphi_s)_{j-1}^i}{2 \cdot \Delta x} \cdot \Delta t \right] + \\
 & + \left(\frac{(D_b)_j \cdot \Delta t}{\Lambda_j} \right) \cdot \left[K_s \frac{(\varphi_s)_{j+1}^i - 2 \cdot (\varphi_s)_j^i + (\varphi_s)_{j-1}^i}{\Delta x^2} \cdot \Delta t \right]
 \end{aligned}
 \tag{4.3.23}$$

and for the concentrations at the downstream boundary according to Eqs (4.3.18) and (4.3.19) in succession

$$\begin{aligned}
 (\varphi_s)_n^{i+1} &= \frac{\beta_n \cdot (D_b)_n \cdot \Delta t}{\Lambda_n} \cdot (\varphi_b)_n^i + \\
 &+ \left(\frac{1 + (D_b)_n \cdot \Delta t}{\Lambda_n} \right) \cdot \left[(\varphi_s)_n^i - u_s \frac{(\varphi_s)_n^i - (\varphi_s)_{n-1}^i}{\Delta x} \cdot \Delta t \right]
 \end{aligned}
 \tag{4.3.24}$$

and

$$\begin{aligned}
 (\varphi_b)_n^{i+1} &= \left[\frac{\beta_n \cdot [(D_b)_n \cdot \Delta t]^2}{\Lambda_n \cdot [1 + (D_b)_n \cdot \Delta t]} + \frac{1}{1 + (D_b)_n \cdot \Delta t} \right] \cdot (\varphi_b)_n^i + \\
 &+ \left(\frac{(D_b)_n \cdot \Delta t}{\Lambda_n} \right) \cdot \left[(\varphi_s)_n^i - u_s \frac{(\varphi_s)_n^i - (\varphi_s)_{n-1}^i}{\Delta x} \cdot \Delta t \right]
 \end{aligned}
 \tag{4.3.25}$$

with

$$\Lambda_{j,n} = 1 + (D_b)_{j,n} \cdot (1 + \beta_{j,n}) \cdot \Delta t
 \tag{4.3.26}$$

4.3.2 Dimensional analysis

As mentioned in Section 4.1 the actual lag-coefficient, related to the actual transport-velocity c of a pollution cloud is not always equal to the dead-zone parameter after Eq.(4.1.2)

$$\beta = \frac{A_b}{A_s}$$

The difference between the actual lag-coefficient $\beta_{act.}$ and the dead-zone parameter β is given by the ratio of actuality after Eq.(4.1.3)

$$\kappa = \frac{\beta_{act.}}{\beta} \quad (0 < \kappa < 1) \quad (4.3.27)$$

Considering a river with one value for the dead-zone parameter (the ratio of the cross-sectional areas of the main stream and the stagnant zones are constant) there will be an adaptation length L_a from the point of release or the point where the groyne-fields start, over which the actual transport-velocity $c_{act.}$ changes from u_s to c after Eq.(4.1.1). Over this distance the actual lag-coefficient $\beta_{act.}$ varies from zero to $\beta = A_b/A_s$, i.e. the κ -value increases continuously from zero to one.

Considering a certain river reach with a variable value of the dead-zone parameter, there might be a difference between the mean value of the dead-zone parameter and the overall lag-coefficient over this river reach, i.e. the κ -value lies between zero and one. In case of an instantaneous adaptation of the transport velocity c to an increase or decrease of the dead-zone parameter after Eq.(4.1.1) the lag coefficient becomes equal to the mean value of the dead-zone parameter ($\kappa = 1$).

Beside the dead-zone parameter β , the actual lag-coefficient also depends on the mass transfer between the main stream and the stagnant zone, which on its turn depends on the concentration differences between the main stream and the stagnant zone. The concentration distribution in the main stream depends primarily on the flow velocity u_s and the longitudinal dispersion-coefficient K_s (see Eq. 2.1.8). The mass transfer is represented by the coefficients D_s and D_b for which yields $D_s/D_b = A_b/A_s = \beta$ (see Eq.2.3.25).

Thus the ratio of actuality κ is influenced by the parameters β , D_b , K_s and u_s . For the examination of relations between the κ -value and these parameters with the help of the numerical dead-zone model after the Eqs (4.3.22) ... (4.3.26), a dimensional analysis for the differential equations (4.3.1) and (4.3.2) has been carried out.

Introducing a time and length scale after

$$x = L \cdot \bar{x} \quad (4.3.28)$$

$$t = \frac{L}{u_s} \cdot \bar{t} \quad (4.3.29)$$

wherein L is the length scale, the Eqs (4.3.1) and (4.3.2) can be rewritten into a dimensionless form

$$\frac{\partial \varphi_s}{\partial \bar{t}} + \frac{\partial \varphi_s}{\partial \bar{x}} - \frac{K_s}{u_s \cdot L} \frac{\partial^2 \varphi_s}{\partial \bar{x}^2} = - \frac{D_s \cdot L}{u_s} (\varphi_s - \varphi_b) \quad (4.3.30)$$

$$\frac{\partial \varphi_b}{\partial t} = \frac{D_b \cdot L}{u_s} (\varphi_s - \varphi_b) \quad (4.3.31)$$

Now three dimensionless parameters can be distinguished

$$\frac{K_s}{u_s \cdot L} \quad ; \quad \frac{D_s \cdot L}{u_s} \quad ; \quad \frac{D_b \cdot L}{u_s}$$

Because the mass transfer coefficients are related to each other by the dead zone parameter β after $D_s/D_b = \beta$, the dimensionless parameters concerned can be rewritten by

$$\frac{K_s}{u_s \cdot L} \quad ; \quad \frac{D_b \cdot L}{u_s} \quad ; \quad \beta \quad (4.3.32)$$

For the dimensionless distance the Péclet number is chosen by setting $L = x$ in the first dimensionless parameter of Eq.(4.3.32)

$$Pe = \frac{u_s \cdot x}{K_s} \quad (4.3.33)$$

In succession the relation of κ with the mass transfer coefficients D_s and D_b can now be given by the dimensionless mass-transfer parameter \mathcal{E} , as a combination of the first and second dimensionless parameter of Eq.(4.3.32) after

$$\mathcal{E} = \frac{D_b \cdot L}{u_s} \cdot \frac{K_s}{u_s \cdot L} = \frac{D_b \cdot K_s}{u_s^2} \quad (4.3.34)$$

Thus the relation to be examined by the numerical dead-zone model is

$$\kappa = f(Pe, \mathcal{E}) \quad (4.3.35)$$

Instead of the Péclet number also the second term of Eq.(4.3.32) could be chosen for the dimensionless distance

$$\frac{D_b \cdot x}{u_s} \quad (4.3.36)$$

4.3.3 Initial behaviour of the transport velocity in a river without dead zones

For the examination of the relations after the Eqs (4.3.35) or (4.3.36) the value of $\beta_{act.}$ has to be determined after

$$\beta_{act.} = \frac{u_s}{c_{act.}} - 1 \quad (4.3.37)$$

The actual transport velocity $c_{act.}$ of a pollution cloud can be related to

- * the time-centroid of the concentration distribution, according to Eq.(2.3.78)
- * the peak value of the concentration distribution.

The space-centroid of the concentration distribution will not be considered, because this definition needs various points of calculation or observation (in case of a tracer experiment) in the x -direction. From a practical point of view this means a too labour-intensive procedure and therefore not performable. Moreover concentration distributions in the space domain are equal to the concentration distributions in the time domain as long as the distributions deform very slowly ("frozen cloud"-approach).

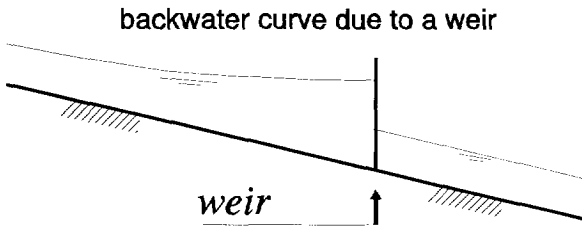


Fig. 4.3.3 Water-level profile at a weir

In case of discontinuities of the flow velocity caused by weirs, there is a remarkable deformation of the pollution cloud, resulting in a so called turn-over process (Kuik, C.A. van & A. van Mazijk, 1994). At the upstream side of the weir the velocity of the space-centroid is already influenced by the larger flow-velocity

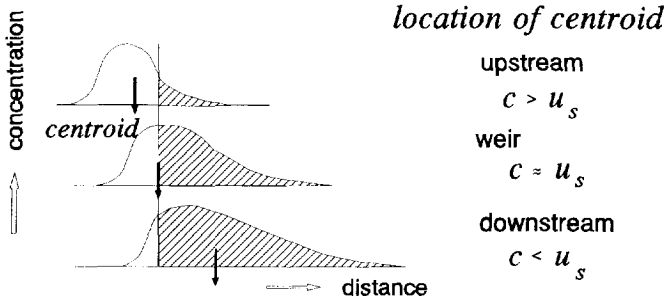


Fig. 4.3.4 Behaviour of a pollution cloud in the vicinity of a weir

downstream of the weir and at the downstream side the upstream flow-velocity still influences the velocity of the space-centroid (Figs 4.3.3 and 4.3.4). As a result the lag coefficient after Eq.(4.3.37) shows negative and positive peak-values (Fig. 4.3.5 and 4.3.6).

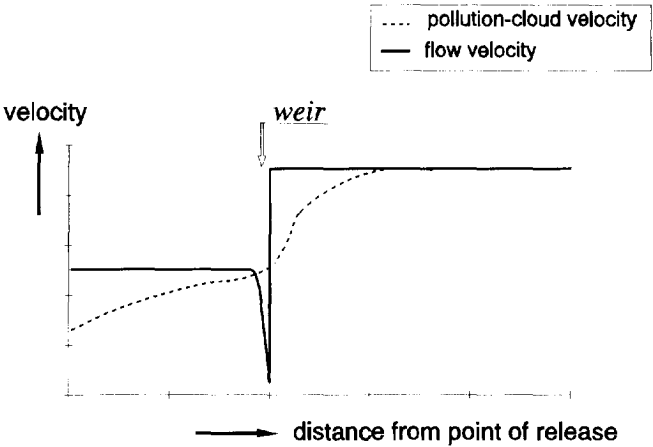


Fig. 4.3.5 Longitudinal distribution of the flow and pollution-cloud velocity in the vicinity of a weir after van Kuik & van Mazijk (1994)

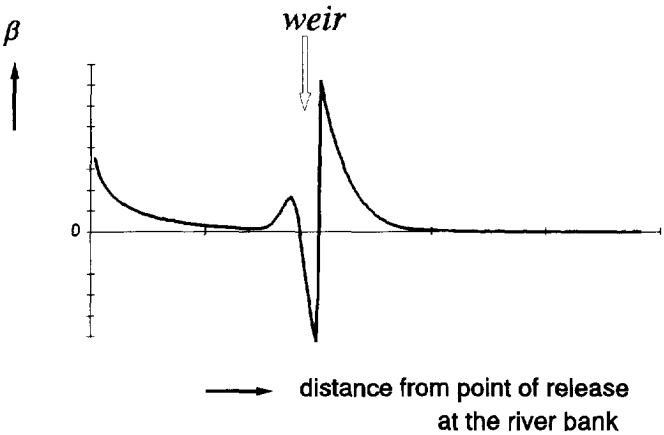


Fig. 4.3.6 Distribution of the lag coefficient β in the vicinity of a weir, based on the space-centroid after van Kuik & van Mazijk (1994)

Therefore generally the time-centroid has to be preferred as the variable for the determination of the transport velocity.

From the point of release the transport velocity c of a pollution cloud based on the time-centroid is equal to the flow velocity in case there are no stagnant zones (the dead-zone parameter $\beta = 0$). It yields after Eq.(2.3.69) (see also Krenkel, 1962)

$$\mu_t = \left(\frac{x}{u_s} + \frac{2 \cdot K}{u_s^2} \right) \quad (4.3.38)$$

With Eq.(2.3.78)

$$c = \left(\frac{d\mu_t}{dx} \right)^{-1} \quad (4.3.39)$$

the transport velocity becomes

$$c = u_s \quad (4.3.40)$$

This means that from the point of release the time-centroid can be used as the parameter for the examination of the influence of artificial stagnant-zones on the actual transport-velocity $c_{act.}$, i.e. the ratio of actuality κ .

If the transport time is related to the peak concentration, this parameter does not always represent the flow velocity in case the dead-zone parameter $\beta = 0$.

Considering Eq.(2.1.8) (the Taylor-model) and Eq.(2.3.85) (Chatwin-model) the transport velocity related to the peak concentration can be determined as a function of the distance from the point of release. The time t_{max} , which corresponds with the peak concentration can be found by

$$\frac{\partial \varphi}{\partial t} = 0 \quad (4.3.41)$$

Applying Eq.(4.3.41) to Eq.(2.1.8), the following expression is found for the time corresponding with the maximum concentration (t_{max}), setting $K = K_s$ and $u = u_s$,

$$t_{max} = \frac{-K_s + \sqrt{K_s^2 + u_s^2 x^2}}{u_s^2} \quad (4.3.42)$$

Thus the average transport-velocity $\bar{c}(x)$ over the distance x from the point of release and related to the peak concentration, is given by

$$\bar{c}(x) = \frac{x}{t_{max}} = \frac{u_s^2 x}{-K_s + \sqrt{K_s^2 + u_s^2 x^2}} \quad (4.3.43)$$

and according to Eq.(4.3.37) the corresponding overall lag-coefficient $\beta_{overall}$ by

$$\beta_{overall}(x) = \frac{u_s}{\bar{c}(x)} - 1 = \frac{-K_s + \sqrt{K_s^2 + u_s^2 x^2}}{u_s x} - 1$$

$$\beta_{overall} = \frac{\sqrt{1+Pe^2} - 1}{Pe} - 1 \quad (4.3.44)$$

with the Péclet number $Pe = u_s \cdot x/K_s$.

For the determination of the local value of the lag coefficient (β_{local}) the local transport-velocity $c(x)$ related to the peak concentration, has to be considered

$$\frac{1}{c(x)} = \frac{dt_{max}}{dx} = \frac{x}{\sqrt{K_s^2 + u_s^2 x^2}} \quad (4.3.45)$$

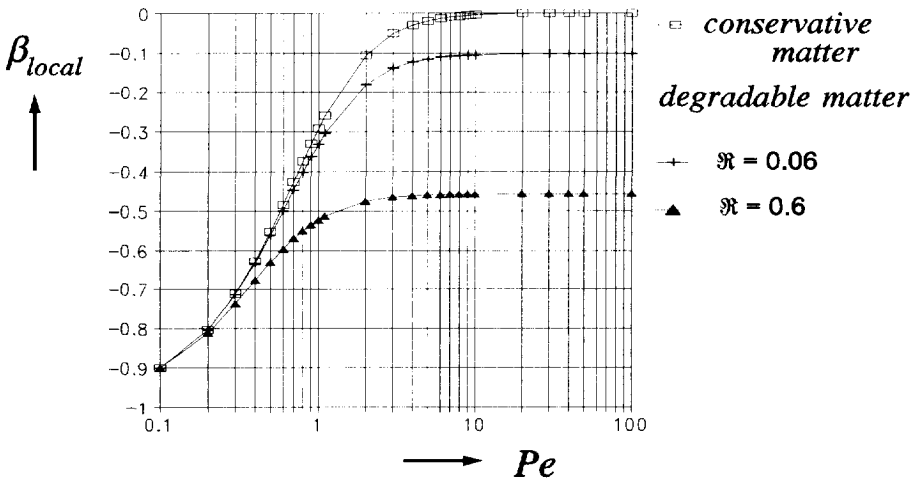


Fig. 4.3.7 Distribution of the local β -value with the dimensionless distance (Pe -number) for conservative and degradable matter after Eqs (4.3.46) and (4.3.49)

Then the corresponding lag-coefficient becomes

$$\beta_{local} = \frac{u_s}{c} - 1 = \frac{u_s x}{\sqrt{K_s^2 + u_s^2 x^2}} - 1$$

$$\beta_{local} = \frac{Pe}{\sqrt{1 + Pe^2}} - 1 \quad (4.3.46)$$

In Fig. 4.3.7 equation (4.3.46) is presented graphically. The negative value of the lag coefficient is caused by the dispersion. Near the point of release the concentration gradients are relatively large and consequently the dispersive transport is large. This gives a relatively steep front of the concentration distribution in the time domain with a relatively large tail: the distribution shows a positive skewness (Fig. 4.3.8). At large distances from the point of release, β becomes zero: Pe -number > 10 . In the River Rhine with a mean flow-velocity of 1 m/s and dispersion coefficients smaller than 3000 m²/s (Fig. 2.3.9), the lag coefficient has become zero at distances within 3 km from the point of release. This means that in case of far-field studies the influence of the dispersion, resulting into a negative value of the lag coefficient, is negligible.

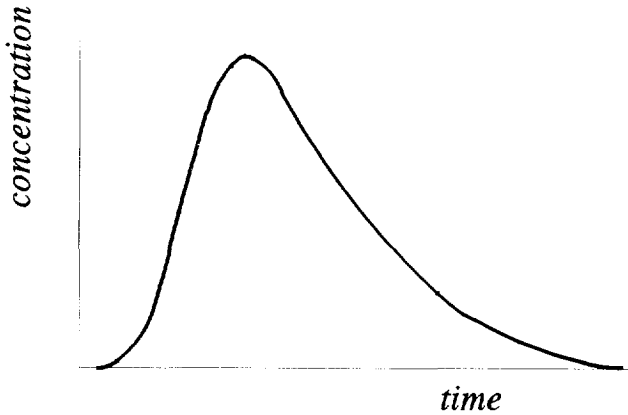


Fig. 4.3.8 Concentration distribution in the time domain with a positive skewness

If the pollution consists of a degradable matter with a first order decomposition process and a decay coefficient k , Eq.(2.1.8) becomes

$$\bar{\varphi}(x,t) = \frac{M/A}{\sqrt{4 \cdot \pi \cdot K \cdot t}} \exp \left[- \frac{(x - u_s \cdot t)^2}{4 \cdot K \cdot t} - k \cdot t \right] \quad (4.3.47)$$

and in succession Eq.(4.3.42)

$$t_{max} = \frac{-K_s + \sqrt{K_s^2 + (4K_s k + u_s^2) \cdot x^2}}{4K_s k + u_s^2} \quad (4.3.48)$$

With the dimensionless distance $Pe = u_s \cdot x/K_s$ and by introducing the dimensionless parameter $\mathfrak{R} = K_s \cdot k/u_s^2$ Eq.(4.3.48) becomes for degradable matter

$$\beta_{local} = \frac{Pe}{\sqrt{1 + (4\mathfrak{R} + 1) \cdot Pe^2}} - 1 \quad (4.3.49)$$

This means, that the decay do increase the distance over which the local β -value is negative (Fig. 4.3.7), moreover for large distances β_{local} reaches a negative limit-value, given by

$$\beta_{local} = \frac{1}{\sqrt{4\mathfrak{R} + 1}} - 1 \quad (4.3.50)$$

In Fig. 4.3.7 two values of the dimensionless parameter \mathfrak{R} are considered. In Table 4.3.1 \mathfrak{R} -values are presented, based on extreme values of the dispersion coefficient K_s , the degradation coefficient k and the flow velocity u_s .

TABLE 4.3.1 \mathfrak{R} -values

	\mathfrak{R}	K_s (m ² /s)	u_s (m/s)	k (day ⁻¹)
mean value	$7 \cdot 10^{-4}$	200	1.0	0.3
large value	$6 \cdot 10^{-1}$	1000	0.1	0.5
small value	$3 \cdot 10^{-5}$	100	2.0	0.1

It can be concluded that also for degradable matter the negative value of β is negligibly small in case of far-field studies (see Eq. 4.3.50).

In a similar way the time corresponding with the peak concentration after the Chatwin-model with a skewness parameter $G_s = 1$ (Eq. 2.3.85) is determined (see also Appendix E). In Fig. 4.3.9 the resulting distribution of the lag coefficient β is compared with the distribution after the Taylor-model. In case of the Chatwin-model the local β -value becomes negligible ($-0.05 < \beta_{local} < 0$) at distances of about 10 times the distance, found in case of the Taylor-model. The reason for this increment is the effect of the Hermite-polynomial, which transforms the concentration distribution after the Taylor-model in order to realise the skewness of the distribution as mostly measured in nature (Fig. 4.3.10).

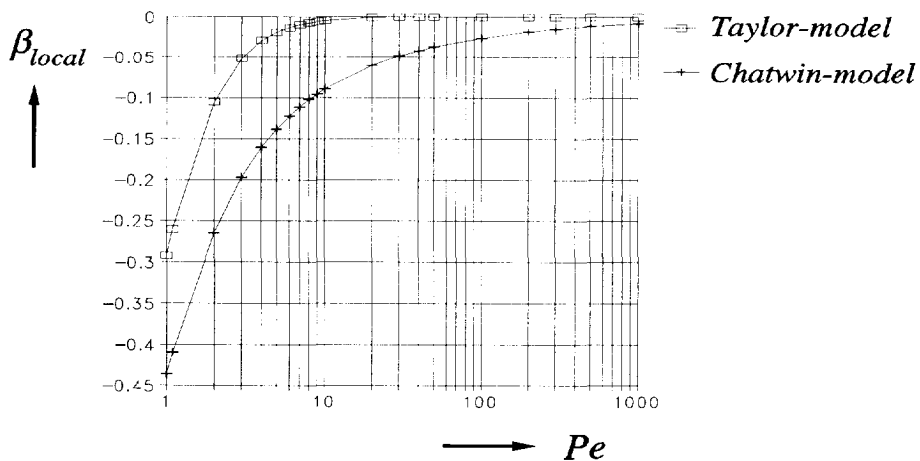


Fig. 4.3.9 Comparison of the distributions of the local β -value with the dimensionless distance (Pe -number) after the Taylor- and the Chatwin-model for conservative matter

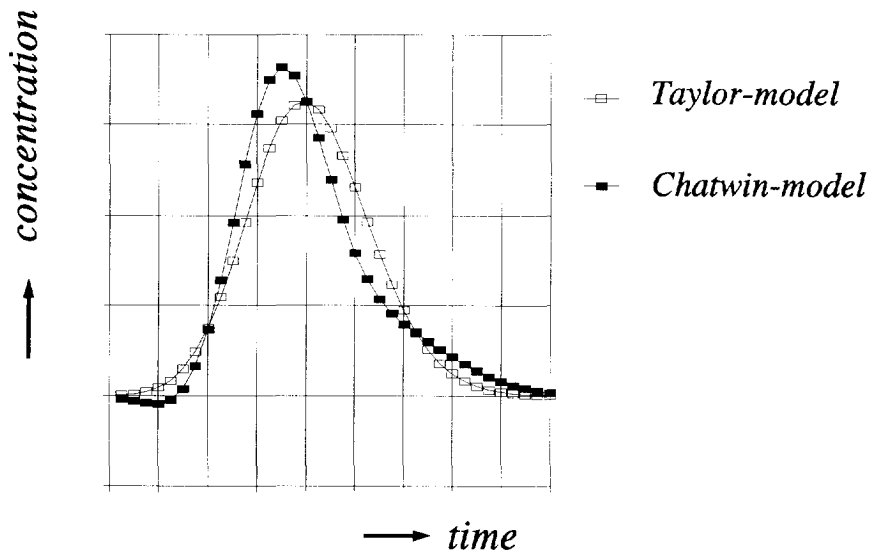


Fig. 4.3.10 Comparison of the concentration distributions after the Taylor- and the Chatwin-model

In Fig. 4.3.11 the distribution of the *overall* value of the lag coefficient for the Taylor- and the Chatwin-model are presented and compared with the distribution after the numerical model, presented in Sub-section 4.3.1 by Eq.(4.3.3) with the neglect of the two terms concerning the exchange of the dead zone ($D_s = 0$). In order to get the time the maximum concentration occurs exactly as possible, the used time-step Δt was 1 second. For the determination of the local value of the lag coefficient the space step was chosen as small as possible. Referring to Eqs (4.3.20) and (4.3.21) the space step Δx becomes 20 m, considering a longitudinal dispersion-coefficient K_s of 100 m²/s and a flow velocity u_s of 1 m/s.

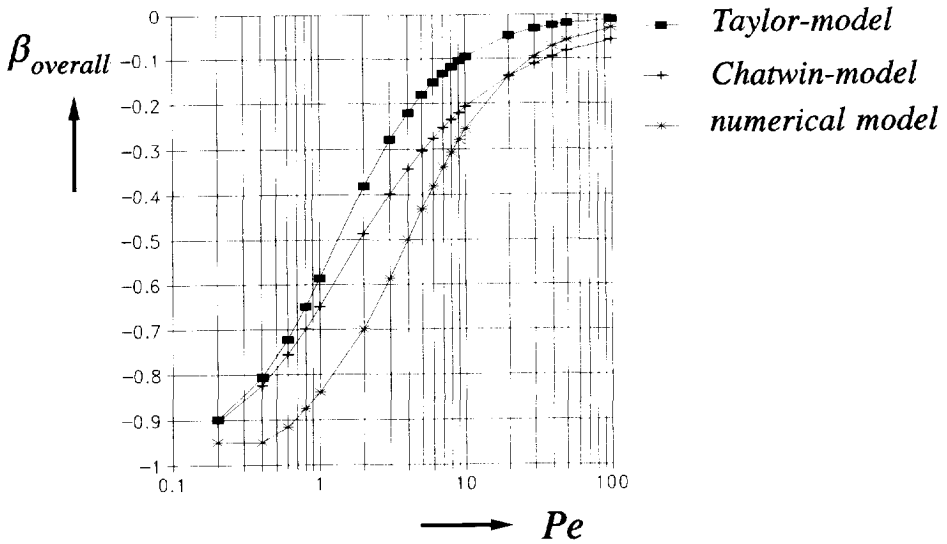


Fig. 4.3.11 Comparison of the distributions of the overall β -value with the dimensionless distance (Pe -number) after the Taylor-, Chatwin- and numerical model

For all models the influence of the dispersion at the transport time of the peak concentration, represented by the overall value of the lag coefficient has nearly been vanished at a distance corresponding with $Pe = 100$. However, the differences in the distribution of the overall lag-coefficient between the Chatwin-model and the numerical model only concerns the transport time of the maximum concentration itself and not the concentration distribution in the time domain as a whole (Fig. 4.3.12). The concentration distribution after the numerical model suits quite well with the Chatwin-model.

In Fig. 4.3.13 the distribution of the *local* β -value for the numerical model after Eq.(4.3.3) with $D_s = 0$ is plotted for two space steps. The step-wise variations in

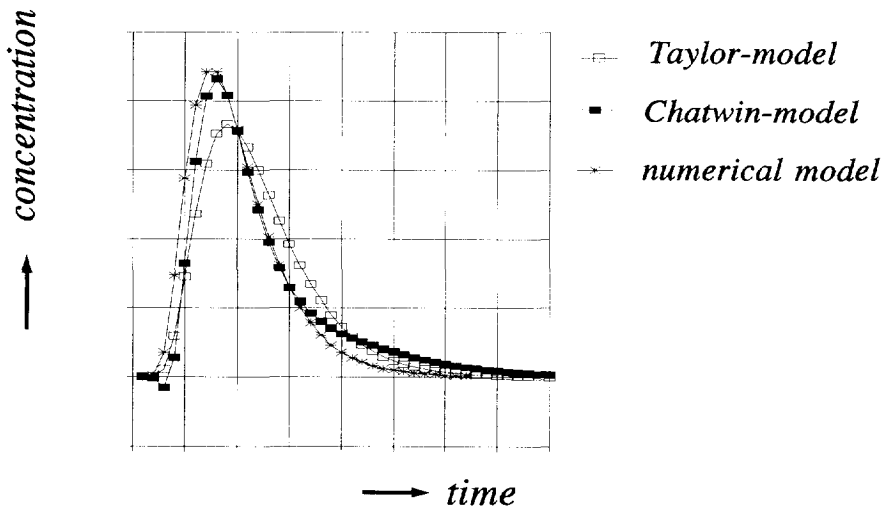


Fig. 4.3.12 Comparison of the concentration distributions after the Taylor-, Chatwin- and numerical model at a distance from the point of release, which corresponds with $Pe = 10$

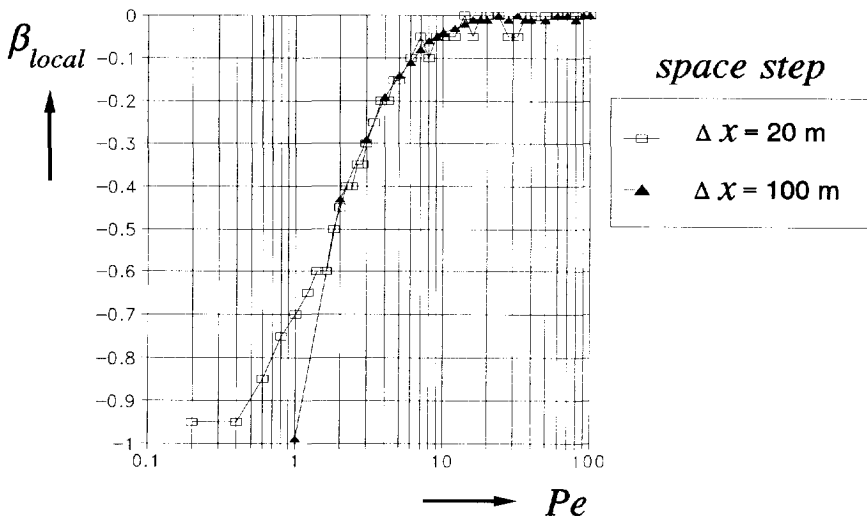


Fig. 4.3.13 Influence of the space step on the distribution of the local lag-coefficient with the dimensionless distance (Pe -number) for the numerical model after Eq.(4.3.3) with $D_s = 0$

in the distribution for $\Delta x = 20$ m is caused by the time and space step

$$\beta_{local} = \frac{u_s \cdot \Delta t_{max}}{\Delta x} - 1 \quad (4.3.51)$$

In the numerical model the time of the maximum concentration is approximated by the time step for which the calculated concentration has a maximum value. Thus the accuracy of Δt_{max} is 0.5 s in this case (time step $\Delta t = 1$ s). After Eq.(4.3.51) the distribution becomes smoother if the space step increases. Because Eq.(4.3.51) is an approximation of

$$\beta_{local} = u_s \cdot \frac{dt_{max}}{dx} - 1 \quad (4.3.52)$$

for small values of Pe the time step as well as the space step have to become smaller in order to get more accurate β -values. In Fig. 4.3.14 the distribution of the local β -value after the numerical model is compared with those after the Taylor- and Chatwin-model.

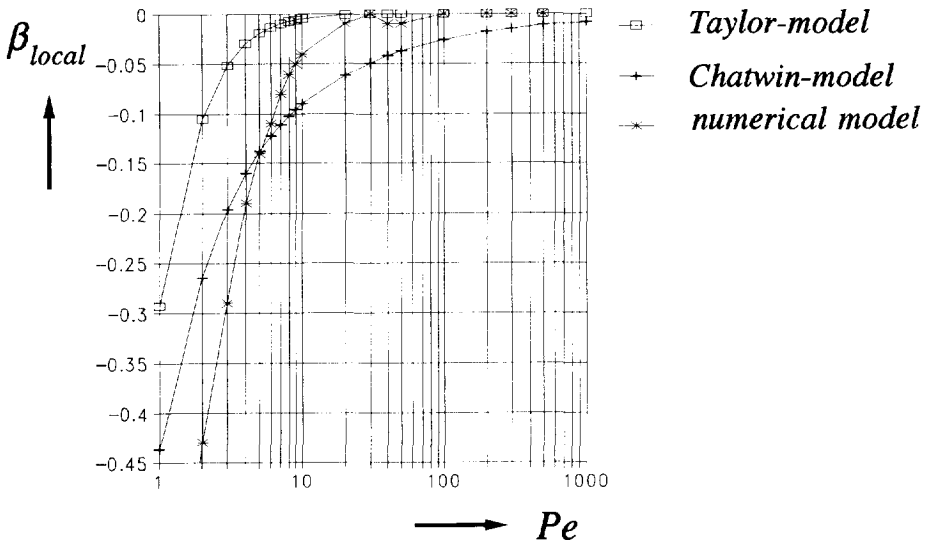


Fig. 4.3.14 Comparison of the distributions of the local β -value after the Taylor- and Chatwin-model with the numerical model ($\Delta x = 100$ m)

Based on the distributions of the overall as well as the local β -value it can be concluded that the influence of the dispersion on the transport velocity of the peak concentration has become negligible at a distance corresponding with a Pe -number

of 100. This means for the examination of the influence of dead zones on the transport velocity of the peak concentration by the numerical model, i.e. for the analysis of the ratio of actuality κ of the lag coefficient in relation with the dead-zone parameter after Eq.(4.3.35) or Eq.(4.3.36), the dead zones in the model concerned, have to begin not until $Pe \geq 100$.

4.3.4 Initial behaviour of the transport velocity in a river with one single dead-zone parameter

For the determination of the influence of the stagnant zones on the transport velocity near the point of release or just downstream of the starting point of the dead zones (e.g. groyne-fields) computations were carried out with the numerical model described in Sub-section 4.3.1. The values of the parameters for the reference situation are mainly based on the situation in the River Rhine. The order of magnitude of the flow velocity in the River Rhine is 1 m/s. The longitudinal dispersion-coefficient is of the order of 10^2 till 10^3 . For an estimation of the magnitude of the mass-transfer coefficient (D_b) Eq.(2.3.73) is considered

$$D_b = \frac{\alpha_s \cdot P_s}{A_b} \cdot E \quad (4.3.53)$$

With Eq.(2.3.74)

$$E \approx 0.02 \cdot u_s$$

and defining the hydraulic radius by

$$R = \frac{A_s}{P_s} \approx a$$

Eq.(4.3.53) becomes for $\alpha_s = 1$

$$D_b \approx 0.02 \cdot \frac{A_s}{A_b} \cdot \frac{u_s}{a} = 0.02 \cdot \frac{u_s}{\beta \cdot a} \quad (4.3.54)$$

Considering the following average values, according to the River Rhine

$$\begin{array}{lll} \beta & \approx & 10^{-1} \\ u_s & \approx & 1 \text{ m/s} \\ a & \approx & 5 \text{ m} \end{array}$$

the value of D_b becomes of the order of

$$O(D_b) = O\left(10^{-2} \cdot \frac{10^0}{10^{-1} \cdot 10^1}\right) = O(10^{-2}) \quad (4.3.55)$$

Therefore the reference value of D_b is 0.01 s^{-1} .

For the examination of the influences of the parameters K_s and D_b on the distribution of the κ -value four computations were carried out with a constant dead-zone parameter of 0.20 (see Table 4.3.2). To be sure that the results show only the effect of the dead zones on the transport velocity, in the model these zones start at a distance corresponding with $Pe = 10$ from the point of release (Fig. 4.3.15). In Table 4.3.3 the applied space and time step of the executed runs are collected.

TABLE 4.3.2 Input data of the computations for the analysis of the initial behaviour of the κ -value, related to the time-centroid of the concentration distribution

run nr.	K_s (m^2/s)	D_b (s^{-1})	u_s (m/s)	β	\mathcal{E} (Eq.4.3.34)
1	100	0.01	1	0.2	1
2	1000	0.01	1	0.2	10
3	100	0.001	1	0.2	0.1
4	1000	0.001	1	0.2	1

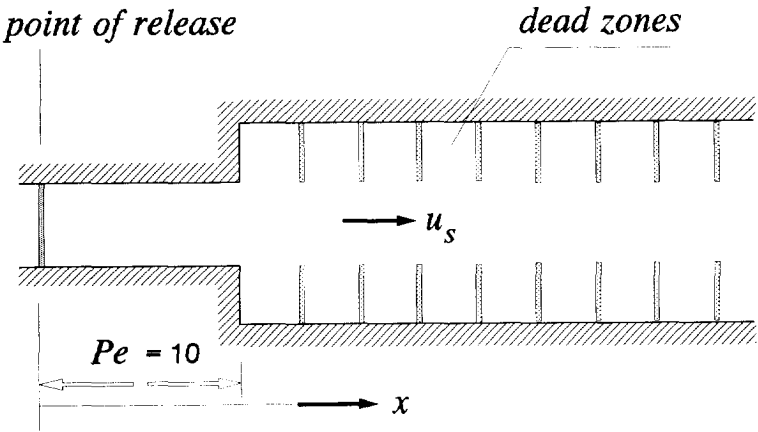


Fig. 4.3.15 Model schematization of the executed computations after Table 4.3.2

Figure 4.3.16 shows the distribution of the local κ -value with the distance in kilometre from the starting point of the dead zones (Fig. 4.3.15) for two values of the mass-transfer coefficient (run nrs 1 and 3). Both distributions of κ are completely

TABLE 4.3.3 Numerical input-data for the computations, executed in the frame work of the analysis of the initial behaviour of the κ -value (see Table 4.3.2)

run nr.	space step Δx (m)	time step Δt (s)	distance without dead zones ($Pe = 10$) (km)
1	50	10	1
2	500	30	10
3	50	10	1
4	500	30	10

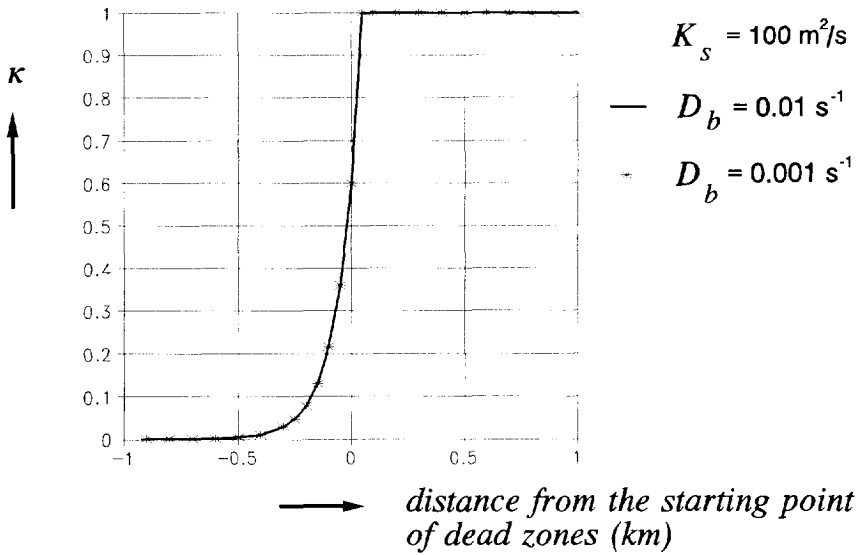


Fig. 4.3.16 Distribution of the local κ -value in the vicinity of the starting point of the dead zones for two values of the mass-transfer coefficient D_b , (run nrs 1 and 3)

equal. Comparing the results of run numbers 1 and 2 with different longitudinal dispersion-coefficients (Fig. 4.3.17), it can be concluded that due to the dispersion the transport velocity upstream of the starting point is also reduced by the stagnant zones: the larger the coefficient the longer the distance over which this phenomena can be observed. In case the dimensionless distance after the Pe -number is used, there is no difference in the local κ -distribution (Fig. 4.3.18). Thus the executed run nrs 1 ... 4 show the same distribution.

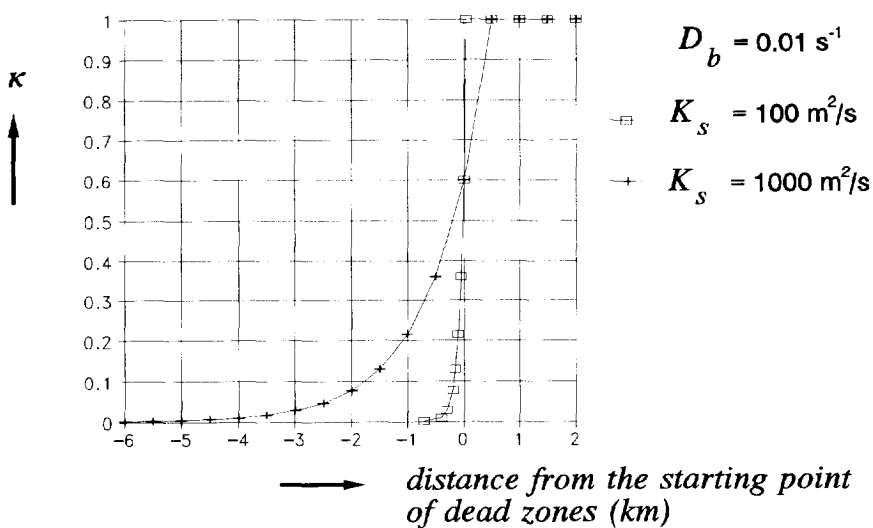


Fig. 4.3.17 Distribution of the local κ -value in the vicinity of the starting point of the dead zones for two values of the longitudinal dispersion-coefficient K_s (run nrs 1 and 2)

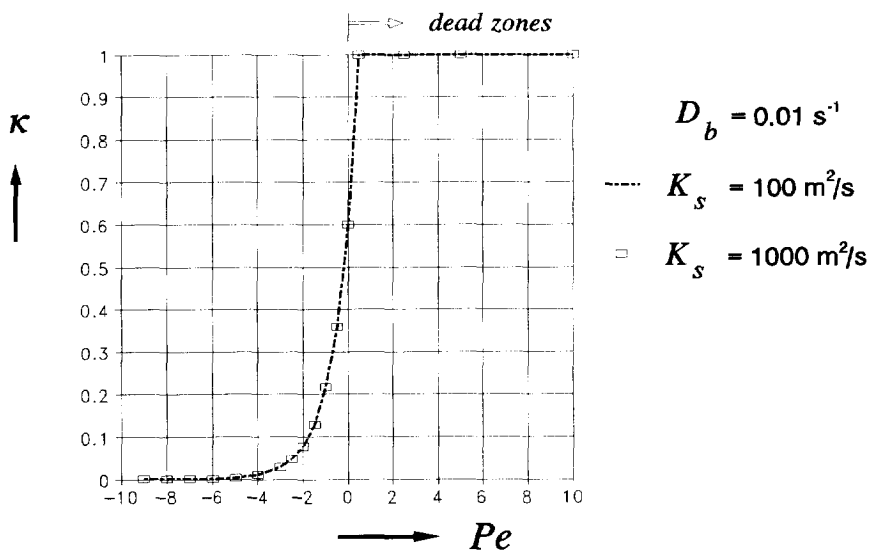


Fig. 4.3.18 Distribution of the local κ -value for two values of the longitudinal dispersion-coefficient K_s as a function of Pe (run nrs 1 and 2)

Further the Figs 4.3.16 ... 4.3.18 present that there is more or less an instantaneous adaptation of the transport velocity c to the dead zones at the beginning of these zones after Eq.(4.1.1)

$$c = \frac{u_s}{1 + \beta} \quad (4.3.56)$$

The reason for the instantaneous adaptation of the transport velocity is because also the whole tail of the concentration distribution at $x = L$ is taken into account for the determination of the time-centroid after Eq.(2.3.62)

$$\mu_t = \frac{1}{m_0} \int_{-\infty}^{\infty} t \cdot \varphi_s(L, t) dt \quad (4.3.57)$$

with

$$m_0 = \int_{-\infty}^{\infty} \varphi_s(L, t) dt \quad (4.3.58)$$

Moreover there seems to be no influence of the mass-transfer coefficient D_b on the results. Only the concentration distributions will be different. In case the mass-transfer coefficient is smaller, there is less exchange of mass during the passage of the pollution cloud. Consequently the peak concentration in the main stream will be reduce less, but the tail will be longer with smaller concentration-values (see Fig. 4.3.19).

Neglecting the dispersion the concentration distribution can be given by Eq.(2.3.49) as a combination of Eqs (2.3.44) and (2.3.48) (Kranenburg, 1988)

$$\begin{aligned} \frac{\varphi_s(x, t)}{\overline{\varphi}} &= \frac{1}{2\sqrt{\pi}} \cdot \frac{[D_s \cdot D_b \cdot (x/u_s) \cdot (t - x/u_s)]^{1/4}}{t - x/u_s} \cdot \\ &\cdot \exp \left[-D_b \cdot t + (D_b - D_s) \cdot (x/u_s) + 2\sqrt{D_b \cdot D_s \cdot (x/u_s) \cdot (t - x/u_s)} \right] + \\ &+ \exp \left[-D_s \cdot (x/u_s) \right] \end{aligned} \quad (4.3.59)$$

After this approximation two 'waves' can be distinguished (Fig 2.3.5). The first 'wave' propagates with the flow velocity u_s and the second 'wave' propagates more slowly after Eq.(4.1.1)

$$c = \frac{u_s}{1 + \beta} \quad (4.3.60)$$

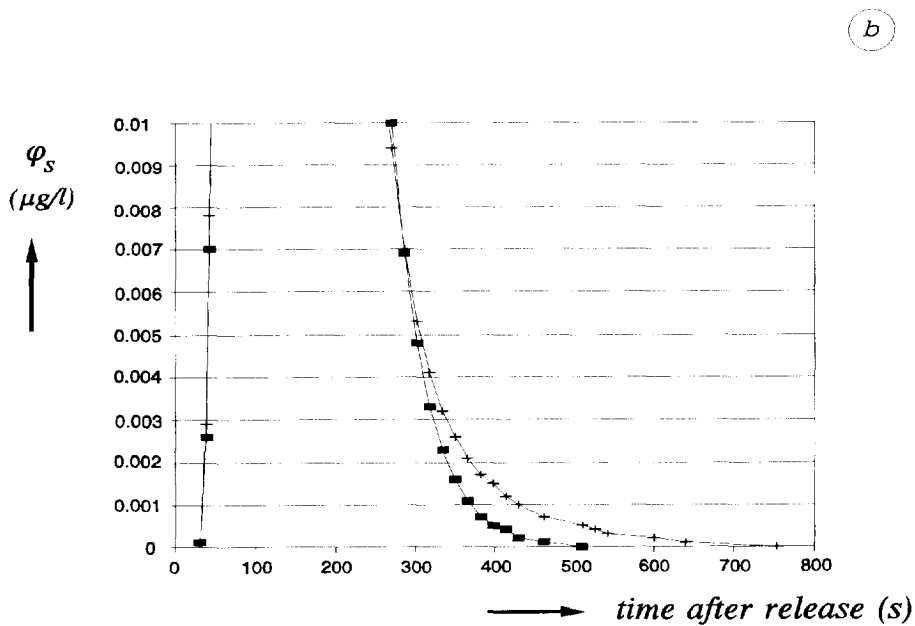
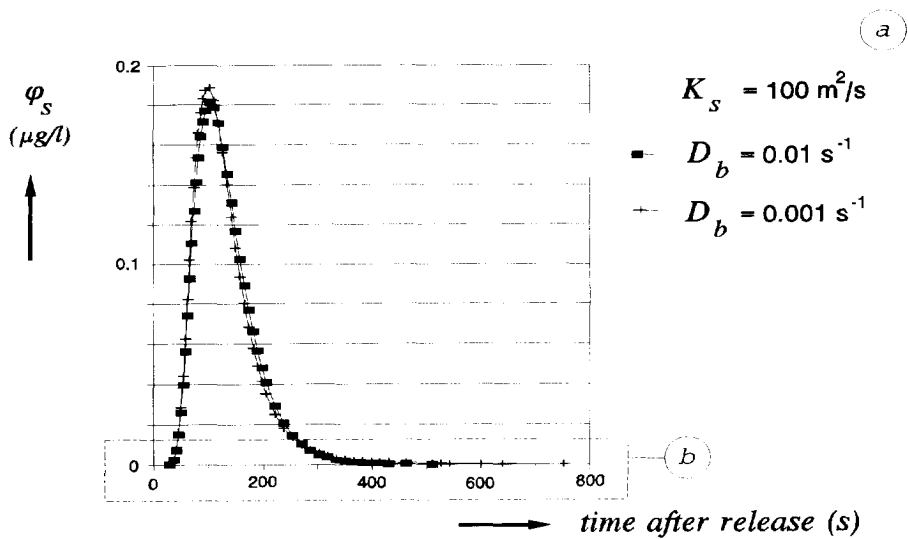


Fig. 4.3.19

Concentration distributions for $Pe = 2.5$ (= 250 m from the starting point of the dead zones), run nrs 1 and 3

Because the first 'wave' decreases with the distance after

$$\frac{\varphi_s(x)}{\varphi} = \exp \left(- D_s \frac{x}{u_s} \right) = \exp \left(- \beta D_b \frac{x}{u_s} \right) \quad (4.3.61)$$

the resulting transport-velocity c of the combination of both 'waves' equals more and more the transport velocity of the second 'wave' with the distance. In other words there is no instantaneous adaptation of the transport velocity to the dead zones, which is in contradiction with the results of the numerical model.

In principle the transport velocity of the combined waves over the distance the first 'wave' has not disappeared, could be determined by applying Eqs (4.3.57) and (4.3.58) to Eq.(4.3.59). For simplicity the integration after Eqs (4.3.57) and (4.3.58) can be executed numerically after

$$\mu_t = \frac{1}{m_0} \sum_{t_1}^{\infty} t \cdot \varphi_s(x, t) \Delta t \quad (4.3.62)$$

$$m_0 = \sum_{t_1}^{\infty} \varphi_s(x, t) \Delta t \quad (4.3.63)$$

with $t_1 > x/u_s$. This restriction means that an accurate determination of the time-centroid by Eqs (4.3.62) and (4.3.63) of the combined 'waves' after Eq.(4.3.59) is not possible. Moreover, Eq.(4.3.59) yields only for large values of

$$p = 2 \sqrt{D_s D_b \frac{x}{u_s} \cdot \left(t - \frac{x}{u_s} \right)} = 2 D_b \sqrt{\beta \cdot \frac{x}{u_s} \cdot \left(t - \frac{x}{u_s} \right)} \quad (4.3.64)$$

Consequently Eq.(4.3.59) does not give reliable results for small distances from the point of release.

In Table 4.3.4 an example of the distribution of the transport velocity with the distance, represented by the κ -value, is given. Figure 4.3.20 shows the concentration distributions concerned. Referring to the condition that Eq.(4.3.59) is not reliable for small values of p after Eq.(4.3.63) (see also the values of p_1), the κ -values larger than unity for small distances in Table 4.3.4 confirm this restriction. On the other hand, if Eq.(4.3.59) is reliable the transport velocity can be given by Eq.(4.3.60), i.e. $\kappa = 1$.

According to Eq.(4.3.64), smaller values of the mass-transfer coefficient D_b means a larger distance over which Eq.(4.3.59) is not correct. Thus in case D_b is ten times smaller ($= 0.001 \text{ s}^{-1}$) the results become accurate at a ten times longer distance ($= 20,000 \text{ m}$) with $\kappa \approx 1$.

TABLE 4.3.4 The distribution of the transport velocity, represented by the κ -value, after Eq.(4.3.59) (Kranenburg, 1988)

$\beta = 0.20 \qquad D_b = 0.01 \text{ s}^{-1} \qquad u_s = 1 \text{ m/s}$				
x (m)	t_1 (s)	p_1 (with $t = t_1$)	κ	
			overall *)	local **)
200	200.02	0.018	2.1	
500	500.05	0.045	1.3	
1000	1000.1	0.089	1.05	0.88
2000	2002	0.56	1.00	0.98
3000	3003	0.85	1.00	1.00

*) over the distance x concerned
 **) at the distance concerned over 10 m

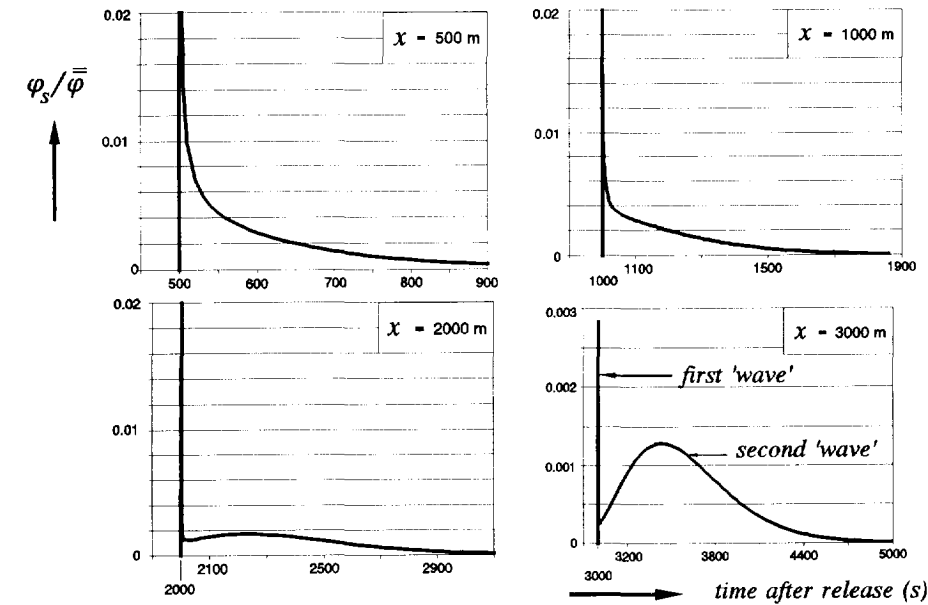


Fig. 4.3.20 Concentration distributions in the time domain after Eq.(4.3.59) at four distances from the point of release (see also Table 4.3.4)

In comparison with the results of the numerical model, it can be concluded that the neglect of the dispersion in the dead-zone model after Eq.(4.3.59) give the same results as far as this approximation is applicable, i.e. at large distances of the point

of release or large values of p ⁵⁾. In this context it has to be mentioned that at short distances of the point of release, where the concentration gradients are large, the dispersive transport has a significant influence on the transport velocity (see also Sub-section 4.3.3).

In nature the very small concentration-values at the end of the tail cannot be measured. Therefore the influence of a truncation of the tail of the concentration distribution on the initial behaviour of the transport velocity has been examined too. For practical sense a truncation of the tail at 1 percent or 3 percent of the peak concentration is common (Yotsukura et al, 1970). In Tables 4.3.5 and 4.3.6 the input data of the executed computations with the numerical model are summarized. Because of the truncation there might be a slight influence of the dispersion on the transport velocity related to the time-centroid as described in Sub-section 4.3.3 if the transport is related to the peak concentration. Therefore in the computations concerned the dead zones start at a distance corresponding with the Pe -number of 25 instead of 10. The resulting distributions of the local κ -value are presented in Figs 4.3.21 ... 4.3.28. The irregularities of the κ -distributions in Figs 4.3.21 ... 4.3.28 is caused by the relation of the truncation to a time step.

TABLE 4.3.5 Input data of the computations for the analysis of the initial behaviour of the κ -value, related to the time-centroid of truncated concentration-distributions

run nr.	K_s (m ² /s)	D_b (s ⁻¹)	u_s (m/s)	β	truncation (%)	\mathcal{E} (Eq.4.3.34)
5	100	0.01	1	0.2	1	1
6	100	0.01	1	0.2	3	1
7	1000	0.001	1	0.2	1	1
8	1000	0.001	1	0.2	3	1
9	100	0.001	1	0.2	1	0.1
10	100	0.001	1	0.2	3	0.1
11	1000	0.01	1	0.2	1	10
12	1000	0.01	1	0.2	3	10
13	400	0.001	2	0.2	1	0.1
14	400	0.001	2	0.2	3	0.1
15	100	0.01	1	0.1	3	1
16	100	0.01	1	0.3	3	1
17	100	0.001	1	0.1	3	0.1
18	100	0.001	1	0.3	3	0.1

⁵⁾ The presented values of p_1 in Table 4.3.4 give a qualification of the expression 'large values of p ': $p > 0.5$

TABLE 4.3.6 Numerical input-data for the computations, executed in the frame work of the analysis of the initial behaviour of the κ -value (Table 4.3.5) and the standard deviation of the κ_m -value

run nr.	space step Δx (m)	time step Δt (s)	distance without dead zones ($Pe = 25$) (km)	$ \sigma_{\kappa_m} $
5	50	5	2.5	0.014
6	50	5	2.5	0.042
7	500	30	25	0.008
8	500	30	25	0.025
9	50	5	2.5	0.014
10	50	5	2.5	0.042
11	500	30	25	0.008
12	500	30	25	0.025
13	100	10	5	0.028
14	100	10	5	0.085
15	50	5	2.5	0.085
16	50	5	2.5	0.028
17	50	5	2.5	0.085
18	50	5	2.5	0.028

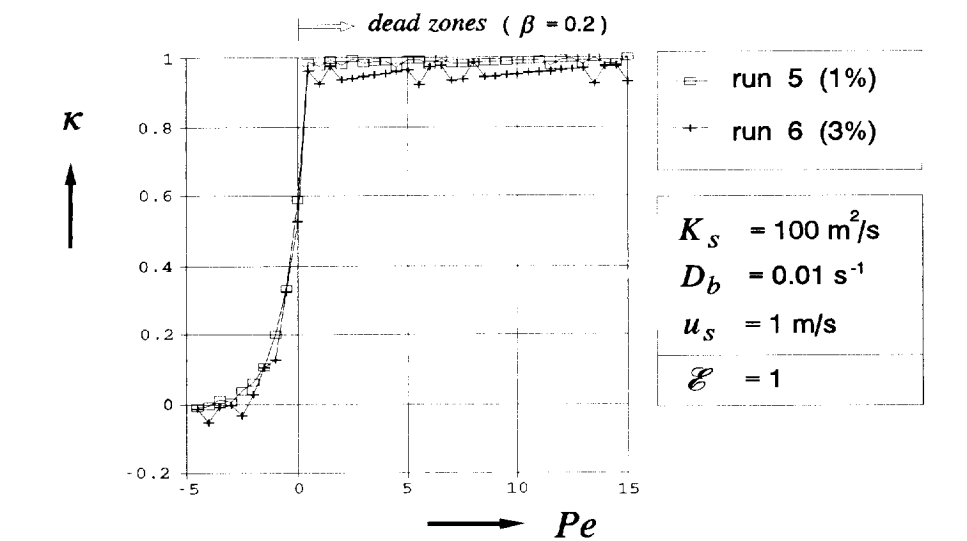


Fig. 4.3.21 Influence of the truncation of the tail of the concentration distribution on the initial distribution of the local κ -value (run nrs 5 and 6)

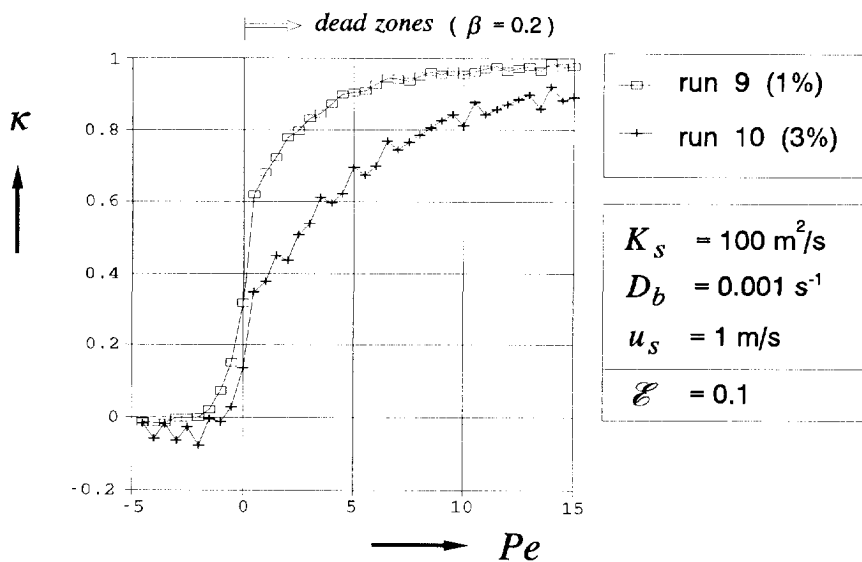


Fig. 4.3.22 Influence of the truncation of the tail of the concentration distribution on the initial distribution of the local κ -value (run nrs 9 and 10)

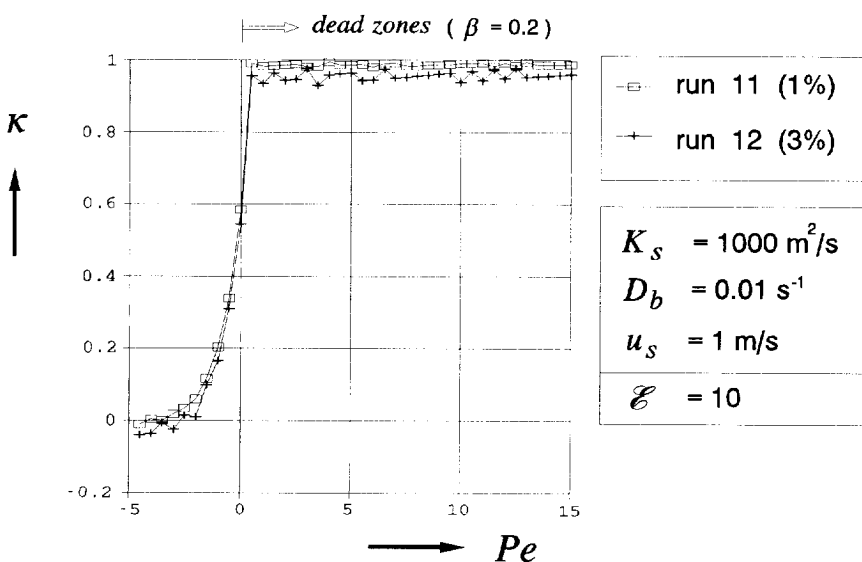


Fig. 4.3.23 Influence of the truncation of the tail of the concentration distribution on the initial distribution of the local κ -value (run nrs 11 and 12)

Because the local value of κ is determined by

$$\kappa_m = \frac{\beta_m}{\beta} = \frac{\left(\frac{(\mu_t)_m - (\mu_t)_{m-1}}{\Delta x} \cdot u_s - 1 \right)}{\beta} \quad (4.3.65)$$

with $(\mu_t)_m$ = time-centroid of the concentration distribution at the upstream boundary of the space step m
 $(\mu_t)_{m-1}$ = time-centroid of the concentration distribution at the downstream boundary of the space step m ,

the accuracy of the local κ_m can be given by the variance of this parameter after (see also Eq. 3.4.2)

$$\sigma_{\kappa_m}^2 = 2 \cdot \sigma_{\mu_t}^2 \cdot \left(\frac{u_s}{\beta \cdot \Delta x} \right)^2 \quad (4.3.66)$$

with σ_{μ_t} = standard deviation of the time-centroid

Beside the influence of the truncation condition and the time step on the variance of the time-centroid, Eq.(4.3.66) shows also the influence of the applied space step

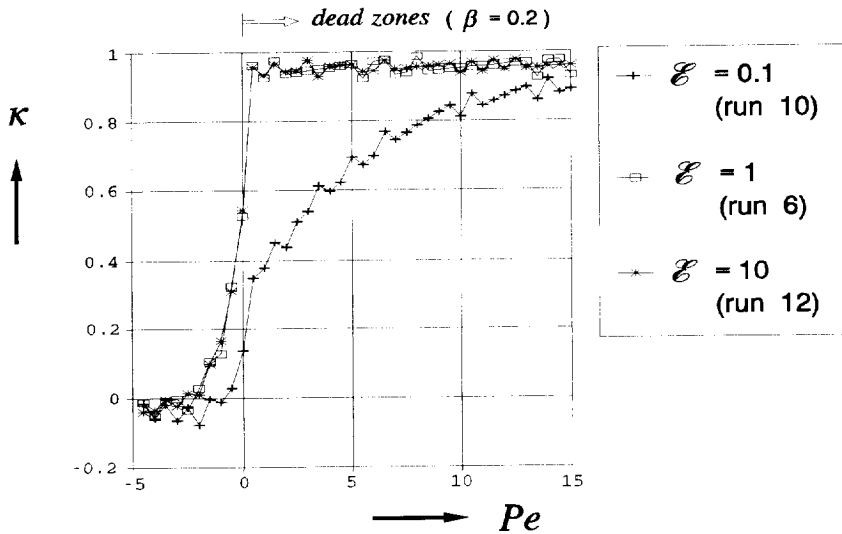


Fig. 4.3.24 Influence of dimensionless mass-transfer parameter \mathcal{E} on the initial distribution of the local κ -value for a 3%-truncation of the tail (runs 6, 10 and 12)

on the accuracy of the κ -value. In Table 4.3.6 the variance of the local κ_m -value after Eq.(4.3.66) is given, assuming that the variance of the time-centroid is twice the percentage of the truncation of the time step, which seems to be a good approximation. The initial distribution of the local κ -value shows a steep increment at the beginning of the dead-zones as in case of no truncation (Fig. 4.3.18), but now up to a certain value smaller than one. Thereafter the κ -value increases slowly with the distance until unity. Figures 4.3.21 ... 4.3.23 show the influence of the percentage of the truncation of the tail. In case of a larger percentage of the truncation the κ -values are systematically smaller than the values in case of a smaller percentage.

In Fig. 4.3.24 the influence of the *mass transfer* between the main stream and the dead zones are presented explicitly by comparing three runs with different values of the mass-transfer parameter \mathcal{E} ($= 0.1, 1$ and 10) for a 3%-truncation. Roughly it can be stated that for values of $\mathcal{E} \geq 1$ there is no difference with the situation without truncation. In Figs 4.3.25 and 4.3.26 a comparison of the different runs with equal mass-transfer parameters \mathcal{E} , but different flow-velocities (u_s), longitudinal dispersion- (K_s) and mass-transfer coefficients (D_b) is made. It shows that the mass-transfer parameter constitutes a good qualification of the influence concerned after Eq.(4.3.35) (see Sub-section 4.3.2).

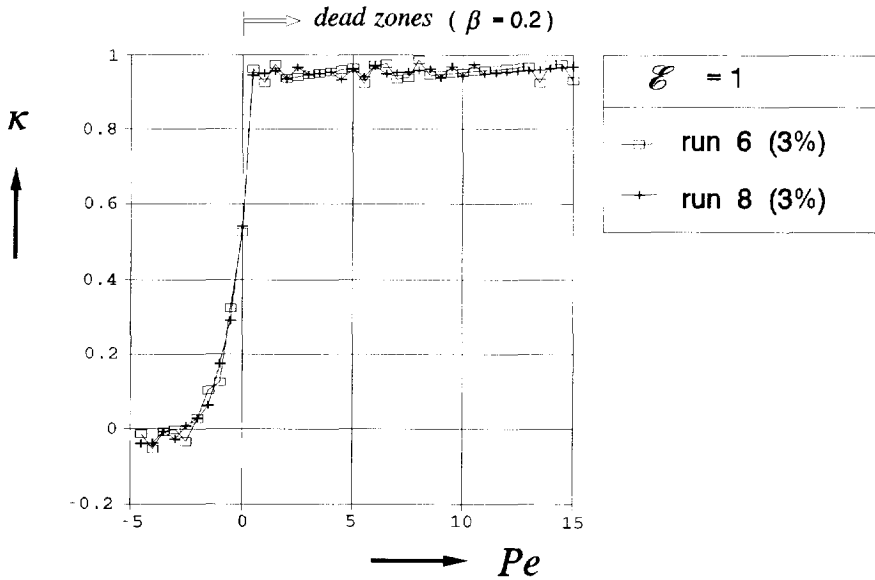


Fig. 4.3.25 Comparison of the local κ -distribution with equal \mathcal{E} -values ($=1$) and truncation percentages, but different longitudinal dispersion- and mass-transfer coefficients (run nrs 6 and 8)

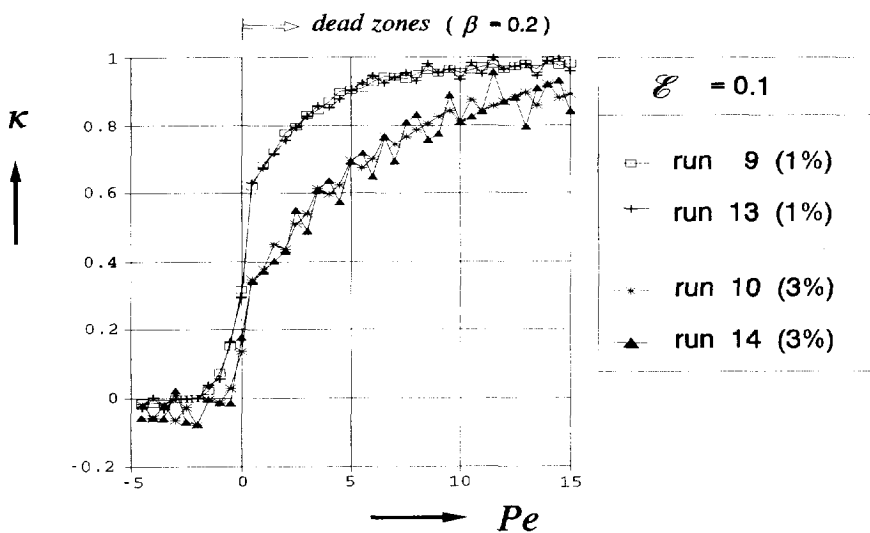


Fig. 4.3.26 Comparison of the local κ -distribution with equal \mathcal{E} -values ($=0.1$), but different longitudinal dispersion- and mass-transfer coefficients for two truncation-percentages (run nrs 9, 10, 13 and 14)

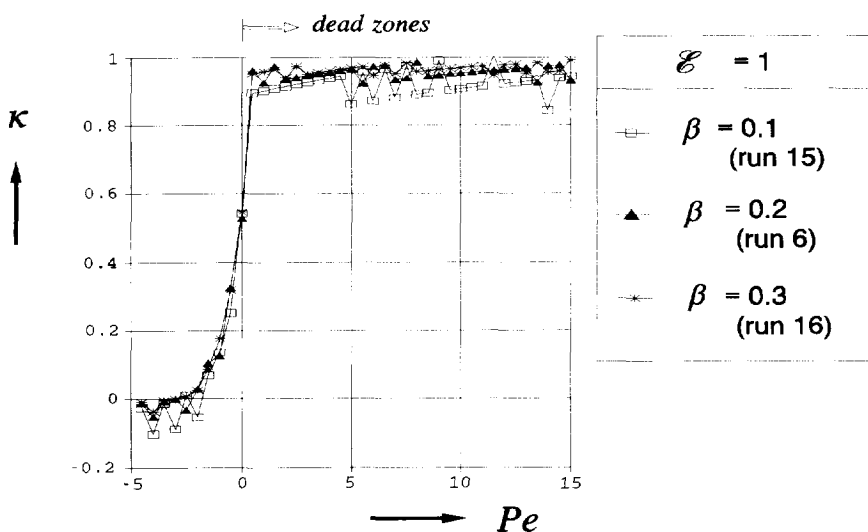


Fig. 4.3.27 Comparison of the local κ -distribution with equal \mathcal{E} -values ($=1$), but different dead-zone parameters for a 3%-truncation (run nrs 6, 15 and 16)

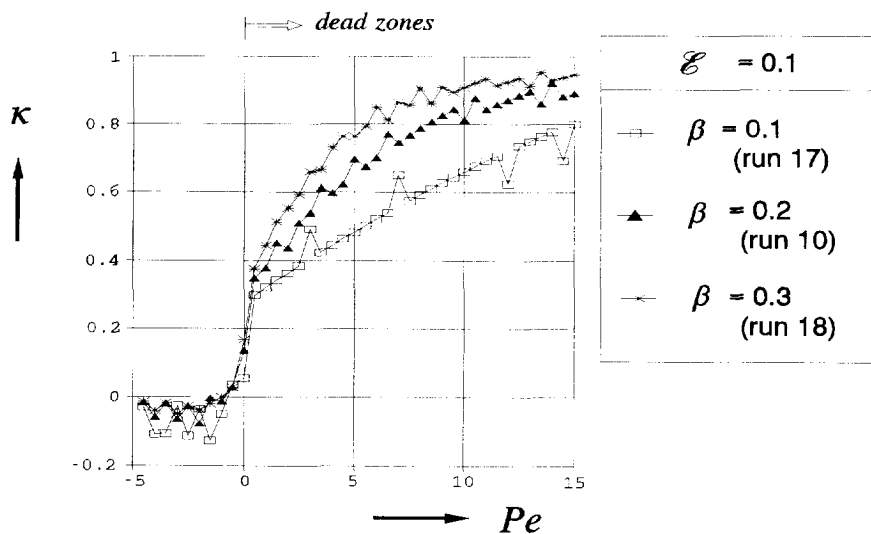


Fig. 4.3.28 Comparison of the local κ -distribution with equal \mathcal{E} -values ($=0.1$), but different dead-zone parameters for a 3%-truncation (run nrs 10, 17 and 18)

However, a variation of the dead-zone parameter β with equal values of the mass-transfer parameter \mathcal{E} shows negligible differences in case $\mathcal{E} = 1$ (Fig. 4.3.27), but large differences in case of $\mathcal{E} = 0.1$ (Fig. 4.3.28). As a matter of fact, the slow exchange of mass in case of a small mass-transfer coefficient D_b and a small amount of exchange of mass in case of a small dead-zone parameter β cause less reduction of the peak concentration in the main stream as well as a longer tail with smaller concentrations than in case of a large values of the parameters D_b and β (Fig. 4.3.29). Therefore a truncation of the tail for concentrations smaller than a certain percentage of the peak concentration means that a relatively large part of the tail is neglected in case of a small β -value. This phenomena effects the time-centroid in such a way, that the instantaneous adaptation to the dead zones as described above, cannot occur. Nevertheless the influence of the dead-zone parameter is limited in case of large values of the mass-transfer parameter ($\mathcal{E} \geq 1$).

Thus, when the mass-transfer coefficient D_b becomes very small (of the order 10^{-3}) and the dispersion coefficient K , remains small as well, which corresponds with a mass-transfer parameter $\mathcal{E} < 1$, there is a significant influence of the truncation on the initial distribution of the transport velocity.

Summarizing, it can be said, that the distribution of the ratio of actuality κ with the distance (Pe -number) not only depends on the value of the mass-transfer parameter

\mathcal{E} after Eq.(4.3.35), but also on the dead-zone parameter β and the truncation percentage.

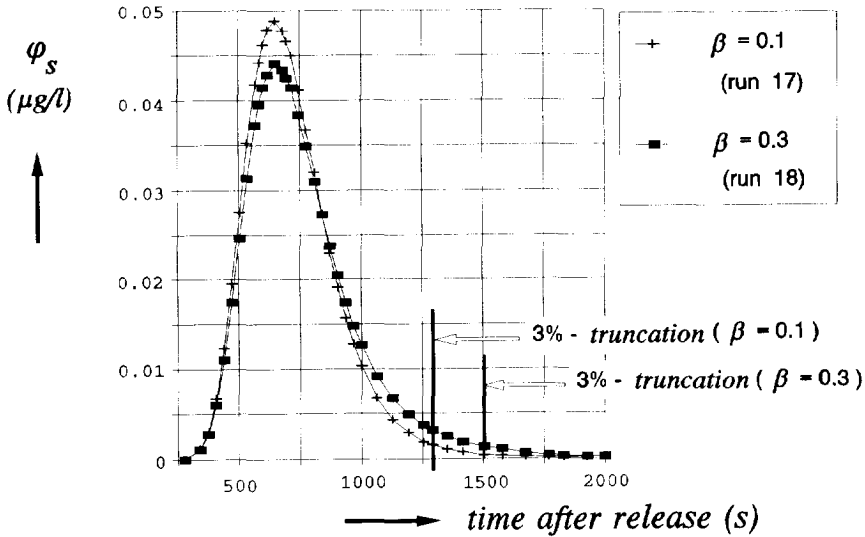


Fig. 4.3.29 Concentration distributions for $Pe = 10$ ($= 1$ km from the starting point of the dead zones), run nrs 17 and 18; comparison of the influence of the dead-zone parameter on the truncation

Because the truncation criterion is more or less arbitrary, this criterion is impracticable for an objective analysis of the distribution of κ just downstream of the starting point of dead zones. Moreover Nordin and Sabol (1974) stated that a truncation will make the distribution more nearly Gaussian, which can lead to a misunderstanding of the physical processes involved.

Therefore it seems better to consider the peak concentration next to the time-centroid, all the more since the transport velocity of the peak concentration can be compared with the transport velocity of the first 'wave' after Eq.(4.3.59) as presented in Fig. 4.3.20. In Tables 4.3.7 and 4.3.8 the input data of the executed computations are collected. Again irregularities in the κ -distributions are caused by the numerical approach: the time of the peak value (t_{max}) is linked with the time step applied. According to Eq.(4.3.65) it yields

$$\kappa_m = \frac{\beta_m}{\beta} = \frac{\left(\frac{(t_{max})_m - (t_{max})_{m-1}}{\Delta x} \cdot u_s - 1 \right)}{\beta} \quad (4.3.67)$$

TABLE 4.3.7 Input data of the computations for the analysis of the initial behaviour of the κ -value, related to the peak concentration

run nr.	K_s (m ² /s)	D_b (s ⁻¹)	u_s (m/s)	β	\mathcal{E} (Eq.4.3.34)
19	100	0.01	1	0.2	1
20	100	0.001	1	0.2	0.1
21	1000	0.01	1	0.2	10
22	1000	0.001	1	0.2	1
23	400	0.001	2	0.2	0.1
24	100	0.01	1	0.1	1
25	100	0.01	1	0.3	1
26	100	0.001	1	0.1	0.1
27	100	0.001	1	0.3	0.1
28	1000	0.01	1	0.1	10
29	1000	0.01	1	0.3	10
30	100	0.0005	1	0.2	0.05
31	100	0.0005	1	0.1	0.05
32	100	0.0005	1	0.3	0.05
33	200	0.0001	1	0.2	0.02
34	100	0.0001	1	0.2	0.01

The inaccuracy in the calculated time of the peak concentration t_{max} is $< 0.5 \Delta t$, thus the inaccuracy in the local κ -value can be given by

$$\Delta \kappa_m = \frac{\left(\frac{\Delta t}{\Delta x} \cdot u_s \right)}{\beta} \quad (4.3.68)$$

This means that the time step Δt has to be chosen as small as possible, while the space step Δx has to be as large as possible. However, on account of the stability, the value of the space step Δx is limited by two conditions. Beside the condition after Eq.(4.3.21)

$$\Delta x \geq \sqrt{2 \cdot K_s \cdot \Delta t} \quad (4.3.69)$$

the space step is also limited by the cell Péclet number (Vreugdenhil, 1989)

$$\frac{u_s \cdot \Delta x}{K_s} < 2$$

or

$$\Delta x < \frac{2 \cdot K_s}{u_s} \quad (4.3.70)$$

This condition is important for the accuracy of the results over the initial distance from the point of release, where the dead-zone parameter equals zero ($Pe < 100$) and the concentration gradients are relatively large.

In Table 4.3.8 the applied time and space steps of the computations after Table 4.3.7 are presented, as well as the inaccuracies after Eq.(4.3.68).

TABLE 4.3.8 Numerical input-data for the computations, executed in the frame work of the analysis of the initial behaviour of the κ -value (see Table 4.3.7) and the inaccuracy of the local κ -value

run nr.	space step Δx (m)	time step Δt (s)	distance without dead zones ($Pe = 100$) (km)	$\Delta \kappa_m$ Eq.(4.3.68)
19	100	1	10	0.05
20	100	1	10	0.05
21	500	1	100	0.01
22	500	1	100	0.01
23	200	1	20	0.05
24	100	1	10	0.10
25	100	1	10	0.03
26	100	1	10	0.10
27	100	1	10	0.03
28	500	1	100	0.02
29	500	1	100	0.007
30	100	1	10	0.05
31	100	1	10	0.10
32	100	1	10	0.03
33	200	2	20	0.05
34	100	1	10	0.05

If the peak concentration is used for the examination of the influence of the dead zone on the transport velocity the dead zones in the model have to begin not until $Pe = 100$ (see Sub-section 4.3.3). This means that in case of a dispersion coefficient of the order 10^3 and a flow velocity of 1 m/s the dead zones have to start at a distance of 100 km (Table 4.3.8).

Figure 4.3.30 shows the influence of the mass-transfer parameter \mathcal{E} on the initial distribution of the local κ -value. The results are comparable with the cases the time-centroid is considered with a 3%-truncation of the tail (Fig. 4.3.24). For values of $\mathcal{E} \geq 1$ the transport velocity reduces more or less instantaneously at the starting point of the dead zones to a value, corresponding with Eq.(4.3.60) after

$$c = \frac{u_s}{1 + \beta_{act.}}$$

with $\beta_{act.}/\beta = \kappa \geq 0.95$

The presented distributions in Fig. 4.3.31 prove again that the mass-transfer parameter \mathcal{E} constitutes a good qualification of the influence concerned after Eq.(4.3.35), based on the dimensional analysis (Sub-section 4.3.2).

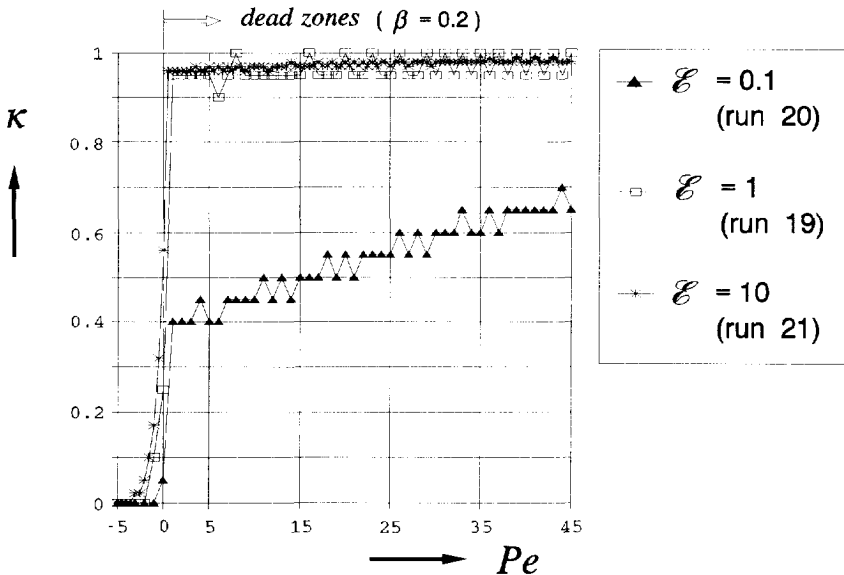


Fig. 4.3.30 Influence of the mass-transfer parameter \mathcal{E} on the initial distribution of the local κ -value, related to the peak concentration (run nrs 19, 20 and 21)

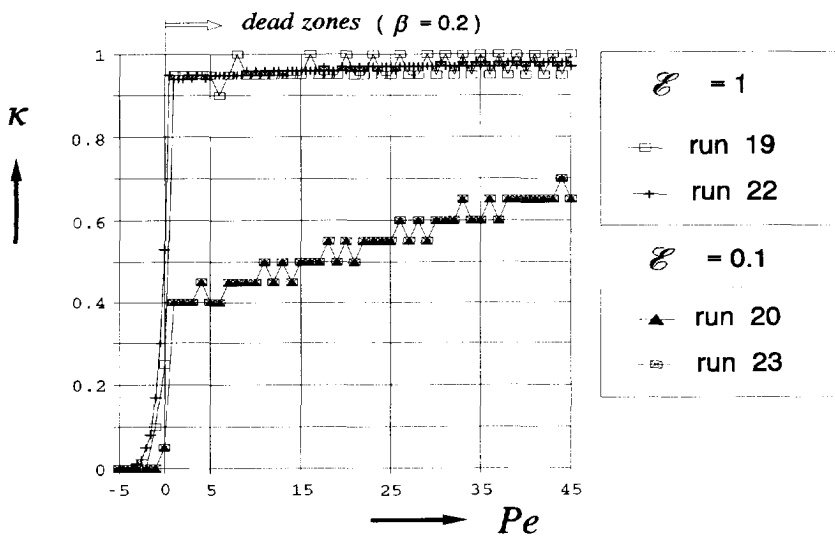


Fig. 4.3.31 Comparison of the local κ -distributions with equal \mathcal{E} -values, but different longitudinal dispersion- and mass-transfer coefficients (run nrs 19, 20, 22 and 23)

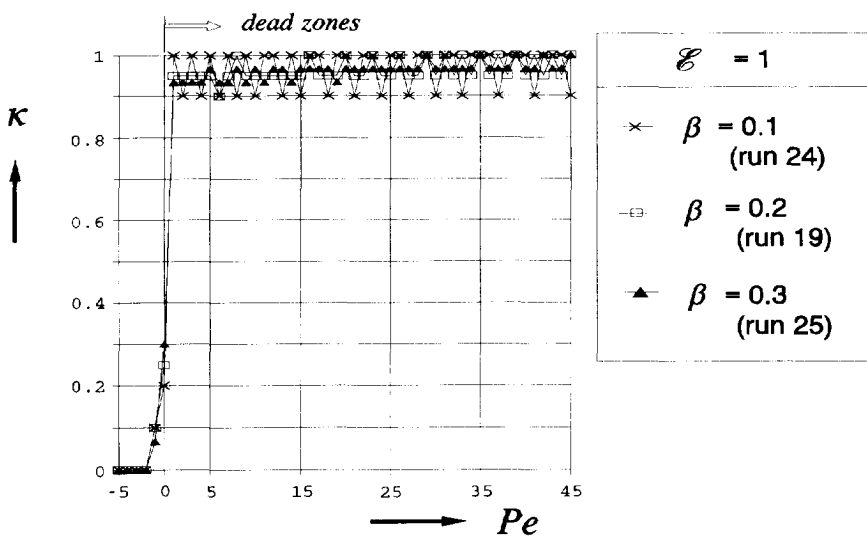


Fig. 4.3.32 Comparison of the local κ -distributions with equal values for the mass-transfer parameter \mathcal{E} , but different dead-zone parameters (run nrs 19, 24 and 25)

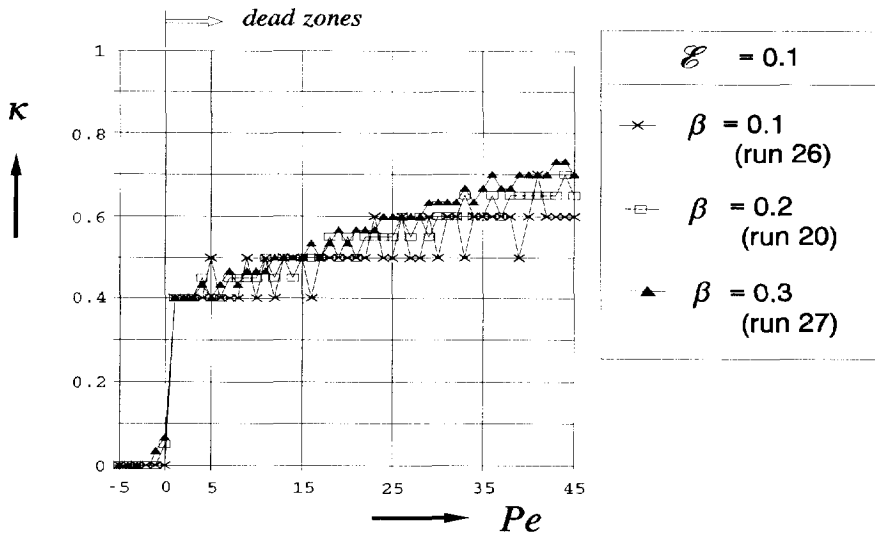


Fig. 4.3.33 Comparison of the local κ -distributions with equal values for the mass-transfer parameter \mathcal{E} , but different dead-zone parameters (run nrs 20, 26 and 27)

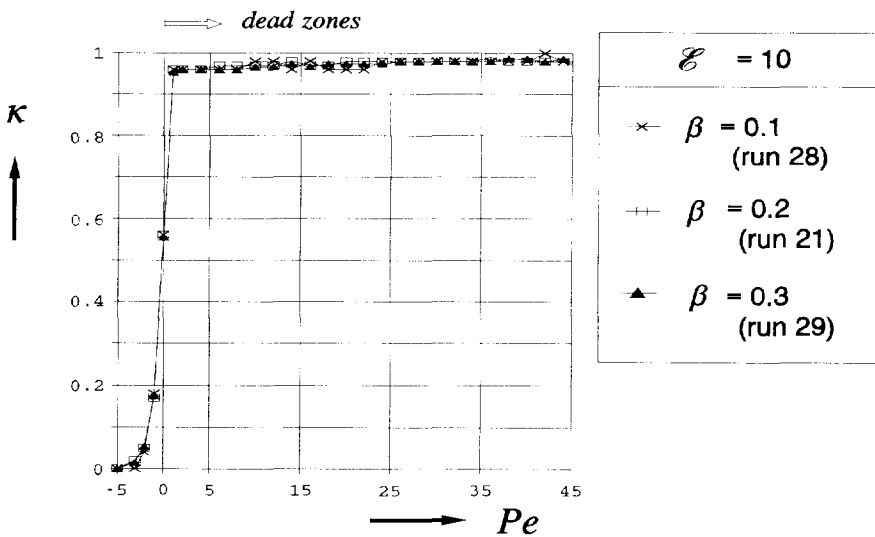


Fig. 4.3.34 Comparison of the local κ -distributions with equal values for the mass-transfer parameter \mathcal{E} , but different dead-zone parameters (run nrs 21, 28 and 29)

However, a variation of the dead-zone parameter β with equal \mathcal{E} -values shows also negligible differences in case $\mathcal{E} \geq 1$ (Figs 4.3.32 and 4.3.34), but significant differences in case of $\mathcal{E} = 0.1$ (Fig. 4.3.33).

For a more detailed examination of the influence of the dead-zone parameter β for $\mathcal{E} < 1$ the fluctuations of the κ -value, due to the numerical inaccuracies after Eq.(4.3.68) are reduced by smoothing the calculated time-distribution of the peak concentration (t_{max}) after

$$(t_{max})_{m+1} = (t_{max})_m + 0.1 \cdot [(t_{max})_{m+10} - (t_{max})_m] \quad (4.3.71)$$

In Fig. 4.3.35 the original κ -distribution of run nr. 20 (Tables 4.3.7 and 4.3.8) is compared with the distribution based on the smoothed time-distribution. It indicates that the smoothed distribution approaches the exact distribution quite well.

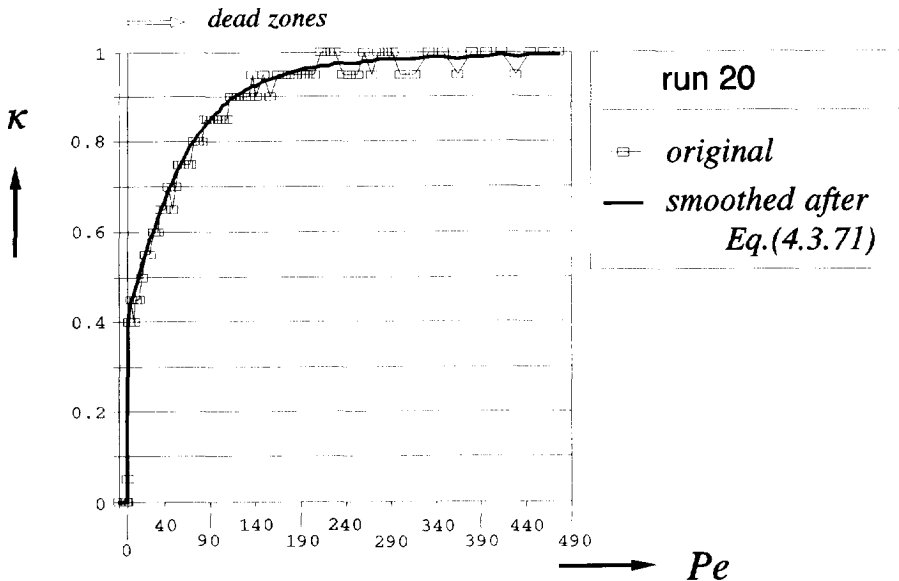


Fig. 4.3.35 Comparison of the original distribution of the κ -value, related to the peak concentration, with the distribution based on the smoothing of the calculated time-distribution of the peak values after Eq.(4.3.71)

In Fig. 4.3.36 the smoothed distributions of the κ -value for different β -values and one \mathcal{E} -value ($= 0.1$), as presented in Fig. 4.3.33, are given. The considered distance from the starting point of the dead zones is ten times longer than in Fig. 4.3.33 ($Pe = 500$ instead of 45).

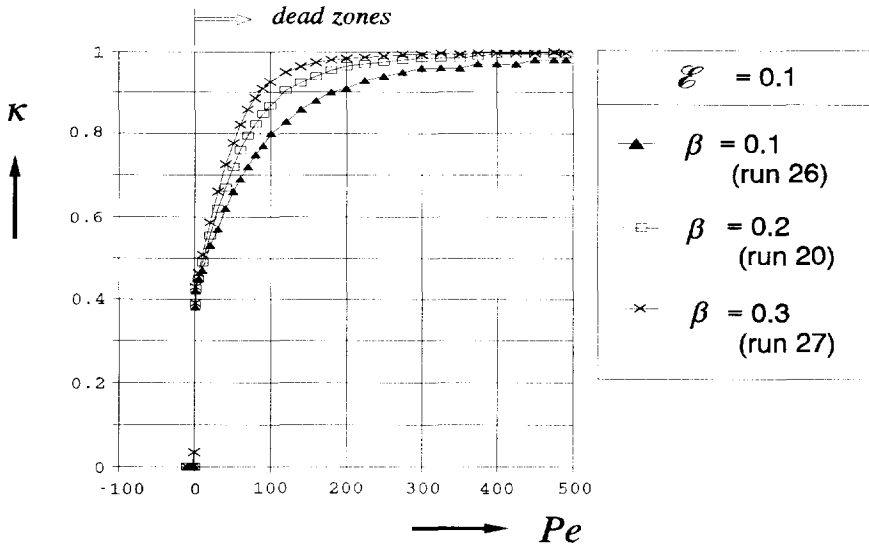


Fig. 4.3.36 Comparison of the initial distributions of the local κ -value with the Pe number, related to the smoothed time of the peak concentration with equal \mathcal{E} -values and different dead-zone parameters

Considering the analytical solution of the degenerated pair of coupled Eqs (2.3.19) and (2.3.18), which is given by Eq.(4.3.59) (Kranenburg, 1988, personal communication), it is stated that this solution holds for large values of the parameter p after Eq.(4.3.64)

$$p = 2D_b \sqrt{\beta \cdot \frac{x}{u_s} \cdot \left(t - \frac{x}{u_s}\right)} \quad (4.3.72)$$

The distribution of the κ -value, presented in Table 4.3.4 suggests that the transport velocity has been adapted to the dead zones at a distance, which corresponds with $p \geq 1$ and $t = 1.001 \cdot (x/u_s)$. The quantification of the corresponding distance can be given after Eq.(4.3.72) by

$$p = p_0 \cdot D_b \cdot \frac{x}{u_s} \cdot \sqrt{\beta} \quad (4.3.73)$$

with $p_0 = 2 \cdot \sqrt{0.001} = 0.06$ and $p > 1$, or

$$D_b \cdot \frac{x}{u_s} \cdot \sqrt{\beta} > 15.8 \quad (4.3.74)$$

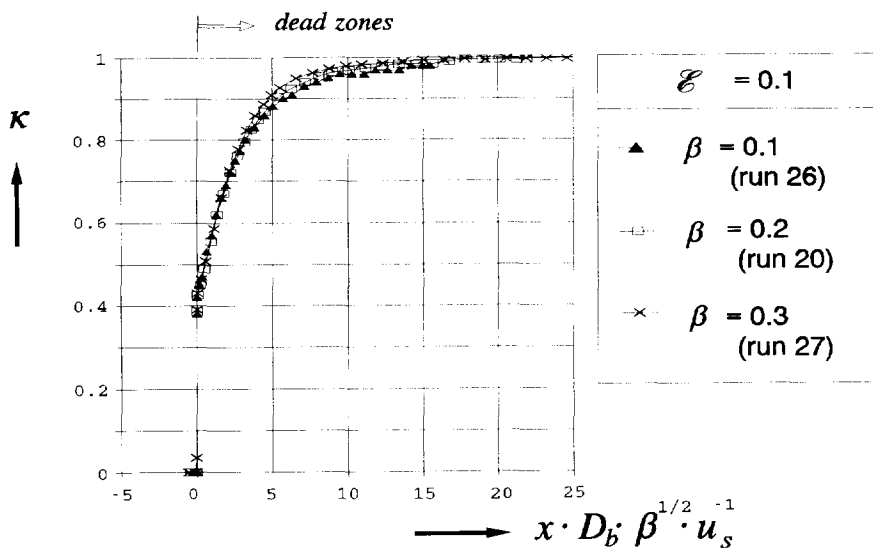


Fig. 4.3.37 Comparison of the local κ -distributions with the dimensionless distance $x \cdot D_b \cdot \beta^{1/2} \cdot u_s^{-1}$ for $\mathcal{E} = 0.1$ and different dead-zone parameters

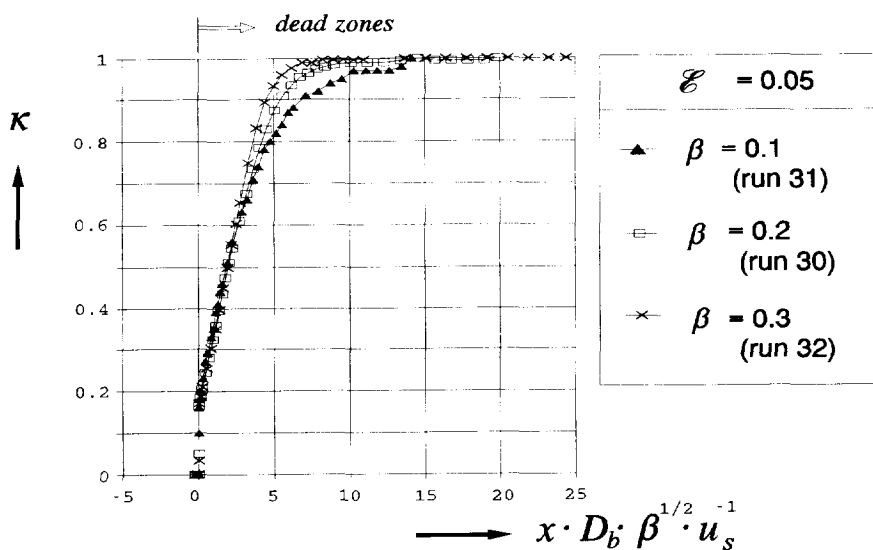


Fig. 4.3.38 Comparison of the local κ -distributions with the dimensionless distance $x \cdot D_b \cdot \beta^{1/2} \cdot u_s^{-1}$ for $\mathcal{E} = 0.05$ and different dead-zone parameters

By way of comparison in Fig. 4.3.37 the κ -distributions, presented in Fig. 4.3.36, are related to the dimensionless distance $x \cdot D_b \cdot \beta^{1/2} \cdot u_s^{-1}$ (see also Sub-section 4.3.2, Eq. 4.3.36). This presentation shows that the distributions for the different β -values become more or less similar, whereas the κ -value achieves the value of unity at a distance, which corresponds with the condition of Eq.(4.3.74): $0.95 \leq \kappa \leq 1$ at a dimensionless distance $x \cdot D_b \cdot \beta^{1/2} \cdot u_s^{-1} = 10$ till 15. Comparable results are found for a two times smaller value of the mass-transfer parameter \mathcal{E} (see Fig. 4.3.38). Still, the respective distributions for the different dead-zone parameters are not as similar as in case of $\mathcal{E} = 0.1$. Consequently there is no univocal relation between the dimensionless parameters κ , \mathcal{E} and $x \cdot D_b \cdot \beta^{1/2} \cdot u_s^{-1}$ in case of small \mathcal{E} -values.

A further reduction of the mass-transfer parameter \mathcal{E} (< 0.05) means naturally a different distribution of the local κ -value (Fig. 4.3.39). Due to the deformation of the concentration distribution as a result of dispersion and mass transfer between the main stream and the dead zones, locally the transport velocity related to the peak concentration can become even smaller than the velocity based on the dead-zone parameter after Eq.(4.3.60). This means that in case of very small \mathcal{E} -values, locally the actual lag-coefficient β_{act} can become larger than the present dead-zone parameter β . However, the distance at which κ becomes equal to unity, does not change.

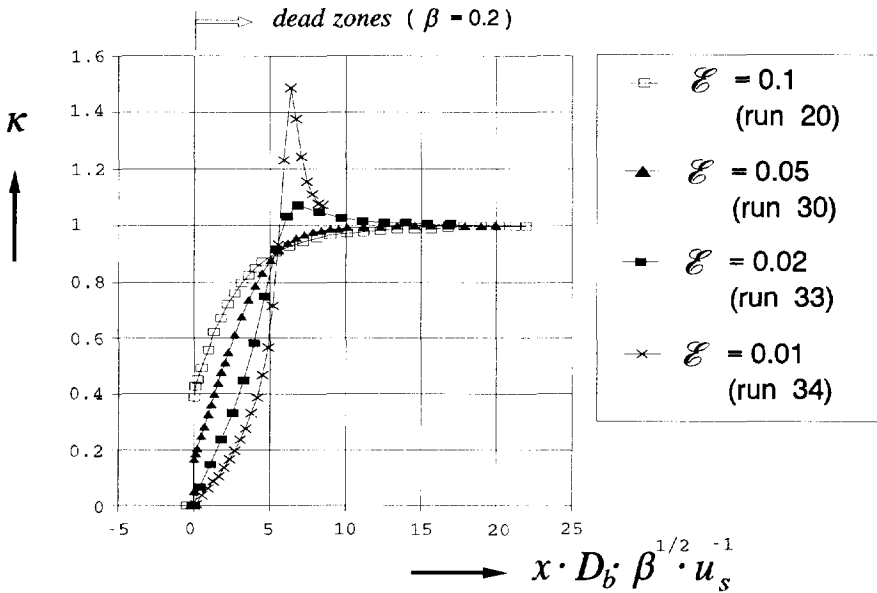


Fig. 4.3.39 Influence of the mass-transfer parameter \mathcal{E} on the initial distribution of the local κ -value, related to the peak concentration (run nrs 20, 30, 33 and 34)

Considering the reference values of the mass-transfer coefficient D_b ($= 0.01 \text{ s}^{-1}$), the longitudinal dispersion-coefficient K_s ($= 100$ till $1000 \text{ m}^2/\text{s}$), the mean flow-velocity u_s ($= 1 \text{ m/s}$) and the dead-zone parameter β ($= 0.2$), based on the situation in the River Rhine, the mass-transfer parameter \mathcal{E} is of the order of 10^0 till 10^1 . In that case it can be concluded that the transport velocity, related to the peak concentration also shows more or less an instantaneous adaptation to the dead-zones ($\kappa \geq 0.95$) as it is in the case the transport is related to the time-centroid ($\kappa = 1$), which is comparable with the distance of adaptation of about 3.5 km after Eq.(4.3.74).

4.3.5 The transport velocity in a river with a variable dead-zone parameter

After the previous Sub-section 4.3.4 there is an instantaneous adaptation of the transport velocity to the dead zones (dead-zone parameter β) after Eq.(4.3.60)

$$c = \frac{u_s}{1 + \beta}$$

in case the velocity c is related to the time-centroid of the concentration distribution. If the transport velocity is related to the peak value of the concentration distribution the adaptation takes place in a more or less similar way ($\kappa \geq 0.95$ at the starting point of the dead zones) with the restriction that the mass-transfer parameter $\mathcal{E} \geq 1$. This means that the resulting lag-coefficient β_j over the river reach j with a variable dead-zone parameter β_i can be given by Eq.(3.3.18)

$$\beta_j = \frac{\sum_{i=1}^j \left(\frac{\Delta x_i}{u_i} \cdot \beta_i \right)}{\sum_{i=1}^j \frac{\Delta x_i}{u_i}} \quad (4.3.75)$$

wherein Δx_i is the length of sub-branch i .

Considering the numerical model with one value for the mean flow-velocity u_i and one space step Δx_i , Eq.(4.3.75) can be simplified by

$$\beta_j = \frac{1}{j} \cdot \sum_{i=1}^j \beta_i \quad (4.3.76)$$

For the verification of this statement a few test-cases are carried out with the numerical model. For the dead-zone parameter the River Waal over a distance of about 80 km between Nijmegen (Rhine-kilometre 867.5, bifurcation Pannerden)

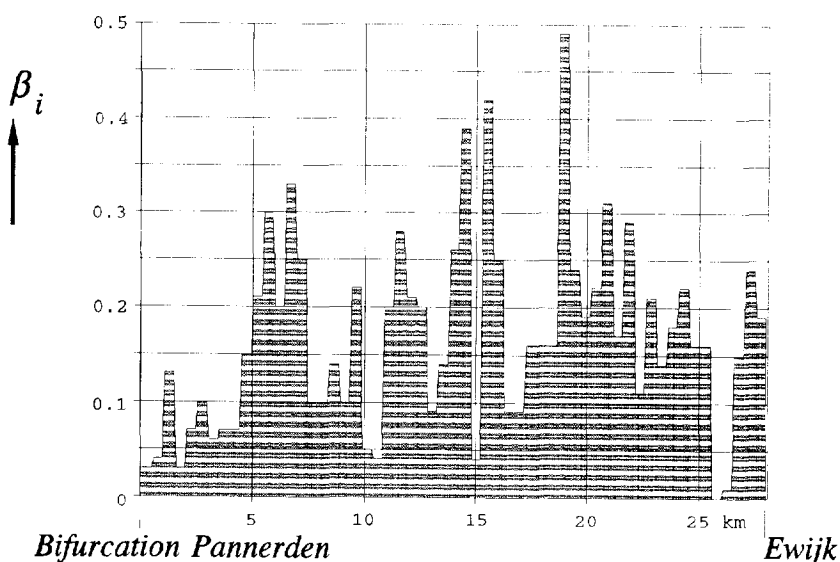


Fig. 4.3.40 Distribution of the dead-zone parameter of the River Waal between bifurcation Pannerden (River-kilometre 867.5) and Ewijk (River-kilometre 896) for $Q_{Lobith} = 3000 \text{ m}^3/\text{s}$

and Vuren (Rhine-kilometre 952.3) for a discharge at Lobith of $3000 \text{ m}^3/\text{s}$ is considered. After the SOBEK-model the dead-zone parameter is given every 500 m river-reach. In Fig. 4.3.40 the considered distribution of the dead-zone parameter is presented for the River Waal over a distance of about 30 km between the bifurcation Pannerden and Ewijk (Rhine-kilometre 896). In Table 4.3.9 the numerical input-data for the computations of the transport velocity related to the time-centroid, are collected. Due to the restrictions of the computer program of the numerical model⁶⁾ the computations of run nrs 35 ... 38 were executed for a river reach of 20 till 30 km, while in case of run nr. 39 with a space step $\Delta x = 500 \text{ m}$ and a time step $\Delta t = 100 \text{ s}$ the River Waal between the bifurcation Pannerden and Vuren was taken into account. The results of the computations are presented in Figs 4.3.41 ... 4.3.50.

⁶⁾ Running the computer program of the numerical model the computed concentrations in the main stream and the dead zone are saved in a file for every space and time step. For the computation of the time-centroid at the space steps concerned, the needed data are loaded from this file. Because the dimensions of this file are restricted, the river reach which can be considered, depends on the dimensions of the space and time step.

TABLE 4.3.9

Input-data of the computations for the analysis of the behaviour of the lag coefficient β_i in relation to the time-centroid, in case of a variable dead-zone parameter β_i

run nr.	K_s (m ² /s)	D_b (s ⁻¹)	u_s (m/s)	\mathcal{E}	space step Δx (m)	time step Δt (s)	distance without dead zones	
							(km)	Pe
35	100	0.01	1	1	100	40	1	10
36	100	0.001	1	0.1	100	40	1	10
37	200	0.01	1	2	100	20	1	5
38	500	0.01	1	5	100	10	1	2
39	500	0.01	1	5	500	100	5	10

Figures 4.3.41 and 4.3.42 show an instantaneous adaptation of the lag coefficient to the value of the dead-zone parameter. In Fig. 4.3.42 the results of run nrs 35 and 36 with different mass-transfer parameters \mathcal{E} are compared. As already observed in Sub-section 4.3.4 (Fig. 4.3.16) the mass-transfer parameter does not effect the distribution of the lag coefficient, if this coefficient is related to the transport velocity of the time-centroid of the concentration distributions.

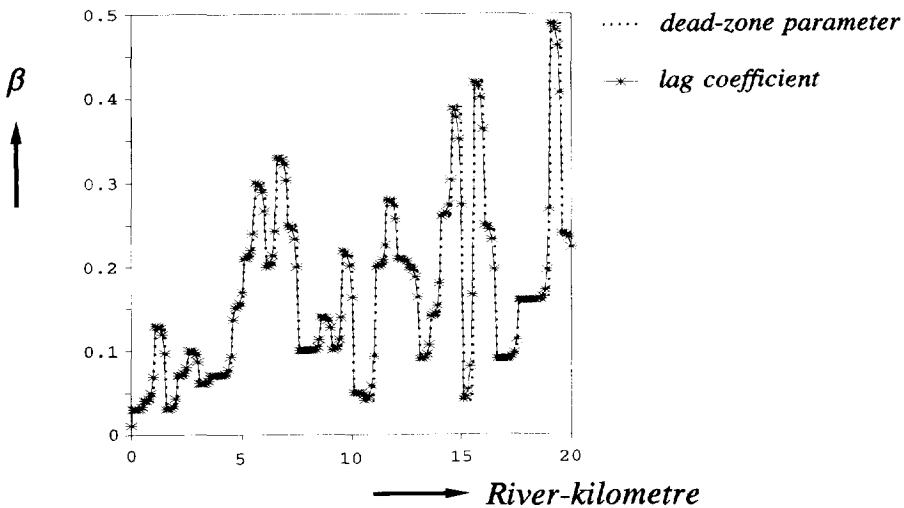


Fig. 4.3.41 Comparison of the distributions of the dead-zone parameter and the local lag-coefficient, related to the time-centroid of the concentration distribution after run nr. 35 ($\mathcal{E} = 1$)

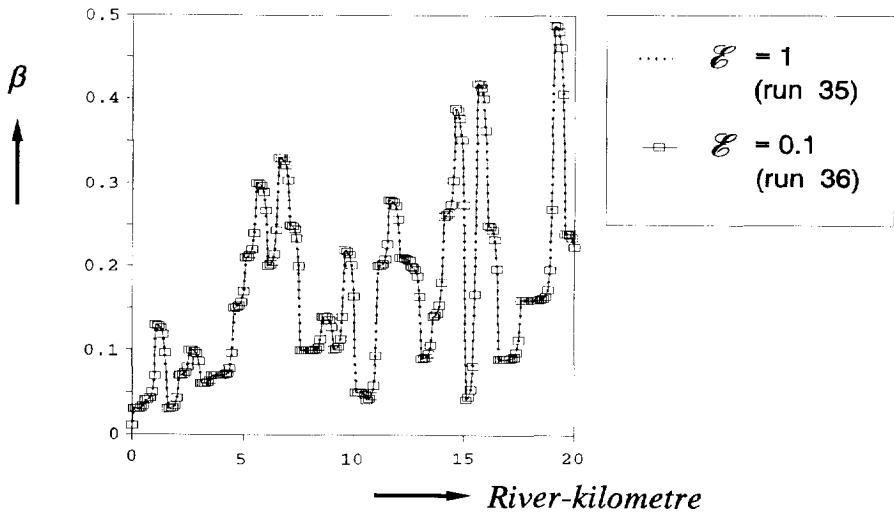


Fig. 4.3.42 Influence of the dimensionless mass-transfer parameter \mathcal{E} on the distribution of the local lag-coefficient (run nrs 35 and 36)

In Fig. 4.3.17 (Sub-section 4.3.4) it is shown that the longitudinal dispersion-coefficient K_L influences the distance over which in the upstream direction the transport velocity is reduced by the dead zones downstream: the larger the coefficient, the longer the distance over which the influence can be observed. This means that in case of a variable dead-zone parameter the local lag-coefficient depends on the local as well as the downstream value of the dead-zone parameter. The contribution of the influence of the downstream dead-zone parameter to the local lag-coefficient increases with the value of the longitudinal dispersion-coefficient (Fig. 4.3.43). If the distance over which the dead-zone parameter varies, is relatively short and the longitudinal dispersion-coefficient is relatively large, the local lag-coefficient cannot adapt completely to the local dead-zone parameter, i.e. the local κ -value will always differ from unity (Fig. 4.3.44). If the value of the dead-zone parameter decreases, the upstream κ -value is smaller than unity and if the dead-zone parameter increases the upstream κ -value is larger than unity.

Therefore a length of the river reach over which the value of the dead-zone parameter and the lag coefficient have to be averaged in order to get a κ -value between 0.9 and 1.1, has been determined. Because the distance of influence depends on the longitudinal dispersion-coefficients the Péclet number is considered. In Fig. 4.3.18 (Sub-section 4.3.4) the distance over which the dead zones effect the transport velocity in the upstream direction, corresponds with a dimensionless

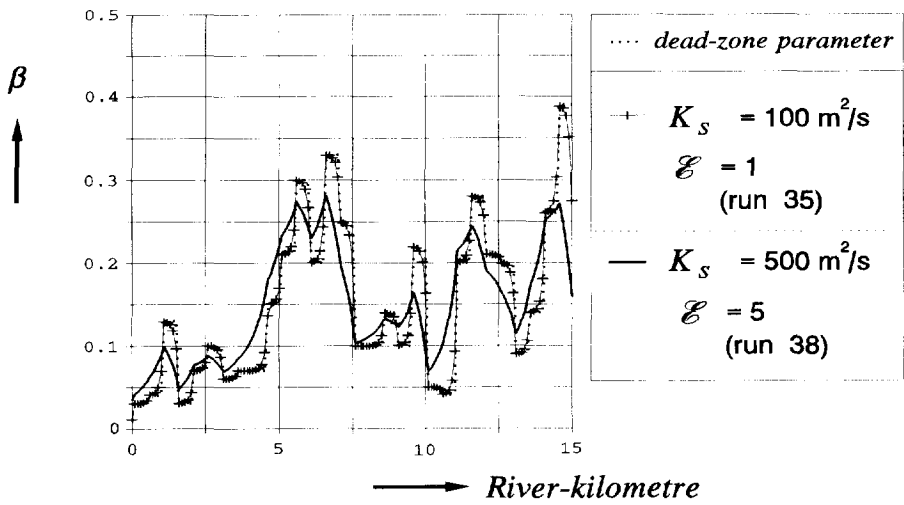


Fig. 4.3.43 Influence of the dispersion on the distribution of the local lag-coefficient in case of a variable dead-zone parameter per 500 m river reach

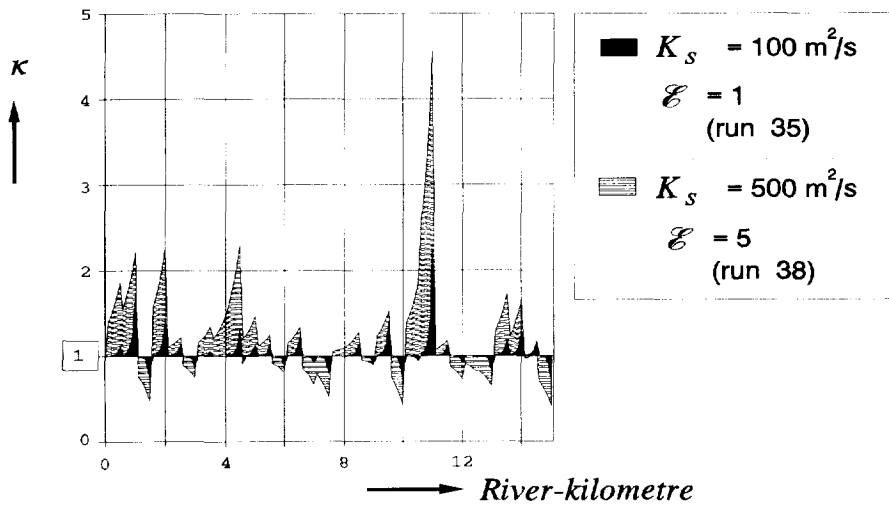


Fig. 4.3.44 Distribution of the deviation of the κ -value from unity; comparison of two computations with different longitudinal dispersion-coefficients (run 35 and 38)

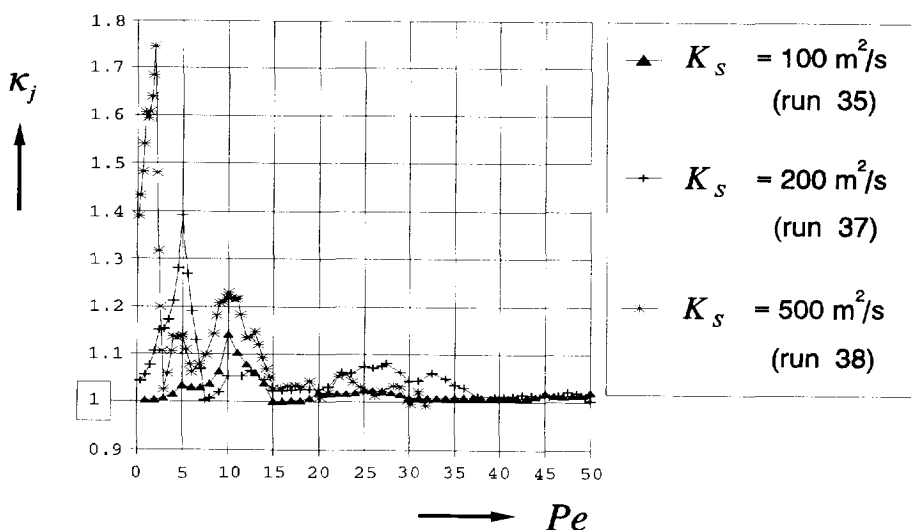


Fig. 4.3.45 Distribution of the overall value of κ for three different values of the longitudinal dispersion-coefficient K_s

distance equal to $Pe = 10$. In Fig. 4.3.45 the overall value of the ratio of actuality κ after

$$\kappa_j = \frac{\beta_j}{\frac{1}{j} \sum_{i=1}^j \beta_i} \quad (4.3.77)$$

with

$$\beta_j = \frac{(\mu_t)_j - (\mu_t)_0}{j \cdot \Delta x} \cdot u_s - 1 \quad (4.3.78)$$

wherein β_i dead-zone parameter of space step i
 $(\mu_t)_j$ time-centroid of the concentration distribution at the downstream boundary of the space step j
 $(\mu_t)_0$ time-centroid of the concentration distribution at the upstream boundary of the space step 1, i.e. the first space step with dead zones

is presented for three different values of the longitudinal dispersion-coefficient K_s . The distance is given by the Péclet number Pe . It shows that the condition

$$0.9 \leq \kappa_j \leq 1.1 \quad (4.3.79)$$

is achieved for $Pe \geq 15$. However, it should be noted that this result is based on the situation in the River Waal. Large variations of the value of the dead-zone parameter over a relatively short distance do increase the κ_j -value. On the other hand, in open channels such variations are mostly caused by harbours or lakes with an open connection with the channel concerned. Because in this case a completely mixed situation of the pollutant in the stagnant zone, i.e. harbour or lake, cannot be expected. Thus the contribution of stagnant zones, caused harbours and lakes to the actual dead-zone parameter and the lag coefficient respectively will be restricted. The contribution depends on the dimensions of the part of the stagnant zone, which exchanges with the main stream.

The dimensionless distance $Pe = 15$ means for the Dutch branches of the River Rhine with a mean flow-velocity $u_s = 1$ m/s and a longitudinal dispersion-coefficient of about $3000 \text{ m}^2/\text{s}$ (see Fig. 3.4.20, Sub-section 3.4.4), an averaging over a distance of about 45 km. Thus, it can be concluded that also from a practical point of view an averaging of the dead-zone parameter and the lag coefficient over a distance, corresponding with $Pe = 15$ is a good starting point for a comparison of the dead-zone parameter and a measured lag-coefficient, based on tracer measurements.

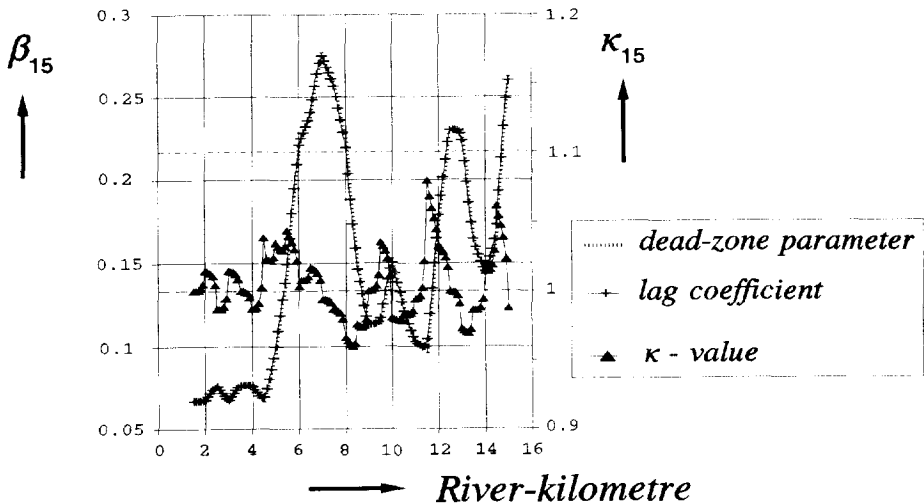


Fig. 4.3.46 Comparison of the dead-zone parameter with the lag coefficient, averaged over a distance, corresponding with $Pe = 15$ ($K_s = 100 \text{ m}^2/\text{s}$, run nr. 35) and the ratio of these parameters

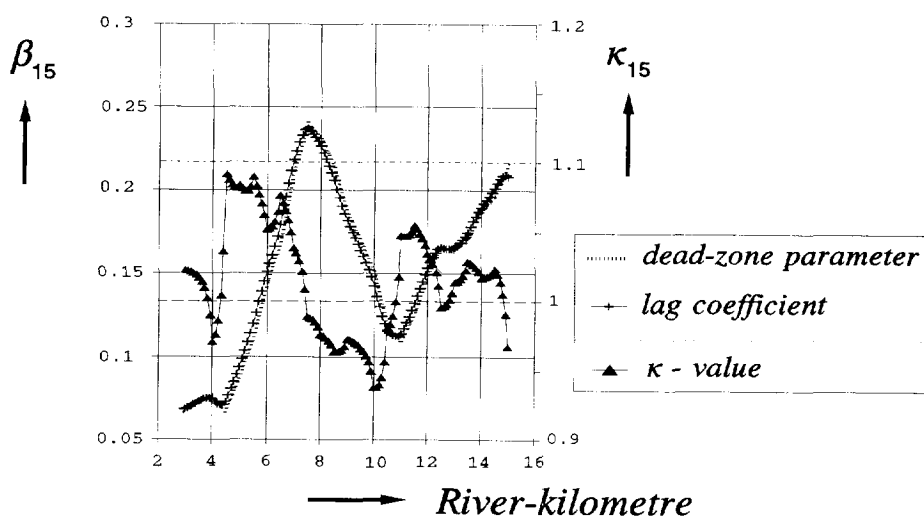


Fig. 4.3.47 Comparison of the dead-zone parameter with the lag coefficient, averaged over a distance, corresponding with $Pe = 15$ ($K_s=200$ m²/s, run nr. 37) and the ratio of these parameters

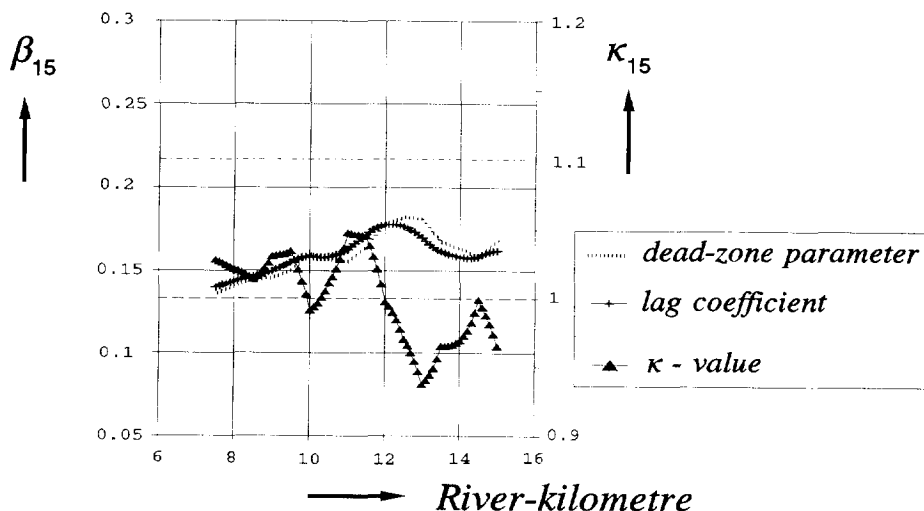


Fig. 4.3.48 Comparison of the dead-zone parameter with the lag coefficient, averaged over a distance, corresponding with $Pe = 15$ ($K_s=500$ m²/s, run nr. 38) and the ratio of these parameters

For verification of this starting point in Figs 4.3.46 ... 4.3.48 the distribution of the averaged values of the dead-zone parameter and the lag coefficient are compared for run nrs 35, 37 and 38 after

dead-zone parameter

$$\beta_{15} = \frac{1}{15} \sum_{i=j}^{j+15} \beta_i \quad (4.3.80)$$

lag coefficient

$$\beta_{15} = \frac{(\mu_t)_{j+15} - (\mu_t)_{j-1}}{15 \cdot \Delta x} \cdot u_s - 1 \quad (4.3.81)$$

for $j = 1, 2, 3, \dots$

The distributions of the dead-zone parameter and the lag coefficient show a good agreement and the presented distribution of the corresponding κ_{15} -value lies between the values 0.9 and 1.1 after Eq.(4.3.79).

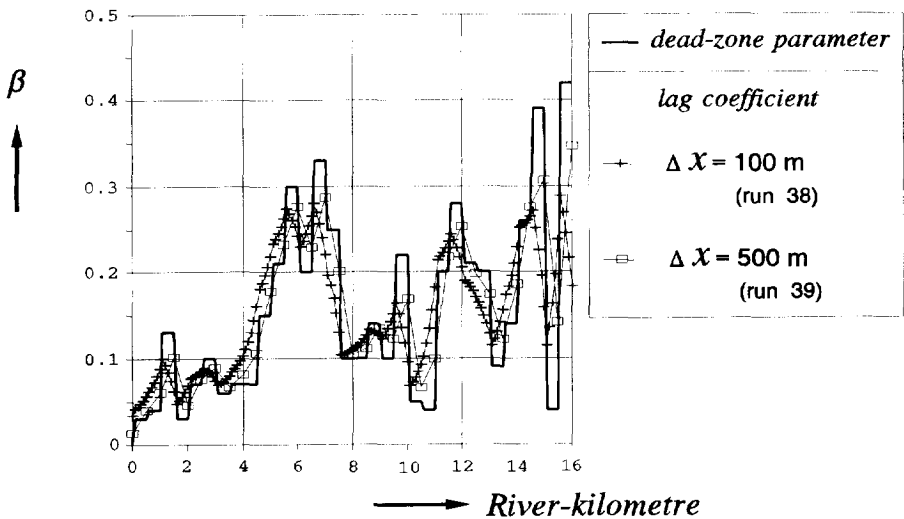


Fig. 4.3.49 Influence of the space step on the distribution of the local lag-coefficient in case of a variable dead-zone parameter per 500 m river reach (run nrs 38 and 39)

In Fig. 4.3.49 the distributions of the local lag-coefficients, computed after run nrs 38 and 39 with different space steps are compared with the dead-zone parameter. It shows that due to the increment of the space step from 100 till 500 m, the

distribution of the lag coefficient is shifted over a distance of 400 m: a numerical consequence of the enlargement of the space step. Figure 4.3.50 shows the comparison of the dead-zone parameter with the lag coefficient after Eqs (4.3.80) and (4.3.81) and the corresponding distribution of the κ_{15} -value. Again the distribution of the lag coefficient agrees quite well with the distribution of the dead-zone parameter, whereas the κ_{15} -value varies between 0.95 and 1.05. This result proves that the averaging of the lag coefficient and the dead-zone parameter over the dimensionless distance, corresponding with $Pe = 15$, is a good starting point indeed for a comparison of these parameters.

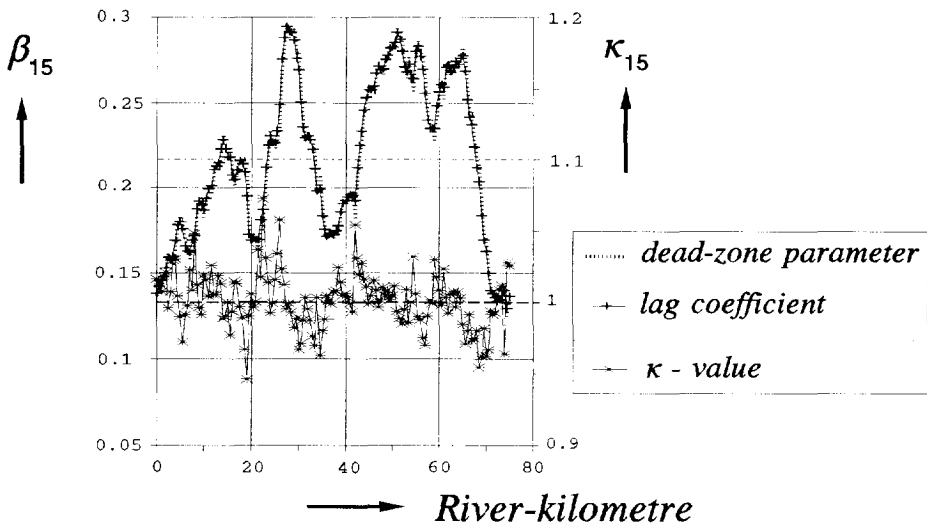


Fig. 4.3.50 Comparison of the dead-zone parameter with the lag coefficient, averaged over a distance, corresponding with $Pe = 15$ ($K_s = 500 \text{ m}^2/\text{s}$, run nr. 39) and the ratio of these parameters

For the examination of the behaviour of the transport velocity related to the peak concentration, additional computations were carried out. The input-data of the computations concerned are listed in Table 4.3.10. The results are presented in Figs 4.3.51 ... 4.3.58.

Referring to the conclusion in Sub-section 4.3.4 that the transport velocity, related to the peak concentration adjusts more or less instantaneously to the dead zones after Eq.(4.3.60) for values of the mass-transfer parameter $\mathcal{E} \geq 1$, the distribution of the local lag-coefficient based on the peak concentration will also follow the distribution of the variable dead-zone parameter as closely as the lag coefficient based on the time-centroid (compare Fig. 4.3.51 with Fig. 4.3.41).

TABLE 4.3.10 Input-data of the computations for the analysis of the behaviour of the lag coefficient β_i in relation to the peak concentration, in case of a variable dead-zone parameter β_i

run nr.	K_s (m ² /s)	D_b (s ⁻¹)	u_s (m/s)	\mathcal{E}	space step Δx (m)	time step Δt (s)	distance without dead zones	
							(km)	Pe
40	100	0.01	1	1	100	1	10	100
41	100	0.001	1	0.1	100	1	10	100
42	100	0.0005	1	0.05	100	1	10	100
43	500	0.01	1	5	100	1	50	100
44	500	0.01	1	5	500	1	50	100
45	500	0.002	1	1	500	1	50	100
46	500	0.001	1	0.5	500	1	50	100
47	500	0.0004	1	0.2	500	1	50	100

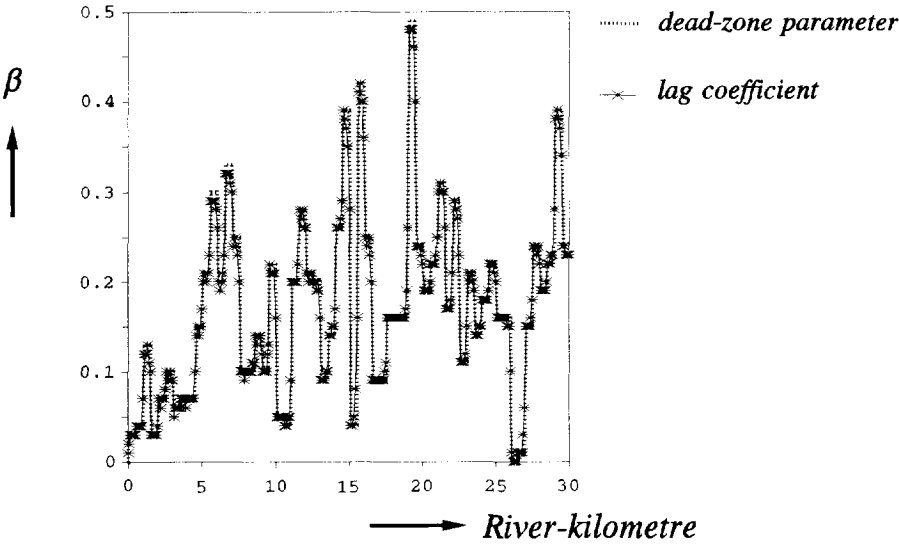


Fig. 4.3.51 Comparison of the distributions of the dead-zone parameter and the local lag-coefficient, related to the peak value of the concentration distribution after run nr. 40 ($\mathcal{E} = 1$)

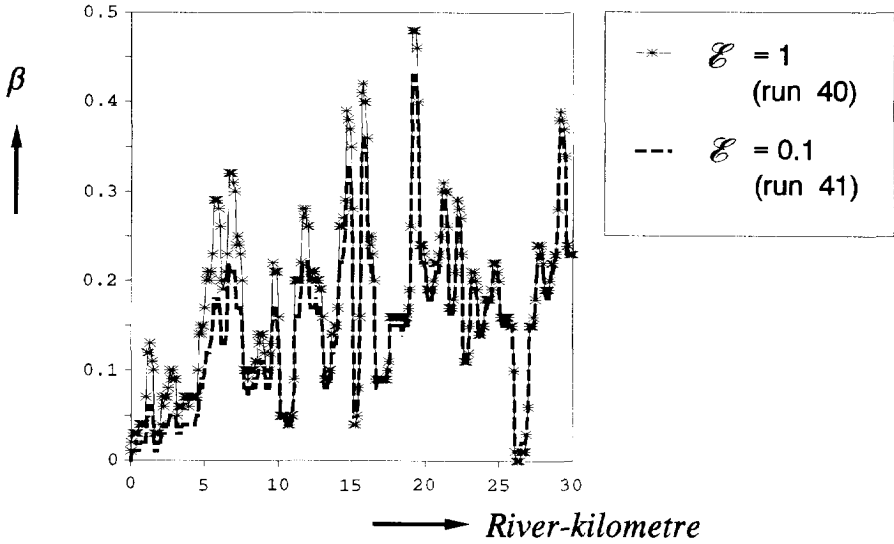


Fig. 4.3.52 Influence of the dimensionless mass-transfer parameter \mathcal{E} on the distribution of the local lag-coefficient (run nrs 40 and 43)

In Figs 4.3.52 and 4.3.53 the influence of the mass-transport parameter \mathcal{E} on the initial distribution of the ratio of the local lag-coefficient and the dead-zone parameter (i.e. the κ -value) is analyzed. Figure 4.3.52 shows that for $\mathcal{E} = 0.1$ the difference between the distributions of the dead-zone parameter and the local lag-coefficient reduces with the distance. According to the analysis of the adaptation length over which the local lag-coefficient (based on the peak concentration) becomes equal to the dead-zone parameter by applying the dimensionless distance $x \cdot D_b \cdot \beta_j^{1/2} \cdot u_s^{-1}$ (Sub-section 4.3.4), the initial distribution of the local κ -value is presented for three values of the mass-transfer parameter in Fig. 4.3.53. The dead-zone parameter in the expression for the dimensionless distance $x \cdot D_b \cdot \beta_j^{1/2} \cdot u_s^{-1}$ is defined by

$$\beta_j = \frac{1}{j} \sum_{i=1}^j \beta_i \quad (4.3.82)$$

Considering the tendency of the presented distribution, it can be concluded that the overall adaptation-length corresponds with a dimensionless distance $x \cdot D_b \cdot \beta_j^{1/2} \cdot u_s^{-1} = 10$ till 15, as found in case of a constant dead-zone parameter (see Sub-section 4.3.4). The local fluctuations of κ are caused by the variation of the dead-zone parameter. Since in case of a mass-transfer parameter $\mathcal{E} < 1$, there is no

instantaneous adaptation of the local lag-coefficient to the dead-zone parameter, if the transport velocity is related to the peak concentration. An additional adaptation-length for the concerned value of the dead-zone parameter is needed. However, because the dead-zone parameter varies every 500 m river-reach, the additional adaptation-length after a variation of the dead-zone parameter is overruled by the adaptation to the next dead-zone parameter. The extremely large fluctuations of κ (larger than 1 or smaller than 0.8) indicate extremely large differences between two successive values of the dead-zone parameter.

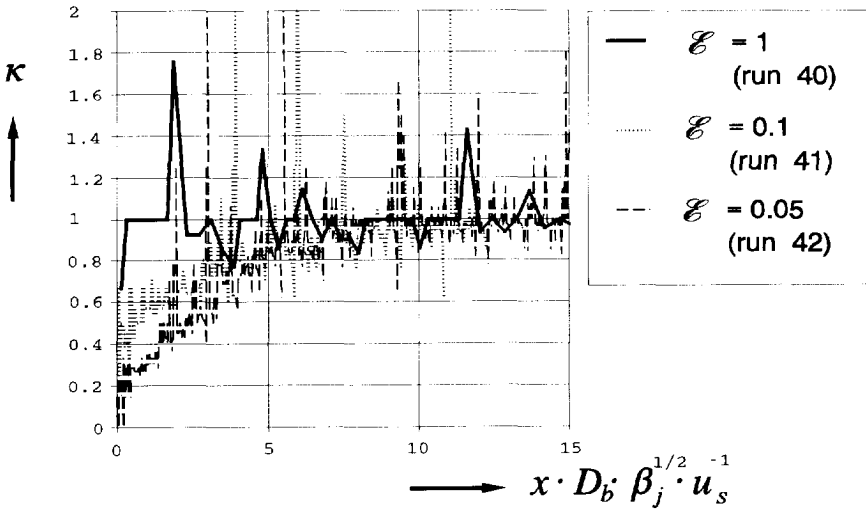


Fig. 4.3.53 Influence of the mass-transfer parameter \mathcal{E} on the initial distribution of the local κ -value, related to the peak concentration (run nrs 40, 41 and 42)

The influence of the longitudinal dispersion-coefficient K_x on the transport velocity, related to the peak concentration is presented for values of the mass-transfer parameter $\mathcal{E} \geq 1$ in Fig. 4.3.54. As already found for the transport velocity related to the time-centroid of the concentration distribution, due to the dispersion the upstream lag-coefficient is influenced by the downstream dead-zone parameter-value (see Sub-section 4.3.4, Fig. 4.3.43). If the distance over which the dead-zone parameter is constant, does not vary, the deviation of the local value of the lag coefficient from the dead-zone parameter will increase with the longitudinal dispersion-coefficient (Fig. 4.3.54).

Also in case of the peak concentration an increment of the space step from 100 to 500 m only means a shift of the distribution of the local lag-coefficient over a distance of 400 m (Fig. 4.3.55). Thus for the analysis of the influence of the

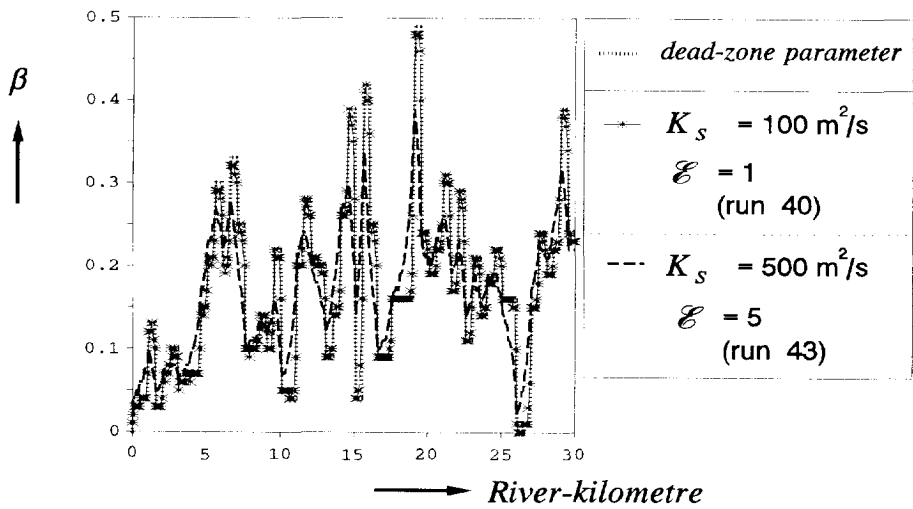


Fig. 4.3.54 Influence of the dispersion on the distribution of the local lag-coefficient, related to the peak concentration, in case of a variable dead-zone parameter per 500 m river reach

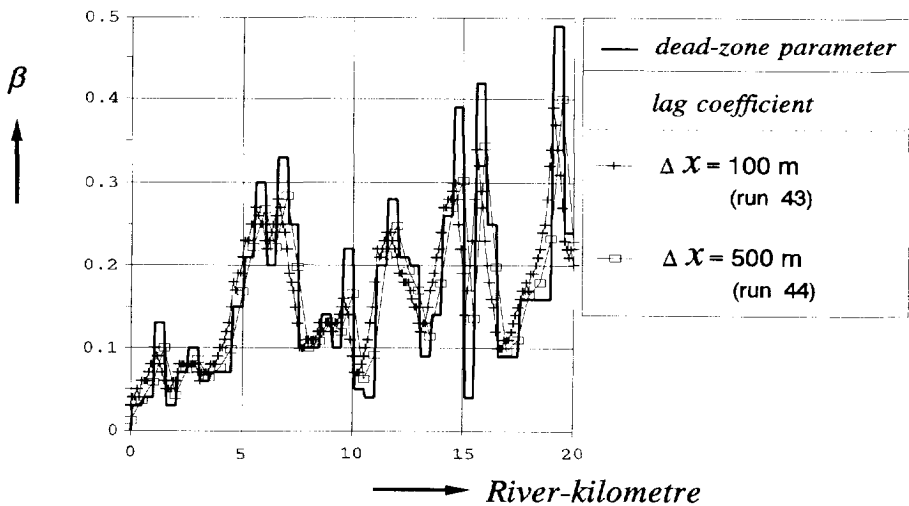


Fig. 4.3.55 Influence of the space step on the distribution of the local lag-coefficient, related to the peak concentration, in case of a variable dead-zone parameter per 500 m river reach (run nrs 43 and 44)

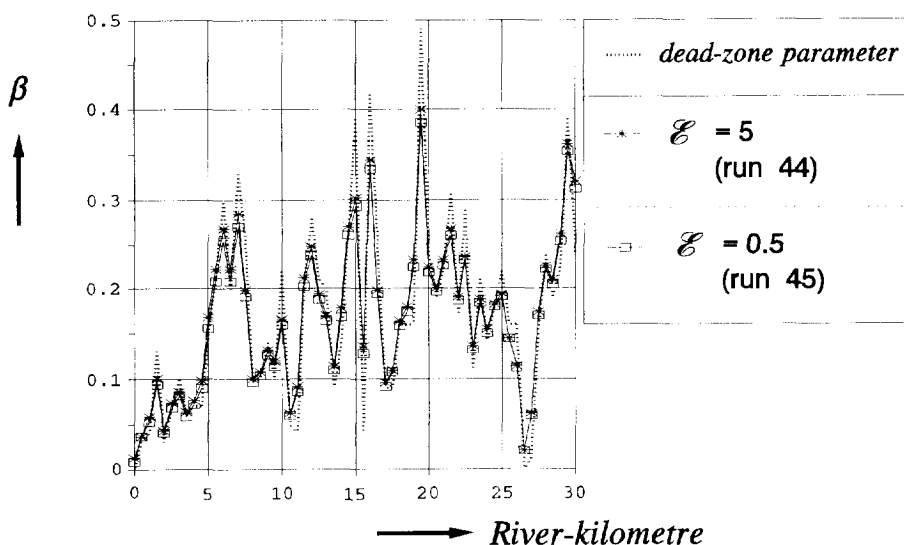


Fig. 4.3.56 Influence of the mass-transfer parameter \mathcal{E} on the distribution of the local lag-coefficient, compared with the dead-zone parameter for a space step of 500 m and $K_s = 500 \text{ m}^2/\text{s}$ (run nrs 44 and 45)

longitudinal dispersion-coefficient for large values, a space step of 500 m can be applied. After the results of run nrs 44 and 45 in Fig. 4.3.56 with a longitudinal dispersion-coefficient $K_s = 500 \text{ m}^2/\text{s}$, a reduction of the mass-transfer parameter \mathcal{E} from 5 to 0.5 has no significant influence on the local lag-coefficient. However, after Fig. 4.3.53 in case of a smaller dispersion-coefficient ($K_s = 100 \text{ m}^2/\text{s}$) a reduction of the mass-transfer parameter shows a large difference between the initial κ -distributions. Defining the relative difference between the local κ -value of two comparable computations by

$$\frac{\Delta \kappa}{\kappa} = \frac{\kappa_{\mathcal{E}_1} - \kappa_{\mathcal{E}_2}}{\kappa_{\mathcal{E}_1}} \quad (4.3.83)$$

wherein $\kappa_{\mathcal{E}_1} = \kappa$ -value in case of a large \mathcal{E} -value
 $\kappa_{\mathcal{E}_2} = \kappa$ -value in case of a comparable small \mathcal{E} -value

the κ -distributions of run nrs 40 and 41 (with $K_s = 100 \text{ m}^2/\text{s}$), as well as run nrs 44 and 45 (with $K_s = 500 \text{ m}^2/\text{s}$) are compared in Fig 4.3.57.

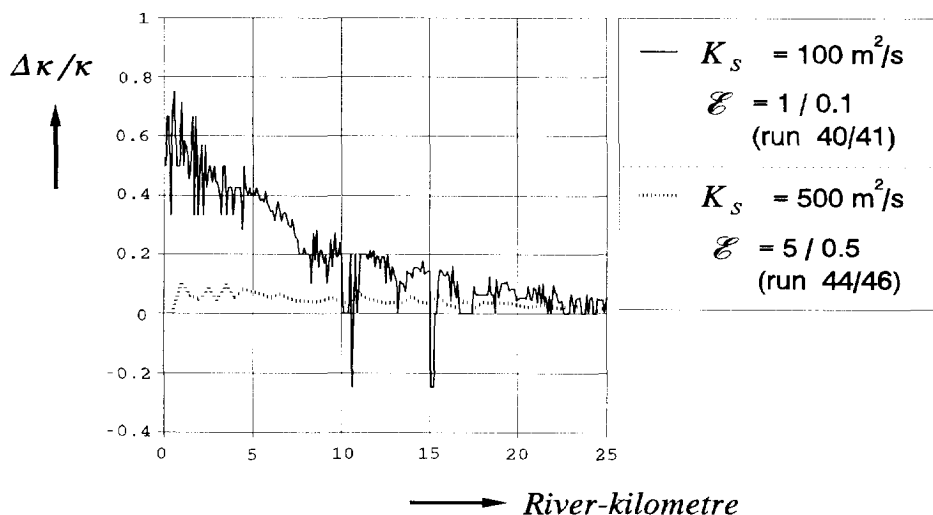


Fig. 4.3.57 Influence of the dispersion on the effect of the mass transfer on the initial distribution of the lag coefficient related to the peak concentration, represented by the relative κ -value after Eq.(4.3.83)

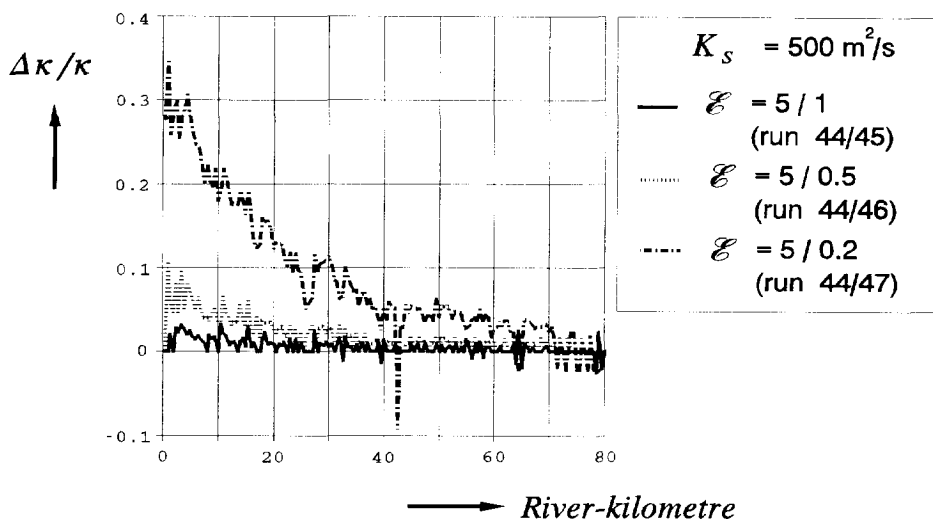


Fig. 4.3.58 Influence of the mass-transfer parameter on the initial distribution of the lag coefficient related to the peak concentration, represented by the relative κ -value after Eq.(4.3.83)

Apparently a large dispersion-coefficient smooths the fluctuations of the κ -distribution, i.e. the dispersion reduces the adaptation length. The reduction depends on the value of the dispersion coefficient K_s as well as the value of the mass-transfer coefficient D_b , i.e. the mass-transfer parameter \mathcal{E} . The smaller the mass-transfer coefficient, the larger the longitudinal dispersion-coefficient must be in order to get a comparable reduction of the influence of the mass transfer on the transport velocity, related to the peak concentration. In Fig. 4.3.58 the influence of the mass-transfer parameter \mathcal{E} on the initial κ -distribution in comparison with the κ -distribution for $\mathcal{E} = 5$ (run nr. 44) is presented. It proves again that for the peak concentration the instantaneous adaptation of the lag coefficient to the dead-zone parameter holds for $\mathcal{E} \geq 1$.

Considering the transport velocity related to the time-centroid of the concentration distributions, it was stated from a practical point of view that for a good agreement between the dead-zone parameter and the lag coefficient an averaging of these parameters over a distance, corresponding a Péclet number of 15 has to be chosen. Figures 4.3.59 and 4.3.60 show that this statement also prevails for the transport velocity related to the peak concentration, if the mass-transfer parameter $\mathcal{E} \geq 1$.

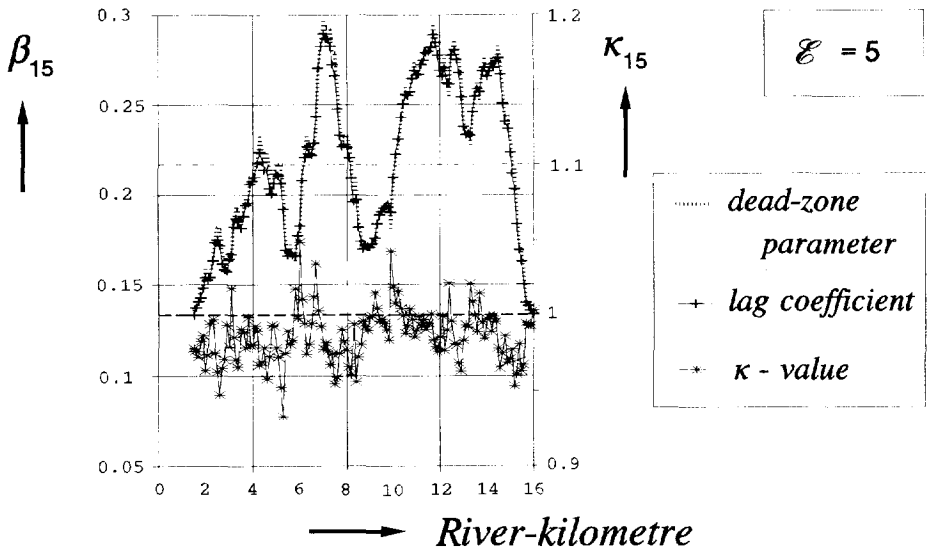


Fig. 4.3.59 Comparison of the dead-zone parameter with the lag coefficient, averaged over a distance, corresponding with $Pe = 15$ ($K_s = 500 \text{ m}^2/\text{s}$, $\mathcal{E} = 5$, run nr. 44) and the ratio of these parameters

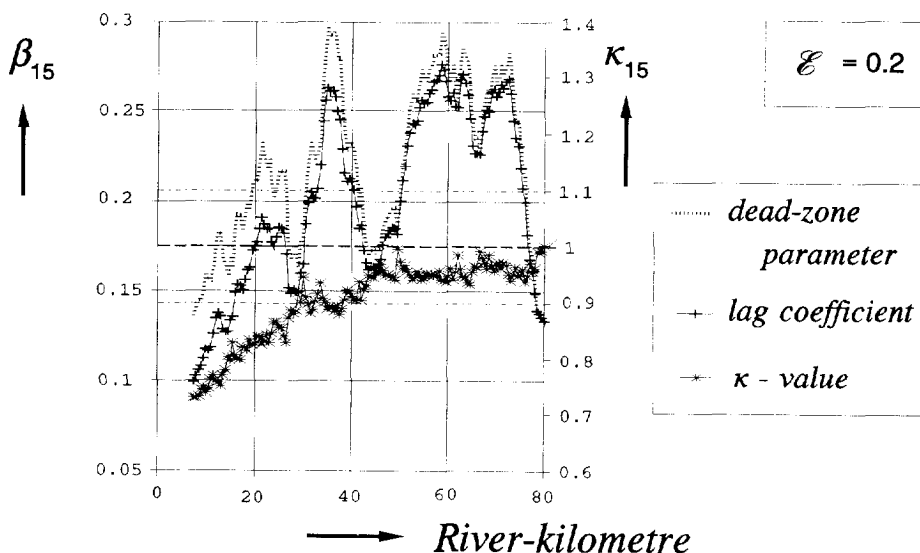


Fig. 4.3.60 Comparison of the dead-zone parameter with the lag coefficient, averaged over a distance, corresponding with $Pe = 15$ ($K_s = 500 \text{ m}^2/\text{s}$, $\mathcal{E} = 0.2$, run nr. 47) and the ratio of these parameters

4.3.6 Conclusions

The transport velocity of a pollution cloud has been related to the time-centroid as well as to the peak value of the concentration distribution. In case of the time-centroid the transport velocity c adjusts instantaneously to the dead-zone parameter after

$$c = \frac{u_s}{1 + \beta} \quad (4.3.84)$$

wherein u_s is the mean flow-velocity in the main stream and β the dead-zone parameter. However, due to the longitudinal dispersion the dead zones influences also the transport velocity upstream of these zones. The distance concerned increases with the longitudinal dispersion-coefficient K_s . The distance can be quantified by the Péclet number: $Pe = 10$ till 15 . The mass-transfer coefficient D_b , representing the exchange of mass between the main stream and the dead zones, has no effect on the transport velocity, related to the time-centroid. It only effects the concentration distribution: the smaller the mass-transfer coefficient the longer the tail of the concentration distribution will be.

The instantaneous adaptation of the transport velocity to the dead zones after Eq.(4.3.84) means in case of a variable dead-zone parameter that the actual lag-coefficient $\beta_{act.}$ after Eq.(4.1.3) varies with the dead-zone parameter, thus the ratio of the actual lag-coefficient and the dead-zone parameter κ will be equal to the unity. However, this holds for small values of the longitudinal dispersion-coefficient. Referring to the influence of the dead zones on the transport velocity in the upstream direction, caused by the dispersion, the variation of the local lag-coefficient will become smaller than the variation of the dead-zone parameter if the dispersion coefficient increases. As a matter of fact, due to the dispersion the distribution of the local lag-coefficient is a smoothed version of the distribution of the dead-zone parameter. Therefore from a practical point of view it is suggested to compare the values of the actual lag-coefficient and the dead-zone parameter averaged over a distance, corresponding with $Pe = 15$, being the upstream river-reach influenced by the down-stream dead-zones. In this case the actual lag-coefficient deviates less than 10% from the dead-zone parameter ($0.9 \leq \kappa \leq 1.1$)

If the transport of the pollutant is related to the peak value of the concentration distribution, the adaptation of the transport velocity c depends on the magnitude of the mass-transfer parameter $\mathcal{E} = D_b \cdot K_s / u_s^2$. For values of $\mathcal{E} \geq 1$ there is more or less an instantaneous adaptation of the local lag-coefficient to the dead-zone parameter value. Consequently in case of a variable dead-zone parameter an averaging over the dimensionless distance of $Pe = 15$ also gives comparable values for these parameters ($0.9 \leq \kappa \leq 1.1$).

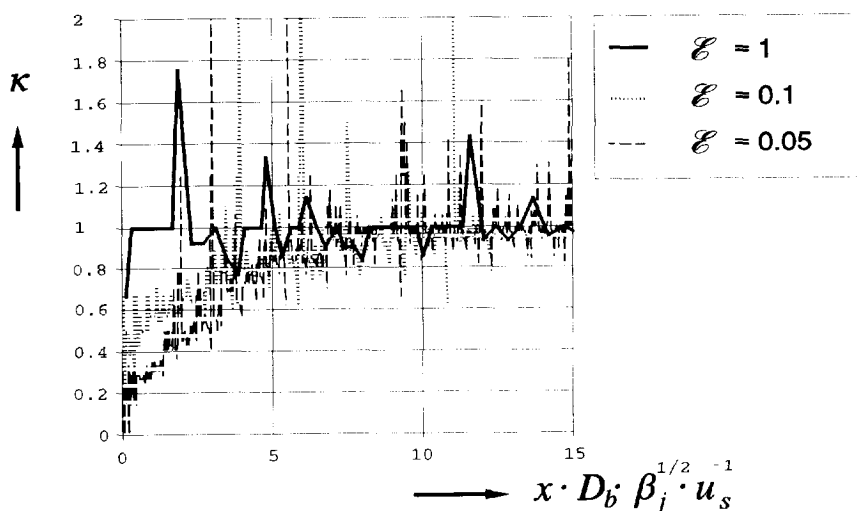


Fig. 4.3.61 Influence of the mass-transfer parameter \mathcal{E} on the initial distribution of the local κ -value, related to the peak concentration

However, for $\mathcal{E} < 1$ there is an adaptation length of the local lag-coefficient to the dead-zone parameter. This distance can be given by the dimensionless parameter $x \cdot D_b \cdot \beta_j^{1/2} \cdot u_s^{-1} = 10$ till 15. In case of a variable dead-zone parameter there are two types of adaptation. There is an overall adaptation-length from the starting point of the dead zones, which can also be given by the parameter $x \cdot D_b \cdot \beta_j^{1/2} \cdot u_s^{-1} = 10$ till 15, wherein β_j is the overall value of the dead-zone parameter. Locally the variations of the dead-zone needs additional adaptation-lengths per change of the dead-zone parameter. Because mostly the adaptation-length is much larger than the distance over which the dead-zone parameter is constant, the adaptation to the local value of the dead-zone parameter cannot be achieved and is overruled by the adaptation to the next dead-zone parameter. The result is an overall adaptation of the lag coefficient to the overall mean-value of the dead-zone parameter with a locally fluctuated deviation, due to the variation of the dead-zone parameter (Fig. 4.3.61, see also Fig. 4.3.53). Relatively large fluctuations of the ratio of the lag coefficient and the dead-zone parameter ($\kappa > 1.5$) indicate relatively large variations of the dead-zone parameter. By increasing of the longitudinal dispersion-coefficient these fluctuations are smoothed.

These results mean that by tracer experiments the mass-transfer coefficient D_b cannot be determined explicitly by the transport velocity of a tracer cloud. If the transport velocity, based on the time-centroid and the peak value of the measured concentration distributions are equal, a lower limit for the mass-transfer parameter can be given: $\mathcal{E} \geq 1$. Considering the Dutch branches of the River Rhine with a mean flow-velocity $u_s = 1$ m/s and a longitudinal dispersion-coefficient $K_s = 3000$ m²/s, for the mass-transfer coefficient D_b a value larger than $3.5 \cdot 10^{-4}$ s⁻¹ is found (see Eq. 4.3.34), whereas the used reference value after Eq.(4.3.54) is equal to 10^{-2} s⁻¹.

If the transport velocity based on the time-centroid and the peak concentration differ, it yields $\mathcal{E} < 1$. In case of the River Rhine the mass-transfer coefficient becomes smaller than $3.5 \cdot 10^{-4}$ s⁻¹.

It is because the mass-transfer coefficient D_b does effect the concentration distribution, its value has to be determined by comparison of measured and calculated concentration-distributions. As already mentioned, an important effect of the mass-transfer coefficient on the concentration distribution considers the tail of the distribution. Therefore the measured concentration-distributions have to be as complete as possible. If the tail of a concentration distribution is hardly measured the determination of the mass-transfer coefficient becomes inaccurate.

4.4

THE DUTCH BRANCHES OF THE RIVER RHINE

4.4.1

General

On account of the shipping traffic groyne-fields are built at both banks of the Dutch branches of the River Rhine (Fig. 4.4.1). By these artificial dead-zones these river branches are pre-eminently appropriate for comparison of the tracer experiments 04/89, 09/90 and 06/91 with computational results of the dead-zone model. However, for a useful comparison the measured concentration-distributions have to be reliable. After the analysis of the lag coefficient based on the measured distributions (see Sub-section 3.4.5), not all measuring-stations seem to be suitable. In Table 4.4.1 the most appropriate measuring-stations are collected.

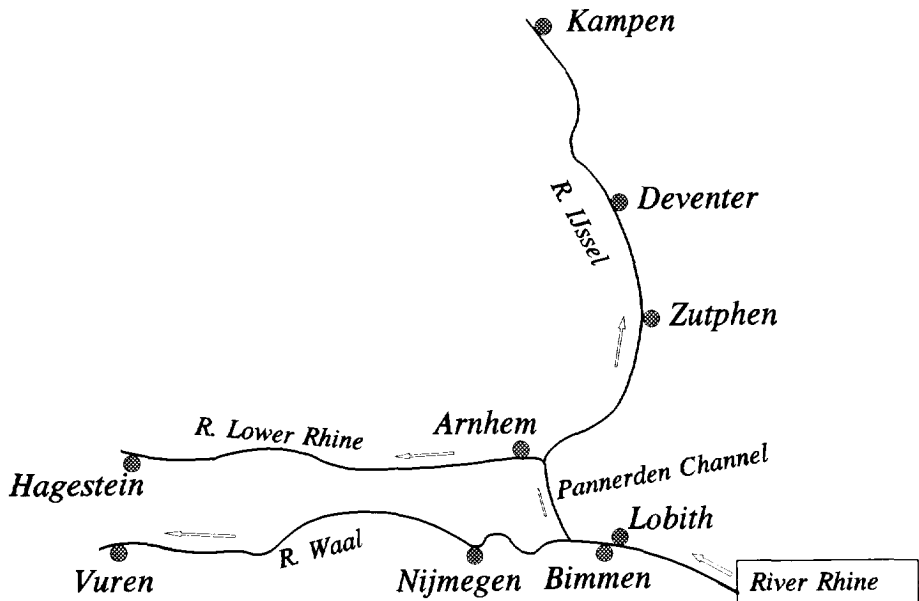


Fig. 4.4.1 Overview of the Dutch branches of the River Rhine

For the analysis of the transport of a pollutant cloud in the Dutch Rhine-branches there two aspects to be taken into consideration:

- * the actual lag-coefficient $\beta_{act.}$ in relation to the dead-zone parameter β , based on the ratio of the cross-sectional areas of the groyne-fields (A_b) and the main stream (A_s), and
- * the mass-transfer coefficient D_b .

TABLE 4.4.1 Appropriate measuring-stations for the analysis of the dead-zone parameter and the mass-transfer coefficient

Tracer experiment	04/89	09/90	06/91
River discharge at Lobith (m ³ /s)	2979	954	2383
measuring station			
Lobith	X	X	
Bimmen			X
Nijmegen		X	X
Vuren	X	(X) *)	X
Hagestein	X		X
Kampen	(X) *)	X	

*) The tail of the concentration is not measured completely

In case of the analysis of the mass-transfer coefficient, next to the reliability of the measured time-centroid or peak concentration the distribution itself must be as complete as possible, i.e. the tail of the concentration distribution. The measured concentration-distributions for which the tail is missing, are marked with (X) (see Fig. 4.1.2).

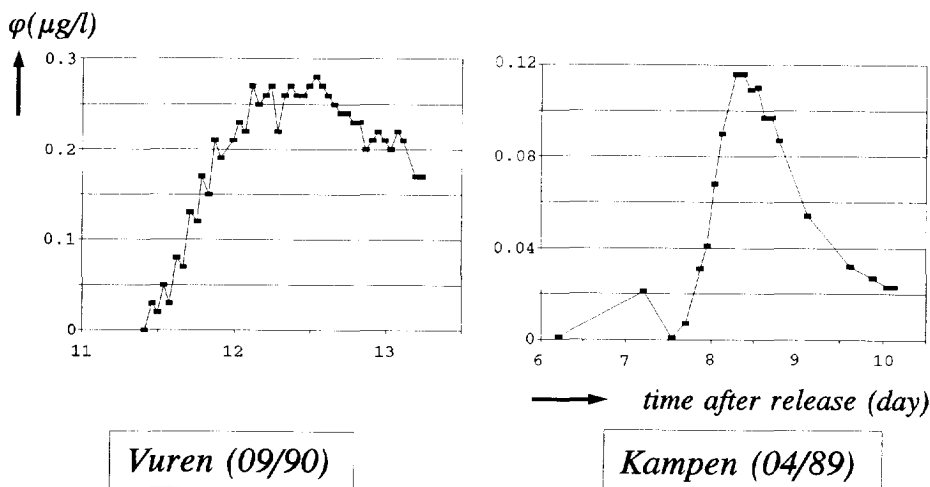


Fig. 4.4.2 Measured concentration-distributions at the measuring-stations Kampen (tracer experiment 04/89) and Vuren (tracer experiment 09/90)

For the comparison of the measured lag-coefficient with the dead-zone parameter, the schematization of the Dutch Rhine-branches after the SOBEK-model are used (Delft Hydraulics & Ministry of Transport, Public Works and Watermanagement, 1995). In Sub-section 3.4.5 the measured lag-coefficients have been compared roughly with the dead-zone parameter. Because the dead-zone parameters after the SOBEK-model are mostly given every 500 m river-reach, for simplicity the averaged values (β_n) have been determined by

$$\beta_n = \frac{1}{n} \sum_{i=1}^n \beta_i \quad (4.4.1)$$

The dead zones caused by lakes, river harbours etc. with an open connection with the river, have been defined by values of the dead-zone parameter $\beta_i > 0.8$. Excluding of these dead zones in the determination of the average dead-zone parameter was made by replacing these values (> 0.8) by zero.

TABLE 4.4.2 Dead-zone parameter for the Dutch branches of the River Rhine after the SOBEK-model

river branch			tracer experiment					
			09/90		06/91		04/89	
			river discharge at Lobith (m³/s)					
			954		2383		2979 **)	
			(1) *)	(2)*)	(1)	(2)	(1)	(2)
Lobith/Bimmen	- Nijmegen	0.57	0.13	0.58	0.18	0.63	0.24	
	- Vuren	0.40	0.16	0.45	0.23	0.50	0.27	
	- Hagestein	0.86	0.29	0.89	0.32	0.97	0.34	
	- Kampen	0.80	0.19	0.79	0.23	0.80	0.28	
Nijmegen	- Vuren	0.34	0.17	0.41	0.24	0.45	0.28	

- *) (1) inclusive harbours and lakes, which have an open connection with the river
 (2) for values of the dead-zone parameter > 0.5 , the dead-zone parameter value is replaced by the value of 0.5

- **) the dead-zone parameter after the SOBEK-model is related to a river discharge at Lobith of 3000 m³/s

Now the mean value of the dead-zone parameter has been determined more precisely by taking the distance Δx_i between two successive values of the dead-zone

parameter into consideration after

$$\beta_n = \frac{\sum_{i=1}^n \left(\frac{\beta_{i-1} + \beta_i}{2} \cdot \Delta x_i \right)}{\sum_{i=1}^n \Delta x_i} \quad (4.4.2)$$

with β_{i-1} dead-zone parameter at the upstream boundary of the considered river reach Δx_i
 β_i dead-zone parameter at the downstream boundary of the considered river reach Δx_i

In Table 4.4.2 the values, averaged over the river branches concerned after Eq.(4.4.2), are presented for the three river discharges at Lobith during the tracer experiments 04/89, 09/90 and 06/91. Because there will not be a completely mixed situation of the transported pollutant in large dead-zones as lakes and river harbours, the dead-zone parameter has to be reduced at these river cross-sections. In Table 4.4.2 the averaged values of the dead-zone parameter is presented, if β_i -values larger than 0.5 are substituted by a value of 0.5.

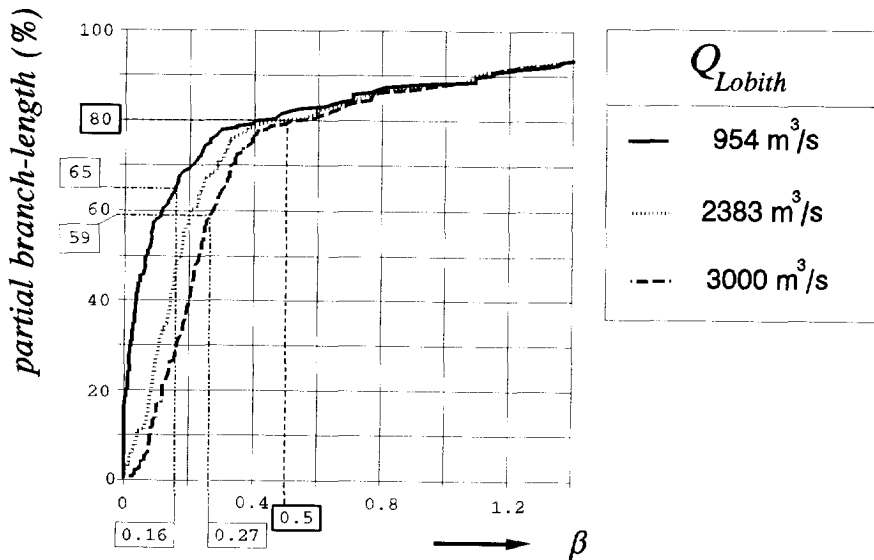


Fig. 4.4.3 Partial branch-length with values of the dead-zone parameter β equal to or less than the considered one for the Rhine-branch between Lobith and Vuren (River Waal) after the SOBEK-model

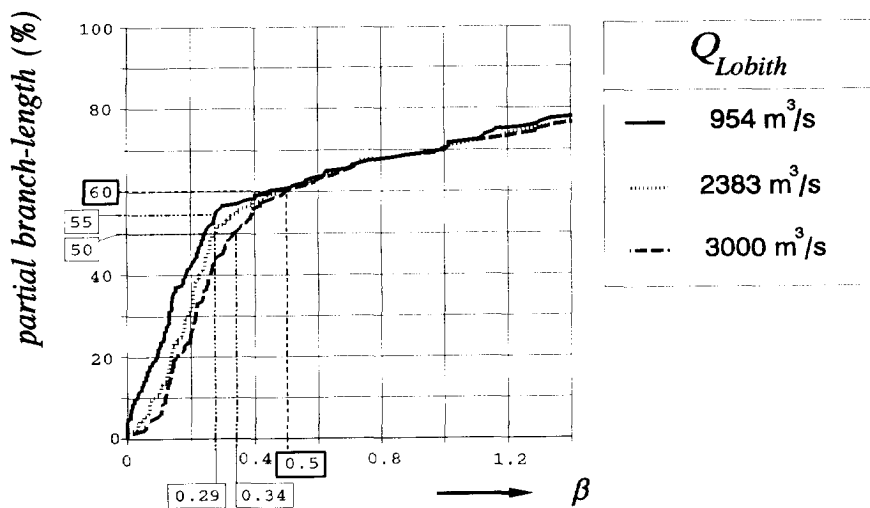


Fig. 4.4.4 Partial branch-length with values of the dead-zone parameter β equal to or less than the considered one for the Rhine-branch between Lobith and Hagestein (Pannerden Channel and R. Lower Rhine) after the SOBEK-model

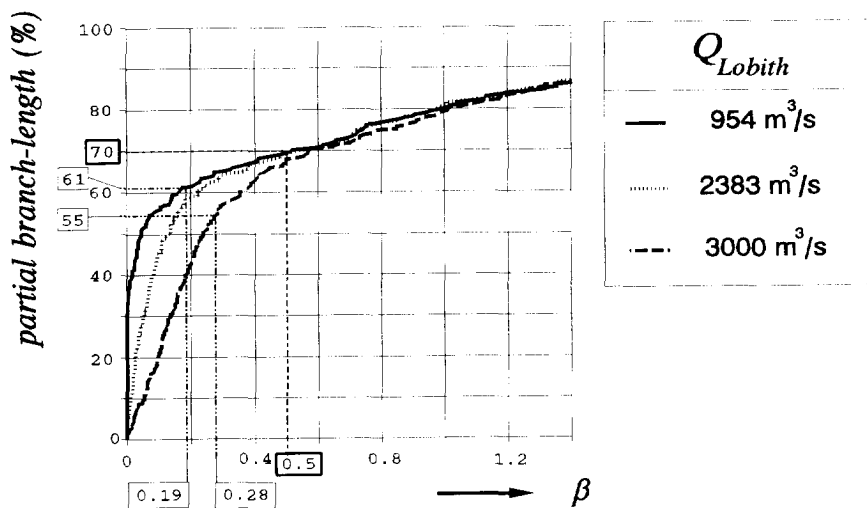


Fig. 4.4.5 Partial branch-length with values of the dead-zone parameter β equal to or less than the considered one for the Rhine-branch between Lobith and Kampen (Pannerden Channel and R. IJssel) after the SOBEK-model

The distribution of the river branch-length for which the dead-zone parameter is smaller than or equal to the value concerned, are presented in succession for the Rhine branches *Lobith-Vuren* (including the River Waal) in Fig. 4.4.3, *Lobith-Hagestein* (including the Pannerden Channel and the River Lower-Rhine) in Fig. 4.4.4 and *Lobith-Kampen* (including the Pannerden Channel and the River IJssel) in Fig. 4.4.5 (see also Fig. 4.4.1). Based on a rough comparison of Figs 4.4.3 ... 4.4.5 it can be concluded that the River Waal shows the smallest contribution of lakes and river harbours to the distribution of the dead zones (about 20% the dead-zone parameter $\beta > 0.5$), whereas the River Lower Rhine has the largest contribution (about 30%), partly caused by the weirs with lateral canals with ship locks at Driel, Amerongen and Hagestein (Fig. 3.2.5). The part of the large stagnant-zone which exchanges with the main stream, depends on the shape and dimensions of the zone itself as well as the connection with the main stream. Because it is impossible to determine on forehand which part of the stagnant zone will exchange with the main stream of the river, the contribution of these zones to the mean value of the dead-zone parameter cannot be given explicitly, unless after an analysis of the local flow phenomena which predominate the exchange of a pollutant. Moreover the pollutant has to be mixed homogeneously over the part of the dead zone, which exchanges with the main stream.

Referring to the average ratio of the total width of the groyne-fields and the main stream along the Dutch Rhine-branches (Section 4.2) of about 0.2 till 0.3, for a first indication of the mean value of the dead-zone parameter the contribution of the large stagnant zones is limited by a value of 0.5. The resulting mean values correspond with a 50 till 60% of the branch-length, for which the dead-zone parameter is smaller than or equal to the mean-value concerned (see Table 4.4.2 and Figs 4.4.3 ... 4.4.5). Due to the uncertainty of the representing dead-zone parameter in case of large stagnant zones, the dead-zone parameter and the measured lag-coefficient becomes less and less comparable, if the contribution of large stagnant zones with incomplete exchange is increasing. Thus the Rhine branch Lobith - Vuren (including the River Waal) will be the most appropriate branch for the analysis of the influence of the dead zones, i.e. groyne-fields on the transport velocity related to the time-centroid or peak concentration of the measured concentration-distributions. The significance of the other Rhine branches will be more indicative. Anyhow, they might give information about the valuation of large stagnant-zones by a dead-zone parameter.

At last it has to be noticed that there is a slight increment of the dead-zone parameter with the river discharge.

In Sub-section 4.4.2 an analysis of the measured lag-coefficient in relation with the dead-zone parameter after the SOBEK-model as well as after the Rhine Alarm-Model, is presented. The mass-transfer coefficient for the Dutch Rhine-branches will be examined in Sub-section 4.4.3.

4.4.2 Transport velocity and the dead-zone parameter

As indicated in Subsection 4.3.6 the lag coefficient becomes comparable with the dead-zone parameter if this parameter is averaged over a distance, corresponding with a Péclet number of at least 10 till 15. Therefore in Table 4.4.3 the Pe-number is presented for the river reaches, considered in Table 4.4.2.

TABLE 4.4.3 The lengths of the river reaches concerned after the Péclet number (*Pe*)

river reach			length	mean flow- velocity u_s	long. dispersion- coefficient K_s	<i>Pe</i> - number
			(km)	(m/s)	(m ² /s)	
tracer experiment 04/89						
Lobith	-	Vuren	89.6	1.17	4476	23.4
	-	Hagestein	84.3	0.98	1016	81.3
	-	Kampen	132.3	0.85	635	177.1
tracer experiment 09/90						
Lobith	-	Nijmegen	21.43	0.96	6103	3.4
		Vuren	88.5	0.84	5650	13.2
		Kampen	131.2	0.51	544	123.0
Nijmegen	-	Vuren	67.07	0.81	5528	9.8
tracer experiment 06/91						
Bimmen	-	Nijmegen	19.71	1.14	4433	5.1
		Vuren	86.78	1.08	4703	19.9
		Hagestein	81.48	0.89	981	73.9
Nijmegen	-	Vuren	67.07	1.06	4776	14.9

The large longitudinal dispersion-coefficients of the river reach Lobith - Vuren (River Waal) can be explained by considering the used semi-empirical expression for the longitudinal dispersion-coefficient K_s as derived by Fischer et al. (1979) (see Eq. 2.3.86)

$$K_s = \alpha_x \cdot \frac{u_s^2 \cdot B^2}{a \cdot u_s} \quad (4.4.3)$$

with α_x = coefficient of proportionality
 B = width of the main stream
 a = depth of the main stream
 u_* = shear velocity: $u_* = u_* \cdot \sqrt{g} / C$

With a calibrated value α_x in the Rhine Alarm-Model for the Dutch Rhine-branches of 0.02 ⁷⁾ and a river width between 250 and 350 m (Table 4.4.4) the value of the dispersion coefficient becomes 4500 till 6000 m²/s. This means that relatively long distances have to be considered for the comparison of the lag coefficient and the dead-zone parameter. Thus the river reach Lobith/Bimmen - Nijmegen will not be taken into consideration. Further, in case of the tracer experiment 06/90 with a low river-discharge at Lobith of 954 m³/s the value of the lag coefficient over the river reach Nijmegen - Vuren (River Waal) will be compared not more than in an indicative sense with the averaged dead-zone parameter over this river reach.

TABLE 4.4.4 River width of the Dutch Rhine-branches after the Rhine Alarm-Model

River reach	river width (m)
- River Rhine Lobith - Panmerden bifurcation	340
- River Waal Panmerden bifurcation - Vuren	260 - 340
- Panmerden Channel	135 - 140
- River Lower Rhine IJssel bifurcation - Hagestein	100 - 150
- River IJssel IJssel bifurcation - Kampen	80 - 150

For the determination of the lag coefficient, based the tracer experiments concerned, the time-centroid of the measured concentration-distributions at the stations mentioned in Table 4.4.1 are collected in Table 4.4.5. For the determination of the time-centroid the measured concentration-distributions are approximated by the concentration distribution after the Chatwin-model (Eq. 2.3.85) by the DUD-method (see Subsection 3.3.1) in order to be independent of the completeness

⁷⁾ Based on velocity profiles in a river Fischer et al. (1979) derived a value 0.011 for the coefficient of proportionality α_x . However, after measurements in open channels the coefficient can become four times larger or smaller (see also Table 3.4.9).

TABLE 4.4.5 Time-centroid of the measured concentration-distributions

measuring station	Rhine-kilometre	time-centroid (μ_t) _m (day)	
		after the Chatwin-model by the DUD-method	after Eq.(4.4.4)
tracer experiment 04/89 (discharge at Lobith 2979 m ³ /s)			
Lobith	862.20	6.9383	7.0645
Vuren	951.80	8.0834	8.1597
Hagestein	946.50	8.2825	8.5679
Kampen	994.50	8.7358	9.1 *)
tracer experiment 09/90 (discharge at Lobith 954 m ³ /s)			
Lobith	863.30	11.340	-
Nijmegen	884.73	11.691	-
Vuren	951.80	12.749	-
Kampen	994.50	14.046	14.5351
tracer experiment 06/91 (discharge at Lobith 2383 m ³ /s)			
Bimmen	865.02	6.5320	-
Nijmegen	884.73	6.7589	-
Vuren	951.80	7.6919	-
Hagestein	946.50	8.0722	-

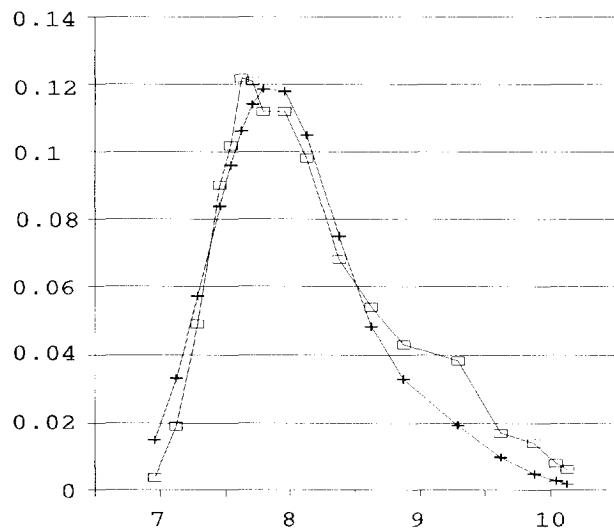
*) Based on the extrapolated concentration-distribution as presented in Fig. 3.4.34

of the measured concentration-distribution. In this way the time-centroid can also be approximated for the distributions with an incompletely measured tail of the distribution as presented in Fig. 4.4.2. On the other hand the approximation does not represent always the tail quite well (see Fig. 3.4.33), which means that the derived time-centroid is too small. Therefore in Table 4.4.5 for a restricted number of measuring stations at distances L from the point of release, the time-centroid derived from the measured concentrations after (see Eq. 3.3.8)

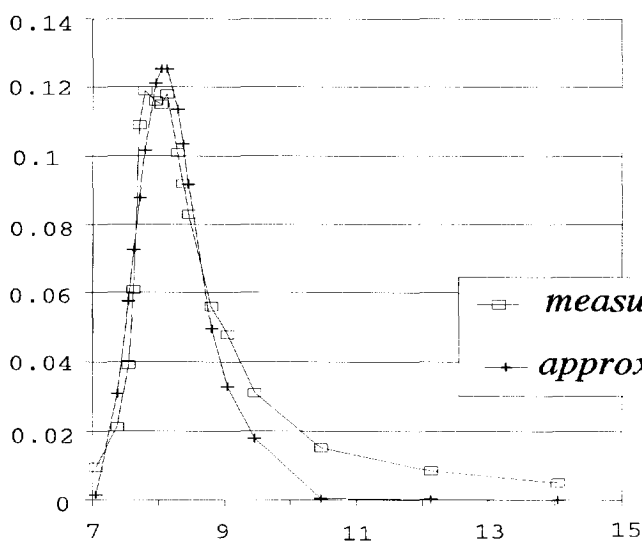
$$\mu_t = \frac{\int_{-\infty}^{+\infty} t \cdot \varphi_{meas.}(L, t) \cdot dt}{\int_{-\infty}^{+\infty} \varphi_{meas.}(L, t) \cdot dt} \quad (4.4.4)$$

is also presented. Figures 4.4.6...4.4.8 illustrate the restrictions of the approximation of the tail of the concentration distribution by the Chatwin-model after the DUD-method. In case of the tracer experiment 09/90 (Fig. 4.4.7) with a low-water

$\varphi(\mu\text{g/l})$



a



b

—□— *measured*
—+— *approximation*

—→ *time after release (day)*

Fig. 4.4.6 Comparison of measured concentration-distributions with the approximation by the Chatwin-model, tracer experiment 04/89, measuring-stations Vuren (a) and Hagestein (b)

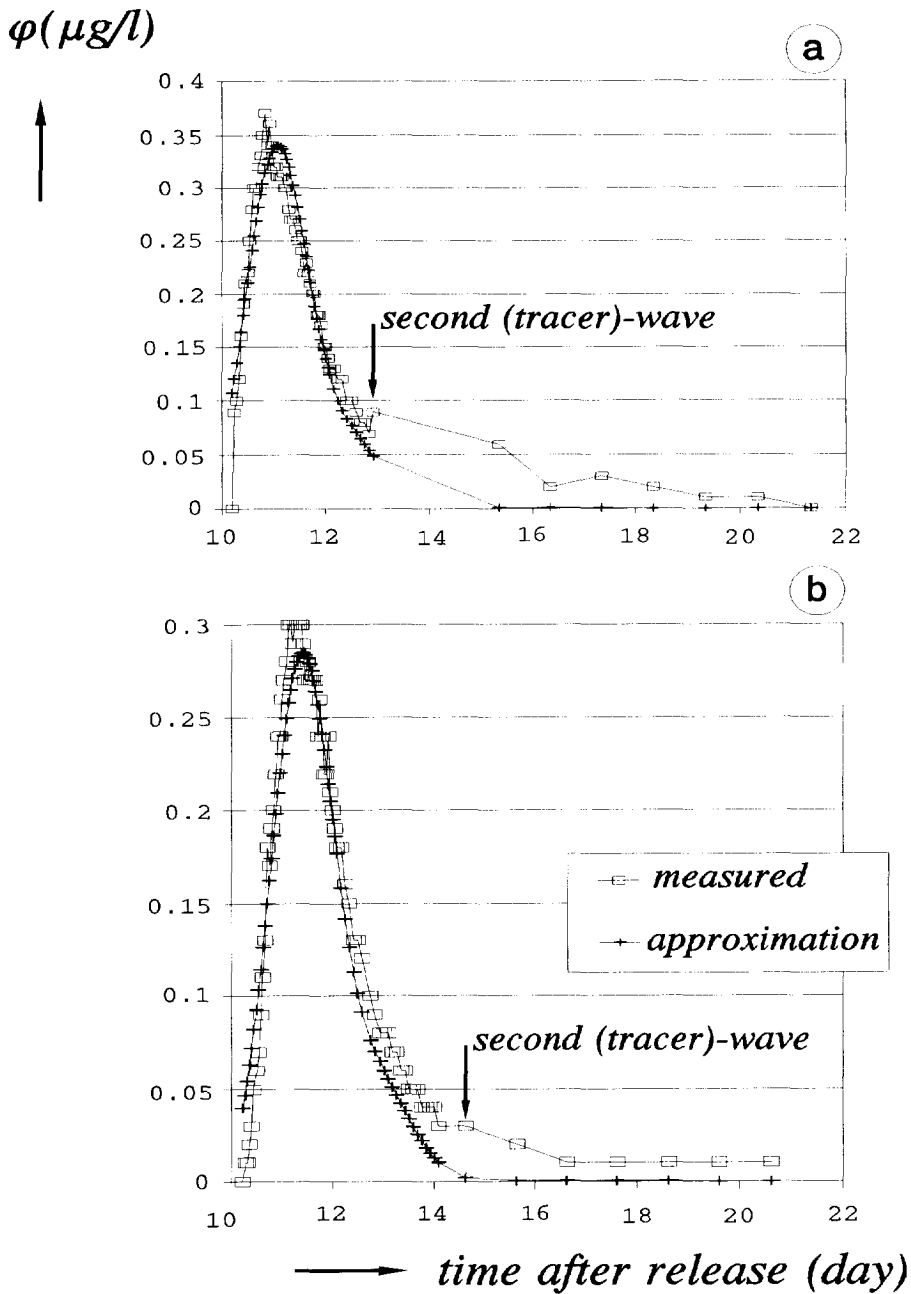


Fig. 4.4.7 Comparison of measured concentration-distributions with the approximation by the Chatwin-model, tracer experiment 09/90, measuring-stations Lobith (a) and Nijmegen (b)

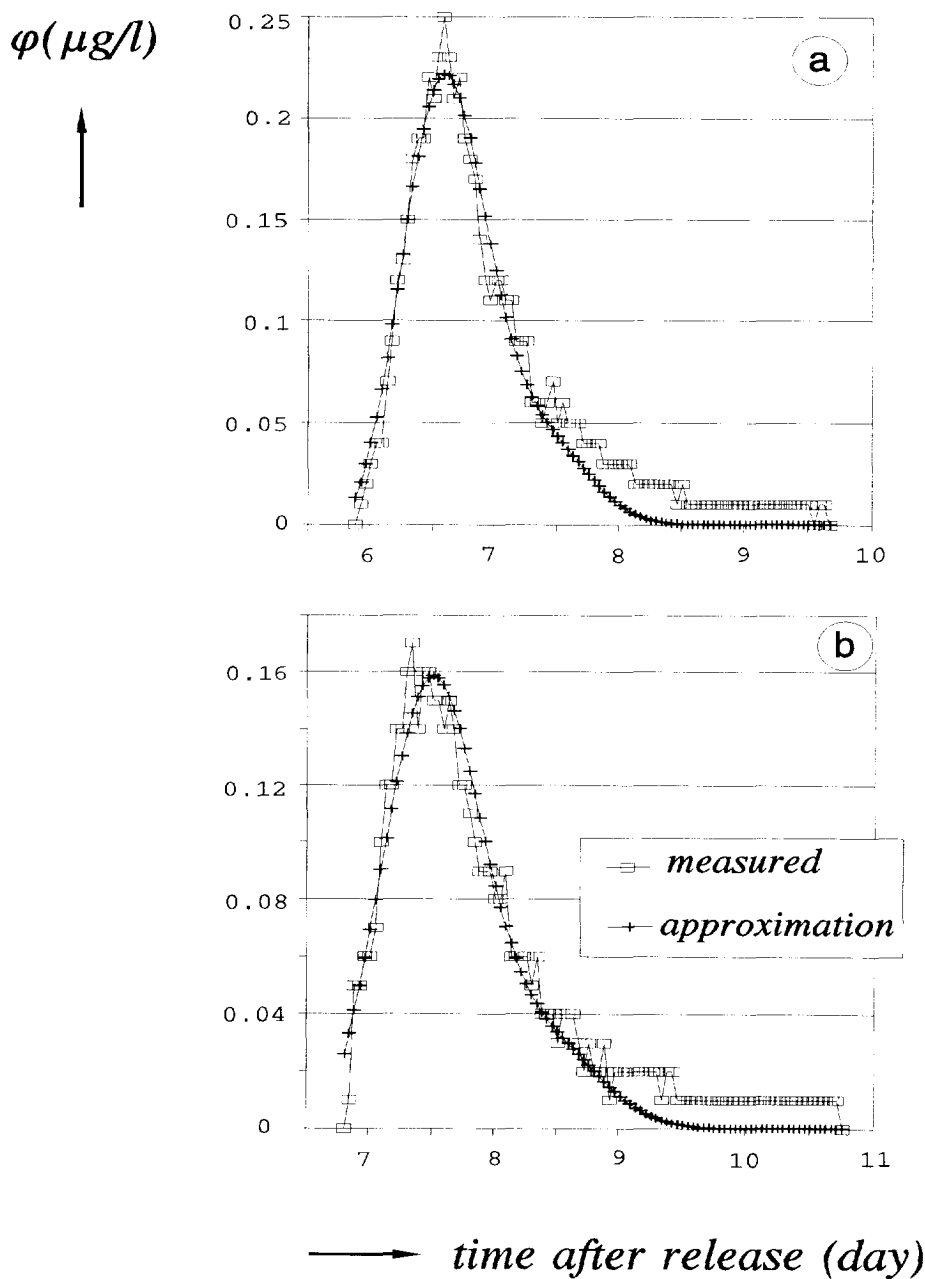


Fig. 4.4.8 Comparison of measured concentration-distributions with the approximation by the Chatwin-model, tracer experiment 06/91, measuring-stations Nijmegen (a) and Vuren (b)

discharge at Lobith of 954 m³/s, the concentration distribution of the tail suggests a second 'tracer' wave, which disturbs the determination of the time-centroid by Eq.(4.4.4) significantly, whereas the DUD-method neglects this wave. Because the tracer Rhodamine WT is measured by the fluorescence, a small additional release of a substance, which apparently can also be measured by the fluorescence, might be the reason of this wave. Anyhow, with the correction for the background concentration this wave was not be recognized as a non-tracer substance.

For a good approximation of the measured concentration-distribution by the Chatwin-model the skewness G_i of the distribution has to be more or less equal to unity (see Sub-section 2.3.2, Eqs 2.3.60 and 2.3.85). Therefore a variation of the skewness in order to improve the reproduction of the tail, is limited and consequently the time-centroid will hardly change.

Thus, the accuracy of the time-centroid still depends on the completeness of the measured concentration-distribution, including the tail.

The presented lag-coefficients in Table 4.4.6 are determined after Eq.(3.4.3)

$$\beta_m = \frac{(\Delta \mu_t)_m}{(\Delta T_u)_m} - 1 \quad (4.4.5)$$

with $(\Delta \mu_t)_m$ = difference between the time-centroid of two successive measuring-stations (river reach m)
 $(\Delta T_u)_m$ = the flow time between the two successive measuring-stations concerned (river reach m)

After the square propagation-law of errors the variance of the lag coefficient β_m can be approximated by (see Eq.3.4.2)

$$\sigma_{\beta_m}^2 = 2 \cdot \sigma_{\mu_t}^2 \cdot \frac{1}{(\Delta T_u)_m^2} + 2 \cdot \sigma_{T_u}^2 \cdot \frac{(\Delta \mu_t)_m^2}{(\Delta T_u)_m^4} \quad (4.4.6)$$

with σ_{μ_t} = standard deviation of the time-centroid
 σ_{T_u} = standard deviation of the flow time

Based on the comparison of the time-centroid, determined with the DUD-method and after Eq.(4.4.4) in Table 4.4.5 the variance of the time-centroid is estimated at 0.1 day.

In Table 4.4.6 also the flow time after the SOBEK-model is considered. The differences between the flow time after the Rhine Alarm-Model and the flow time

TABLE 4.4.6 Transport time and lag coefficient based on the time-centroid of the measured concentration-distributions after Table 4.4.5

River reach	transport time after time-centroid ($\Delta\mu_t$) _m (day)	flow-time (ΔT_u) _m (day)		lag coefficient β_m after		$ \sigma_{\beta_m} $ 2)
		(1) 1)	(2) 1)	(1) 1)	(2) 1)	
tracer experiment 04/89						
Lobith - Vuren	1.1451	0.8867	0.8659 4)	0.29	0.32	0.16
Lobith - Hagestein	1.3442	0.9786	1.1101 4)	0.37	0.21	0.14
Lobith - Kampen	1.7975 (2.0355) ³⁾	1.6762	1.7784 4)	0.07 (0.21) ⁵⁾	0.01 (0.14) ⁵⁾	0.08
tracer experiment 09/90						
Lobith - Vuren	1.409	1.2125	1.3348	0.16	0.06	0.11
Nijmegen - Vuren	1.058	0.9553	1.0307	0.11	0.03	0.14
Lobith - Kampen	2.706 (3.195) ³⁾	2.7572	2.9093	-0.02 (0.16) ⁵⁾	-0.07 (0.10) ⁵⁾	0.05
tracer experiment 06/91						
Bimmen - Vuren	1.1599	0.9303	0.9093	0.25	0.28	0.15
Nijmegen - Vuren	0.9330	0.7309	0.6990	0.28	0.33	0.20
Bimmen - Hagestein	1.5402	1.0379	1.3147	0.48	0.17	0.13

¹) (1) Rhine Alarm-Model

(2) SOBEK-model

²) after Eq.(4.4.5) with $\sigma_{\mu_t} = 0.1$ day and $\sigma_{T_u} = 0.014$ day.

³) transport after the time-centroid, determined by Eq.(4.4.4) at Kampen, whereas the time-centroid at Lobith is approximated by the Chatwin-model

⁴) flow time is related to a river discharge at Lobith of 3000m³/s instead of 2979m³/s.

⁵) based on the transport time after ³)

after the SOBEK-model are remarkable. For the river reach Lobith - Vuren (the River Waal) they vary between 0.02 day for discharges larger than 2000 m³/s at Lobith till 0.1 day for low-water discharges. The differences at the river reach

Lobith - Kampen is more than 0.1 day and at the river reach Lobith - Hagestein the difference increases up to 0.3 day in case of the tracer experiment 06/91. These large differences might be caused by changes of the morphology since the schematization of the Dutch Rhine-branches, used for the Rhine Alarm-Model⁸⁾. In Fig. 4.4.9 the flow-time differences between the Rhine Alarm-Model and the SOBEK-model for the river reach Arnhem (IJssel bifurcation) - Hagestein is presented. It shows an large increment of the flow-time differences for river discharges of 1400 till 2000 m³/s up to 1 till 2 days. These river discharges concern the range for which the weirs in the River Lower Rhine are lowered.

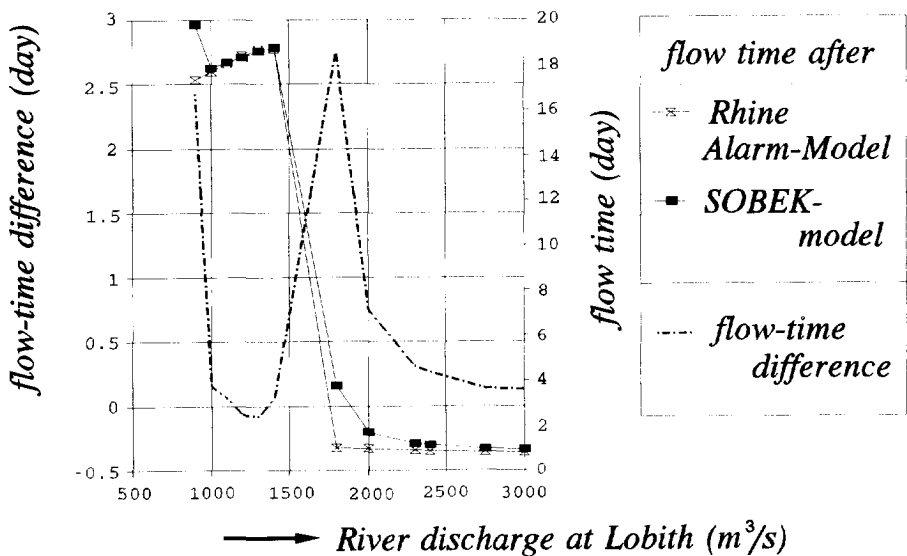


Fig. 4.4.9 Comparison of the flow times after the Rhine Alarm-Model and the SOBEK-model for the River Lower Rhine and the River Lek between the IJssel bifurcation (Arnhem) and Hagestein

Because of these large flow-times differences, the lag coefficient is listed for both models in Table 4.4.6.

As already discussed in Sub-section 4.4.1 the dead-zone parameter along the Dutch Rhine-branches is not so homogeneously distributed as it should be for a good comparison with the measured lag-coefficient (see Figs 4.4.3, 4.4.4 and 4.4.5). Moreover, the dead-zone parameter of a significant part of the river reaches concerned is larger than 0.5. Because for these zones a completely mixed situation

⁸⁾ For the flow times in the Rhine Alarm-Model the schematization after the ZWENDL-model has been used, a one-dimensional hydrodynamic model.

becomes doubtful, the average value β_n after Eq.(4.4.2) has been determined for three restrictive conditions: the considered β_i -values are less or equal to 0.3, 0.5 or 0.8. For instance, if $\beta_i \leq 0.8$ all values larger than 0.8 are substituted by a value of 0.8. In Figs 4.4.10 ... 4.4.13 the β_n -distributions as a function of the discharge at Lobith are compared with the lag coefficients, including the variance as presented in Table 4.4.6.

Apart from the relatively large variance, the lag coefficient of the river reach Lobith - Vuren (Fig. 4.4.10) corresponds fairly well with the average dead-zone parameter with the restriction condition $\beta_i \leq 0.5$. As already indicated in Sub-section 4.4.1, this agreement might be a result of the relatively homogeneous distribution of the dead-zone parameter: over 80% of the river reach concerned the dead-zone parameter is smaller than 0.5 (see Fig. 4.4.3). For low-water discharges the results show a slight reduction of the dead-zone influence on the transport velocity. The lag coefficient reduces more than the dead-zone parameter.

Although the length of the river reach Nijmegen - Vuren corresponds with a Pléclet number smaller than 15 (10 till 15, see Table 4.4.2) and the concentration distribution at Nijmegen shows a 'second wave' (Fig. 4.4.7), the results show the same tendency (Fig. 4.4.11).

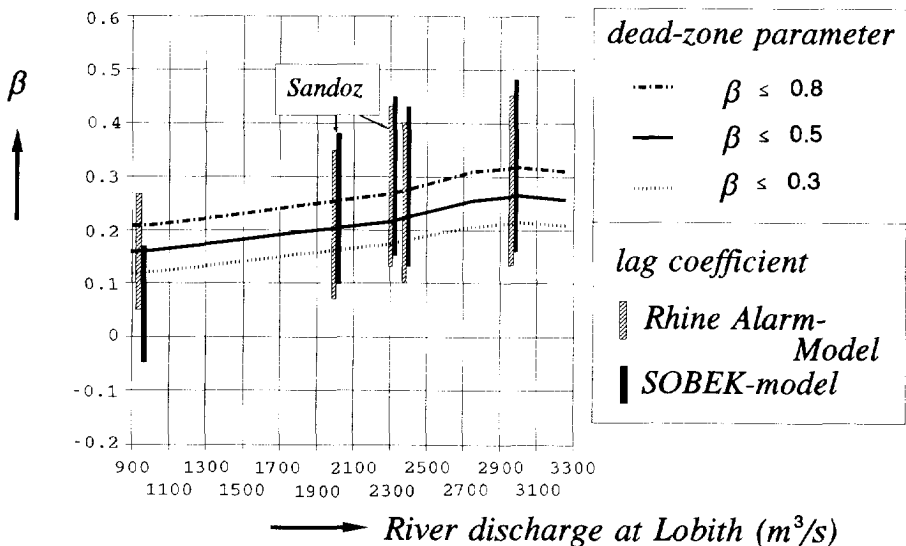


Fig. 4.4.10 Comparison of the average dead-zone parameter with the measured lag-coefficient for the river reach Lobith - Vuren (R. Waal); tracer experiments 04/89, 09/90, 06/91 and Sandoz-spill

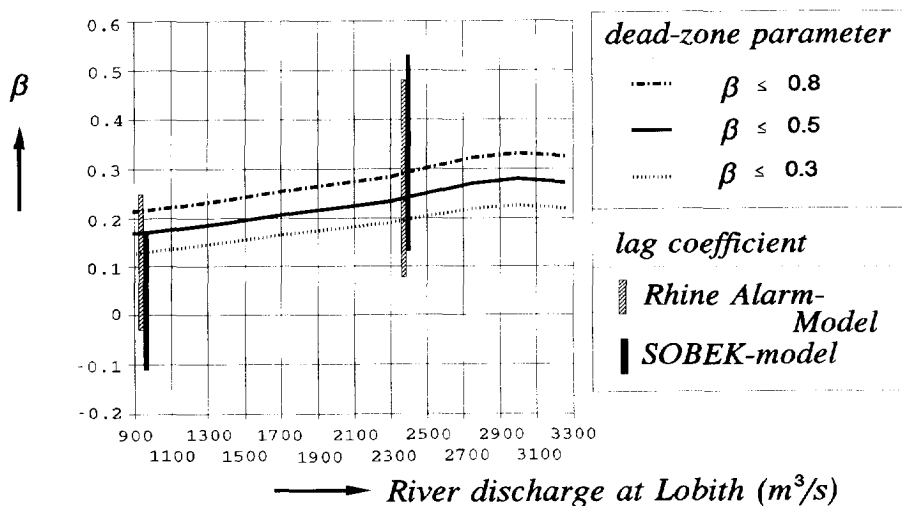


Fig. 4.4.11 Comparison of the average dead-zone parameter with the measured lag-coefficient for the river reach Nijmegen - Vuren (River Waal), tracer experiments 09/90 and 06/91

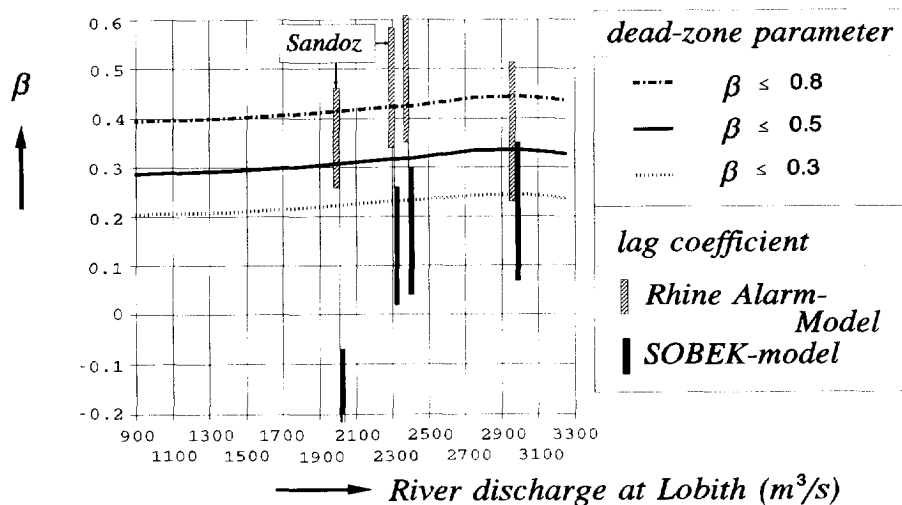


Fig. 4.4.12 Comparison of the average dead-zone parameter with the measured lag-coefficient for the river reach Lobith - Hagestein (River Lower Rhine); tracer experiments 04/89, 06/91 and Sandoz-spill

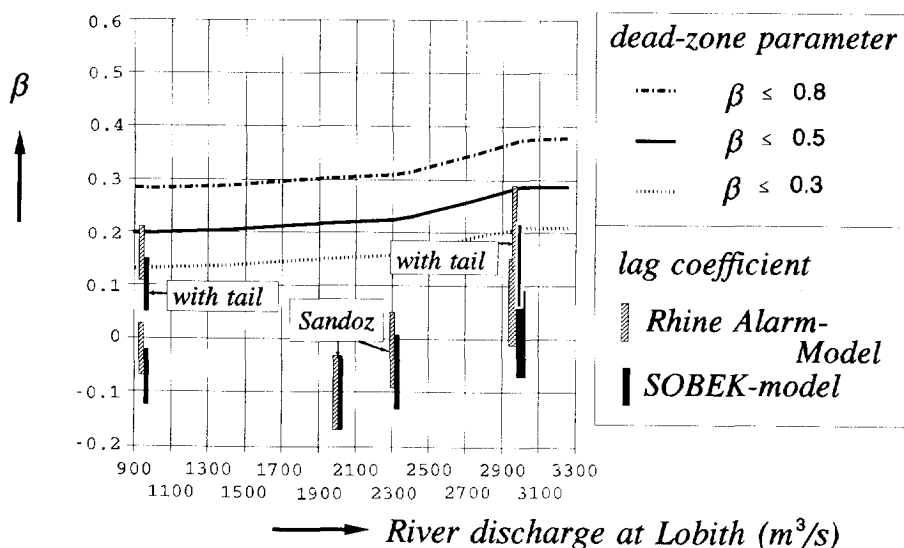


Fig. 4.4.13 Comparison of the average dead-zone parameter with the measured lag-coefficient for the river reach Lobith - Kampen (River IJssel); tracer experiments 04/89, 09/90 and Sandoz-spill

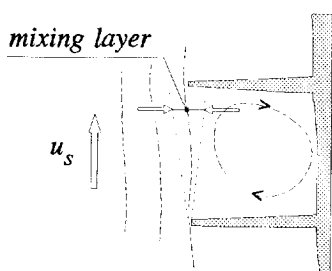


Fig. 4.4.14 Mixing layer downstream of a groyne

As discussed in Section 4.2 the velocity head Δh_1 , defined by

$$\Delta h_1 = \frac{u_s^2}{2 \cdot g} \quad (4.4.7)$$

has to be larger than the loss of energy head over the longitudinal distance between the groynes in order to get an eddy in the groyne-field, needed for a completely mixed situation (Fig. 4.4.14). Although this condition is independent of the flow velocity

(see Eq. 4.2.2), it will be reasonable to expect that for very small values of the velocity head (less than 0.01 or 0.02m) the strength of the eddy as a mixing tool will reduce. This might be an explanation for the slight reduction of the value of the lag coefficient in comparison with the dead-zone parameter for low-water discharges in Figs 4.4.10 and 4.4.11.

The results of the river reach Lobith - Hagestein (Fig. 4.4.12) present the effect of the flow-time difference between the Rhine Alarm-Model and the SOBEK-model

explicitly. The difference decreases with the increase of the river discharge (see also Fig. 4.4.9). Averaging the flow-time differences it can be stated that for river discharges larger than 2300 m³/s at Lobith (free runoff) the lag coefficient corresponds more or less with the average dead-zone parameter with the same restriction condition as for the River Waal: $\beta_i \leq 0.5$.

During the tracer experiment 09/90 with low-water conditions the tracer cloud passed the measuring station Hagestein about a week earlier than expected (see Fig. 3.4.32), thus no measurements are available. Analysis of the transport times between Lobith and Hagestein by time-series of chloride concentrations for low-water conditions proved, that the transport velocity can be described by the flow time plus/minus 10 till 15%, based on detailed information of the discharge and water-level distribution along this river reach during the passage of the pollutant (van Mazijk and Wuijts, 1995). This means that the influence of the dead zones with an averaged value 0.30 (Fig. 4.4.12) can be neglected for low-water conditions. This agrees with the assumption, that for small values of the velocity head the mixing in the groyne-fields reduces. In Fig. 4.4.15 the velocity head for the Dutch Rhine-branches is related to the river discharge at Lobith. If the discharge is controlled by the weirs in the River Lower Rhine, the velocity head becomes about 0.003 m.

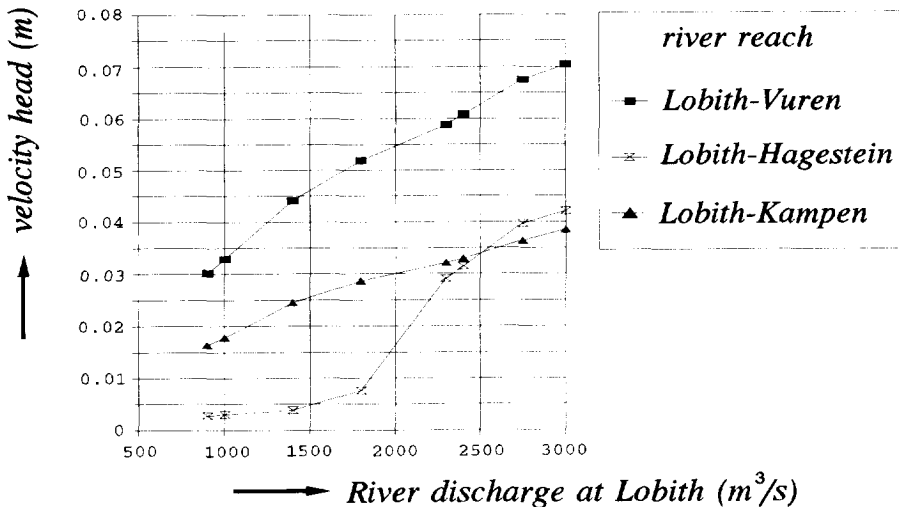


Fig. 4.4.15 Mean velocity-head for the Dutch Rhine-branches

In case of the river reach Lobith - Kampen (River IJssel) the lag coefficient is about zero (Fig. 4.4.13). If the tail of the concentration distribution is taken into account for the determination of the time-centroid more properly by applying Eq.(4.4.4) (see Table 4.4.5 and Figs 3.4.33 and 3.4.34) the lag coefficient

corresponds with an average dead-zone parameter for the restriction condition of $\beta_i \leq 0.3$ or less. The velocity head of the river reach Lobith - Kampen lies between 0.02 and 0.04 m, which corresponds with the velocity head of the river reach Lobith - Vuren in case of low-water conditions for which a reduced influence of the dead zones is found (Fig. 4.4.10). A first provisional conclusion could be that for a velocity head of 0.01 till 0.05 m the lag coefficient corresponds with an average dead-zone parameter with the restriction condition of $\beta_i \leq 0.2$ (Fig. 4.4.16). Further investigations about the relation between the flow velocity, i.e. velocity head and the effect of dead zones on the transport velocity of a pollution cloud are necessary for the confirmation of the assumptions concerned.

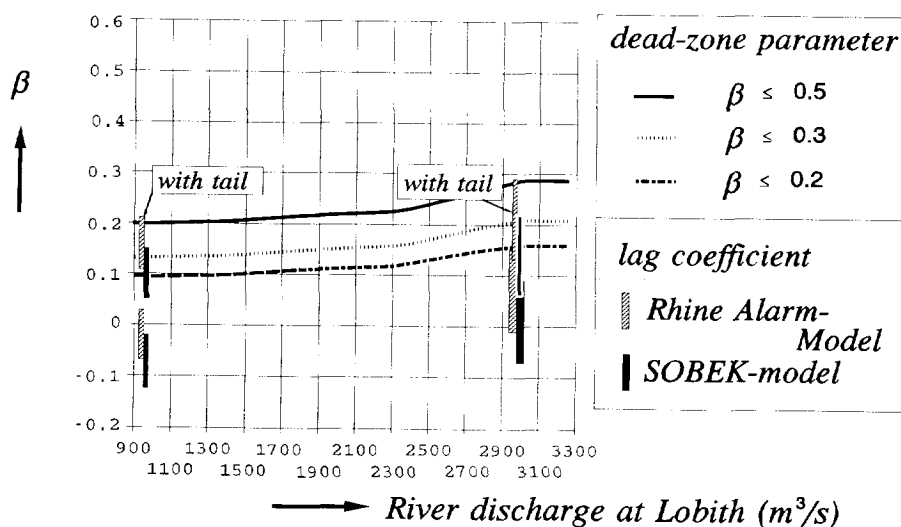


Fig. 4.4.16 Comparison of the average dead-zone parameter with the measured lag-coefficient for the river reach Lobith - Kampen (R. IJssel); tracer experiments 04/89 and 09/90

During the transport of the pollution cloud, caused by the fire at the Sandoz plant at Schweizerhalle (Switzerland), a lot of chemical and biological parameters has been measured at Lobith, Vuren, Hagestein and Kampen, as Rhodamine determined by the fluorescence. With the measured Rhodamine concentration-distributions the lag coefficient for the Dutch Rhine-branches has been determined, based on the time-centroid after the Chatwin-approximation with the DUD-method. In Table 4.4.7 the results are collected. Because during the passage of the pollution cloud (from the 9th till the 13th November 1986) the discharge at Lobith varied significantly (Fig. 4.4.17), two river discharges at Lobith are considered. In Figs 4.4.10, 4.4.12 and 4.4.13 the resulting lag-coefficients are compared with the dead-zone parameters.

TABLE 4.4.7 Transport time and lag coefficient based on the time-centroid of the measured concentration-distributions of the Rhodamine, released at the Sandoz plant

River reach	transp.time after time-centroid	flow-time (ΔT_u) _m		lag coefficient β_m after		$ \sigma_{\beta_m} $ ²⁾
	$(\Delta \mu_t)$ _m	(day)				
	(day)	(1) ¹⁾	(2) ¹⁾	(1) ¹⁾	(2) ¹⁾	
river discharge at Lobith 2316 m ³ /s						
Lobith-Vuren	1.2382	0.9674	0.9494	0.28	0.30	0.15
Lobith-Hagestein	1.5804	1.0785	1.3884	0.46	0.14	0.12
Lobith-Kampen	1.8554	1.8942	1.9799	-0.02	-0.06	0.07
river discharge at Lobith 2010 m ³ /s						
Lobith-Vuren	1.2382	1.0183	0.9978	0.21	0.24	0.14
Lobith-Hagestein	1.5804	1.1568	1.8969	0.36	-0.17	0.10
Lobith-Kampen	1.8554	2.0568	2.0603	-0.10	-0.10	0.07

- 1) (1) Rhine Alarm-Model
 (2) SOBEK-model
 2) after Eq.(4.4.5) with $\sigma_{\mu_t} = 0.1$ day and $\sigma_{T_u} = 0.014$ day.

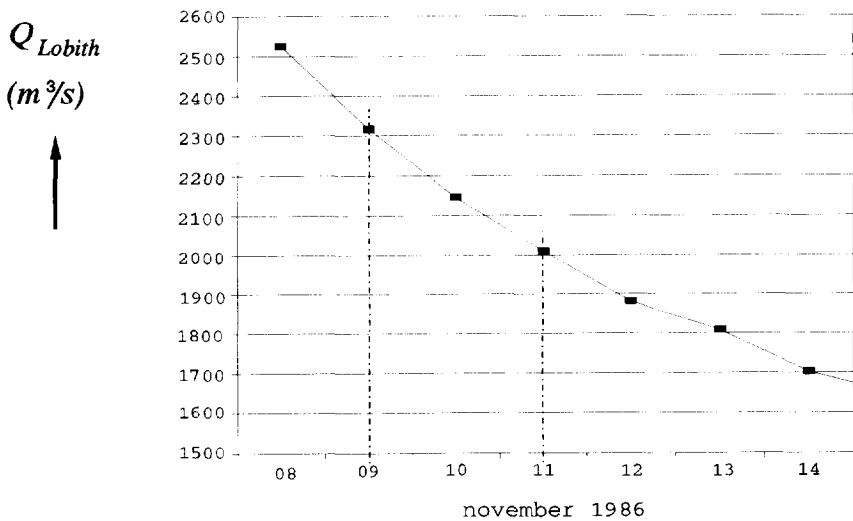
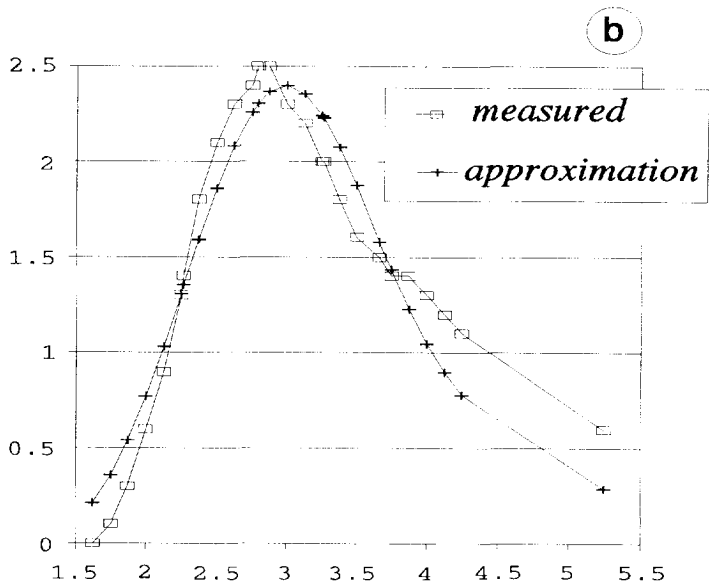
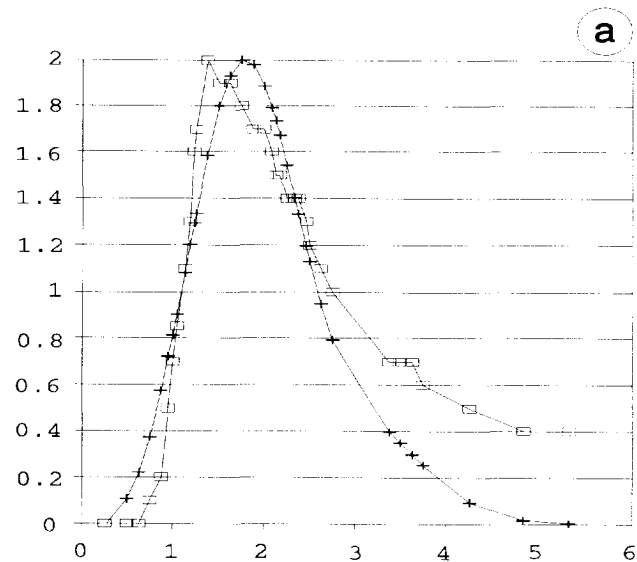


Fig. 4.4.17 River discharge at Lobith during the passage of the pollution cloud of the Sandoz-plant

$\varphi(\mu\text{g/l})$



time since 08.11.86 ; 0:00 hr (day)

Fig. 4.4.18 Comparison of measured concentration-distributions with the approximation by the Chatwin-model; Rhodamine-concentration originating from the Sandoz plant in 1986, measuring-stations Lobith (a) and Vuren (b)

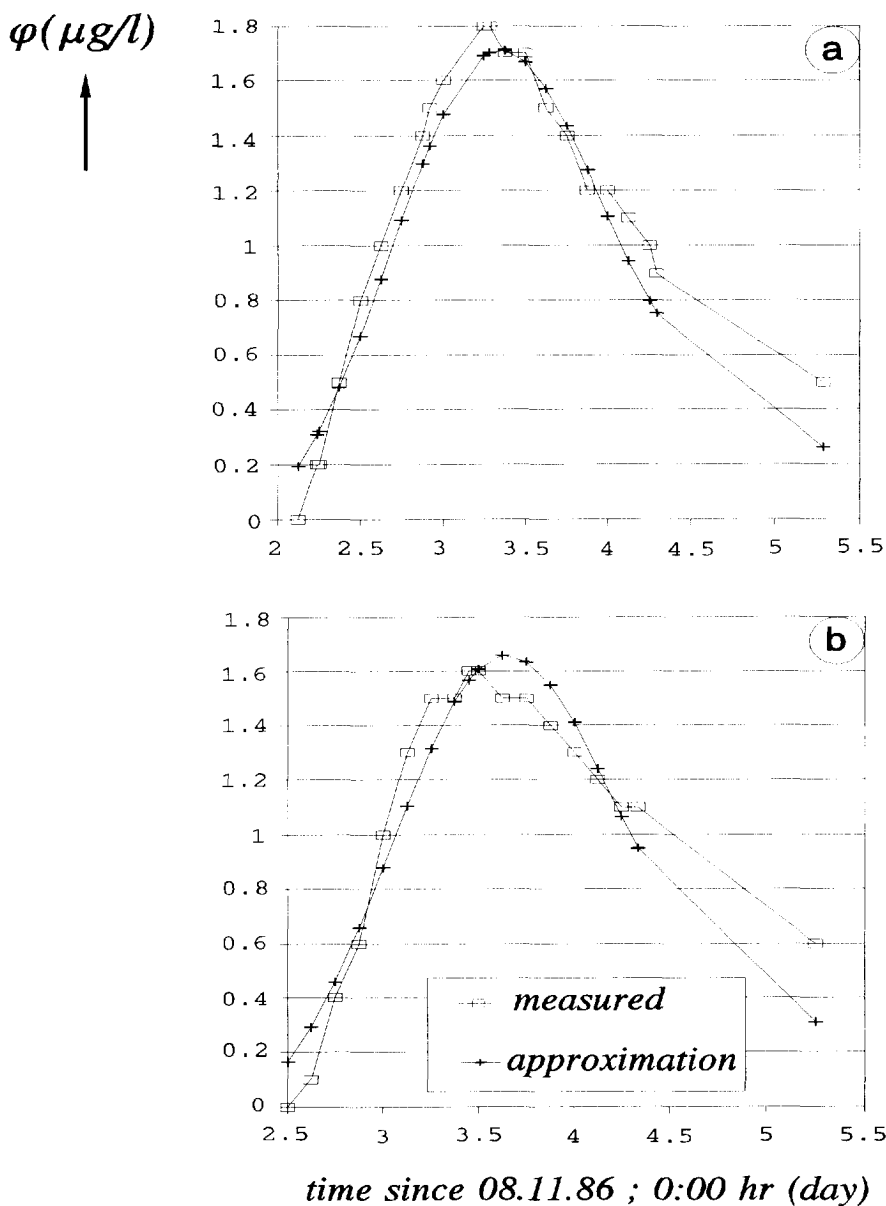


Fig. 4.4.19 Comparison of measured concentration-distributions with the approximation by the Chatwin-model, Rhodamine-concentration originating from the Sandoz plant, measuring-stations Hagestein (a) and Kampen (b)

For the river reach Lobith - Vuren (Fig. 4.4.10) the lag coefficients are comparable with those after the tracer experiments. According to the increase of the flow-time difference between the Rhine Alarm-Model and the SOBEK-model for river discharges between 2300 and 2000 m³/s at Lobith there is a large difference between the lag coefficient related to the flow time after the Rhine Alarm-Model and to the flow time after the SOBEK-model (Fig. 4.4.12). Assuming that the flow time after the SOBEK-model is more true than the flow time after the Rhine Alarm-Model, the results show a decrease of the influence of the dead zones with the decrease of the river discharge. Referring to the decrease of the velocity head for smaller discharges (Fig. 4.4.15), such a decrease might confirm the conclusion that the influence of the dead zones becomes negligible in case of low-water conditions for which the discharge is controlled by the weirs in the River Lower Rhine.

The lag coefficients for the river reach Lobith - Kampen (Fig. 4.4.13) show the same deviation from the dead-zone parameter as the tracer experiments 04/89 and 09/90. In Figs 4.4.18 and 4.4.19 the measured concentration-distributions are compared with the approximation after the Chatwin-model by the DUD-method⁹⁾. All the concentration distributions missed the tail, thus it cannot be stated that the negative values of the lag coefficient is only caused by the failing of the tail of the concentration distribution. On the other hand it might confirm that due to the small velocity head of a few centimetres (Fig. 4.4.15), the effect of the dead zones on the transport of a solved substance becomes negligible.

TABLE 4.4.8 Mean value of the actual dead-zone parameter of the Dutch Rhine-branches ($Q_{Lobith} \geq 2300 \text{ m}^3/\text{s}$)

River reach	lag coefficient / actual dead-zone parameter	dead-zone parameter after the Rhine Alarm-Model
Lobith/Bimmen - Vuren	0.24	0.18
Lobith/Bimmen - Hagestein	0.32	0.27
Lobith/Bimmen - Kampen	0 till 0.14	0.02
Nijmegen - Vuren	0.26	0.18

⁹⁾ Notice that the peak concentration at Lobith is smaller than at the measuring-station Vuren. The presented concentrations are the measured values corrected by a background-value, for which the value just before the front of the pollution wave, is taken.

In Table 4.4.8 the lag coefficient e.g. the actual dead-zone parameter is summarized in case of a free-runoff situation in the River Lower Rhine ($Q_{Lobith} \geq 2300 \text{ m}^3/\text{s}$). The values are compared with those after the calibration of the Rhine Alarm-Model. The dead-zone parameter after the Rhine Alarm-Model is systematically smaller than the values, based on the time-centroid of the approximated distribution after the Chatwin-model. Besides of the differences between the flow times of the Rhine Alarm-Model (ZWENDL-model) and the SOBEK-model, it has to be noticed that for the calibration of the dead-zone parameter in the Rhine Alarm-Model the concentration distribution around the peak value has been considered (concentration values larger than 0.3 of the peak value, see Sub-section 3.3.1).

On account of the inaccuracy of the lag coefficient (Tables 4.4.6 and 4.4.7) a determination of the lag coefficient based on the *peak value* of the concentration distribution in order to get a first indication about the value of the mass-transfer parameter \mathcal{E} has been dropped.

4.4.3 Mass-transfer coefficient

For the determination of the mass-transfer parameter \mathcal{E} , i.e. the mass-transfer coefficient D_b in the Dutch Rhine-branches the river reach Bimmen - Vuren, tracer experiment 06/91 is considered. This river reach has been chosen preferably, because the concentration distributions at Bimmen and Vuren seem to be completely measured (Fig. 4.4.20, see also Table 4.4.1).

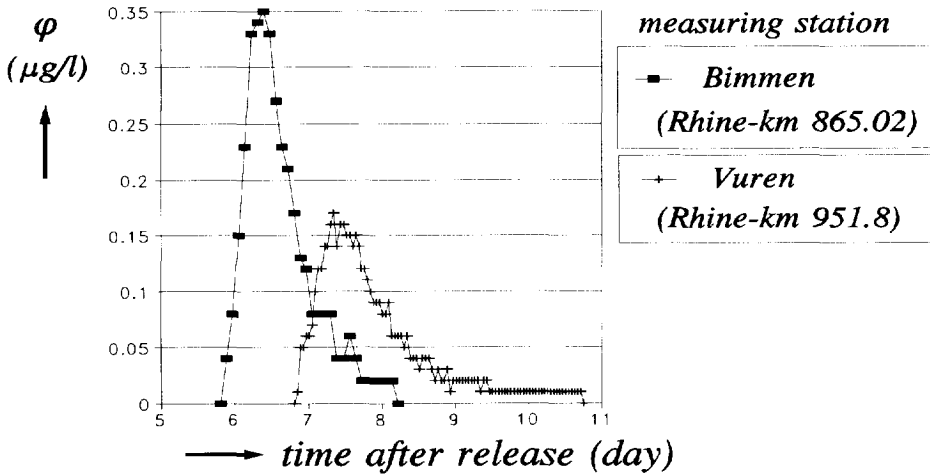


Fig. 4.4.20 Measured concentration-distributions at Bimmen and Vuren, tracer experiment 06/91

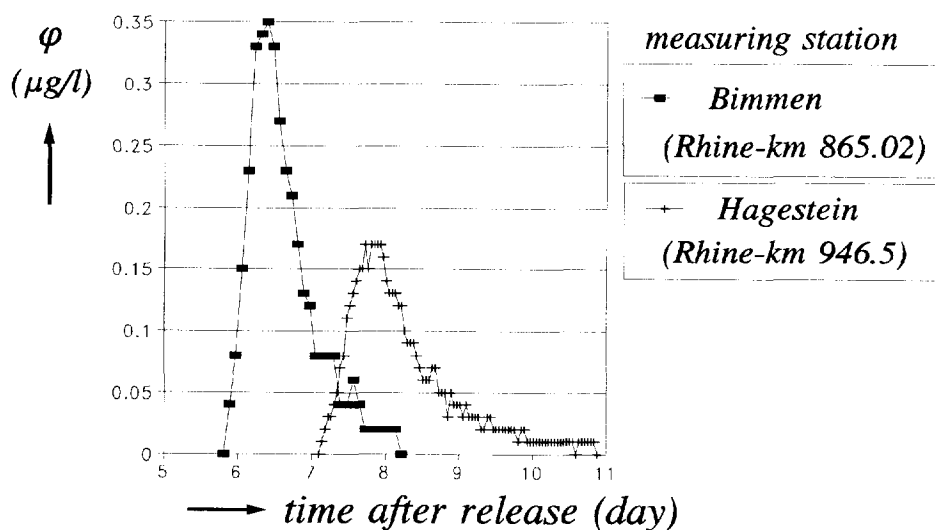


Fig. 4.4.21 Measured concentration-distributions at Bimmen and Hagestein, tracer experiment 06/91

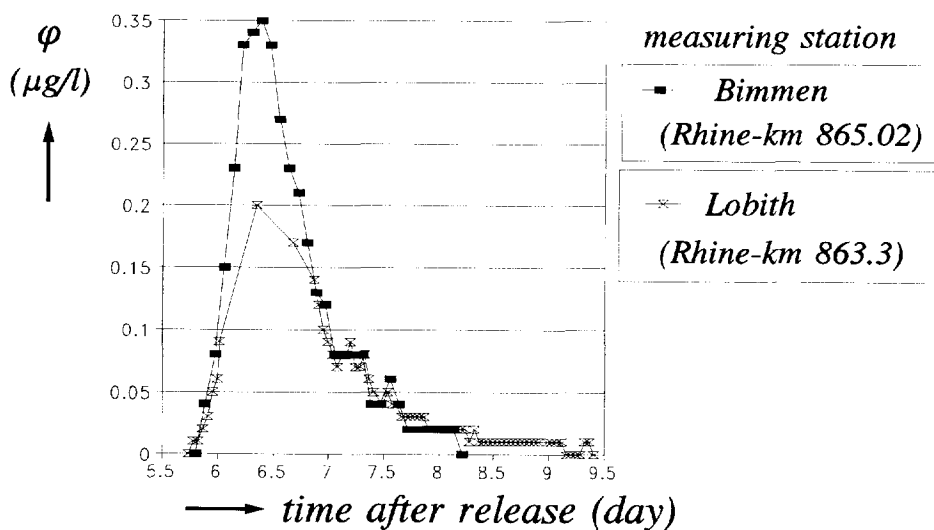


Fig. 4.4.22 Comparison of the measured concentration-distributions at Lobith (right river-bank) and Bimmen (left river-bank), tracer experiment 06/91

For the verification of the results of the river reach Bimmen - Vuren, the river reach Bimmen - Hagestein is used. In Fig. 4.4.21 the measured concentration-distribution of the stations concerned, are presented. The concentration level of the distributions at Vuren and Hagestein is much less than the level of the distribution, measured at Bimmen. The differences cannot be explained by the decomposition of the used tracer Rhodamine WT. A comparison of the concentration distributions at Lobith and Bimmen in Fig. 4.4.22 (see also Sub-section 3.4.5, Fig. 3.4.23) shows the same differences. In Table 4.4.9 the mass flux \mathcal{F} per unit of discharge of the station concerned, are collected, whereas \mathcal{F} is defined by

$$\mathcal{F} = \int_{-\infty}^{\infty} \varphi_{meas.}(L, t) \cdot dt = \sum_{i=1}^{m_1} [\varphi_{meas.}(L, t)]_i \cdot (t_i - t_{i-1}) \quad (4.4.8)$$

wherein $[\varphi_{meas.}(L, t)]_i$ is the measured concentration at the time t_i and m_1 the total number of measured concentration-values.

TABLE 4.4.9 Mass flux per unit of river discharge F after Eq.(4.4.8), tracer experiment 06/91

measuring station	mass flux \mathcal{F} (g·m ⁻³ ·day)
Bimmen	0.300
Lobith	0.236
Vuren	0.197
Hagestein	0.207

For the analysis of the mass-transfer coefficient D_b the numerical dead-zone model after Eqs (4.3.22) and (4.3.23) in Sub-section 4.3.1 has been applied. In this model the decomposition of a substance is not taken into account and therefore the flux \mathcal{F} after Eq.(4.4.8) will be constant. Consequently, if the measured concentration-distribution at Bimmen is used as the initial concentration distribution in the main stream φ_s after (see Sub-section 4.3.1)

$$0 \leq t \leq i \cdot \Delta t \quad \text{and} \quad x = 0 \quad \varphi_s(0, t) = [\varphi_{meas.}]_i$$

the measured concentrations at Vuren and Hagestein have to be adjusted after the mass-flux ratio $\mathcal{F}_{Bimmen}/\mathcal{F}_{Vuren}$ and $\mathcal{F}_{Bimmen}/\mathcal{F}_{Hagestein}$ respectively for a correct comparison of the measured and calculated concentration-distributions. In Table 4.4.10 the input data for the computations, executed with the numerical model, are collected.

TABLE 4.4.10 Input data of the computations for the analysis of the mass-transfer coefficient D_b with the numerical dead-zone model

river reach (length)	mean flow- velocity u_s (m/s)	long. disp. coeff. K_s (m ² /s)	dead-zone parameter β (-)	mass- transfer coeff. D_b (s ⁻¹)	Δx (km)	Δt (s)
Bimmen - Vuren (85 km)	1.082	4700	0.2756	0.0100 0.0010 0.0002 0.0001	8.5	7200
Bimmen - Hagestein (80 km)	0.704	980	0.1715	0.0100 0.0010 0.0002 0.0001	2.0	1800

The time and space step are based on the time step of the measured concentration distribution, as well as the conditions for stability and accuracy of the calculations after Eqs (4.3.20), (4.3.21) and (4.3.70) (see Sub-sections 4.3.1 and 4.3.4). For simplicity the dead-zone parameter is kept constant over the whole river-reaches concerned, and is equal to the mean value based on the time-centroid, approximated by the Chatwin-model and the flow-time after the SOBEK-model (see Table 4.4.6). Consequently, the mean flow-velocity is also based on the flow times after the SOBEK-model as presented in Table 4.4.6. For the longitudinal dispersion-coefficients the values of Table 4.4.2 are used. Because the initial condition for the concentration in the main stream is given by a concentration distribution, the dead zones are present from the beginning of the model: $x = 0$ corresponds with the measuring-station Bimmen.

The results of the computations are presented in Fig. 4.4.23 ... 4.4.26. Figures 4.4.23 and 4.4.24 show the influence of the mass-transfer coefficient D_b on the calculated distributions explicitly. The influence of the magnitude of the mass-transfer coefficient is mainly demonstrated by the differences in the peak value of the calculated concentration-distribution, whereas the differences in the tail of the distributions are negligible small (0.001 $\mu\text{g/l}$, or $< 0.5\%$ of the peak value). As suggested in Sub-section 4.3.6, a comparison of the measured with calculated tails for the quantification of the mass-transfer coefficient seems to be useless, all the more since the accuracy of the measured concentrations in the tail of the distribution amounts 0.005 $\mu\text{g/l}$. This means that the quantification of the mass-transfer coefficient has to be left to the fitting of the peak of the concentration distribution.

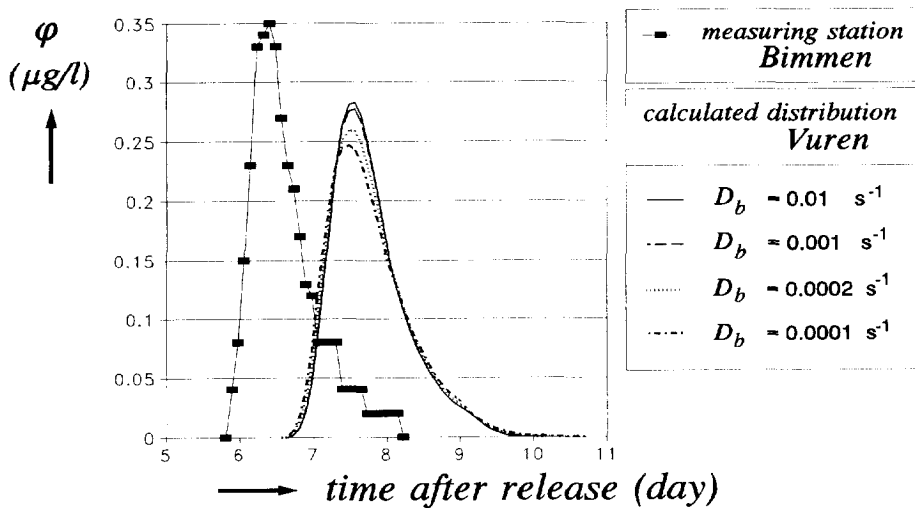


Fig. 4.4.23 Influence of the mass-transfer coefficient D_b on the concentration distribution at Vuren, based on the measured concentration-distribution at Bimmen, tracer experiment 06/91

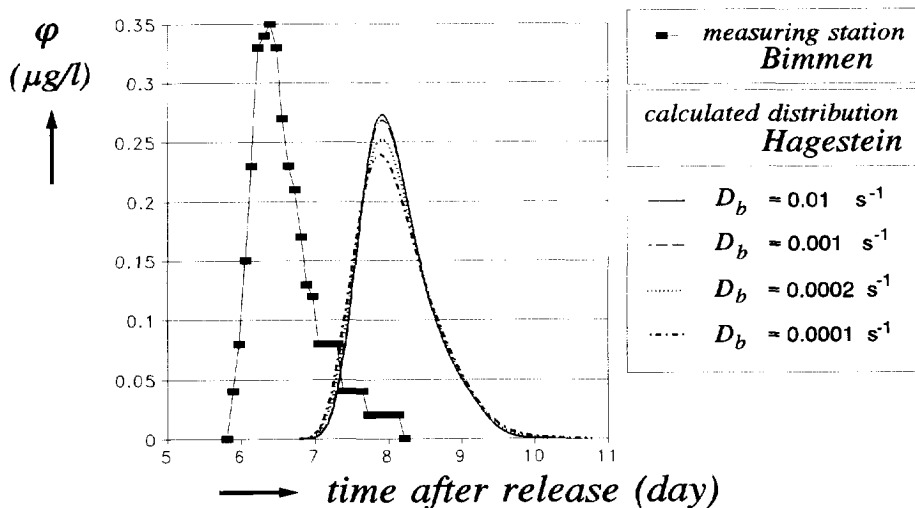


Fig. 4.4.24 Influence of the mass-transfer coefficient D_b on the concentration distribution at Hagestein, based on the measured concentration-distribution at Bimmen, tracer experiment 06/91

The decrease of the calculated peak-value is due to the increase of the difference between the mass transfer from the main stream into the dead zones and in the opposite direction. After Eqs. (4.3.1) and (4.3.2) in Sub-section 4.3.1 the mass transfer can be described as a decomposition process of the first order for

the concentration in the main stream, if $\varphi_s > \varphi_b$ by

$$\frac{d\varphi_s}{dt} = -D_s(\varphi_s - \varphi_b) = -\beta \cdot D_b(\varphi_s - \varphi_b) \quad (4.4.9)$$

and the concentration in the dead zone, if $\varphi_s < \varphi_b$ by

$$\frac{d\varphi_b}{dt} = D_b(\varphi_s - \varphi_b) \quad (4.4.10)$$

A small value of the mass-transfer coefficient D_b means that the transport from the main stream into the dead zone will last relatively long: a relatively large part of the passage time of the tracer cloud, it yields $\varphi_s > \varphi_b$. During the passage of the tail of the cloud it yields $\varphi_s < \varphi_b$ and the transport takes place in the opposite direction.

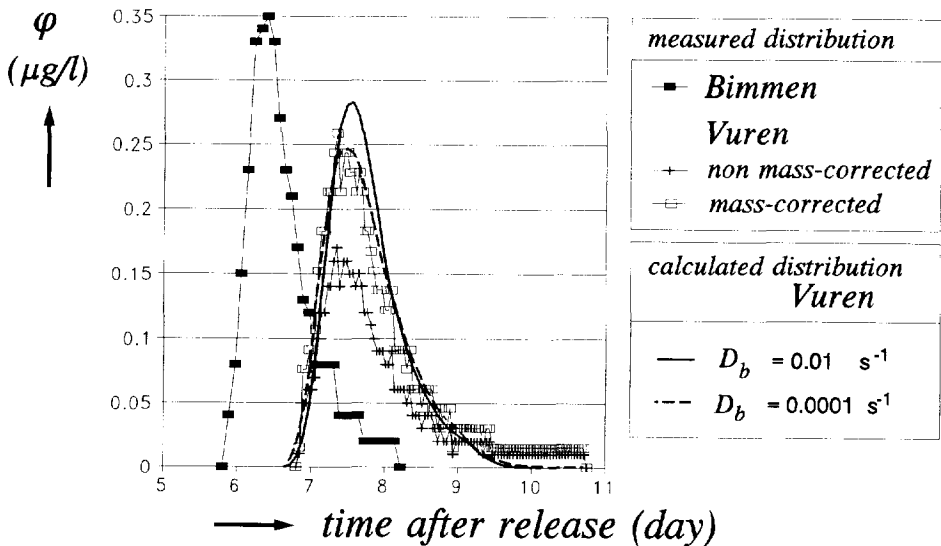


Fig. 4.4.25 Comparison of the measured non mass-corrected and mass-corrected concentration-distribution at Vuren with the calculated distributions for two mass-transfer coefficients D_b , tracer experiment 06/91

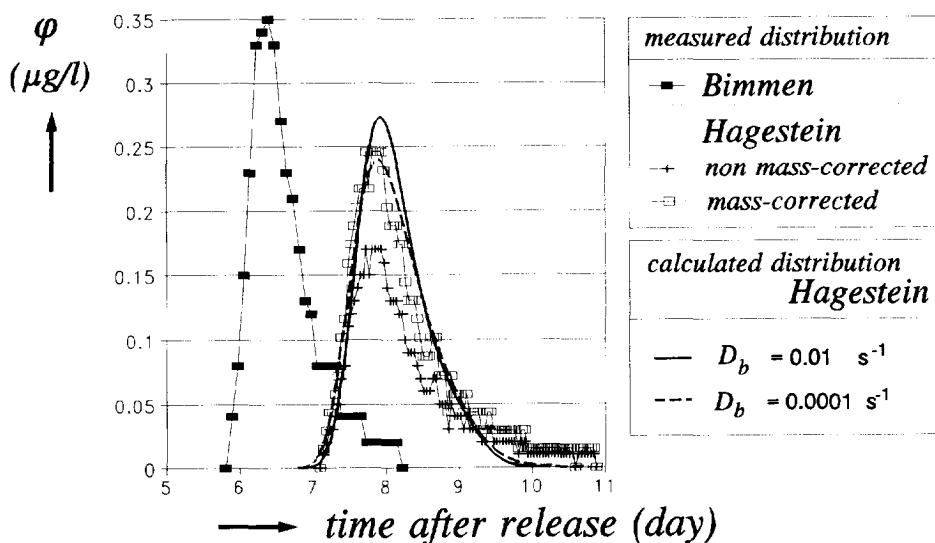


Fig. 4.4.26 Comparison of the measured non mass-corrected and mass-corrected concentration-distribution at Hagestein with the calculated distributions for two mass-transfer coefficients D_b , tracer experiment 06/91

In Figs 4.4.25 and 4.4.26 the calculated distributions for two values of the D_b -coefficient are compared with the non mass-corrected and mass-corrected measured concentration distributions at Vuren (Fig. 4.4.25) and Hagestein (Fig. 4.4.26). It shows that the adjustment of the concentration distributions by the mass-flux ratios results into a good agreement with the calculated distribution for a mass-transfer coefficient $D_b = 10^{-4} \text{ s}^{-1}$, which, however, is 100 times smaller than based on Eq.(4.3.54) (see Sub-section 4.3.4). Because the applied mass-flux ratio depends on the accuracy and completeness of the distributions concerned, whereas the variation of the peak concentration is relatively small in comparison with the related variation of the mass-transfer coefficient, the reliability of this result is questionable. The difference between the peak concentrations at Lobith and Bimmen (Fig. 4.4.22) underlines this conclusion.

Further, the tail of the distribution, measured at Bimmen is much shorter than the tails, measured at Lobith (Fig. 4.4.22), Vuren (Fig. 4.4.20) and Hagestein (Fig. 4.4.21). For that reason additional computations have been carried out for the river reach Lobith/Bimmen - Vuren with the concentration distribution, measured at Lobith as the initial boundary-condition in the main stream. The results are presented in Fig. 4.4.27. Using the same input data as in case of the measuring-station Bimmen (Table 4.4.10), a good agreement with the measured concentration-

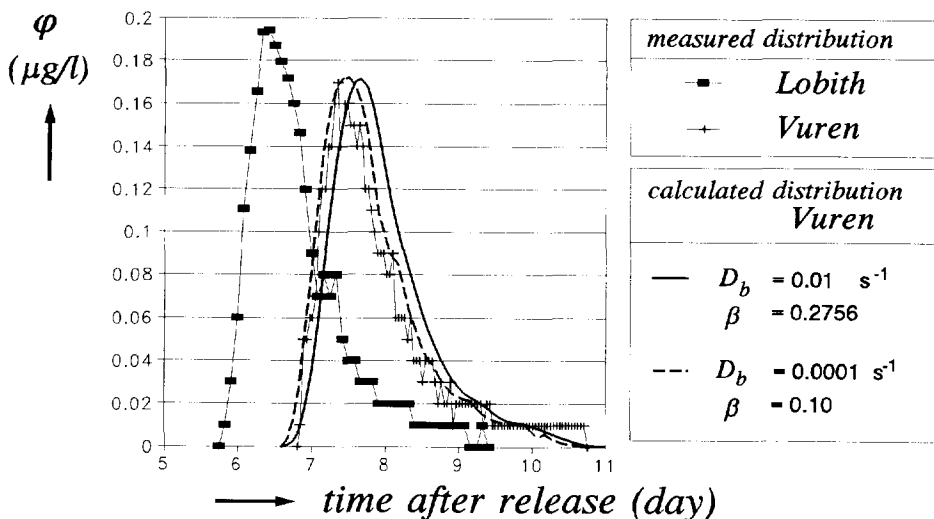


Fig. 4.4.27 Comparison of the measured concentration-distribution at Vuren with calculated distributions for different parameter-values, based on the measured concentration-distribution at Lobith, tracer experiment 06/91

distribution at Vuren without any adjustment of the mass flux, is obtained for a value of 10^{-2} s^{-1} for the mass-transfer coefficient D_b , if the shape of the distributions are considered. However, the calculated distribution shows a time shift with the measured one, due to the 4-hours difference between the measured distributions at Lobith and Bimmen (see Sub-section 3.4.5, p.110). The tracer cloud passes Bimmen earlier than Lobith, although Lobith lies upstream of Bimmen. This means that the measured transport-time between Lobith and Vuren is smaller than between Bimmen and Vuren. Consequently the lag coefficient, i.e. the dead-zone parameter has to be reduced up to about 0.10 in order to get a good fit. However, after Eq.(4.4.9) a reduction of the dead-zone parameter means less "decomposition" in the main stream and in succession a larger peak-concentration. In order to reduce the peak concentration (see also Figs 4.4.23 and 24) the mass-transfer coefficient has to become smaller: after Eq.(4.4.10) the increment of the concentration in the dead zone reduces and the "decomposition" in the main stream lasts longer. Apparently the period of "decomposition" is predominant compared to the magnitude of the "decomposition parameter" $\beta \cdot D_b$ after Eq.(4.4.9).

Further, the results in Fig. 4.4.27 show a better fit of the tail of the concentration distribution than in Figs 4.4.25 and 4.4.26. This caused by the initial condition of the measuring station Lobith with a longer tail than measured at Bimmen.

Referring to the differences in the mass flux of the measured concentration-distributions on one hand (Table 4.4.9) and the relatively small effect of large variations of the mass-transfer coefficient on the calculated concentration-distributions on the other hand (Figs 4.4.24 and 4.4.25), further analysis of the mass-transfer coefficient, based on the tracer experiments 04/89 and 09/90 have been left out of consideration. Moreover, due to these differences of the mass flux and the relatively small effects of the mass-transfer coefficients, the determination of a representative D_b -value for the Dutch Rhine-branches by the measured concentration-distributions turns out to be impossible.

4.4.4 Conclusions

In case of artificial dead-zones, like groyne-fields, the reproduction of the transport velocity of a pollution cloud, i.e. the actual lag-coefficient, representing the difference between the mean flow-velocity and the transport velocity is equal to the dead-zone parameter β : the ratio of the cross-sectional areas of the main stream and the dead zone. However, the influence of large dead-zones as river harbours is restricted. A good approximation of their influence is given by the limitation of the β -values at 0.5.

Because fluctuations of the lag coefficient, due to a variable dead-zone parameter are smoothed by the longitudinal dispersion-coefficient, a river reach with a length, corresponding with a Péclet number of at least 10 has to be considered in order to get a good agreement of the lag coefficient and the dead-zone parameter. For shorter distances the deviation of the average lag-coefficient from the mean dead-zone parameter depends on the magnitude of the dispersion-coefficient as well as the local dead-zone parameter. The deviation increases with the dispersion coefficient as well as the fluctuations of the dead-zone parameter.

The equivalence of the lag coefficient and the dead-zone parameter presumes a completely mixed situation in the dead zone. In case of groyne-fields this situation is achieved if the distance in the flow direction between two successive groynes is smaller than 30 times the water depth of the main stream, which is mostly the case along the Dutch Rhine-branches. This condition is related to the velocity head in comparison with the slope of the energy head (see Section 4.2). The analysis of the relation between the lag coefficient and the dead-zone parameter showed that the completely mixed situation also depends on the velocity head itself. For values smaller than 0.05 m, a reduction of the influence of the dead zone has been observed. Apparently for very small values of the velocity head the propulsion force for the eddy in the groyne-field is vanishing. This means among others that for suppressed flow the influence of the dead zones on the transport velocity of a pollution cloud is negligible.

The lag coefficient is determined by comparison of the transport time, related to the time-centroid of the measured concentration-distributions, and the flow time. For the flow time, two models have been considered:

- * the Rhine Alarm-Model with tables for the relation between the water level at Lobith and the flow times in the Dutch Rhine-branches, based on the schematization after the ZWENDL-model, and
- * the SOBEK-model for which recently the cross-sectional areas of the main stream and the stagnant zones have been determined every 500 m river reach of the Dutch Rhine-branches. The cross sections are related to the river discharge at Lobith as well as the discharges in the Rhine branches.

The observed differences in the flow times between both models, especially in case of the transition of a free runoff and a suppressed flow in the River Lower Rhine, oblige to update the flow times in the Rhine Alarm-Model.

The transport velocity related to the time-centroid is not influenced by the mass-transfer coefficient. This coefficient only influences the shape of the concentration distribution. It appears that large variations of the coefficient ($D_b = 10^{-2}$ till 10^{-4} s^{-1}) cause variations in the tail of the distribution, which are negligible in relation to the accuracy of the measured concentrations. Although the resulting variations in the peak concentration are significant, they still are smaller than the concentration differences, caused by the decay of the tracer or otherwise. Thus, it turns out that tracer experiments with degradable matter are unsuitable for the determination of the mass-transfer coefficient. Moreover, the measured concentration-distributions have to be complete, including the tail with a high accuracy of measurement.

Chapter 5

TRANSPORT VELOCITY IN CASE OF A RELEASE AT A RIVER BANK

5.1 INTRODUCTION

The transport velocity just downstream of the release at a river bank is strongly influenced by the transversal flow-velocity distribution. Near the river bank the flow velocity is smaller than in the centre of the river. Consequently the transport velocity will be smaller than the mean flow-velocity, if the moment of inertia at the point of release is so small, that the transport of released substance is completely determined by the local flow-velocity. Based on the exponential velocity-profile an analytical expression has been derived in Sub-section 2.2.1 after the '*linear-spreading method*'. The overall value over the dimensionless distance X is given by (see Appendix A, Eqs A.12 and A.18)

$$\overline{\beta(X_1)} = \frac{n^3}{(n+1)(n-1)^2} \cdot (2 \cdot X_1)^{-1/n} - 1 \quad (5.1.1)$$

for $X \leq 0.5$ and

$$\begin{aligned} \overline{\beta(X_1)} = & \frac{1}{X_1} \cdot \left(0.5 \left[\frac{n^3}{(n+1)(n-1)^2} - 1 \right] \right) + \\ & + \frac{1}{X_1} \cdot \left(\int_{0.5}^{X_1} \left[\frac{n^2}{n^2-1} \cdot \frac{1}{2\xi} \cdot \left[2 - (2-2\xi)^{\frac{n-1}{n}} \right] - 1 \right] d\xi \right) \end{aligned} \quad (5.1.2)$$

for $0.5 < X < 1$.

The second term at the right part of Eq.(5.1.2) is solved numerically with steps $\Delta X = 0.01$. In Eqs (5.1.1) and (5.1.2) the parameter n reproduces the transversal flow-velocity distribution. In rivers the n -value is about 8 to 12. The dimensionless distance X is related to the transverse mixing distance L_m after

$$X = \frac{x}{L_m} \quad (5.1.3)$$

with

$$L_m \approx 0.4 \cdot \frac{u_s \cdot B^2}{K_y} \quad (5.1.4)$$

(see Section 2.1, Eq.(2.1.4))

In Fig. 5.1.1 the distribution of the overall lag-coefficient after Eqs (5.1.1) and (5.1.2) is presented graphically for three values of the parameter n . Because after the linear-spreading method the influence of the transversal flow-velocity distribution on the transport velocity can be given by analytical expressions (Eqs 5.1.1 and 5.1.2), the practical applicability of this theoretical approach will be simpler than the '*flux method*', as presented in Sub-section 2.2.1.

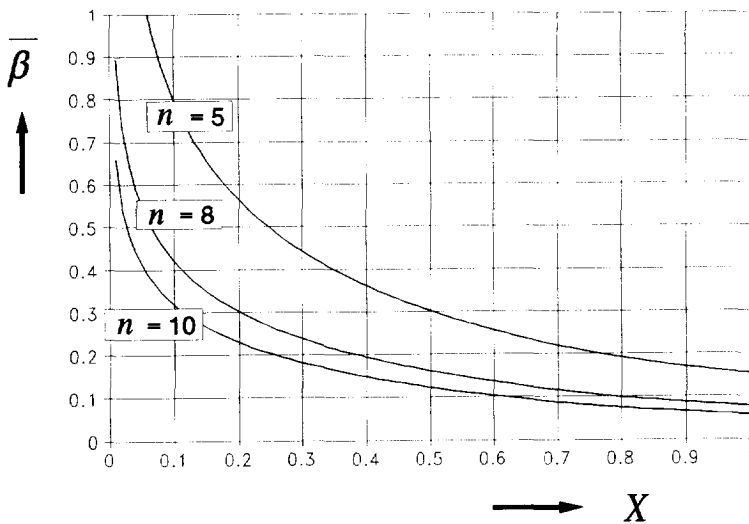


Fig. 5.1.1 The distribution of the overall lag-coefficient, due to the transversal flow-velocity distribution after Eqs (5.1.1) and (5.1.2) for three values of the exponent n

For the examination of the practical applicability of the linear-spreading method, the tracer experiments 05/90 and 07/91 are considered (see Section 3.1). The river reach, which will be taken into account for this examination, concerns the River Rhine with its lateral canals from the point of release at Huningue at the left bank (Rhine-kilometre 169.0, see Fig. 3.1.4) downstream to the end of the Rheinseiten Canal (Rhine-kilometre 226.6). The verification of the calibrated Rhine Alarm-Model by these two tracer experiments shows deviations of the travel time T_d of

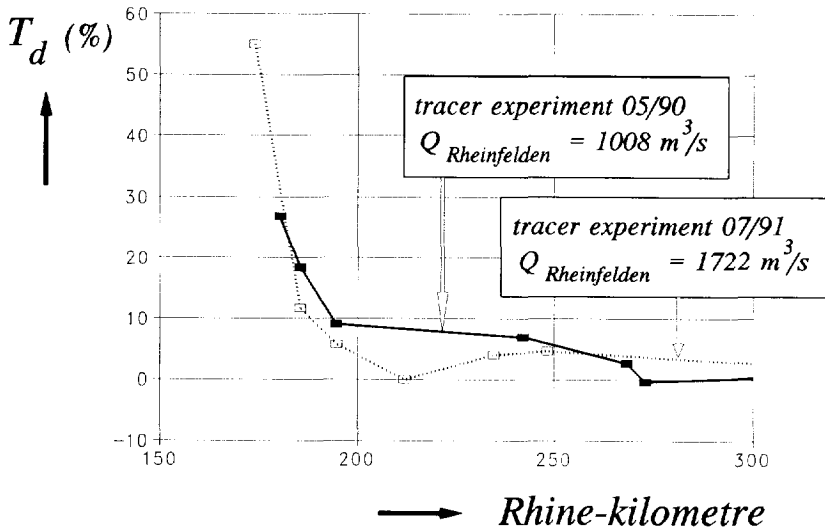


Fig. 5.1.2 Deviation of the travel time T_d in case of a release at the bank of the river (tracer experiments 05/90 and 07/91)

more than 10% along this river reach (Fig. 5.1.2, see also Fig. 3.4.2, Sub-section 3.4.1), for which the deviation is defined by (see Eq. 3.3.5)

$$T_d = \frac{(T_c)_{meas.} - (T_c)_{comp.}}{(T_c)_{meas.}} \quad (5.1.5)$$

wherein $(T_c)_{meas.}$ concerns the measured travel-time related to the peak concentration and $(T_c)_{comp.}$ the calculated travel-time after the Rhine Alarm-Model.

The distribution of the deviation in Fig. 5.1.1 confirms the influence of the transversal flow-velocity distribution. In Section 5.2 the overall lag-coefficient, based on the time-centroid of the measured concentration-distributions will be compared with the theoretical approach after Fig. 5.1.1. In Section 5.3 conclusions will be drawn for the practical applicability in the Rhine Alarm-Model.

5.2 COMPARISON OF EXPERIMENTAL DATA WITH COMPUTATIONAL RESULTS

For the analysis of the lag coefficient, due to the transversal flow-velocity distribution the measured concentration-distributions at a distance smaller than the

transverse mixing distance L_m from the point of release will be considered. For the determination Eq.(5.1.4) has been rewritten. Because the transversal dispersion-coefficient K_y is defined by (see Eq. 2.1.5)

$$K_y = \alpha_y \cdot a \cdot u_* \quad (5.2.1)$$

and the shear velocity u_*

$$u_* = \frac{u_s \cdot \sqrt{g}}{C} \quad (5.2.2)$$

Eq.(5.1.4) becomes

$$L_m = 0.4 \cdot \frac{B^2 \cdot C}{\alpha_y \cdot a \sqrt{g}} \quad (5.2.3)$$

In Table 5.2.1 the transverse mixing distances of the measuring stations concerned, is presented for $\alpha_y = 0.6$, as a mean value⁹⁾. The mean values of the river width B and depth a , as well as the Chézy-coefficient C are based on the river schemati-

TABLE 5.2.1 Transverse mixing distance L_m and the dimensionless distance X after Eq.(5.1.3), tracer experiments 05/90 and 07/91

measuring station	Rhine-km	averaged values of the river reach/canal concerned					
		distance	width	depth	Chézy-coeff.		
		x (km)	B (m)	a (m)	C (m ^{1/2} /s)	L_m (km)	X
tracer experiment 05/90 point of release at Rhine-km 169.0							
Kembs	174.0	5.0	176	8.75	47	35	0.14
Kembs	180.5	11.5	154	8.04	46	29	0.40
Kembs-Niffer	185.5	16.5	148	7.88	46	27	0.60
Ottmarsheim	194.6	25.5	144	7.74	46	26	0.97
tracer experiment 07/91 point of release at Rhine-km 169.1							
Kembs	174.1	5.0	176	8.87	47	35	0.14
Kembs-Niffer	185.5	16.4	148	8.00	46	27	0.61
Ottmarsheim	194.6	25.5	144	7.86	46	26	1.00

⁹⁾ For natural streams the coefficient α_y lies between 0.3 and 0.9 (Fischer et al, 1979).

zation in the Rhine Alarm-Model. Figure 5.2.1 shows the schematized river-reach from Basel (Rhine-km 167) downstream to the end of the lateral canal of Marckolsheim (Rhine-km 242.5) with the measuring stations concerned. The point of release is situated at Huningue, Rhine-kilometre 169.0 or 169.1 (see Table 5.2.1).

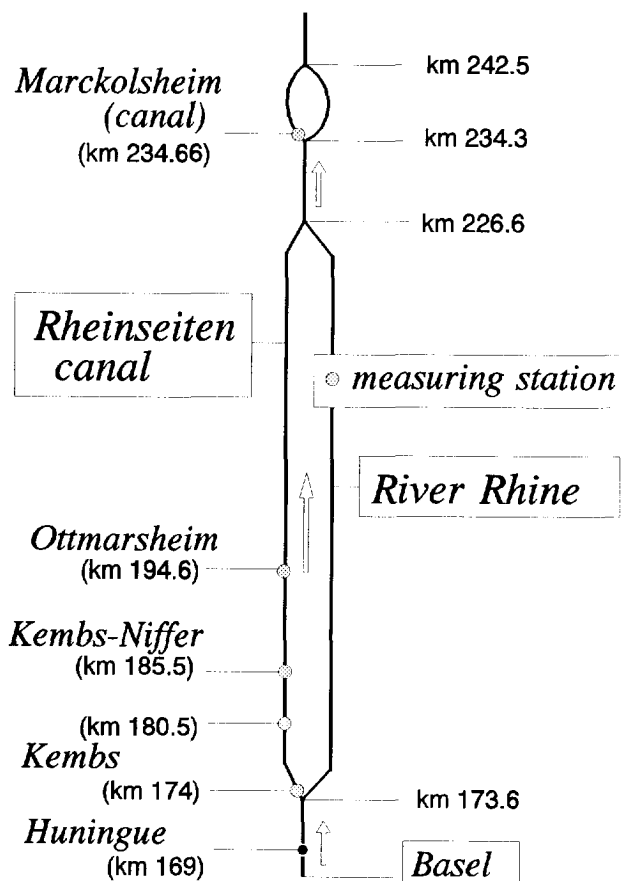


Fig. 5.2.1 Schematized river-reach Basel - Marckolsheim with the measuring stations, tracer experiments 05/90 and 07/91

In case of the tracer experiment 05/90 with a river discharge of $1008 \text{ m}^3/\text{s}$ at Rheinfelden, the discharge of the River Rhine downstream of the bifurcation at Kembs (Rhine-km 173.6) will be negligibly small (about $30 \text{ m}^3/\text{s}$). Thus, the tracer released at the left bank of the river at a distance less than 5 km upstream of the bifurcation, will flow completely into the Rheinseiten canal. However, in case of

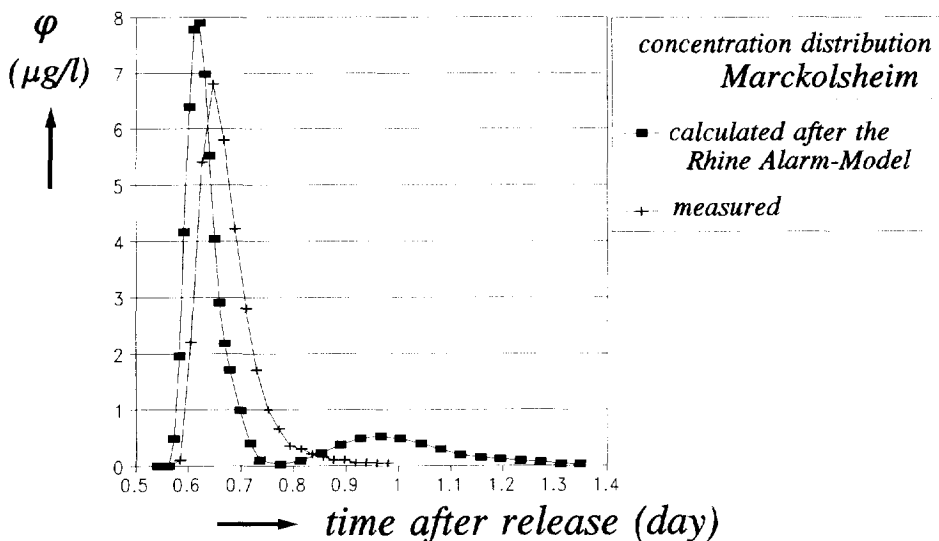


Fig. 5.2.2 Comparison of the measured and calculated concentration-distributions at Markolsheim (canal), tracer experiment 07/91

the tracer experiment 07/91 with a discharge of 1722 m³/s at Rheinfelden, the discharge of the River Rhine downstream of the bifurcation amounts more than 300 m³/s. Because the distance between the point of release and the bifurcation is relatively small in comparison with the transverse mixing length of 35 km (see Table 5.2.1), it is not improbable that even in this situation the tracer will flow completely into the Rheinseiten canal. The concentration distribution, measured in the lateral canal at Marckolsheim (Rhine-km 234.66) confirms this assumption by showing one tracer wave (Fig. 5.2.2). After the one-dimensional Rhine Alarm-Model, which presumes a completely mixed situation over the cross-sectional area of the river at the point of release, there are two tracer waves due to the two flow-paths (by way of the Rheinseiten canal and the River Rhine) between the point of release and the measuring point at Marckolsheim (Fig. 5.2.1).

After these considerations the concentration distributions of the measuring stations along the Rheinseiten canal of both tracer experiments can be used for the analysis of the theoretical approach of the lag coefficient, described by the Eqs (5.1.1) and (5.1.2).

For the determination of the overall lag-coefficient $\bar{\beta}$ from the point of release downstream to the measuring station concerned, the transport time based on the time-centroid after the DUD-method has been used. However, because the tracer

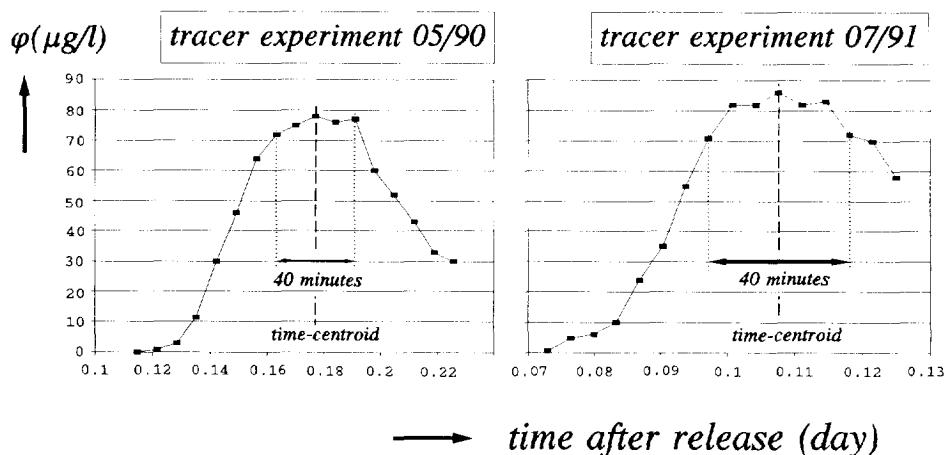


Fig. 5.2.3 Measured concentration-distributions at Kembs (Rhine-km 174)

has been released into the river during a period of 40 minutes (tracer experiment 05/90; van Mazijk, June 1991), the concentration distribution, measured at the nearest station Kembs (Rhine-km 174) show still a period, the tracer concentration is more or less constant (Fig. 5.2.3). Therefore the time-centroid of the concentration distributions at this station is related to the centre of this period. Moreover, because the time is related to the beginning of the release, the time-centroid of this station has been reduced with half of the release period (the release period of the tracer experiment 07/91 is assumed to be equal) in order to get an accurate transport-time¹⁰⁾.

In Table 5.2.2 the results are presented. The flow time has been deduced from the hydrological schematization after the Rhine Alarm-Model, which is related to the river discharge at Rheinfelden (see also Section 3.2). In Fig. 5.2.4 the results of Table 5.2.2. are compared with the distribution of the overall value of the lag coefficient for three n -values of the exponential velocity-profile. It shows that the best fit is achieved for a n -value between 3 and 5, which, however, is much smaller than the usual value of 8 to 12.

As a matter of fact, the dimensionless distance X in Table 5.2.2 depends on the transverse mixing distance after Eq.(5.1.3). Beside the dimensions of the cross-sectional area of the river reach concerned, the transverse mixing distance L_m also depends on the value of the coefficient α_y (Eq. 5.2.3). A large α_y -value means a

¹⁰⁾ The release period of the tracer experiment 07/91 is assumed to be the same as in case of the tracer experiment 05/90.

TABLE 5.2.2 Overall lag-coefficient in case of a bank release, tracer experiments 05/90 and 07/91

measuring station	Rhine-kilometre	dimensionless distance X	transp. time μ_t (day)	flow-time T_u (day)	overall lag-coefficient $\bar{\beta}$
tracer experiment 05/90 ($Q_{\text{Rheinfelden}} = 1008 \text{ m}^3/\text{s}$) point of release at Rhine-km 169.0					
Kembs	174.0	0.14	0.1632	0.0889	0.84
Kembs	180.5	0.40	0.2362	0.1650	0.43
Kembs-Niffer	185.5	0.60	0.2894	0.2235	0.29
Ottmarsheim	194.6	0.97	0.3899	0.3300	0.18
tracer experiment 07/91 ($Q_{\text{Rheinfelden}} = 1722 \text{ m}^3/\text{s}$) point of release at Rhine-km 169.1					
Kembs	174.1	0.14	0.0937	0.0533	0.76
Kembs-Niffer	185.5	0.61	0.1824	0.1510	0.21
Ottmarsheim	194.6	1.00	0.2573	0.2290	0.12

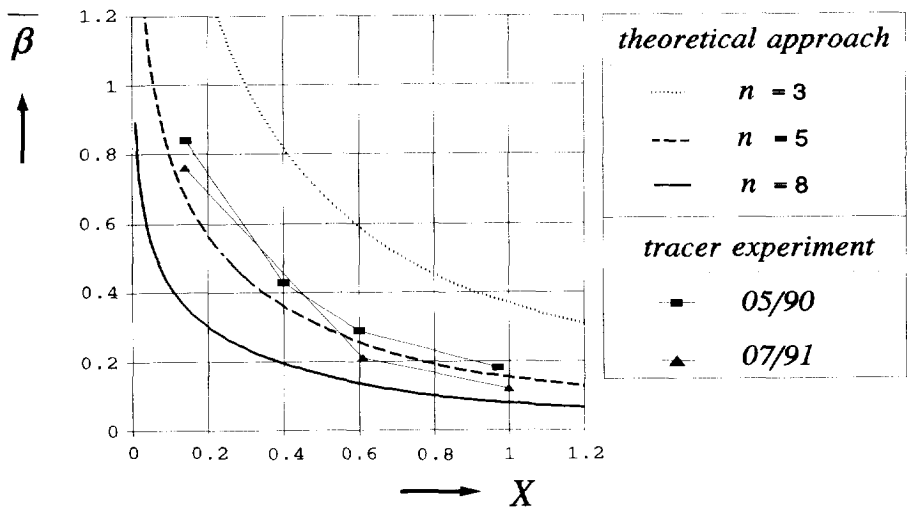


Fig. 5.2.4 Comparison of the overall lag-coefficient after the tracer experiments 05/90 and 07/91 with the theoretical approach after Eqs (5.1.1) and (5.1.2)

fast transversal spreading and consequently a short transverse mixing-distance. This means on its turn that the value of the transverse mixing-coefficient α_y can be fitted, if the n -value should be known explicitly by measurements of the transversal velocity-profile. Because the 25 km river-reach between Rhine-km 169 and Rhine-km 194.6 concerns the Rheinseiten canal over a distance of more than 20 km, a value of 8 for the velocity-profile exponent n is assumed to be a good approximation. The fitted α_y -values for $n = 8$ are collected in Table 5.2.3 and presented graphically in Fig. 5.2.5.

TABLE 5.2.3 Distribution of the fitted transverse mixing-coefficient α_y for a transverse exponential velocity-profile with $n = 8$, tracer experiments 05/90 and 07/91

measuring station	Rhine-kilometre	transverse mixing coeff. α_y	dimensionless distance X	mean flow-velocity u_s (m/s)
tracer experiment 05/90 ($Q_{\text{Rheinfelden}} = 1008 \text{ m}^3/\text{s}$)				
Kembs	174.0	0.06	0.0133	0.65
Kembs	180.5	0.14	0.0933	0.81
Kembs-Niffer	185.5	0.22	0.2100	0.85
Ottmarsheim	194.6	0.27	0.4365	0.90
tracer experiment 07/91 ($Q_{\text{Rheinfelden}} = 1722 \text{ m}^3/\text{s}$)				
Kembs	174.1	0.08	0.0182	1.08
Kembs-Niffer	185.5	0.35	0.3558	1.26
Ottmarsheim	194.6	0.40	0.6667	1.29

It shows that the transverse mixing increases with the distance from the point of release. The more the tracer is spread over the cross section of the river or canal, the larger the transverse mixing-coefficient α_y becomes, i.e. the transverse mixing. Apparently, the increase of the flow velocity with the distance y from the river bank, described by the exponential velocity-profile after Eq.(2.2.1) for $y \leq 0.5 B$

$$u(y) = \frac{n+1}{n} \cdot \left(\frac{y}{0.5B} \right)^{\frac{1}{n}} \cdot u_s \quad (5.2.4)$$

corresponding with an increase of the turbulence, causes this increase of the transverse mixing-coefficient. The influence of the flow velocity on the transverse mixing-coefficient can also be observed by comparing the fitted α_y -values of both

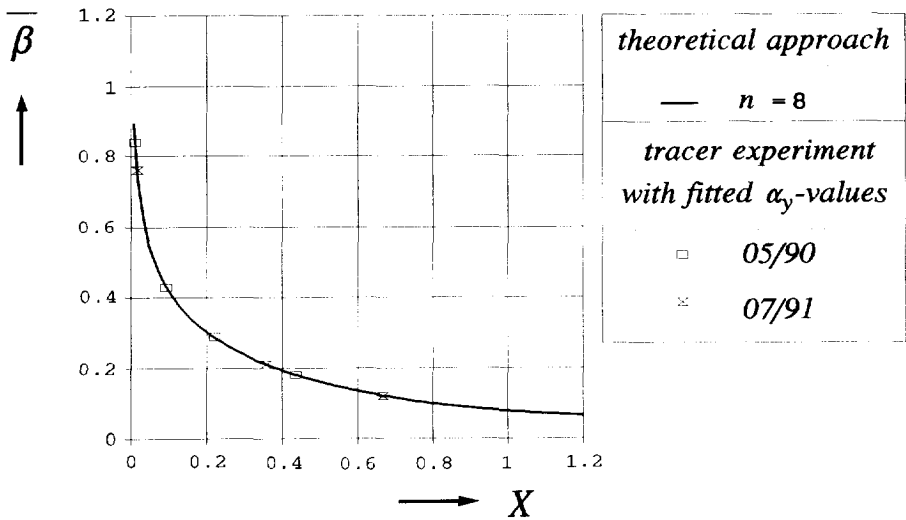


Fig. 5.2.5. The distribution of the overall lag-coefficient after Eqs (5.1.1) and (5.1.2) for $n = 8$ and the measured lag-coefficients for fitted α_y -values (Table 5.2.3)

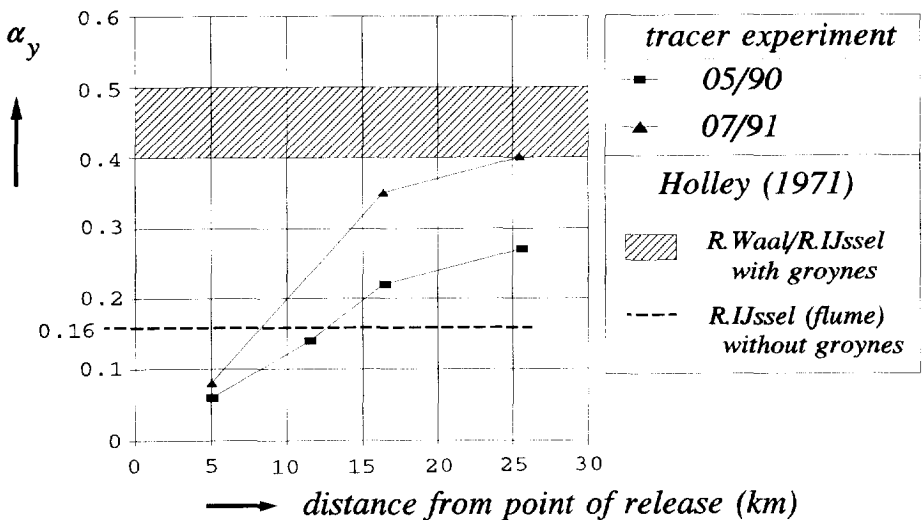


Fig. 5.2.6 Distribution of the transverse mixing-coefficient α_y in comparison with data after Holley (1971)

tracer experiments (Fig. 5.2.6). In case of the tracer experiment 07/91 with a river discharge at Rheinfelden of 1722 m³/s the flow velocities are larger than in case of the tracer experiment 05/90 with a river discharge of 1008 m³/s (Table 5.2.3).

Partly due to the influence of the flow velocity, i.e. the turbulence on the transverse mixing-coefficient, in Fig. 5.2.6 the fitted α_y -values are compared with the results of tracer experiments, carried out by Holley (1971) in two Dutch Rhine-branches: the River Waal and the River IJssel. Because of the groynes along the river banks of these Rhine branches, which generate additional turbulence, he found relatively large transverse mixing-coefficients: between 0.4 and 0.5. In order to demonstrate the effect of the groynes explicitly, he also examined the transverse mixing in an undistorted, fixed bed river model of the River IJssel (with groynes) as well as in a rectangular flume with and without groynes. The dimensions and spacing of the groynes in the rectangular flume were chosen to correspond to the average conditions in the river model. Based on the results of the experiments, he concluded that in case of no groynes the transverse mixing-coefficient becomes about three times smaller: $\alpha_y = 0.16$. This result agrees quite well with the fitted α_y -values after the tracer experiments 05/90 and 07/91, referring to the fact that the river reach between Rhine-km 169 and 194.6 has no groynes. Moreover, 80% of this river reach concerns the Rheinseiten canal, which will be more or less comparable with a rectangular flume.

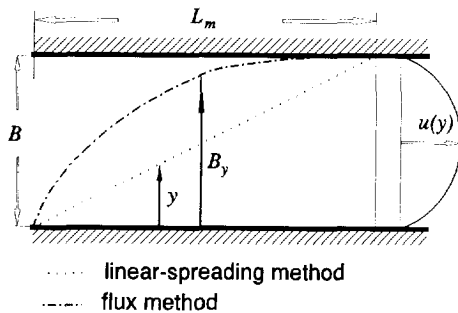


Fig. 5.2.7 Difference of the tracer width along the river for the *linear-spreading method* and the *flux method*

In Sub-section 2.2.1 the *flux method* is presented next to the *linear-spreading method* after Eqs (5.1.1) and (5.1.2). Because the flux method takes into account the spreading of the tracer over the width, described by Eq.(2.1.3) (see Section 2.1), which results into a spreading of the tracer near the point of release over a larger part of the river width as assumed by the linear-spreading method (Fig. 5.2.7), it has been concluded that the influence of velocity profile is not as much as the linear-spreading method suggests. Therefore, in order to get comparable values for

the overall lag-coefficient unusual n -values of about 36 has to be applied for the linear-spreading method. However, this conclusion is in contradiction with the presented comparison of the fitted α_y -values and the overall lag-coefficient after the linear-spreading method for $n = 8$ in Fig. 5.2.5. Obviously, the transverse mixing near the point of release in case of the tracer experiments 05/90 and 07/91 is so

small, that the linear-spreading method with a usual n -value gives a good approximation of the overall lag-coefficient. Moreover, the relatively small values for the transverse mixing-coefficient confirm this. Because the transverse mixing also depends on the occurrence of net transverse velocities, which can exist due to changes in channel geometry and velocity distributions, the practical applicability of the results of the tracer experiments 05/90 and 07/91 are restricted.

5.3 PRACTICAL APPLICATION

The transport velocity of a pollutant, released at the river bank is mainly determined by the local flow-velocity in relation to the amount of spreading of the pollutant over the cross section of the channel. If the transversal velocity-distribution is described by the exponential profile after (see Sub-section 2.2.1, Eqs 2.2.1 and 2.2.2)

$$u(y) = \frac{n+1}{n} \cdot \left(\frac{y}{0.5B} \right)^{\frac{1}{n}} \cdot u_s \quad (5.3.1)$$

for $y \leq 0.5 B$

$$u(y) = \frac{n+1}{n} \cdot \left(\frac{B-y}{0.5B} \right)^{\frac{1}{n}} \cdot u_s \quad (5.3.2)$$

for $0.5 B < y < B$

and the spreading of the pollutant is assumed to be homogeneous over a part of the channel width, determined by linear interpolation between the point of release and the transverse mixing distance L_m after (see Eq. 5.2.3)

$$L_m = 0.4 \cdot \frac{B^2 \cdot C}{\alpha_y \cdot a \sqrt{g}} \quad (5.3.3)$$

the actual transport-velocity, i.e. the overall lag-coefficient can be given by Eqs (5.1.1) and (5.1.2)

for $X \leq 0.5$

$$\overline{\beta(X_1)} = \frac{n^3}{(n+1)(n-1)^2} \cdot (2 \cdot X_1)^{-1/n} - 1 \quad (5.3.4)$$

and for $0.5 < X < 1$.

$$\begin{aligned} \overline{\beta(X_1)} = & \frac{1}{X_1} \cdot \left(0.5 \left[\frac{n^3}{(n+1)(n-1)^2} - 1 \right] \right) + \\ & + \frac{1}{X_1} \cdot \left(\int_{0.5}^{x_1} \left[\frac{n^2}{n^2-1} \cdot \frac{1}{2\xi} \cdot \left[2 - (2 - 2\xi)^{\frac{n-1}{n}} \right] - 1 \right] d\xi \right) \end{aligned} \quad (5.3.5)$$

wherein the dimensionless distance X is defined by

$$X = \frac{x}{L_m} \quad (5.3.6)$$

For a good estimation of the lag coefficient after Eqs (5.3.4) and (5.3.5), beside the channel geometry, two parameters have to be estimated:

- the transverse mixing-coefficient α , and
- the exponent n of the velocity profile.

The transverse mixing coefficient α , depends on the intensity of turbulence and the occurrence of net transverse velocities. Generally spoken, in rivers with protective structures such as groynes, which cause additional turbulence the transverse mixing coefficient is three times larger than in case the river cross-section is more rectangular like canals. Based on the results of tracer experiments, the transverse mixing-coefficient can be estimated at 0.5 for river reaches with groynes and at 0.15 for river reaches without groynes.

If there are no transversal velocity-profiles available, a first estimation of the overall lag-coefficient can be made by $n = 10$, referring to the usual values for rivers and canals of 8 to 12. If it is done so for the River Rhine from Basel (Rhine-km 163.8) downstream to Vuren (River Waal, Rhine-km 951), at first the transverse mixing distance L_m has to be determined after Eq.(5.3.3). On account of the variation of the river width and the presence of groyne-fields the river is split up into a number of river branches as presented in Fig. 5.3.1. Based on the hydrological conditions during the tracer experiment 04/89 the mean values of the parameters concerned for these river branches are derived from the Rhine Alarm-Model (Table 5.3.1). The results show the large influence of the transverse mixing coefficient α , as well as the river width B on the magnitude of the transverse mixing distance L_m .

In order to get in succession an indication about the magnitude of the overall lag-coefficient β in comparison with the calibrated dead-zone parameter in the Rhine Alarm-Model, a distance of 20 km from the point of release is considered (Table 5.3.2). For the exponent n of the transversal velocity-profile two values have been

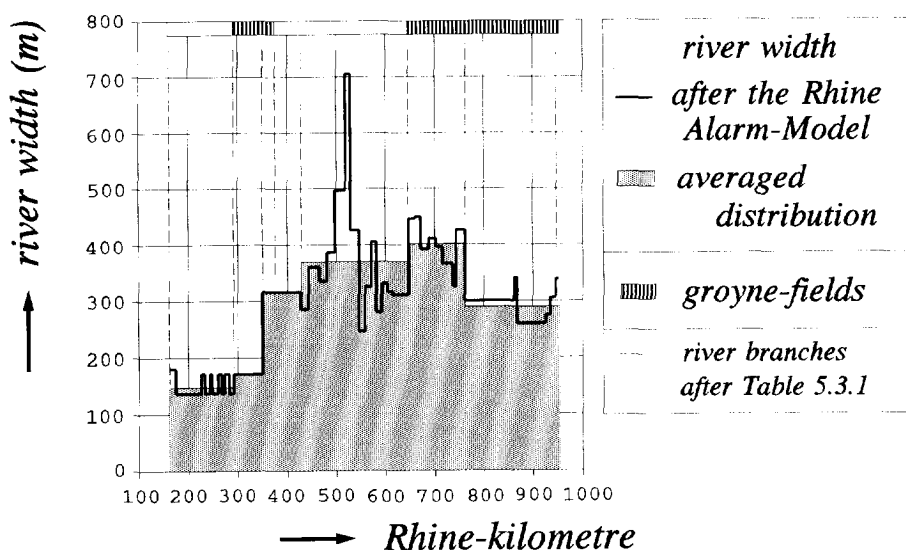


Fig. 5.3.1 The splitting of the River Rhine between Basel (Rhine-km 163.8) and Vuren (R.Waal, Rhine-km 951), based on the presence of groyne fields and the variation of the river width

TABLE 5.3.1 Distribution of the transverse mixing distance L_m for the River Rhine between Basel (River Rhine) and Vuren (River Waal)

River branch		groynes	α_y	averaged values			L_m (km)
Rhine-km	length (km)			width B (m)	depth a (m)	Chézy- coeff. C (m ^{1/2} /s)	
163.8 - 291.4	127.6	no	0.15	147	8.33	47	104
291.4 - 351	59.6	yes	0.5	170	9.63	47	36
351 - 376	25.0	yes	0.5	315	3.49	40	290
376 - 428.5	52.5	no	0.15	315	3.31	40	1020
428.5 - 647.5	219.0	no	0.15	369	4.61	42	1056
647.5 - 762	114.5	yes	0.5	401	5.06	43	349
762 - 951	189.0	yes	0.5	289	7.49	46	131

used: the usual value of 10 as well as the value of 36, for which the flux method with $n = 10$ corresponds with the applied linear-spreading method (see Fig. 2.2.8, Sub-section 2.2.1). The results are visualized in Fig. 5.3.2. The distribution of the dead-zone parameter β after the Rhine Alarm-Model is also plotted for comparison.

TABLE 5.3.2 Indication of the overall lag-coefficient along the River Rhine for two n -values of the transversal velocity-profile

River branch	distance from point of release $x = 20$ km	overall value of the lag coefficient $\bar{\beta}$	
Rhine-km	X after Eq.(5.3.6)	$n = 10$	$n = 36$
163.8 - 291.4	0.19	0.23	0.06
291.4 - 351	0.55	0.11	0.03
351 - 376	0.07	0.37	0.09
376 - 428.5	0.02	0.55	0.13
428.5 - 647.5	0.02	0.56	0.13
647.5 - 762	0.06	0.39	0.09
762 - 951	0.15	0.26	0.06

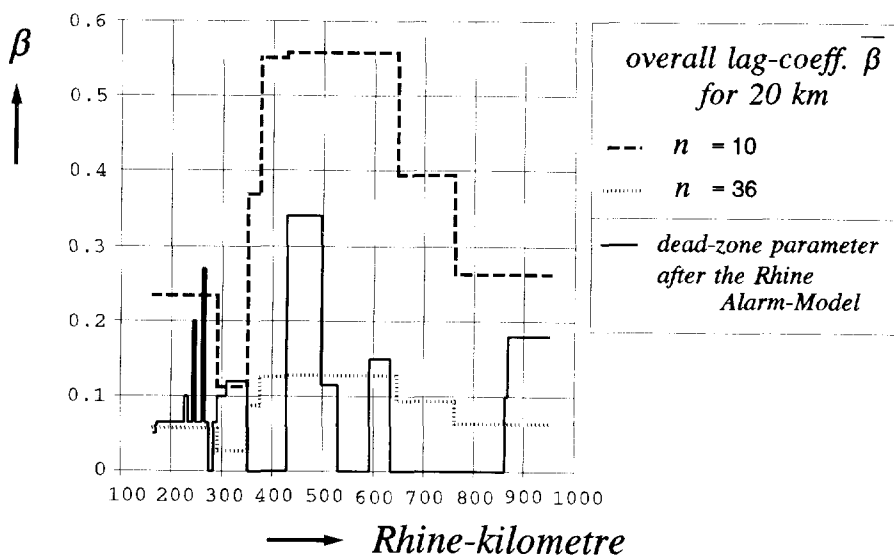


Fig. 5.3.2 Distribution of the overall lag-coefficient in case of a release at the river bank for two n -values in comparison with the dead-zone parameter after the Rhine Alarm-Model

As concluded in Sub-section 2.2.1, due to the larger transversal spreading than assumed by the linear spreading-method the overall lag-coefficient is not as much as this method suggests. However, if the transversal mixing-coefficient α_y increases

with the distance from the point of release (Fig. 5.2.6), the transversal spreading will be less than found by Eq.(2.1.3) for a constant α_y -value

$$\frac{\varphi(x',y')}{\varphi_0} = \frac{1}{\sqrt{\pi \cdot x'}} \cdot \sum_{n=-\infty}^{n=\infty} \left(\exp \left[- \frac{(y' - 2n)^2}{4 \cdot x'} \right] \right) \quad (5.3.7)$$

This means that after all the linear spreading-method might be a better approximation than the flux method. In that case the additional lag-coefficient due to the inhomogeneous cross-sectional mixing downstream of a release at the river bank can become as much as 0.2 till 0.5 (Fig. 5.3.2, with $n = 10$).

However, it has to be noticed that relatively small variations of the n -value as well as the α_y -value have large influence on the additional lag-coefficient. Because the reliability of these values without verification by tracer experiments in the river concerned are restricted, it has to be emphasized that the results for $n = 10$ and $\alpha_y = 0.15$ (without groynes) or 0.5 (with groynes) have to be handle very cautiously, since the prediction of a late arrival-time of a pollution cloud is mostly unacceptable.

Chapter 6

CONCLUSIONS AND RECOMMENDATIONS

In the Rhine Alarm-Model the transport of a pollution cloud is calibrated by the lag coefficient β , which describes the difference between the mean flow-velocity u_s , based on the hydraulic schematization of the River Rhine and the measured transport-velocity c after

$$c = \frac{u_s}{1 + \beta} \quad (6.1)$$

For the calibration and verification of this parameter a series of tracer experiments has been carried out between Basel downstream to the Dutch Rhine-branches.

In this study the determination of the lag coefficient β is based on the comparison of the measured transport-time and the flow time. The transport time can be related to the time-centroid of the measured concentration-distribution as well as to the peak value of the distribution. For the determination of the time-centroid the zeroth and first moment of the distribution has to be computed. Because in practice the measured concentration-distribution is mostly incomplete (a part of the distribution is missed, which is mostly the tail) the time-centroid has been determined by minimizing the difference between the measured distribution and the theoretical approximation after the adapted Taylor-solution by the third Hermite-polynomial after Chatwin. For the minimizing a derivative-free Gauss-Newton algorithm, called DUD (*Doesn't Use Derivatives*) has been applied. The accuracy of the calculated lag-coefficient, based on two successive measured concentration-distributions is highly influenced by the distance between the measuring stations concerned: the smaller the distance the smaller the difference in transport and flow time between these stations. This means that the flow time between two stations must be at least more than the passage time of the tracer cloud at the considered measuring-stations. Due to the long distance over which the tracer experiments were carried out (Basel - Netherlands), this condition could not be fulfilled all the time.

The flow velocity u_s , i.e. the flow time has been derived from the relevant data of the Rhine Alarm-Model. For the Dutch Rhine-branches these data are based on a schematization after the one-dimensional hydrodynamic ZWENDL-model. Recently the SOBEK-model for the Dutch Rhine-branches has been developed. In this model the cross-sectional areas of the main stream and the dead zones have been determined every 500 m river reach. The cross sections are related to the river discharge at Lobith as well as the discharges in the Rhine branches. The observed

differences in the flow times between the SOBEK-model and the Rhine Alarm-Model, especially in case of the transition of a free runoff and a suppressed flow in the River Lower Rhine, oblige to update the flow times in the Rhine Alarm-Model.

For the calibration of the lag coefficient in the Rhine Alarm-Model the peak concentration was considered as well as the concentration distribution for values larger than 30% of the calculated peak-value. This meant that the tail of the concentration distribution was not taken into account. The difference between the calibrated β -values after the Rhine Alarm-Model and the values obtained by the DUD-method were within the range of accuracy

A detailed analysis of the distribution of the lag coefficient along the River Rhine, based on the tracer experiments, shows that in general a significant lag-coefficient (>0.05) is obtained if artificial dead-zones like groyne-fields are present.

Downstream of the main tributaries of the River Rhine (River Neckar, River Main and River Mosel) β -values larger than 0.05 have been observed too. This in contrast with the expectation, based a theoretical approximation of the two-dimensional transport-phenomena downstream of a tributary by schematizing the traced river-branch as a number of point releases over a certain width of the river. It has been demonstrated that the value of the local lag-coefficient depends on the discharge ratio between the tributary concerned and the River Rhine as well as on the discharge of the River Rhine itself. In case of low-water the tributaries Neckar and Main influence the transport of substances significantly ($\beta \sim 0.20$). In case of high-water situations there is also a significant influence, if the discharge of the tributary constitutes a significant part of the total discharge of the River Rhine (more than 10%). Conversely, the inflow of the River Mosel effects the transport of the pollution cloud only in case of low-water conditions.

Therefore, it is assumed that the retardation of the transport downstream of a tributary is mainly caused by the exchange of substances between the main stream and the inflow of the tributary and the difference of the flow velocities between both zones. Thus, for a more detailed quantification of the lag coefficient in relation to the river discharges, measurements of flow-patterns downstream of the tributaries are recommended.

Further, it can be concluded that the theoretical approximation mentioned above, might be a simplification, which does not hold without any restriction.

The influence of islands in the middle of the river on the overall transport-velocity remains negligible as long as the length of the lateral branch does not differ significantly from the length of the main branch. Because in the River Rhine the branches, surrounded islands are more or less equal, there have not been found any influence on the lag coefficient explicitly. On the other hand the islands might

influence the shape of a measured concentration-distribution. In case of relatively short distances between two successive measuring-stations (see above), the significance of the calculated lag-coefficient is restricted, especially if the peak concentration has been considered.

Between Basel and Strasbourg the River Rhine has five lateral canals with power stations. Here the lag coefficient represents deviations of the actual flow-velocity from the flow velocity, based on the German-French agreement concerning the discharge ratio between the canals and the River Rhine. This deviation depends on the rise-level control by the power stations. Because for small river-discharges the storage period of water is mostly longer than during larger river-discharges, the difference between the mean flow-velocity after the German-French agreement and the actual transport-velocity will be *larger* in case of *small* river-discharges and *smaller* in case of *larger* discharges. Consequently the lag coefficient varies with the river discharge: large values for low-water situations and small values for high-water situations. However, because the lag coefficient is constant in the Rhine Alarm-Model, an average value has been used. An adaptation of the Rhine Alarm-Model by which it becomes possible to feed the model with the actual discharges at the power stations has to be avoided from a practical point of view. Moreover, this adaptation is not a necessity, since the verification of the calibrated model by tracer experiments during low- and high-water conditions showed differences between calculated and measured transport-times of about 5% or less.

For the analysis of the influence of the artificial dead-zones, as groyne-fields, a numerical with an explicit scheme has been used. The Dutch Rhine-branches were considered for the verification of the model results. If the transport velocity is related to the time-centroid, it has been shown that the actual lag-coefficient varies instantaneously with the dead-zone parameter $\beta_{dead-zone}$, defined by

$$\beta_{dead-zone} = \frac{A_b}{A_s} \quad (6.2)$$

with A_b = cross-sectional area of the dead zone
 A_s = cross-sectional area of the main stream

The dead-zone parameter has been derived from the schematization of the Dutch Rhine-branches after the SOBEK-model.

As a matter of fact the local lag-coefficient and the dead-zone parameter are similar. However, because fluctuations of the lag coefficient, due to a variable dead-zone parameter are smoothed by the longitudinal dispersion-coefficient K_s , a river reach with a length x , corresponding with a Péclet number Pe , defined by

$$Pe = \frac{u_s \cdot x}{K_s} \quad (6.3)$$

of 10 till 15 has to be considered in order to get a good agreement of the lag coefficient and the mean dead-zone parameter over this distance (The deviation of the actual lag-coefficient from the averaged dead-zone parameter is less than 10%). Beside groyne-fields, there are large dead-zones as river harbours and lakes. The contribution of these dead zones to the actual lag-coefficient is restricted. A good approximation of their influence is given by the limitation of the $\beta_{dead-zone}$ -values at 0.5.

It is recommended to verify these results by comparing the measured lag-coefficients with the dead-zone parameter of the German reaches of the River Rhine, which are regulated by groyne-fields (between Rhine-km 290 and 375, and between Rhine-km 740 and 862).

However, it has to be realized that the equivalence of the lag coefficient and the dead-zone parameter presumes a completely mixed situation in the groyne-field. This situation is achieved if the distance in the flow direction between two successive groynes is smaller than 30 times the water depth of the main stream, which is mostly the case along the Dutch Rhine-branches. This condition is related to the velocity head in comparison with the slope of the energy head. The analysis of the relation between the lag coefficient and the dead-zone parameter showed that the completely mixed situation also depends on the velocity head itself. For values smaller than 0.05 m, a reduction of the influence of the dead zone has been observed. Apparently for very small values of the velocity head the propulsion force for the eddy in the groyne-field is vanishing. This means among others that for suppressed flow the influence of the dead zones on the transport velocity becomes negligible. A verification of this statement by tracer measurements in the main stream and the in the groyne-fields is recommended.

The mass transfer between the main stream and the dead zones only effects the shape of the concentration distribution in the main stream, but not the transport velocity related to the time-centroid. It appears that large variations of the mass-transfer coefficient D_b from 10^{-2} till 10^{-4} s^{-1} cause variations in the tail of the distribution, which are negligible in relation to the accuracy of the measured concentrations. The influence of the mass-transfer coefficient on the shape of the concentration distribution means also that the transport velocity related to the peak concentration is effected by this coefficient and consequently the adaptation of the transport velocity c to the dead-zone parameter after Eq.(6.1). For the analysis of this influence the dimensionless mass-transfer parameter $\mathcal{E} = D_b \cdot K_s / u_s^2$ has been used. It came out that for values of $\mathcal{E} \geq 1$ there is more or less an instantaneous adaptation of the local lag-coefficient to the dead-zone parameter value.

Consequently in case of a variable dead-zone parameter an averaging over the dimensionless distance of $Pe = 15$ also gives comparable values for these parameters.

It has been tried to quantify the mass-transfer coefficient D_b for the Dutch Rhine-branches by fitting the measured concentration-distributions with the numerical model. Although the considered variations of the mass-transfer coefficient (10^{-2} till 10^{-4} s^{-1}) result into significant variations in the calculated peak-concentration, these variations were still smaller than the measured concentration-differences, caused by the decay of the tracer or otherwise. Thus, it turns out that tracer experiments with degradable matter are unsuitable for the determination of the mass-transfer coefficient. Moreover, the measured concentration-distributions have to be complete, including the tail with a high accuracy of measurement.

Apart from the reduction of the transport velocity of a dissolved substance by stagnant zones in case of a completely mixed situation over the cross section of the main stream, the transport velocity can also differ from the mean flow-velocity in case the substance is inhomogeneously distributed over the cross section. Now the difference is caused by the variation of the flow velocity over the river width. The analyzed situation concerned a release from the river bank. The distance L_m over which a completely mixed situation is achieved, is given by

$$L_m = 0.4 \cdot \frac{u_s \cdot B^2}{K_y} \quad (6.4)$$

with K_y = transversal dispersion-coefficient
 B = river width

The transversal dispersion-coefficient is defined by

$$K_y = \alpha_y \cdot a \cdot u_* \quad (6.5)$$

wherein α_y = transverse mixing-coefficient
 u_* = shear velocity
 a = water depth

If the flow-velocity profile over the river width B is approximated by an exponential expression with the exponent n after

$$u(y) = \frac{n+1}{n} \cdot \left(\frac{y}{0.5B} \right)^{\frac{1}{n}} \cdot u_s \quad (6.6)$$

for $y \leq 0.5 B$

and

$$u(y) = \frac{n+1}{n} \cdot \left(\frac{B-y}{0.5B} \right)^{\frac{1}{n}} \cdot u_s \quad (6.7)$$

for $0.5 B < y < B$

the overall lag-coefficient from the point of release downstream to a certain distance x can be determined, assuming a linear spreading of the substance between the point of release and the distance $x = L_m$ with a homogeneous distribution over the spreading width. There are two important parameters, determining the overall lag-coefficient: the transverse mixing-coefficient α_y and the exponent n . The verification of this approximation of the lag coefficient by two tracer experiments with a release at the river bank, about 5 km downstream of Basel demonstrates its applicability. Thus, a good fit has been obtained for $\alpha_y \sim 0.2$, which agrees with other investigations in rivers without groynes. The corresponding value of the exponent n is about 10, which is a usual value for rivers. Based on the results of other investigators the transverse mixing-coefficient should be about 0.5 or more in case of groynes: a larger value, due to the additional mixing caused by these groynes. However, it has been noticed that relatively small variations of the n -value as well as the α_y -value have large influence on the lag coefficient. Thus, a first estimation for the River Rhine, based on these α_y - and n -values results in overall lag-coefficients for a distance of 20 km of 0.1 till more than 0.5. Therefore, it has to be emphasized that the use of these values without verification by flow-velocity measurements as well as tracer experiments in the river concerned, has to be discouraged, since the prediction of a late arrival-time of a pollution cloud is mostly unacceptable.

The longitudinal dispersion-coefficient K_s has been analyzed roughly. Instead of the coefficient itself the coefficient of proportionality α_x of the semi-empirical expression after Fischer et al. (1979) has been considered for the dead-zone model

$$K_s = \alpha_x \cdot \frac{u_s^2 \cdot B^2}{a \cdot u_x} \cdot (1 + \beta_{dead-zone}^2) \quad (6.8)$$

The α_x -value varies from 0.001 between Basel and Strasbourg, with an averaged value of 0.007 between Strasbourg and Lobith, till about 0.02 for the Dutch Rhine-branches. After Fischer et al. (1979) the semi-empirical value of α_x is 0.011, but can be 4 times smaller and larger. Tracer experiments in the Albert Canal and the Kempen Canals (Belgium) gave values of about ten times smaller, due to the small flow-velocities and therefore relatively uniform flow-velocity profiles over the cross section (Craenenbroeck et al., 1985). Thus it can be concluded that the calibrated values for the canal-reaches between Basel and Strasbourg confirm the values of the Belgium canals, while the values for the river-reaches correspond with those,

found by Fischer et al. (1979). The α_x -values for the Dutch Rhine-branches are twice the semi-empirical value of 0.011. The reason for these relatively large values could be the presence of the groyne-fields along the Rhine branches in the Netherlands. The additional turbulence, they excite as well as their influence on the cross-sectional velocity-profile, can increase the longitudinal dispersion.

LIST OF SYMBOLS

symbol	dimension	definition
A	$[L^2]$	cross-sectional area
A_s	$[L^2]$	cross-sectional area of the main stream
A_b	$[L^2]$	cross-sectional area of the dead zone
a	$[L]$	water depth
a_s	$[L]$	water depth in the main stream
a_b	$[L]$	water depth in the groyne-field
B	$[L]$	river width; width of the main stream
B_1	$[L]$	width of the polluted branch at a confluence
B_y	$[-]$	dimensionless width over which the pollutant has been spread in case of a release at the river bank ($= B_y / B$)
B_b	$[L]$	width of the groyne-field (perpendicular to the flow direction in the main stream)
b_0	$[L]$	river width downstream of a tributary (Fig. 2.2.12 only)
b_s	$[L]$	maximum width of the stagnant zone (i.e. eddy downstream of a tributary)
C	$[L^{1/2} \cdot T^{-1}]$	Chézy-coefficient
c	$[L \cdot T^{-1}]$	transport velocity
$c_{act.}$	$[L \cdot T^{-1}]$	actual transport-velocity
$c_{1,2,3,4}$	$[-]$	coefficients
D_s	$[T^{-1}]$	mass-transfer coefficient for the transport from the main stream into the dead zone
D_b	$[T^{-1}]$	mass-transfer coefficient for the transport from the dead zone into the main stream
D_{bb}	$[T^{-1}]$	mass-transfer coefficient for the bottom dead-zone
D_{bw}	$[T^{-1}]$	mass-transfer coefficient for the wall dead-zone
d	$[L]$	depth of the trapped eddy in the dead zone
d_b	$[L]$	depth of the trapped eddy in the bottom dead-zone
d_w	$[L]$	depth of the trapped eddy in the wall dead-zone
E	$[L \cdot T^{-1}]$	transfer velocity of the pollutant
F	$[M \cdot L^{-2} \cdot T^{-1}]$	mass transport; flux
\mathcal{F}	$[M \cdot L^{-3} \cdot T]$	mass flux per unit of discharge
f	$[-]$	wall roughness after Darcy-Weisbach ($= 8 g / C^2$)
g	$[L \cdot T^{-2}]$	acceleration due to gravity
G_t	$[-]$	skewness coefficient
$H_3(\tau)$	$[-]$	$H_3(\tau) = \tau^3 - 3 \cdot \tau$ (third Hermite-polynomial)
$H_4(\tau)$	$[-]$	$H_4(\tau) = \tau^4 - 6 \cdot \tau^2 + 3$ (fourth Hermite-polynomial)
$H_6(\tau)$	$[-]$	$H_6(\tau) = \tau^6 - 15 \cdot \tau^4 + 45 \cdot \tau^2 - 15$ (sixth Hermite-polynomial)

i	[-]	energy gradient
i_b	[-]	mean slope of bottom; slope of the energy gradient, which is equal to the bottom slope in case of uniform flow-conditions
K	$[L^2 \cdot T^{-1}]$	one-dimensional longitudinal dispersion-coefficient
K_s	$[L^2 \cdot T^{-1}]$	one-dimensional longitudinal dispersion-coefficient for the dead-zone model
K_x	$[L^2 \cdot T^{-1}]$	dispersion coefficient in x -direction
K_y	$[L^2 \cdot T^{-1}]$	dispersion coeff. in y -direction; transversal dispersion-coefficient
K_{xs}	$[L^2 \cdot T^{-1}]$	dispersion coeff. in the main stream in the x -direction
K_{ys}	$[L^2 \cdot T^{-1}]$	dispersion coeff. in the main stream in the y -direction
K_{zs}	$[L^2 \cdot T^{-1}]$	dispersion coeff. in the main stream in the z -direction
k	$[T^{-1}]$	decay coefficient
k_N	[L]	equivalent sand roughness after Nikuradse
L	[L]	distance; distance from point of release; length of a river branch (around an island)
L_a	[L]	length of adaptation of the actual lag-coefficient to the dead-zone parameter
L_b	[L]	length of groyne-field (distance in flow direction between two successive groynes)
L_m	[L]	transverse mixing distance
L_s	[L]	length of stagnant zone (i.e eddy downstream of a tributary)
M	[M]	mass of an instantaneous release; measured flux
m_0	$[M \cdot L^{-3} \cdot T]$	zeroth moment of concentration distribution
n	[-]	exponent of the exponential velocity-profile
Pe	[-]	Péclet number
P_s	[L]	wetted perimeter
p	[-]	dimensionless parameter defined by
		$p = 2D_b \sqrt{\beta \cdot (x/u_s) \cdot [t - (x/u_s)]}$
Q	$[L^3 \cdot T^{-1}]$	discharge
R	[L]	hydraulic radius
s	$[T^{-1}]$	Laplace variable
T	[T]	travel time; flow time
T_u	[T]	travel time related to the flow velocity
T_c	[T]	travel time related to the transport velocity of the dissolved substance
T_d	[T]	deviation of the measured travel time from the calculated one, related to the measured travel time
t	[T]	time
t_c	[T]	truncation time of the tail of a concentration distribution
t_{max}	[T]	time corresponding with the maximum concentration

u	$[L \cdot T^{-1}]$	mean flow-velocity
$u(y)$	$[L \cdot T^{-1}]$	flow velocity in x -direction as a function of y
u_s	$[L \cdot T^{-1}]$	mean flow-velocity in the main stream
u_c	$[L \cdot T^{-1}]$	mean flow-velocity in the middle of the main stream
u_b	$[L \cdot T^{-1}]$	net flow in the dead zone; mean flow-velocity in the slow-moving zone
u_w	$[L \cdot T^{-1}]$	average velocity in the vicinity of the walls
u_n	$[L \cdot T^{-1}]$	average velocity in a eddy
u_*	$[L \cdot T^{-1}]$	shear velocity $(= \sqrt{(g a i_b)} = u_s \sqrt{(g)/C})$
W	$[M \cdot T^{-1}]$	mass of a constant release
X	$[-]$	dimensionless distance defined by $X = x/L_m$
x	$[L]$	coordinate in flow direction
x'	$[-]$	dimensionless distance defined by $x' = x \cdot K_y / u_s \cdot B^2$
$x_{0,1}$	$[L]$	distance
y	$[L]$	coordinate in transversal direction
y'	$[-]$	dimensionless position in the cross section $y' = y/B$
z	$[L]$	vertical coordinate
α_s	$[-]$	constant of proportionality in relation to the contact area between main stream and dead zone ($0 < \alpha_s < 1$)
α_x	$[-]$	coeff. of proportionality, concerning the longitudinal dispersion-coefficient
$\overline{\alpha_x}$	$[-]$	overall value of α_x from the point of release downstream to the distance concerned
$(\alpha_x)_m$	$[-]$	mean α_x -value over the distance between two successive measuring-stations
$(\alpha_x)_{n_m}$	$[-]$	overall value of α_x from the point of release downstream to the measuring station concerned
α_y	$[-]$	transverse mixing-coefficient
β	$[-]$	lag coefficient; dead-zone parameter
$\overline{\beta}, \beta_{overall}$	$[-]$	overall value of β from the point of release downstream to the distance concerned
β_{local}	$[-]$	local value of β
β_m	$[-]$	mean lag-coefficient β over the distance between two successive measuring-stations
β_{n_m}	$[-]$	overall lag-coefficient β from the point of release downstream to the measuring station concerned
$\beta_{act.}$	$[-]$	actual lag-coefficient
β_{15}	$[-]$	mean value of the lag coefficient over a distance corresponding with $Pe = 15$
Γ	$[-]$	dimensionless parameter defined by $\Gamma = (s/D_b + 1)^{-1}$
Γ_t	$[-]$	kurtosis of the concentration distribution in the time domain

Δh_1	[L]	velocity head
Δh_2	[L]	loss of energy head
Δt	[T]	time step in the description of the numerical model
Δx	[L]	space step in the description of the numerical model
$\delta(x)$	[-]	Diracdelta-function
\mathcal{E}	[-]	dimensionless mass-transfer parameter ($= D_b \cdot K_s / u_s^2$)
Θ	[-]	rate of loss of matter over the distance between two successive measuring-stations
κ	[-]	ratio of actual lag-coefficient and the dead-zone parameter
κ_{15}	[-]	mean value of κ over a distance corresponding with $Pe = 15$
Λ	[-]	parameter in the description of the numerical model after $\Lambda = 1 + (D_s + D_b) \cdot \Delta t$
μ_t	[T]	time-centroid of the concentration distribution
σ	[-]	mean deviation of measured and calculated concentrations
σ_t	[T]	standard deviation of the concentration distribution in the time domain
σ_{T_u}	[T]	standard deviation of the flow time
σ_{β_m}	[-]	standard deviation of the lag coefficient per river reach between two successive measuring-stations
σ_{κ_m}	[-]	standard deviation of κ_m
σ_{μ_t}	[T]	standard deviation of the time-centroid
τ	[-]	dimensionless parameter, defined by $\tau = (t - \mu_t) / (\sigma_t)$
φ	[M·L ⁻³]	concentration
$\overline{\varphi}$	[M·L ⁻³]	concentration, averaged over the cross section
φ_0	[M·L ⁻³]	concentration, averaged over the cross section after $\varphi_0 = W/Q$; average concentration at the point of release; initial concentration-distribution
$\overline{\overline{\varphi}}$	[M·L ⁻³]	concentration, averaged over the cross section after $\overline{\overline{\varphi}} = M / (A_s \cdot u_s)$
φ_s	[M·L ⁻³]	concentration in the main stream
φ_b	[M·L ⁻³]	concentration in the dead zone
φ_{sz}	[M·L ⁻³]	average concentration in the flow zone just above the bottom with dead zones
φ_{sy}	[M·L ⁻³]	average concentration in the flow zone just aside of the walls with dead zones
\mathfrak{R}	[-]	dimensionless decay-parameter defined by $\mathfrak{R} = K_s \cdot k / u_s^2$

super-/subscripts

1	main-stream branch; fast-flowing zone
2	by-pass branch; slow-flowing zone
s	main stream; fast-flowing zone
b	dead zone; slow-flowing zone
i	number of the (sub-)branch; river reach; space step
i	number of the time step in the description of the numerical dead-zone model
j	number of the concerned series of (sub-)branches or river reaches i , counting from the point of release
j	number of the space step in the description of the numerical dead-zone model
m	number of the river reach between two successive measuring-stations; indication of the downstream boundary of the river reach m
m	total number of time steps in the description of the numerical dead-zone model
n	number of the concerned series of (sub-)branches; river reaches or space steps i
n_m	number of the considered series of river reaches m , while n indicates the concerned (sub-)branches or parts of (sub-) branches i , counting from the point of release
n	total number of space steps in the description of the numerical dead-zone model

REFERENCES

- Abramowitz, M. and I.A. Stegun (1965), *Handbook of mathematical functions*, Dover Public. Inc., New York
- Aris, R. (1956), On the dispersion of a solute in a fluid flowing through a tube, Proc. Royal Society, London, England, Vol. 235, Series A, pp. 67...77
- Craenenbroeck, W. van, J. Marivoet and P. Stas (1985), Watermanagement and dispersion in the Albert Canal and the Kempen Canals (in Dutch), Free University of Brussels, Hydrological Department, report nr. 11, 1985
- Beer T. and P.C. Young (1983), Longitudinal Dispersion in Natural Streams, Proc. ASCE J. Envir. Engrg. Vol. 109, No. 5, pp 1049...1067
- Becker, A. and P. Sosnowski (1969)
An impulse response for the prediction of the river discharge in case of a flood wave (in German), Wasserwirtschaft - Wassertechnik, 19. Volume, No. 12, pp 410...418
- Best, J. L. and I. Reid (1984), Separation zone at open-channel junctions, Proc. ASCE J. Hydraul. Eng. Vol 110 HY11, pp.1588...1594
- Best, J.L. (1987), Flow dynamics at river channel confluences: implications for sediment transport and bed morphology. In: recent developments in Fluvial Sedimentology (Ed. by F.G. Ethridge, R.M. Flores and M.D. Harvey) Spec. Publs Soc. econ. Paleont. Miner. Tulsa, 39, pp. 27...35
- Bremicker, M. (1989), Method for the analysis and simulation of transport of dissolved matter in rivers (in German), MSc-thesis at Albert-Ludwigs-University Freiburg, Institute of Physical Geography, Chair of Hydrology, Freiburg i.Br (1989)
- Buck, W., K.Felkel, H.Gerhard, H.Kalweit, J.van Malde, K.-R.Nippes,B.Ploeger, W.Schmitz (1993), The Rhine under the influence of man - river engineering works, shipping, water management - (in German), CHR Committee "Anthropogenic influences on the discharge regime", Report Nr. I-11 of the CHR, Secretariat CHR, Lelystad
- Chatwin P.C. (1980), Presentation of Longitudinal Dispersion Data, Proc. ASCE J. Hydr. Div. Vol. 106, HY1, pp. 71...83
- Chikwendu, S.C. and G.V. Ojiakor (1985), Slow-zone model for longitudinal dispersion in two-dimensional shear flows J. Fluid Mech. Vol.152, pp. 15...38
- Delft Hydraulics & Ministry of Transport, Public Works and Watermanagement (1995), SOBEK 1.0 - User's Guide -, Version 1.00, January 1995
- Fischer, H.B., E.J.List, R.C.Y.Koh, J.Imberger and N.H.Brooks (1979), *Mixing in inland and coastal waters*, Academic press, New York
- Hartley, H.O (1961), Modified Gauss-Newton method for fitting on non-linear regression functions, Technometrics, No. 3, pp. 269...280
- Hays, J.R., P.A. Krenkel and K.B. Schnelle (1966), Mass transport mechanisms in open-channel flow, Report, 138 pp., Dep. of Civil Eng., Vanderbilt Univ., Nashville, Tenn.

- Holley, E.R. (1971), Transverse mixing in rivers. Report on analytical, laboratory and field studies for non-buoyant substances, Delft Hydraulics Laboratory, S 132, Delft, December 1971
- Holley, E.R. and G. Abraham (1973), Field tests on transverse mixing in rivers, J. Hydraul. Div., Proc. ASCE, Vol. 99, No. HY 12, December 1973, pp. 2313...2331
- International Commission for the Hydrology of the Rhine Basin (CHR) (1993), The Rhine under the influence of man - river engineering works, shipping, water management - (in German), CHR-working group "Anthropogenic Influences on the discharge regime", Report Nr. I-11 of the CHR, Secretariat CHR, Lelystad
- Jennrich, R.I. and P.F. Sampson (1968), Application of stepwise regression to non-linear least squares estimation, Technometrics, No. 10, pp. 63...72
- Kranenburg C. (1988), personal communication
- Kendall, M.G. and A. Stuart (1958), The Advanced Theory of Statistics, Vol. 1, Griffin, London, England
- Krenkel, P.A. (1962), Waste Dispersion characteristics of streams using turbulent diffusion phenomenon, Journal WPCF, Vol.34, No.12, pp. 1203...1212, Dec. 1962
- Kuik, C.A. and A. van Mazijk (1994), Analysis of the transport of a pollution cloud in the Upper-Rhine River between Lake of Constance and Basel, Communications on Hydraulic and geotechnical engineering, Delft University of Technology, Faculty of Civil Engineering, May 1994
- Lean, G.H. and T.J. Weare (1979), Modelling Two-Dimensional Circulating Flow, J. Hydraul. Div., Proc. ASCE, Vol. 105, No. HY 1, January 1979, pp. 17...26
- Mazijk, A. van (1984), Dispersion in rivers (in Dutch), Delft University of Technology, Faculty of Civil Engineering, Report no. 16-83, Delft, January 1984
- Mazijk, A. van (1987), Dispersion in the River Rhine and its consequences for the policy in water management (in German), 11th Symposium of the IAWR, 1987, Secretariat of the IAWR, Amsterdam
- Mazijk, A. van, P. Verwoerd, J. van Mierlo, M. Bremicker and H. Wiesner (1991), Alarm model 'Rhine' version 2.0, Calibration and Verification (in German), IRC/CHR Committee of experts, Report Nr. II-4 of the CHR, Secretariat CHR, Lelystad
- Mazijk, A. van, P. Verwoerd and J. van Mierlo (1991), Calibration of the Rhine Alarm-Model, based on the tracer experiment 04/89 Village Neuf - Netherlands (in German), Delft University of Technology, Faculty of Civil Engineering and Ministry of Transport, Public Works and Watermanagement, Institute for Inland Water Management and Waste Water Treatment, Lelystad, March 1991

- Mazijk, A. van, J. van Mierlo and H. Wiesner (1991),
Verification of the Rhine Alarm-Model, Version 2.0 (in German), Delft University of Technology, Faculty of Civil Engineering, and Albert-Ludwigs-University Freiburg, Institute of Physical Geography, June 1991
- Mazijk, A. van & J.C.M. van Mierlo (1992), Checking of the calibration of the Rhine Alarm-Model, Version 2.1, based on the tracer experiment 04/89 Village Neuf - Netherlands (in German), Delft University of Technology, Faculty of Civil Engineering, and Albert-Ludwigs-University Freiburg, Institute of Physical Geography, Dec. 1992
- Mazijk, A. van, H.Th. Reitsma and S. Wuijts (1992), Improvement of the determination of the travel time on the river reach Lobith - Hagestein (the Netherlands) of the River Rhine (in Dutch), Association of the Rhine and Meuse Water Supply Companies (RIWA) and Delft University of Technology - Faculty of Civil Engineering, Secretariat of the RIWA, P.O.Box 8169, 1005 AD Amsterdam, June 1992
- Mazijk, A. van & S. Wuijts (1995), Prediction of the travel time of the pollutant cloud between Lobith and Hagestein (the Netherlands) on the River Rhine (in Dutch), *H₂O* (28) 1995, nr. 11, pp. 320...323
- Mierlo, J.M.C. (1993), Control Analysis of the calibration of the Rhine Alarm-Model (in German), MSc-thesis at Albert-Ludwigs-University Freiburg, Institute of Physical Geography, Chair of Hydrology, Freiburg i.Br (1993)
- Ministry of Transport, Public Works and Watermanagement (1986), Dutch Report on the Sandoz-spill (in Dutch), Report D.B.W./RIZA 86-53, Institute for Inland Water Management and Waste Water Treatment, Lelystad, December 1986
- Noppene, R.M. (1988), Sensitivity analysis Rhine Alarm-Model - The transverse mixing reach downstream of confluences (in Dutch), Communications on sanitary engineering and water management No. 20, Delft University of Technology - Faculty of Civil Engineering
- Nordin, C. F., Jr. and G.V. Sabol (1974), Empirical data on longitudinal dispersion in rivers, United States Department of the Interior, U.S. Geological Survey, Water-Resources Investigations 20-74, U.S. Geological Survey, Building 25, Denver Federal Center, Lakewood, Colorado 80225, August 1974
- Nordin C.F. and B.M. Troutman (1980), Longitudinal Dispersion in rivers: the persistence of skewness in observed data, *Wat. Resour. Res.* Vol. 16, No.1, pp. 123...128
- Ralston, M.L. and R.I. Jennrich (1978), DUD, a derivative-free algorithm for non-linear least squares, *Technometrics*, Vol. 20, No. 1, February 1978, pp. 7...14
- Reichert P. and O. Wanner (1987), Simulation of a severe case of pollution of the Rhine river, Paper presented at IAHR-Congress, Lausanne

- Reichert P. and O. Wanner (1991), Enhanced one-dimensional modelling of transport in rivers, Proc. ASCE J. Hydraul. Eng. Vol. 117 HY9, pp. 1165...1183
- Spreafico, M. and A. van Mazijk (ed.) (1993), Alarm model Rhine, A model for the operational prediction of the transport of pollutants in the River Rhine (in German), IRC/CHR Committee of experts, Report Nr. I-12 of the CHR, Secretariat CHR, Lelystad
- Taylor, G.I. (1953), Dispersion of soluble matter in solvent flowing slowly through a tube, Proc. R. Soc. London Ser. A 219, pp. 186...203
- Taylor, G.I. (1954), The dispersion of matter in turbulent flow through a pipe, Proc. R. Society London Ser. A 223, pp. 446...468
- Thackston E.L and K.B. Schnelle (1970), Predicting effects of dead zones on stream mixing, Proc. ASCE Sanit. Engrg. Div. Vol. 96 SA2, pp 319...331.
- Veling, E.J.M. (1996), personal communication
- Valentine E.M. and I.R. Wood (1977), Longitudinal Dispersion with Dead Zones, Proc. ASCE J. Hydr. Div. Vol. 103 HY9, pp. 975...990
- Valentine E.M. and I.R. Wood (1979), Experiments in Longitudinal Dispersion with Dead Zones, Proc. ASCE J. Hydr. Div. Vol. 105 HY8, pp. 999...1016
- Vreugdenhil, C.B. (1989), *Computational Hydraulics, An Introduction*, Springer-Verlag, Berlin 1989
- Wang (1989), Mathematical modelling of morphological processes in estuaries, PhD-Thesis, Delft University of Technology, Faculty of Civil Engrg, Communications on Hydraulic and geotechnical engineering, Report No. 89-1
- Yotsukura, Nobuhiro, H.B. Fischer and W.W. Sayre (1970), Measurements of mixing characteristics of the Missouri River between Sioux City, Iowa and Plattsmouth, Nebraska: U.S. Geol. Survey Water-Supply Paper 1899-G

ACKNOWLEDGEMENTS

This doctoral thesis is the result of the writer's research on transport phenomena in rivers during the last ten years. Since 1987 the main goal of this research was the further development and improvement of the Rhine Alarm-Model in the framework of the 'Rhine' plan of action, which was initiated December 1986 at the conference of Ministers from the Rhine riparian states after the blaze at the Sandoz AG chemical factory at Basel in 1986. It was Professor J.H. Kop who roused in 1991 my interest in writing a doctoral thesis on this subject.

The writer wishes to express his deep gratitude to Professor M. de Vries for acting as thesis advisor. His inspiring support with respect to the content of the thesis as well as to the organizational aspects, has been effected that beside the teaching and managerial tasks, the thesis could be realised within a period of about four years. It was Professor J.B.M. Wiggers finally, who made this possible by offering five sabbatical months to finish the job.

Many thanks to Dr. Z.B. Wang of the Delft University of Technology and Delft Hydraulics, for his critical reading of the thesis, especially the mathematical descriptions.

A special thank to Mr. J.F.X. Urbanus of the Watercompany Europoort, who wrote the computer program for the numerical dead-zone model. For additional wishes he always was willing to include them as soon as possible.

The International Rhine Commission (IRC) and the international Commission for the Hydrology of the Rhine basin (CHR), represented by Dr. M. Spreafico, chairman of the joint IRC and CHR committee of experts, which was charged with the development, calibration and verification of the Rhine Alarm-Model, and Dr. F.H.M. van de Ven, former secretary of the CHR are acknowledged for the availability of the Rhine Alarm-Model as well as the results of the tracer experiments, carried out in the period of 1989 till 1991.

Further I should like to acknowledge Mr. E.H. van Velzen of the Institute for Inland Water Management and Waste Water Treatment (RIZA) of the Ministry of Transport, Public Works and Watermanagement, for his collecting of the data of the dead zones along the Dutch Rhine-branches, which made the comparison of theoretical results with the tracer experiments possible.

Delft Hydraulics is acknowledged for the availability of the DUD-program, which was very useful for the optimizing of several parameters. Thanks to Dr. H.F.P. van den Boogaard, who introduced the DUD-program to me.

At last a special thank to my family, that took care for so many various things when I was working on this thesis. In particular to my wife, Gabriele, I owe much gratitude. She offered a lot of the family and social life. She helped me to get through the tough periods.

CURRICULUM VITAE

Albertus van Mazijk, geboren in 1944 te Utrecht, behaalde in 1962 het HBS-B diploma. In datzelfde jaar begon hij aan de vijfjarige opleiding tot Civiel Ingenieur aan de Technische Hogeschool Delft, Afdeling der Weg- en Waterbouwkunde. In 1969 is hij afgestudeerd op het ontwerp van een stalen hangdakconstructie voor een IJstadion met deelontwerpen op het gebied van de grondmechanica en de spoorweg bovenbouw. Tijdens zijn studie is hij studentassistent geweest bij de Vakgroepen "Grondmechanica" en "Verkeerskunde, Spoorwegbouwkunde en Railverkeers-techniek". In deze periode heeft hij stage gelopen bij de Nederlandsche Spoorwegen (Spoorwegtunnel Schiphol), Soil Mechanics Laboratory, British Railway Board, Engineering Research Laboratories in Derby (Engeland) en bij de Technische Universität München, Afd. Civiele Techniek, Onderafdeling Spoorwegen.

In juli 1969 is hij begonnen als Projectingenieur bij het Waterloopkundig Laboratorium Delft, Afd. Dichtheidsstromen. Fundamenteel onderzoek op het gebied van de zoutpenetratie in getijrivieren, gericht op de situatie in de Nieuwe Waterweg vormde zijn hoofdtak. In september 1974 trad hij in dienst bij de Rijkswaterstaat in Maastricht: eerst bij de Directie Limburg, Afd. Rivierkunde als stafingenieur en vanaf oktober 1975 als hoofd van de Afdeling Maas van het District Zuidoost van de Directie Waterhuishouding en Waterbeweging. Zijn activiteiten lagen in deze periode met name op het gebied van de hoogwaterproblematiek van de Maas, de koelwatercapaciteit van de Maas en haar grindgaten en de hydrologie van de Limburgse en Noord-Brabantse kanalen. In 1979 werd hij overgeplaatst naar de Deltadienst, Afdeling Waterbouwkundige Werken West te Burghsluis, die belast was met het ontwerp en de uitvoering van de Stormvloedkering in de Oosterschelde. Hier beklede hij de functie van hoofd van de onderafdeling "Ontwikkeling Nieuwe Werkmethoden". Een belangrijk aandachtsgebied vormde de bodem- en oever-beschermingsconstructies en het ontwerp van de drempel in de Stormvloedkering.

In oktober 1980 kreeg hij een aanstelling bij de toen nog geheten Technische Hogeschool in Delft, Afdeling Civiele Techniek, Vakgroep Vloeistofmechanica als Wetenschappelijk Hoofdmedewerker. Naast het basisonderwijs vloeistofmechanica is hij in deze periode begonnen met het onderzoek op het gebied van de dispersie in rivieren in samenwerking met de Werkgroep Hydrologie van de RIWA (Samenwerkende Rijn- en Maaswaterleidingbedrijven). In september 1984 kwam hij bij de Vakgroep Civiele Gezondheidstechniek, die kort daarop in het kader van een reorganisatie samenging met de Vakgroep Hydrologie & Waterhuishouding en thans bekend staat onder de naam Vakgroep Waterbeheer, Milieu- & Gezondheidstechniek. Binnen deze Vakgroep behoorde hij tot de Sectie Gezondheidstechniek. Werkzaam als Universitair Hoofddocent heeft hij met name het onderwijs verzorgd op het gebied van de "winning, transport en distributie van drinkwater" en de

"modellering van de waterkwaliteit van oppervlaktewater", terwijl het onderzoek "dispersie in rivieren" zich ging concentreren op het ontwikkelen van stoftransport modellen: calamiteitenmodellen en representativiteit van waterkwaliteitsmeetpunten langs rivieren. Daarbij was er een nauwe samenwerking met zowel de RIWA als de Rijkswaterstaat en in het verlengde daarvan met de Internationale Rijncommissie (IRC). Centraal stond naast de ontwikkeling van het één-dimensionale Maascalamiteitenmodel en het twee-dimensionale Calamiteitenmodel voor het IJsselmeer, het Rijnalarmmodel. Met betrekking tot het laatste is hij gastlid geweest van de IRC/CHR comité van deskundigen, die belast was namens de Internationale Rijncommissie (IRC) en Internationale Commissie voor de Hydrologie van de Rijn (CHR) met de verdere ontwikkeling, calibratie en evaluatie van het Rijnalarmmodel. Tijdens deze activiteiten heeft hij een nauwe samenwerking opgebouwd met de Albert-Ludwigs-Universität, Professur für Hydrologie te Freiburg.

Vanuit zijn onderwijstaak met betrekking tot het transport van drinkwater heeft hij nauwe banden met het Keuringsinstituut van Waterleidingartikelen (KIWA) te Nieuwegein.

Tussen 1984 en 1987 is hij betrokken geweest bij een viertal postacademiale cursussen: Vloeistofmechanica voor de waterleidingingenieur, Transportverschijnselen in Grond- en Oppervlaktewater, Waterkwaliteit en Waterkwaliteitsbeheer. Bij de laatste twee was hij cursusleider.

Appendices

Appendix A

Linear spreading method

The solution of the convection-diffusion equation for a continuous release at a river bank can be given by

$$\frac{\varphi(x', y')}{\varphi_0} = \frac{1}{\sqrt{\pi \cdot x'}} \sum_{n=-\infty}^{\infty} \left[\exp \left(- \frac{(y' - 2n)^2}{4x'} \right) \right] \quad (\text{A.1})$$

with

φ_0 average cross-sectional concentration (W/A)

W constant release

A cross-sectional area of the river

B width of the river

and the dimensionless parameters for

the concentration $\varphi(x', y') / \varphi_0$

the longitudinal distance $x' = x \cdot K_y / [u \cdot B^2]$

the transversal distance $y' = y / B$

wherein K_y stands for the transversal dispersion-coefficient.

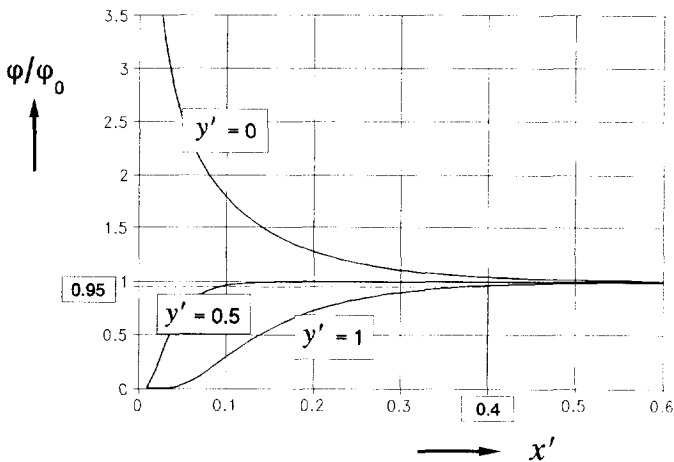


Fig. A.1 Distribution of φ/φ_0 as a function of x' and y' (constant release of a conservative substance at $y' = 0$)

In Fig. A.1 the dimensionless concentration $\varphi(x',y')/\varphi_0$ is presented as a function of the dimensionless distance x' for some dimensionless positions in the cross section y' .

If the completely mixed situation is defined by $\varphi(x',y')/\varphi_0 \geq 0.95$ for $y' = 1$, then the "transverse mixing distance" $x = L_m$ can be derived from Fig. A.1, being the distance over which the released substance is "completely mixed" over the cross section. Because the corresponding dimensionless $x' = 0.4$, the "transverse mixing distance" becomes

$$L_m \approx 0.4 \cdot \frac{u_s \cdot B^2}{K_y} \quad (\text{A.2})$$

Over the transverse mixing reach the transport velocity c will be less than the mean flow velocity u_s due to the velocity distribution over the cross-sectional area of the river (Fig. A.2).

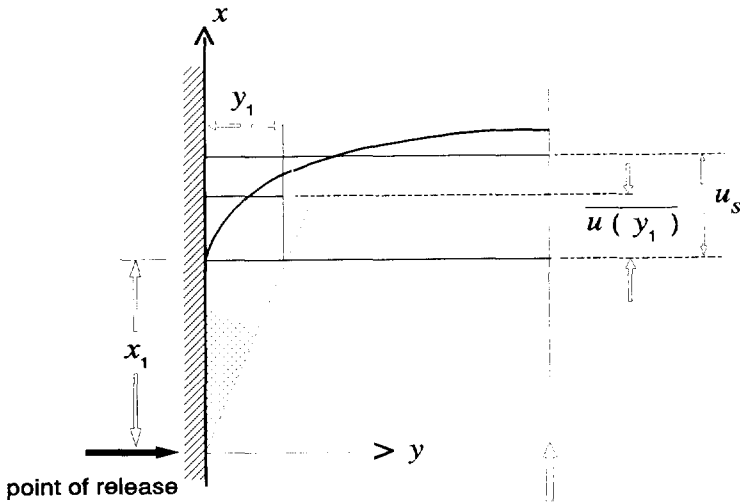


Fig. A.2 Average velocity over the width of the plume of the released substance

In order to formulate a relation between these two velocities, the velocity distribution over the width of the river (depth averaged) is supposed to be symmetrical to the centre of the river and is defined by (for $0 \leq y \leq 0.5 B$)

$$u(y) = \frac{n+1}{n} \cdot \left(\frac{y}{0.5 B} \right)^{1/n} \cdot u_s \quad (\text{A.3})$$

wherein n stands for a constant between 3 and 10, depending on the distribution of the velocity profile in relation to the wall roughness (Fig. A.3).

Because in practice the transport velocity is determined by the travel time of a pollution, the average of the reciprocal value of the velocity has to be considered

$$T_c = \overline{\left(\frac{1}{u(y_1)} \right)} \quad (\text{A.4})$$

with
 T_c travel time per unit of distance.

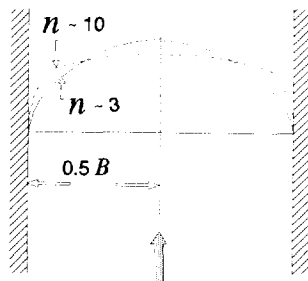


Fig. A.3 Velocity profiles in relation to the n -value

Integration of Eq.(A.3) from 0 to y_1 ($y_1 \leq 0.5 B$) after the relation, given by Eq.(A.4) gives in succession

$$T_c(x) = \frac{1}{c(x)} = \overline{\left(\frac{1}{u(y_1)} \right)} = \frac{1}{y_1} \int_0^{y_1} \frac{1}{u(\psi)} d\psi \quad (\text{A.5})$$

$$\frac{1}{c(x)} = \frac{1}{y_1} \int_0^{y_1} \frac{n}{n+1} \left(\frac{\psi}{0.5B} \right)^{-\frac{1}{n}} \cdot \frac{1}{u_s} d\psi$$

$$\frac{u_s}{c(x)} = \frac{1}{y_1} (0.5 \cdot B)^{\frac{1}{n}} \cdot \frac{n}{n+1} \cdot \frac{n}{n-1} \cdot \left[\psi^{1-\frac{1}{n}} \right]_0^{y_1}$$

$$\frac{u_s}{c(x)} = \frac{n^2}{n^2-1} \left[\frac{0.5 \cdot B}{y_1} \right]^{\frac{1}{n}} \quad (\text{A.6})$$

Assuming a linear transversal spreading of the pollutant with the distance to the point of release and a completely mixed situation over the distance y_1 (see also Fig. 2.2.3 in Section 2.2), the travel time, i.e. the transport velocity at a certain distance x_1 is determined by the average value of $1/u(y)$ over the spreading width y_1 with (Fig. A.2)

$$y_1 = \frac{x_1}{L_m} \cdot B \quad (\text{A.7})$$

thus Eq.(A.6) becomes, dropping the subscript 1

$$\frac{u_s}{c(x)} = \frac{n^2}{n^2 - 1} \left(\frac{0.5 \cdot L_m}{x} \right)^{1/n} \quad (\text{A.8})$$

and with the dimensionless distance $X = x/L_m$

$$\frac{u_s}{c(X)} = \frac{n^2}{n^2 - 1} \cdot (2 \cdot X)^{-\frac{1}{n}} \quad (\text{A.9})$$

Substitution of Eq.(A.9) into the expression for the lag coefficient β

$$\beta = \frac{u_s}{c} - 1 \quad (\text{A.10})$$

gives

$$\beta(X) = \frac{n^2}{n^2 - 1} \cdot (2 \cdot X)^{-1/n} - 1 \quad (\text{A.11})$$

being the local value of β at a distance X from the point of release.

The overall value of the lag coefficient between the point of release and $X = X_1 \leq 0.5$ is found by integration of Eq.(A.11)

$$\begin{aligned} \overline{\beta(X_1)} &= \frac{1}{X_1} \int_0^{X_1} \left[\frac{n^2}{n^2 - 1} \cdot (2 \cdot \xi)^{-1/n} - 1 \right] d\xi \\ &= \frac{n^3}{(n + 1)(n - 1)^2} \cdot (2 \cdot X_1)^{-1/n} - 1 \end{aligned} \quad (\text{A.12})$$

For values of $B \geq y_1 > 0.5 B$ the average travel time T_c becomes with $y_1 = B - y_1'$, while y_1' is the distance from the opposite river-bank.

$$\begin{aligned} T_c &= \frac{1}{c(x)} = \left(\frac{1}{u(y_1)} \right) = \\ &= \frac{n}{n + 1} \cdot \frac{1}{u_s} \cdot \frac{1}{y_1} \cdot \left[2 \cdot \int_0^{0.5 \cdot B} \left(\frac{\Psi}{0.5 B} \right)^{-\frac{1}{n}} d\Psi - \int_0^{y_1'} \left(\frac{\Psi}{0.5 B} \right)^{-\frac{1}{n}} d\Psi \right] \end{aligned} \quad (\text{A.13})$$

which gives in succession

$$\frac{u_s}{c(x)} = \frac{n}{n+1} \cdot \frac{1}{y_1} \cdot (0.5 B)^{\frac{1}{n}} \cdot \left[2 \int_0^{0.5B} \Psi^{-\frac{1}{n}} d\Psi - \int_0^{y_1'} \Psi^{-\frac{1}{n}} d\Psi \right]$$

$$\frac{u_s}{c(x)} = \frac{n^2}{n^2-1} \cdot \frac{1}{y_1} \cdot (0.5 B)^{\frac{1}{n}} \cdot \left(2 \cdot \left[\Psi^{1-\frac{1}{n}} \right]_0^{0.5B} - \left[\Psi^{1-\frac{1}{n}} \right]_0^{y_1'} \right)$$

$$\frac{u_s}{c(x)} = \frac{n^2}{n^2-1} \cdot \frac{1}{y_1} \cdot (0.5 B)^{\frac{1}{n}} \cdot \left(2 \cdot [0.5B]^{1-\frac{1}{n}} - [y_1']^{1-\frac{1}{n}} \right)$$

Substitution of $y_1' = B - y_1$ gives

$$\frac{u_s}{c(x)} = \frac{n^2}{n^2-1} \cdot \frac{1}{y_1} \cdot (0.5 B)^{\frac{1}{n}} \cdot \left[2 - \left(\frac{B-y_1}{0.5B} \right)^{\frac{n-1}{n}} \right] \quad (\text{A.14})$$

Substitution of Eq.(A.7) and applying the dimensionless distance $X = x/L_m$ into Eq.(A.14) yields

$$\frac{u_s}{c(X)} = \frac{n^2}{n^2-1} \cdot \frac{1}{2X} \cdot \left[2 - (2 - 2X)^{\frac{n-1}{n}} \right] \quad (\text{A.15})$$

Applying Eq.(A.10) gives the following expression for the local lag-coefficient

$$\beta(X) = \frac{n^2}{n^2-1} \cdot \frac{1}{2X} \cdot \left[2 - (2 - 2X)^{\frac{n-1}{n}} \right] - 1 \quad (\text{A.16})$$

The overall value of the lag coefficient for $1 \geq X_1 > 0.5$ is found by integration of Eqs (A.11) and (A.16)

$$\begin{aligned} \overline{\beta(X_1)} &= \frac{1}{X_1} \cdot \left(\int_0^{0.5} \left[\frac{n^2}{n^2-1} \cdot (2\xi)^{-\frac{1}{n}} - 1 \right] d\xi \right) + \\ &+ \frac{1}{X_1} \cdot \left(\int_{0.5}^{X_1} \left[\frac{n^2}{n^2-1} \cdot \frac{1}{2\xi} \cdot \left[2 - (2 - 2\xi)^{\frac{n-1}{n}} \right] - 1 \right] d\xi \right) \end{aligned} \quad (\text{A.17})$$

Because the second term at the right part of Eq.(A.17) cannot be solved analytically, it can be done numerically with steps $\Delta X = 0.01$.

$$\begin{aligned} \overline{\beta}(X_1) = & \frac{1}{X_1} \cdot \left(0.5 \left[\frac{n^3}{(n+1)(n-1)^2} - 1 \right] \right) + \\ & + \frac{1}{X_1} \cdot \left(\int_{0.5}^{x_1} \left[\frac{n^2}{n^2-1} \cdot \frac{1}{2\xi} \cdot \left[2 - (2 - 2\xi)^{\frac{n-1}{n}} \right] - 1 \right] d\xi \right) \end{aligned} \quad (\text{A.18})$$

In Fig. A.4 the expression for $\overline{\beta}(X_1)$ according to Eqs (A.12) and (A.18), is presented graphically.

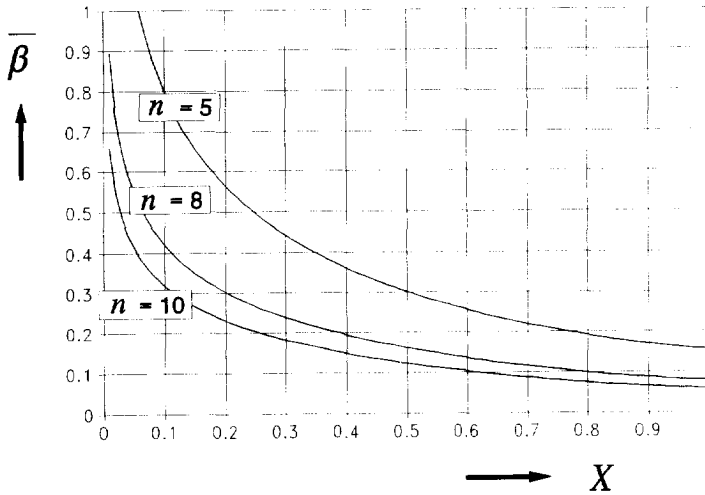


Fig. A.4 Effect of the velocity distribution on the travel time, i.e. the transport velocity

Appendix B

Influence of islands on the lag coefficient

An island in a river can be regarded as a bifurcation and a confluence connected by two branches with different geometry. This difference in geometry will cause a difference in the magnitude of the mean flow-velocity, which will give additional dispersion. For the estimation of this effect on the lag coefficient β , i.e. the transport time of a pollutant, passing an island the *flux method* is applied. Backwater effects as well as differences in longitudinal dispersion-coefficients and two-dimensional effects of both bifurcation and confluence are neglected.

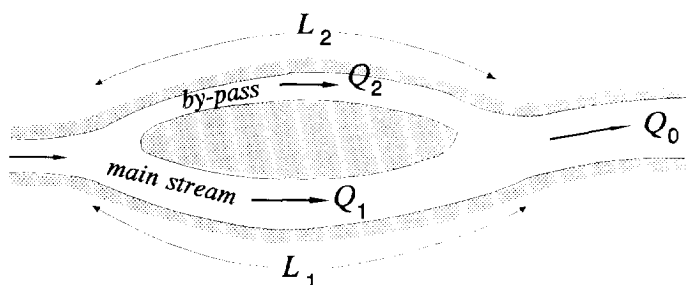


Fig. B.1 Schematization of an island in a river

When the pollutant is completely mixed over the cross-sectional area of the river at the upstream end of the island, i.e. the concentration distribution over the cross section is homogeneous, the mass will distribute over the branches in the same ratio as the discharges. The average travel-time of the pollutant T_c from the upstream end of the island to the downstream end can be given by

$$T_c = \frac{T_{c1} \cdot M_1 + T_{c2} \cdot M_2}{M_1 + M_2} = \frac{Q_1 \cdot \frac{L_1}{u_1} + Q_2 \cdot \frac{L_2}{u_2}}{Q_1 + Q_2} \quad (\text{B.1})$$

wherein

T_c = travel time
 M = mass, passing the branch

Q = discharge of the branch
 L = length of the branch
 u = mean flow-velocity in the branch
 index 1: main-stream branch
 index 2: by-pass branch

The "time of arrival" of the water is determined by the mean flow-velocity over the total area of the two branches (*flow time*), with a correction to counteract for the difference in length

$$T_u = \frac{L_1}{\left(\frac{u_1 \cdot A_1 + u_2 \cdot A_2 \cdot \frac{L_1}{L_2}}{A_1 + A_2} \right)} = \frac{L_1}{\left(\frac{Q_1 + Q_2 \cdot \frac{L_1}{L_2}}{\frac{Q_1}{u_1} + \frac{Q_2}{u_2}} \right)} \quad (\text{B.2})$$

The lag coefficient β can be found by

$$\beta = \frac{T_c}{T_u} - 1 \quad (\text{B.3})$$

Substitution of Eqs (B.1) and (B.2) into Eq.(B.3) yields

$$\beta = \frac{\left(1 + \frac{A_2 \cdot L_2}{A_1 \cdot L_1} \right)}{1 + \frac{Q_2}{Q_1}} \cdot \frac{\left(1 + \frac{Q_2 \cdot L_1}{Q_1 \cdot L_2} \right)}{1 + \frac{A_2}{A_1}} - 1 \quad (\text{B.4})$$

The relation between the discharge ratio Q_2/Q_1 and the ratio of the cross-sectional areas of the branches (A_2/A_1) is determined by applying the Chézy-formula on both branches, assuming the flow is uniform

$$Q = C \cdot A \cdot R^{1/2} \cdot i^{1/2} \quad (\text{B.5})$$

with

C = Chézy-coefficient
 R = hydraulic radius
 i = energy gradient

Assuming that the water depth a in both branches is relatively small in relation to the width B , the hydraulic radius R can be approximated by the water depth

$$R = \frac{B \cdot a}{B + 2a} \approx a \quad (\text{B.6})$$

The ratio of the equilibrium discharges according to Chézy yields

$$\frac{Q_1}{Q_2} = \frac{C_1 \cdot A_1 \cdot a_1^{1/2} \cdot i_1^{1/2}}{C_2 \cdot A_2 \cdot a_2^{1/2} \cdot i_2^{1/2}} \quad (\text{B.7})$$

Equation (B.7) can be simplified by the assumption that the water depths as well as the Chézy-coefficients in the branches do not differ significantly

$$\frac{Q_1}{Q_2} \approx \frac{A_1 \cdot i_1^{1/2}}{A_2 \cdot i_2^{1/2}} \quad (\text{B.8})$$

Because the head over both branches is equal, Eq.(B.8) can be rewritten by

$$\frac{Q_1}{Q_2} \approx \frac{A_1 \cdot L_2^{1/2}}{A_2 \cdot L_1^{1/2}} \quad (\text{B.9})$$

Thus the ratio of the cross-sectional areas of the branches becomes

$$\frac{A_2}{A_1} \approx \frac{Q_2 \cdot L_2^{1/2}}{Q_1 \cdot L_1^{1/2}} \quad (\text{B.10})$$

Substitution of Eq.(B.9) into Eq.(B.4) gives

$$\beta = \frac{\left(1 + \frac{Q_2}{Q_1} \cdot \left[\frac{L_2}{L_1}\right]^{1.5}\right) \cdot \left(1 + \frac{Q_2}{Q_1} \cdot \frac{L_1}{L_2}\right)}{\left(1 + \frac{Q_2}{Q_1}\right) \cdot \left(1 + \frac{Q_2}{Q_1} \cdot \left[\frac{L_2}{L_1}\right]^{0.5}\right)} - 1 \quad (\text{B.11})$$

In case the flow time T_u is based on the flow velocity in the main stream

$$T_u = \frac{L_1}{u_1} \quad (\text{B.12})$$

Thus Eq.(B.4) becomes

$$\beta = \frac{\left(1 + \frac{Q_2}{Q_1} \cdot \frac{L_2}{L_1} \cdot \frac{u_1}{u_2}\right)}{\left(1 + \frac{Q_2}{Q_1}\right)} - 1 = \frac{\left(1 + \frac{A_2}{A_1} \cdot \frac{L_2}{L_1}\right)}{\left(1 + \frac{Q_2}{Q_1}\right)} - 1 \quad (\text{B.13})$$

Substitution of Eq.(B.10) into Eq.(B.13) gives

$$\beta = \frac{\left(1 + \frac{Q_2}{Q_1} \cdot \left[\frac{L_2}{L_1}\right]^{1.5}\right)}{\left(1 + \frac{Q_2}{Q_1}\right)} - 1 \quad (\text{B.14})$$

If the difference of the lengths of the branches is not taken into account, Eq.(B.2) becomes

$$T_u = \frac{L_1}{\left(\frac{u_1 \cdot A_1 + u_2 \cdot A_2}{A_1 + A_2}\right)} = \frac{L_1}{\left(\frac{Q_1 + Q_2}{\frac{Q_1}{u_1} + \frac{Q_2}{u_2}}\right)} \quad (\text{B.15})$$

and Eq.(B.4)

$$\beta = \frac{\left(1 + \frac{A_2}{A_1} \cdot \frac{L_2}{L_1}\right)}{1 + \frac{A_2}{A_1}} - 1 \quad (\text{B.16})$$

which gives with Eq.(B.10)

$$\beta = \frac{\left(1 + \frac{Q_2}{Q_1} \cdot \left[\frac{L_2}{L_1}\right]^{1.5}\right)}{\left(1 + \frac{Q_2}{Q_1} \cdot \left[\frac{L_2}{L_1}\right]^{0.5}\right)} - 1 \quad (\text{B.17})$$

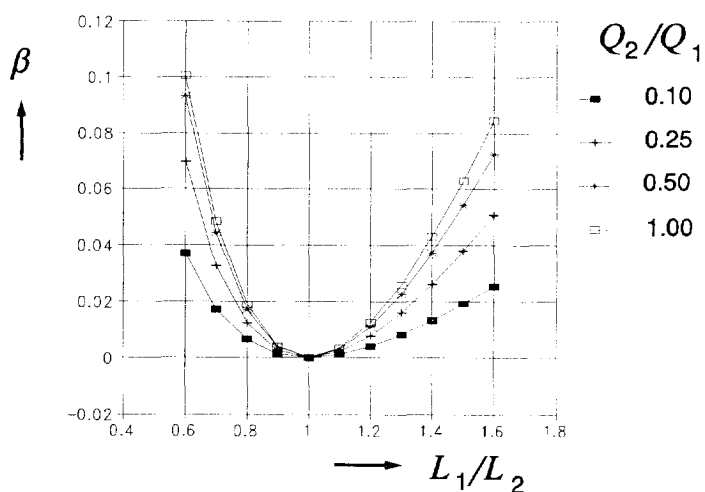


Fig. B.2 Influence of the length ratio of the river branches surrounding an island on the lag coefficient β for several discharge ratios after Eq.(B.11)

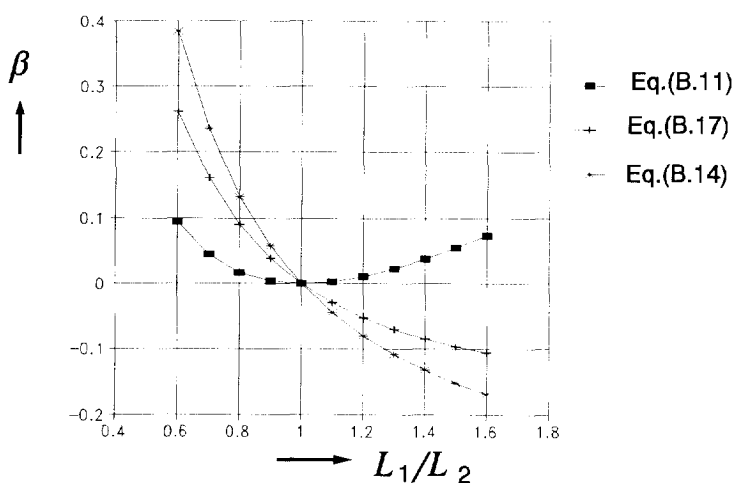


Fig. B.3 Influence of the length ratio of the river branches surrounding an island on the lag coefficient β after Eqs (B.11), (B.14) and (B.17) with a discharge ratio of 0.5

Figure B.2 presents the relation after Eq.(B.11). In Fig. B.3 the relations of the Eqs (B.11), (B.14) and (B.17) are compared for $Q_2/Q_1 = 0.5$. It can be concluded that in all cases the lag coefficient is negligible as long as the difference in lengths of the branches remains small.

Appendix C

Determination of the lag coefficient and the longitudinal dispersion-coefficient in the Rhine Alarm-Model

The calibration of the Rhine Alarm-Model concerns two parameters

- the transport velocity c after

$$c = \frac{u_s}{1 + \beta} \quad (\text{C.1})$$

i.e. *the lag coefficient* β , by which the model flow-time T_u is corrected in order to get a good fit with the measured transport-time T_c of the tracer

$$\beta = \frac{T_c}{T_u} - 1 \quad (\text{C.2})$$

- the longitudinal dispersion-coefficient after Fischer et al. (1979)

$$K = \alpha_x \cdot \frac{u_s^2 \cdot B^2}{a \cdot u_*} \quad (\text{C.3})$$

i.e. *the coefficient of proportionality* α_x in Eq.(C.3).

Because in the model the River Rhine and its tributaries are split up in a number of branches and sub-branches, these parameters have to be determined per river (sub-) branch i .

For the determination of these parameters the moments of the measured concentration-distributions are used:

- for the lag coefficient β , the time-centroid μ_t is considered
- and
- for the dispersion coefficient, i.e. the coefficient of proportionality α_x the variance in the time domain σ_t^2

Because the time-centroid as well as the variance of the concentration distributions concerned, are related to the release time of the tracer. Consequently the values of β and α_x based on these parameters concern the river reaches from the point of release to the considered measuring-point. For the calibration of the Rhine Alarm-Model these overall values (subscript j) have to be related to the values per river (sub-)branch (subscript i).

The lag coefficient

In terms of overall values Eq.(C.1) becomes

$$c_j = \frac{u_j}{1 + \beta_j} \quad (\text{C.4})$$

The overall transport-time $(T_c)_j$ from the point of release to the considered measuring-station can be given by

$$(T_c)_j = (\mu_r)_j = \frac{L_j}{c_j} = \sum_{i=1}^j \frac{\Delta x_i}{c_i} = \sum_{i=1}^j \left(\frac{\Delta x_i}{u_i} \cdot (1 + \beta_i) \right) \quad (\text{C.5})$$

with

L_j = overall distance from the point of release to the measuring point

$$L_j = \sum_{i=1}^j \Delta x_i$$

Δx_i = length of the river (sub-)branch i as well as the distance between the point of release or the measuring station and the downstream or upstream boundary of the (sub-)branch concerned

From Eqs (C.4) and (C.5) the following relation can be derived

$$(1 + \beta_j) \cdot \frac{\sum_{i=1}^j \Delta x_i}{u_j} = \sum_{i=1}^j \left(\frac{\Delta x_i}{u_i} \cdot (1 + \beta_i) \right) \quad (\text{C.6})$$

The mean flow-velocity from the point of release to the measuring station, i.e. the overall flow-velocity can be given by

$$u_j = \frac{L_j}{(T_u)_j} = \frac{\sum_{i=1}^j \Delta x_i}{\sum_{i=1}^j \frac{\Delta x_i}{u_i}} \quad (\text{C.7})$$

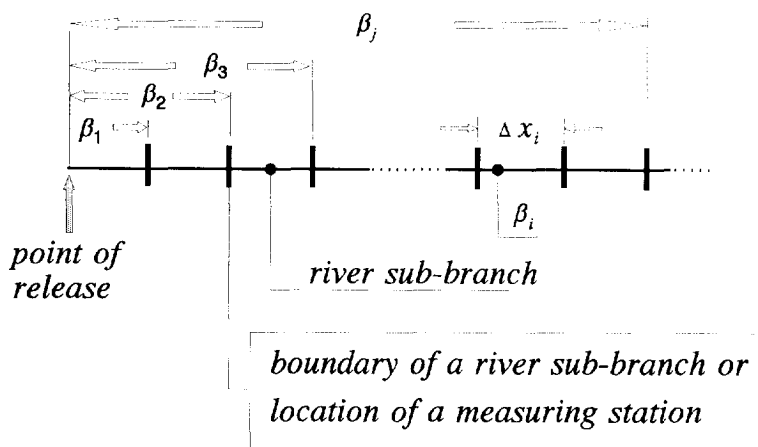


Fig. C.1 Model schematization with sub-branches and the relation between the overall value β_j and the local value β_i per sub-branch

Substitution of Eq.(C.7) into Eq.(C.6) gives the relation between the overall value of the lag coefficient β_j and the local value per (sub-)branch β_i

$$\beta_j \cdot \sum_{i=1}^j \frac{\Delta x_i}{u_i} = \sum_{i=1}^j \left(\frac{\Delta x_i}{u_i} \cdot \beta_i \right) \quad (\text{C.8})$$

Because the overall values for the flow velocity and the transport velocity is defined by

$$u_s = u_j = \frac{L_j}{(T_u)_j} \quad c_j = \frac{L_j}{(T_c)_j} = \frac{L_j}{(\mu_t)_j}$$

the overall value of the lag coefficient can be determined from the measured time-centroid after Eq.(C.4) by

$$\beta_j = \frac{(\mu_t)_j}{(T_u)_j} - 1 = \frac{(\mu_t)_j}{\sum_{i=1}^j \frac{\Delta x_i}{u_i}} - 1 \quad (\text{C.9})$$

In general the measuring stations do not coincide with the boundaries of the river (sub-)branches. Therefore the river reaches between two successive measuring stations are numbered by 1, ..., m and the model (sub-)branches between two successive measuring stations by n_{m-1} , ..., n_m while n indicates the (sub-)branches

concerned, counted from the point of release. Thus Eq.(C.8) can be rewritten into

$$\beta_{n_m} = \frac{\beta_1 \sum_{i=1}^{n_1} \frac{\Delta x_i}{u_i} + \beta_2 \sum_{i=n_1+1}^{n_2} \frac{\Delta x_i}{u_i} + \dots + \beta_m \sum_{i=n_{m-1}+1}^{n_m} \frac{\Delta x_i}{u_i}}{\sum_{i=1}^{n_m} \frac{\Delta x_i}{u_i}} \quad (C.10)$$

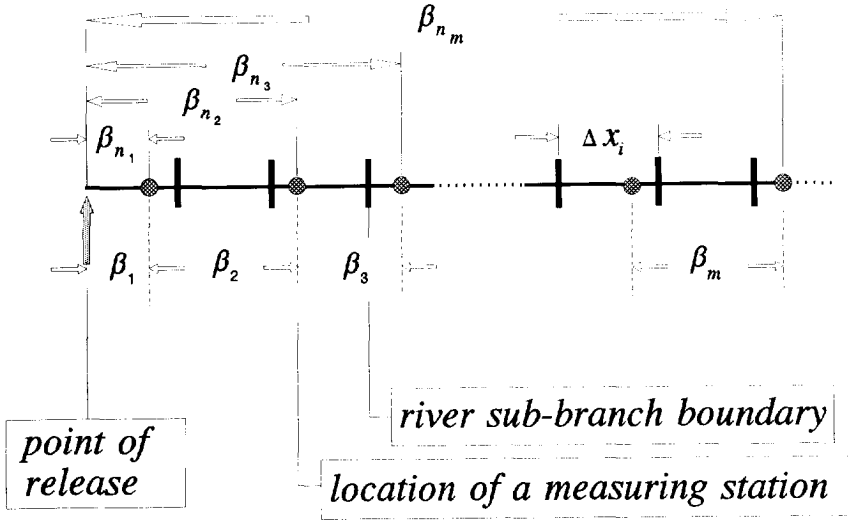


Fig. C.2 Model schematization with sub-branches and the relation between the overall value β_{n_m} and the local value β_m between successive measuring-stations

Starting from the point of release the local lag-coefficients per river reach between two successive measuring stations are determined stepwise (see also Fig. C.2)

$$\beta_1 = \frac{\beta_{n_1} \sum_{i=1}^{n_1} \frac{\Delta x_i}{u_i}}{\sum_{i=1}^{n_1} \frac{\Delta x_i}{u_i}} = \beta_{n_1} \quad (C.11)$$

$$\beta_2 = \frac{\beta_{n_2} \sum_{i=1}^{n_2} \frac{\Delta x_i}{u_i} - \beta_1 \sum_{i=1}^{n_1} \frac{\Delta x_i}{u_i}}{\sum_{i=n_1+1}^{n_2} \frac{\Delta x_i}{u_i}} \quad (C.12)$$

$$\beta_3 = \frac{\beta_{n_3} \sum_{i=1}^{n_3} \frac{\Delta x_i}{u_i} - \left(\beta_1 \sum_{i=1}^{n_1} \frac{\Delta x_i}{u_i} + \beta_2 \sum_{i=n_1+1}^{n_2} \frac{\Delta x_i}{u_i} \right)}{\sum_{i=n_2+1}^{n_3} \frac{\Delta x_i}{u_i}} \quad (C.13)$$

or generally written

$$\beta_m = \frac{\beta_{n_m} \sum_{i=1}^{n_m} \frac{\Delta x_i}{u_i} - \left(\beta_1 \sum_{i=1}^{n_1} \frac{\Delta x_i}{u_i} + \beta_2 \sum_{i=n_1+1}^{n_2} \frac{\Delta x_i}{u_i} + \dots + \beta_{m-1} \sum_{i=n_{m-2}+1}^{n_{m-1}} \frac{\Delta x_i}{u_i} \right)}{\sum_{i=n_{m-1}+1}^{n_m} \frac{\Delta x_i}{u_i}} \quad (C.14)$$

Now the lag coefficients β_i of all the river (sub-)branches between two successive measuring-stations will be equal to β_m .

If the location of the measuring station is between the boundaries of a sub-branch the lag coefficient of this branch ($\beta_{composed}$) is the average value of the lag coefficients of the upstream and downstream river-reach

$$\beta_{composed} \cdot \left(\frac{\Delta x_i}{u_i} + \frac{\Delta x_{i+1}}{u_{i+1}} \right) = \frac{\beta_i \cdot \Delta x_i}{u_i} + \frac{\beta_{i+1} \cdot \Delta x_{i+1}}{u_{i+1}} \quad (C.15)$$

wherein β_i = upstream value of the lag coefficient
 β_{i+1} = downstream value of the lag coefficient

Because the flow velocity in a sub-branch is constant $u_i = u_{i+1} = u$, thus Eq. (C.15) can be simplified by

$$\beta_{composed} = \frac{\beta_i \cdot \frac{\Delta x_i}{u} + \beta_{i+1} \cdot \frac{\Delta x_{i+1}}{u}}{\frac{\Delta x_i + \Delta x_{i+1}}{u}} = \frac{\beta_i \cdot \Delta x_i + \beta_{i+1} \cdot \Delta x_{i+1}}{\Delta x_i + \Delta x_{i+1}} \quad (C.16)$$

The coefficient of proportionality

For the determination of the coefficient of proportionality $(\alpha_x)_i$ per sub-branch the composed longitudinal dispersion-coefficient $\overline{K_s}$ after the Rhine Alarm-Model (van Mazijk et al., 1991) is considered

$$\overline{K_s} = \frac{K}{c^2} \cdot t \quad (C.17)$$

with K is longitudinal dispersion-coefficient after Fischer (1979)

$$K = \alpha_x \cdot \frac{u_s^2 \cdot B^2}{a \cdot u_*} = \alpha_x \cdot \frac{u_s \cdot B^2 \cdot C}{a \sqrt{g}} \quad (C.18)$$

For the determination of the relation between the overall value (subscript $j \rightarrow n_m$) and the local values (subscript i) of the coefficient of proportionality the time t in Eq.(C.17) is substituted by the transport time T_c . It yields

$$(\overline{K_s})_{n_m} = \sum_{i=1}^{n_m} \frac{K_i}{c_i^2} \cdot T_i = \frac{K_{n_m}}{c_{n_m}^2} \cdot T_{n_m} \quad (C.19)$$

wherein T stands for the transport time T_c .

Because $T = T_c = L/c$, Eq.(C.19) becomes

$$\sum_{i=1}^{n_m} \frac{K_i}{c_i^3} \cdot \Delta x_i = \frac{K_{n_m}}{c_{n_m}^3} \cdot L_{n_m} \quad (C.20)$$

Thus substitution of the Eqs (C.1) and (C.18) into Eq.(C.20) gives

$$\sum_{i=1}^{n_m} \left(\frac{(\alpha_x)_i \cdot B_i^2 \cdot C_i}{a_i} \cdot \frac{(1 + \beta_i)^3}{u_i^2} \cdot \Delta x_i \right) = \frac{\alpha_{x_{n_m}} \cdot B_{n_m}^2 \cdot C_{n_m}}{a_{n_m}} \cdot \frac{(1 + \beta_{n_m})^3}{u_{n_m}^2} \cdot L_{n_m} \quad (C.21)$$

With

$$L_{n_m} = \sum_{i=1}^{n_m} \Delta x_i \quad u_{n_m} = \frac{L_{n_m}}{\sum_{i=1}^{n_m} \frac{\Delta x_i}{u_i}} \quad (C.22)$$

Equation (C.21) gives the following relation between the overall $[(\alpha_x)_{n_m}]$ and local $[(\alpha_x)_i]$ values of the proportionality coefficient

$$(\alpha_x)_{n_m} = \frac{a_{n_m}}{B_{n_m}^2 \cdot C_{n_m} \cdot (1 + \beta_{n_m})^3} \cdot \frac{\sum_{i=1}^{n_m} \Delta x_i}{\left[\sum_{i=1}^{n_m} \frac{\Delta x_i}{u_i} \right]^2} \cdot \sum_{i=1}^{n_m} \left[\frac{(\alpha_x)_i \cdot B_i^2 \cdot C_i}{a_i} \cdot \frac{\Delta x_i}{u_i^2} \cdot (1 + \beta_i)^3 \right] \quad (C.23)$$

Considering the situation along the River Rhine the relation between the longitudinal dispersion-coefficient and the time-variance can be given by (see also Subsection 2.3.3, Eq.(2.3.76))

$$\sigma_t^2 = \left(\frac{2 \cdot x}{u_s^3} \right) \cdot [K \cdot (1 + \beta)^2]$$

or

$$(\sigma_t)_{n_m}^2 = \left(\frac{2 \cdot L_{n_m}}{u_{n_m}^3} \right) \cdot [K_{n_m} \cdot (1 + \beta_{n_m})^2] \quad (C.24)$$

Substitution of Eqs (C.18) and (C.22) into Eq.(C.24) gives the expression for the overall value of the coefficient of proportionality, using the measured time-variance

$$(\alpha_x)_{n_m} = \frac{(\sigma_t)_{n_m}^2}{2} \cdot \frac{a_{n_m} \cdot \sqrt{g}}{B_{n_m}^2 \cdot C_{n_m} \cdot (1 + \beta_{n_m})^2} \cdot \frac{\sum_{i=1}^{n_m} \Delta x_i}{\left[\sum_{i=1}^{n_m} \frac{\Delta x_i}{u_i} \right]^2} \quad (C.25)$$

with

$$a_{n_m} = \frac{\sum_{i=1}^{n_m} a_i \cdot \Delta x_i}{\sum_{i=1}^{n_m} \Delta x_i} \quad B_{n_m} = \frac{\sum_{i=1}^{n_m} B_i \cdot \Delta x_i}{\sum_{i=1}^{n_m} \Delta x_i} \quad C_{n_m} = \frac{\sum_{i=1}^{n_m} C_i \cdot \Delta x_i}{\sum_{i=1}^{n_m} \Delta x_i}$$

and

$$\beta_{n_m} = \frac{(\mu_t)_{n_m}}{\sum_{i=1}^{n_m} \frac{\Delta x_i}{u_i}} - 1$$

For the determination of the local coefficient of proportionality per (sub-)branch of the Rhine Alarm-Model Eq.(C.23) is considered. To be able to find an explicit expression for the local value the following substitutions are made

$$H_{n_m} = \frac{B_{n_m}^2 \cdot C_{n_m}}{a_{n_m}} \quad H_i = \frac{B_i^2 \cdot C_i}{a_i} \quad (C.26)$$

Thus Eq.(C.23) becomes

$$(\alpha_x)_{n_m} = \frac{1}{H_{n_m} \cdot (1 + \beta_{n_m})^3} \cdot \frac{\sum_{i=1}^{n_m} \Delta x_i}{\left[\sum_{i=1}^{n_m} \frac{\Delta x_i}{u_i} \right]^2} \cdot \sum_{i=1}^{n_m} \left[(\alpha_x)_i \cdot H_i \cdot \frac{\Delta x_i}{u_i^2} \cdot (1 + \beta_i)^3 \right] \quad (C.27)$$

For further simplification the next substitutions are introduced

$$P_{n_1} = \sum_{i=1}^{n_1} H_i \cdot \frac{\Delta x_i}{u_i^2} \cdot (1 + \beta_i)^3$$

$$P_{n_2} = \sum_{i=n_1+1}^{n_2} H_i \cdot \frac{\Delta x_i}{u_i^2} \cdot (1 + \beta_i)^3$$

or in general

$$P_{n_m} = \sum_{i=n_{m-1}+1}^{n_m} H_i \cdot \frac{\Delta x_i}{u_i^2} \cdot (1 + \beta_i)^3$$

by which Eq. (C.27) can be rewritten into

$$(\alpha_x)_{n_m} = \frac{\sum_{i=1}^{n_m} \Delta x_i}{H_{n_m} \cdot (1 + \beta_{n_m})^3 \cdot \left[\sum_{i=1}^{n_m} \frac{\Delta x_i}{u_i} \right]^2} * \quad (C.28)$$

$$* \left[(\alpha_x)_1 \cdot P_{n_1} + (\alpha_x)_2 \cdot P_{n_2} + \dots + (\alpha_x)_m \cdot P_{n_m} \right]$$

From Eq.(C.28) the local coefficient of proportionality $(\alpha_x)_m$ can be expressed explicitly

$$(\alpha_x)_m = \frac{(\alpha_x)_{n_m} \cdot H_{n_m} \cdot \left[\sum_{i=1}^{n_m} \frac{\Delta x_i}{u_i} \right]^2 \cdot (1 + \beta_{n_m})^3}{P_{n_m} \cdot \sum_{i=1}^{n_m} \Delta x_i} + \quad (C.29)$$

$$- \left[(\alpha_x)_1 \cdot \frac{P_{n_1}}{P_{n_m}} + (\alpha_x)_2 \cdot \frac{P_{n_2}}{P_{n_m}} + \dots + (\alpha_x)_{m-1} \cdot \frac{P_{n_{m-1}}}{P_{n_m}} \right]$$

As in case of the lag coefficient, the coefficients of proportionality $(\alpha_x)_i$ of all the river (sub-)branches between two successive measuring-stations will be equal $(\alpha_x)_m$.

In case the measuring station lies between the boundaries of the sub-branch the coefficient of this branch $[(\alpha_x)_{composed}]$ is the average value of the coefficients of the upstream and downstream river-reach

$$(\alpha_x)_{composed} \cdot \left(\frac{\Delta x_i}{u_i} + \frac{\Delta x_{i+1}}{u_{i+1}} \right) = \frac{(\alpha_x)_i \cdot \Delta x_i}{u_i} + \frac{(\alpha_x)_{i+1} \cdot \Delta x_{i+1}}{u_{i+1}} \quad (C.30)$$

wherein $(\alpha_x)_i$ = upstream value of the lag coefficient
 $(\alpha_x)_{i+1}$ = downstream value of the lag coefficient

Referring to the fact that the flow velocity in a sub-branch is constant, Eq.(C.30) can be simplified by

$$(\alpha_x)_{composed} = \frac{(\alpha_x)_i \cdot \Delta x_i + (\alpha_x)_{i+1} \cdot \Delta x_{i+1}}{\Delta x_i + \Delta x_{i+1}} \quad (C.31)$$

Appendix D

Derivation of the convolution integral

The one-dimensional convection-diffusion equation reads

$$\frac{\partial \bar{\varphi}(x,t)}{\partial t} + u_s \cdot \frac{\partial \bar{\varphi}(x,t)}{\partial x} - K \cdot \frac{\partial^2 \bar{\varphi}(x,t)}{\partial x^2} = 0 \quad (\text{D.1})$$

$$(x > 0, t > 0)$$

with $\bar{\varphi}(x,t)$	=	concentration
x	=	coordinate in flow direction
t	=	time
K	=	longitudinal dispersion-coefficient
u_s	=	mean flow-velocity

For the solution of Eq.(D.1) two boundary conditions and one initial condition are needed:

Boundary conditions

$$\lim_{x \rightarrow \infty} \bar{\varphi}(x,t) = 0 \quad (\text{D.2})$$

$$\bar{\varphi}(0,t) = \psi(t) \quad \text{with } t \geq 0 \quad (\text{D.3})$$

$\psi(t)$ is an arbitrary function of t .

Initial condition

$$\bar{\varphi}(x,0) = 0 \quad \text{with } x > 0 \quad (\text{D.4})$$

The Laplace transforms of the Eqs (D.1) ... (D.4) after

$$\Phi(x,s) = \int_0^{\infty} e^{-st} \cdot \bar{\varphi}(x,t) dt \quad (\text{D.5})$$

become

$$[e^{-st} \cdot \bar{\varphi}(x,t)]_0^{\infty} + s \cdot \Phi(x,s) + u_s \cdot \frac{\partial \Phi(x,s)}{\partial x} - K \cdot \frac{\partial^2 \Phi(x,s)}{\partial x^2} = 0 \quad (\text{D.6})$$

$$\lim_{x \rightarrow \infty} \Phi(x, s) = 0 \quad (\text{D.7})$$

$$\Phi(0, s) = \int_0^{\infty} e^{-st} \cdot \psi(t) \, dt = \bar{\psi}(s) \quad (\text{D.8})$$

$$\Phi(x, 0) = 0 \quad (\text{D.9})$$

Because after Eq.(D.4) it yields

$$\left[e^{-st} \cdot \bar{\varphi}(x, t) \right]_0^{\infty} = -\bar{\varphi}(x, 0) = 0$$

Equation (D.6) becomes

$$s \cdot \Phi + u_s \cdot \frac{\partial \Phi}{\partial x} - K \cdot \frac{\partial^2 \Phi}{\partial x^2} = 0 \quad (\text{D.10})$$

The general solution of Eq.(D.10) is achieved by

$$\Phi(x, s) = a_1 \cdot \exp(\Omega_1 \cdot x) + a_2 \cdot \exp(\Omega_2 \cdot x) \quad (\text{D.11})$$

with

$$\Omega_1 = \frac{u_s}{2 \cdot K} - \frac{\sqrt{u_s^2 + 4 \cdot K \cdot s}}{2 \cdot K}$$

$$\Omega_2 = \frac{u_s}{2 \cdot K} + \frac{\sqrt{u_s^2 + 4 \cdot K \cdot s}}{2 \cdot K}$$

After Eq.(D.7) it yields $a_2 = 0$, so Eq.(D.11) becomes

$$\Phi(x, s) = a_1 \cdot \exp(\Omega_1 \cdot x) \quad (\text{D.12})$$

After Eq.(D.8) a_1 becomes for $x = 0$

$$a_1 = \bar{\psi}(s)$$

by which the solution of Eq.(D.10) results into

$$\Phi(x,s) = \bar{\Psi}(s) \cdot \exp\left(\frac{u_s \cdot x}{2K} - \frac{x}{\sqrt{K}} \cdot \sqrt{\frac{u_s^2}{4K} + s}\right) \quad (D.13)$$

With

$$\alpha = \frac{x}{\sqrt{K}} \quad \wedge \quad \beta = \frac{u_s^2}{4K} \quad (D.14)$$

Eq.(D.13) can be rewritten into

$$\Phi(x,s) = \bar{\Psi}(s) \cdot \exp(\alpha \cdot \sqrt{\beta}) \cdot \exp(-\alpha \cdot \sqrt{s + \beta}) \quad (D.15)$$

In order to get the solution of Eq.(D.1), - i.e. an explicit expression for the concentration $\bar{\varphi}(x,t)$ -, the inverse Laplace-transform of Eq.(D.15) has to be derived. If the inverse Laplace-transform is indicated by \mathcal{L} , the following functions can be defined

$$F(s) = \mathcal{L}[f(\tau)] = \exp(\alpha \cdot \sqrt{\beta}) \cdot \exp(-\alpha \cdot \sqrt{s + \beta}) \quad (D.16)$$

and

$$G(s) = \mathcal{L}[g(\tau)] = \bar{\Psi}(s) \quad (D.17)$$

or

$$\Phi(x,s) = F(s) \cdot G(s) \quad (D.18)$$

After Eq.(D.8) it yields

$$g(\tau) = \psi(\tau) \quad (D.19)$$

Using the properties of the inverse Laplace-transforms, indicated by \mathcal{L}^{-1}

$$\mathcal{L}^{-1}[A \cdot H(s)] = A \cdot \mathcal{L}^{-1}[H(s)] \quad (D.20)$$

$$\mathcal{L}^{-1}[A \cdot H(s + \varepsilon)] = A \cdot \exp(-\varepsilon \cdot \tau) \cdot \mathcal{L}^{-1}[H(s)] \quad (D.21)$$

the function $f(\tau)$ in Eq.(D.16) can be rewritten in succession by

$$\begin{aligned}
f(\tau) &= \mathcal{L}^{-1} [F(s)] = \mathcal{L}^{-1} [\exp(\alpha \cdot \sqrt{\beta}) \cdot \exp(-\alpha \cdot \sqrt{s + \beta})] = \\
&= \exp(\alpha \cdot \sqrt{\beta}) \cdot \exp(-\beta \cdot \tau) \cdot \mathcal{L}^{-1} [\exp(-\alpha \cdot \sqrt{s})] = \\
&= \exp(\alpha \cdot \sqrt{\beta}) \cdot \exp(-\beta \cdot \tau) \cdot \frac{\alpha}{2 \cdot \sqrt{\pi \cdot \tau^3}} \cdot \exp \left[\frac{-\alpha^2}{4 \cdot \tau} \right]
\end{aligned} \tag{D.22}$$

if $\alpha > 0$ (Abramowitz and Stegun, 1965)

Substitution of α and β after Eq.(D.14) transforms Eq.(D.22) into

$$f(\tau) = \frac{x}{2 \cdot \sqrt{\pi \cdot K \cdot \tau^3}} \cdot \exp \left(- \frac{(x - u_s \cdot \tau)^2}{4 \cdot K \cdot \tau} \right) \tag{D.23}$$

Applying the following property of the inverse Laplace-transform

$$\mathcal{L}^{-1} [F(s) \cdot G(s)] = \int_0^t f(\tau) \cdot g(t - \tau) d\tau \tag{D.24}$$

and considering Eqs (D.19) and (D.23) the solution concerned becomes

$$\bar{\varphi}(x, t) = \mathcal{L}^{-1} [\Phi(x, s)] = \mathcal{L}^{-1} [F(s) \cdot G(s)]$$

or

$$\bar{\varphi}(x, t) = \int_0^t \psi(t - \tau) \cdot \frac{x}{2 \cdot \sqrt{\pi \cdot K \cdot \tau^3}} \cdot \exp \left[- \frac{(x - u_s \cdot \tau)^2}{4 \cdot K \cdot \tau} \right] \cdot d\tau \tag{D.25}$$

The derivation of the solution after Eq.(D.25) for the one-dimensional convection-diffusion equation (D.1) has been formulated by analogy with Becker and Sosnowski (1969).

For $x = 0$ the integrand becomes singular. This means that it is not allowed to evaluate $\bar{\varphi}(x, t)$ for $x = 0$ by taking $x = 0$ in the integrand. By means of the

following reasoning (Veling, 1996) it becomes clear that still

$$\lim_{x \rightarrow 0} \bar{\varphi}(x, t) = \Psi(t) \quad (\text{D.26})$$

With the substitution of $\tau = \rho^2$ Eq.(D.25) becomes

$$\begin{aligned} \bar{\varphi}(x, t) = & \int_0^{\sqrt{t}} \Psi(t - \rho^2) \cdot \frac{x}{2 \cdot \sqrt{\pi \cdot K}} \cdot \frac{2}{\rho^2} * \\ & * \exp \left(- \frac{x^2}{4K\rho^2} - \frac{u_s^2}{4K} \rho^2 + \frac{u_s x}{2K} \right) d\rho \end{aligned} \quad (\text{D.27})$$

Rewriting of Eq.(D.27) gives in succession

$$\begin{aligned} \bar{\varphi}(x, t) = & \exp \left(\frac{u_s x}{2K} \right) \left[\int_0^{\sqrt{t}} \Psi(t - \rho^2) \cdot \frac{x}{2\sqrt{\pi}} \cdot \frac{2}{\sqrt{K}} * \right. \\ & * \left\{ \exp \left[- \left(\frac{u_s}{2\sqrt{K}} \rho + \frac{x}{2\sqrt{K}} \frac{1}{\rho} \right)^2 \right] \cdot \exp \left[\frac{u_s x}{2K} \right] \cdot \left(\frac{u_s}{2\sqrt{K}} - \frac{x}{2\sqrt{K}\rho^2} \right) + \right. \\ & - \exp \left[- \left(\frac{u_s}{2\sqrt{K}} \rho - \frac{x}{2\sqrt{K}} \frac{1}{\rho} \right)^2 \right] \cdot \exp \left[- \frac{u_s x}{2K} \right] \cdot \left(\frac{u_s}{2\sqrt{K}} + \frac{x}{2\sqrt{K}\rho^2} \right) \left. \right\} * \\ & * \left(\frac{-2\sqrt{K}}{2x} \right) d\rho \left. \right] = \\ & = - \exp \left(\frac{u_s x}{2K} \right) \int_0^{\sqrt{t}} \Psi(t - \rho^2) \cdot \frac{1}{\sqrt{\pi}} * \\ & * \left\{ \exp(-z_+^2) \cdot \exp \left(\frac{u_s x}{2K} \right) \frac{dz_+}{d\rho} - \exp(-z_-^2) \cdot \exp \left(- \frac{u_s x}{2K} \right) \frac{dz_-}{d\rho} \right\} d\rho \end{aligned} \quad (\text{D.28})$$

with

$$z_{\pm} = \frac{u_s}{2\sqrt{K}} \rho \pm \frac{x}{2\sqrt{K}} \frac{1}{\rho} \quad (\text{D.29})$$

Since Eq.(D28) is a nonlinear transformation, special attention has to be paid to the substitution of Eq.(D.29) into Eq.(D.28). Therefore the integration range is split up into two parts $(0, \sqrt{x/u_s})$, $(\sqrt{x/u_s}, \sqrt{t})$. Because the verification of Eq.(D.25) for $x \downarrow 0$ is concerned, there is no doubt about that $\sqrt{x/u_s} < \sqrt{t}$.

After Eq.(D.29) it yields in succession

$$\begin{aligned} z_{\pm} &= \frac{u_s}{2\sqrt{K}} \rho_{\pm} + \frac{x}{2\sqrt{K}} \frac{1}{\rho_{\pm}} \\ \frac{u_s}{2\sqrt{K}} \rho_{\pm}^2 - z_{\pm} \rho_{\pm} + \frac{x}{2\sqrt{K}} &= 0 \\ (\rho_{\pm})_{1,2} &= \frac{z_{\pm} \sqrt{K}}{u_s} \cdot \left(1 \pm \sqrt{1 - \frac{u_s x}{z_{\pm}^2 K}} \right) \end{aligned} \quad (\text{D.30})$$

where the $+$ -sign holds for the interval $(\sqrt{x/u_s}, \sqrt{t})$, and the $-$ -sign for the interval $(0, \sqrt{x/u_s})$ (see Fig. D.1)

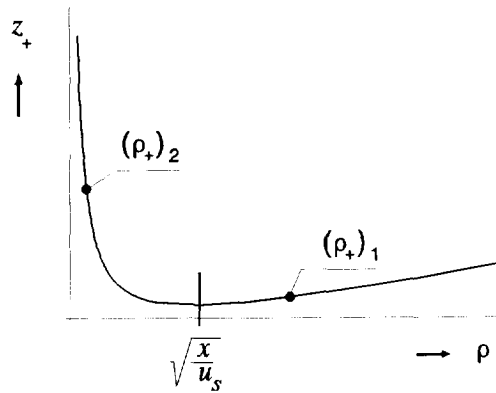


Fig. D.1

In a similar way it yields

$$(\rho_-)_{1,2} = \frac{z_- \sqrt{K}}{u_s} \cdot \left(1 \pm \sqrt{1 + \frac{u_s x}{z_-^2 K}} \right) \quad (\text{D.31})$$

where the $+$ -sign holds for the interval $(\sqrt{x/u_s}, \sqrt{t})$, and the $-$ -sign for the interval $(0, \sqrt{x/u_s})$. Remark that for $0 < \rho < \sqrt{x/u_s}$, the value of z_- is negative (see Fig. D.2)

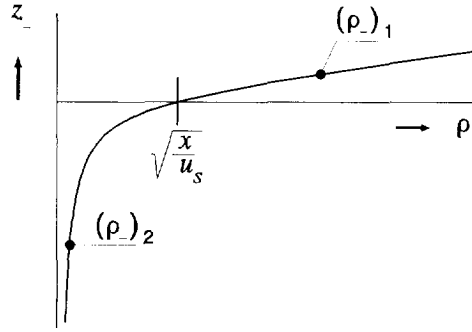


Fig. D.2

Now Eq.(D.28) becomes

$$\begin{aligned} \bar{\varphi}(x,t) = & - \exp \left(\frac{u_s x}{2K} \right) * \\ & * \left[\int_{-\infty}^{\frac{\sqrt{u_s x}}{\sqrt{K}}} \Psi \left(t - (\rho_-)_2^2 \right) \cdot \frac{1}{\sqrt{\pi}} \cdot \exp(-z^2) \cdot \exp \left(\frac{u_s x}{2K} \right) dz + \right. \\ & + \left. \int_{\frac{\sqrt{u_s x}}{\sqrt{K}}}^{\frac{u_s \sqrt{t}}{2\sqrt{K}} + \frac{x}{2\sqrt{K}t}} \Psi \left(t - (\rho_+)_1^2 \right) \cdot \frac{1}{\sqrt{\pi}} \cdot \exp(-z^2) \cdot \exp \left(\frac{u_s x}{2K} \right) dz + \right] \end{aligned}$$

$$\begin{aligned}
& - \int_{-\infty}^0 \Psi \left(t - (\rho_-)_2^2 \right) \cdot \frac{1}{\sqrt{\pi}} \cdot \exp \left(-z^2 \right) \cdot \exp \left(\frac{u_s x}{2K} \right) dz + \\
& - \left[\int_0^{\frac{u_s \sqrt{t}}{2\sqrt{K}} - \frac{x}{2\sqrt{K}t}} \Psi \left(t - (\rho_-)_1^2 \right) \cdot \frac{1}{\sqrt{\pi}} \cdot \exp \left(-z^2 \right) \cdot \exp \left(\frac{u_s x}{2K} \right) dz \right]
\end{aligned}
\tag{D.32}$$

For $x \downarrow 0$, there holds (all following approximations are valid up to order $O(x)$, $x \rightarrow 0$)

$$\begin{aligned}
(\rho_+)_2 &= \frac{z_+ \sqrt{K}}{u_s} \cdot \left(1 - \sqrt{1 - \frac{u_s x}{z_+^2 K}} \right) \sim \frac{z_+ \sqrt{K}}{u_s} \cdot \left(1 - \left(1 - \frac{u_s x}{2z_+^2 K} \right) \right) = \\
&= \frac{x}{2z_+ \sqrt{K}}
\end{aligned}$$

$$\begin{aligned}
(\rho_-)_2 &= \frac{z_- \sqrt{K}}{u_s} \cdot \left(1 - \sqrt{1 + \frac{u_s x}{z_-^2 K}} \right) \sim \frac{z_- \sqrt{K}}{u_s} \cdot \left(1 - \left(1 + \frac{u_s x}{2z_-^2 K} \right) \right) = \\
&= \frac{x}{2(-z_-) \sqrt{K}}
\end{aligned}$$

and

$$(\rho_+)_1 \sim \frac{2z_+ \sqrt{K}}{u_s}$$

$$(\rho_-)_1 \sim \frac{2z_- \sqrt{K}}{u_s}$$

So, for $x \downarrow 0$ Eq.(D.32) becomes

$$\begin{aligned}
 \overline{\varphi}(x,t) \sim & - \left[\int_{-\infty}^0 \psi(t) \cdot \frac{1}{\sqrt{\pi}} \cdot \exp(-z^2) dz + \right. \\
 & + \int_0^{\frac{u_s \sqrt{t}}{2\sqrt{K}}} \psi\left(t - \frac{4z^2 K}{u_s^2}\right) \cdot \frac{1}{\sqrt{\pi}} \cdot \exp(-z^2) dz + \\
 & - \int_{-\infty}^0 \psi(t) \cdot \frac{1}{\sqrt{\pi}} \cdot \exp(-z^2) dz + \\
 & \left. - \int_0^{\frac{u_s \sqrt{t}}{2\sqrt{K}}} \psi\left(t - \frac{4z^2 K}{u_s^2}\right) \cdot \frac{1}{\sqrt{\pi}} \cdot \exp(-z^2) dz \right] = \\
 & = \psi(t) \int_{-\infty}^{\infty} \frac{1}{\sqrt{\pi}} \cdot \exp(-z^2) dz = \psi(t)
 \end{aligned}$$

Appendix E

Transport velocity related to the peak concentration after the Chatwin-model

Considering the Chatwin-model after Eq.(2.3.85) in Sub-section 2.3.3, neglecting the stagnant zones ($\beta = 0$)

$$\varphi_E(x, t) = \frac{M/Q}{\sqrt{4 \cdot \pi \cdot K \cdot t/u^2}} \cdot \exp \left[- \frac{(t - x/u)^2}{4 \cdot K \cdot t/u^2} \right] * \left[1 + \frac{G_t}{6} \cdot H_3 \left(\frac{t - x/u}{\sqrt{2 \cdot K \cdot t/u^2}} \right) \right] \quad (\text{E.1})$$

with (third Hermite-polynomial)

$$H_3 \left(\frac{t - L/c}{\sqrt{2 \cdot K \cdot t/c^2}} \right) = \left(\frac{t - L/c}{\sqrt{2 \cdot K \cdot t/c^2}} \right)^3 - 3 \cdot \left(\frac{t - L/c}{\sqrt{2 \cdot K \cdot t/c^2}} \right) \quad (\text{E.2})$$

and (skewness)

$$G_t = 1 \quad (\text{E.3})$$

wherein

M	=	released mass
Q	=	river discharge
u	=	u_x , mean flow-velocity
K	=	longitudinal dispersion-coefficient
x	=	L , distance from the point of release

For the determination of the transport velocity c of a pollution cloud related to the peak concentration, for which the concentration distribution is well fitted by the Chatwin-model, the peak-value time t_{max} of the distribution in the time domain has to be considered. The time t_{max} as a function of the distance $x = L$ from the point of release will be given by

$$\frac{\partial \varphi_E}{\partial t} = 0 \quad (\text{E.4})$$

and the transport velocity c for the peak concentration by

$$c = \frac{dt_{max}}{dx} \quad (\text{E.5})$$

Elaboration of Eq.(E.2) gives an implicit relation for t_{max}

$$\begin{aligned}
 & \left[\left(\frac{2Kt_{max}}{u^2} \right)^{1.5} + \frac{G_t}{6} \cdot \left(t_{max} - \frac{x}{u} \right)^3 - \frac{G_t}{2} \cdot \left(t_{max} - \frac{x}{u} \right) \cdot \left(\frac{2Kt_{max}}{u^2} \right) \right] * \\
 & \quad * \left[\frac{\left(\frac{x}{u} \right)^2 - t_{max}^2}{\left(\frac{2Kt_{max}}{u^2} \right)} - 1 \right] \cdot \frac{1}{2t_{max}} + \\
 & \quad + \frac{G_t}{2} \cdot \left[\left(t_{max} - \frac{x}{u} \right)^2 - \left(\frac{2Kt_{max}}{u^2} \right) \right] * \left[1 - \frac{\left(t_{max} - \frac{x}{u} \right)}{2t_{max}} \right] = 0 \quad (E.6)
 \end{aligned}$$

Therefore t_{max} is determined by trial and error by comparing the two terms

term 1

$$\begin{aligned}
 & \left[\left(\frac{2Kt_{max}}{u^2} \right)^{1.5} + \frac{G_t}{6} \cdot \left(t_{max} - \frac{x}{u} \right)^3 - \frac{G_t}{2} \cdot \left(t_{max} - \frac{x}{u} \right) \cdot \left(\frac{2Kt_{max}}{u^2} \right) \right] * \\
 & \quad * \left[\frac{\left(\frac{x}{u} \right)^2 - t_{max}^2}{\left(\frac{2Kt_{max}}{u^2} \right)} - 1 \right] \cdot \frac{1}{2t_{max}} \quad (E.7)
 \end{aligned}$$

term 2

$$\frac{G_t}{2} \cdot \left[\left(t_{max} - \frac{x}{u} \right)^2 - \left(\frac{2Kt_{max}}{u^2} \right) \right] * \left[\frac{\left(t_{max} - \frac{x}{u} \right)}{2t_{max}} - 1 \right] \quad (E.8)$$

The accuracy of t_{max} depends on the value of ε in

$$| \text{term 1} - \text{term 2} | = \varepsilon \quad (E.9)$$

In the following computations $\varepsilon < 0.01$.

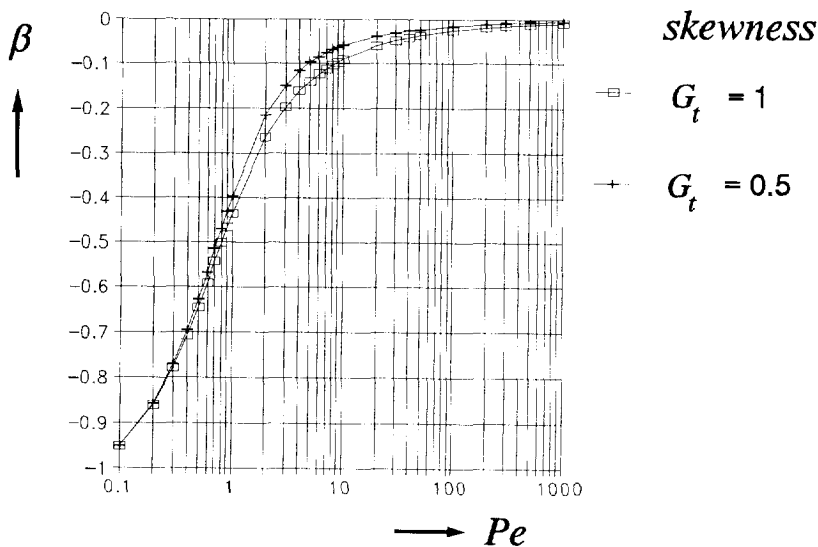


Fig. E.1 Distribution of the local lag-coefficient β as a function of the Pe -number for two values of the skewness G_t after the Chatwin-model

Now the transport velocity c has to be determined numerically

$$c(x_{i+1}) = \frac{(t_{\max})_{i+1} - (t_{\max})_i}{x_{i+1} - x_i} = \frac{\Delta t_{\max}}{\Delta x} \quad (\text{E.10})$$

With $\Delta x = 10$ m the distribution of the local lag-coefficient β can be determined after

$$\beta(x_{i+1}) = \frac{u}{c(x_{i+1})} - 1 \quad (\text{E.11})$$

or with the Péclet number after $Pe = x_{i+1} \cdot u / K$

$$\beta(Pe) = \frac{u}{c(Pe)} - 1 \quad (\text{E.12})$$

The results are presented in Fig. E.1 for two values of the skewness G_t . In Fig. E.2 these results are compared with the Taylor-model, which is equal to the Chatwin-model for $G_t = 0$. The comparison shows that the negative value of the lag coefficient reduces with the skewness.

These results are caused by the large concentration-gradients near the point of release, by which the dispersive transport is relatively large. The result is a relatively steep front of the concentration distribution with a relatively long tail. Consequently the concentration distribution becomes skew. In the Chatwin-model the third Hermite-polynomial enlarges this skewness of the concentration distribution after Taylor-model. The enlargement depends on the value of the skewness G_t .

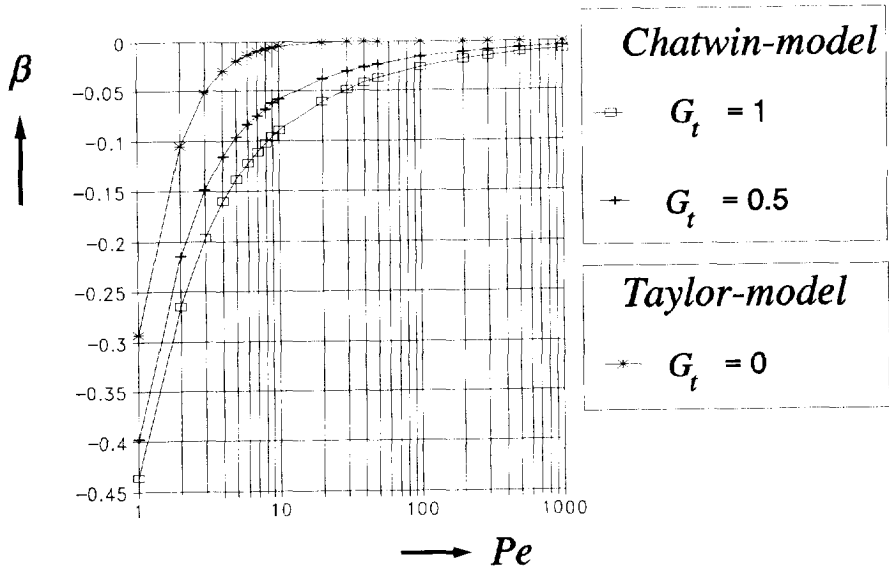


Fig. E.2 Comparison of the distributions of the local lag-coefficient β as a function of the Pe -number after the Chatwin-model and the Taylor-model

Figure E.2 shows that these effects on the lag coefficient related to the peak concentration are significant for $Pe \leq 30$ ($\beta < -0.05$). In case of the River Rhine with a mean flow-velocity of 1 m/s and an average dispersion-coefficient of about 1000 m²/s, the negative β -value occurs over a distance of about 30 km downstream of the point of release.